Focus Meeting #3:
Radio Galaxies –
Resolving the AGN Phenomenon

Articles related to invited and contributed talks, and to poster presentations

August 22 - 23, 2018

Contents

Astronomy in Focus, Volume 1
XXXth IAU General Assembly, August 2018
Teresa Lago, ed.

DOI: 00.0000/X000000000000000X

Focus Meeting #3: Radio Galaxies – Resolving the AGN Phenomenon

Volker Beckmann

CNRS / IN2P3, 3 rue Michel Ange, 75016 Paris, France
email: beckmann@in2p3.fr

Radio galaxies provide excellent laboratories for investigating the physical aspects, unification and cosmic evolution of active galactic nuclei (AGN). Thanks to recent multi-wavelength observations, we are now able to separate many different physical components of radio galaxies through imaging and spectroscopy. Observations from radio through X-ray wavelengths can probe the ejection of matter into jets and monitor decades of jet evolution. Gamma-ray observations have shown that radio galaxies are detectable up to the very-high-energy range despite unfavorable jet alignment.

We observe radio galaxies out to redshifts greater than $z = 5$, which makes them important cosmological probes. Planck maps have provided us with new insights into the populations of radio galaxies and their distributions in space in the $30 - 900$ GHz range. NuSTAR provides high-quality spectra in the hard X-ray range. The Event Horizon Telescope (EHT) has begun mapping close to the event horizon of the Milky Way?s central black hole, and the Square Kilometre Array (SKA), the next generation of extremely large telescopes (ELTs) and other future telescopes will open up a new and vast discovery space.

Focus Meeting #3 brought together multiwavelength observers and theorists to synthesize progress made over the last three years and to define future directions. In order to channel the presentations and discussions, the meeting was organized into five sessions:

• During the first session, starting on August 22nd, we discussed the radio-galaxy structures that are produced on kiloparsec scales and beyond, with an emphasis on plasma composition, and sought to address their underlying causes. Daniel Schwartz (Harvard-Smithsonian Center for Astrophysics, USA) talked about high-resolution studies of 100 kpc jets based on data from the Chandra X-ray Observatory. For example, a new Chandra survey for jets in radio quasars at $z > 3$ has revealed X-ray jets and lobes extending beyond the region of detected radio emission (Schwartz 2018).

• The second session will focus on the central engine and production of the jet(s). Alexander Tchekhovskoy (University of California, Berkeley, USA) introduced the topic with a presentation about how numerical simulations incorporating general relativity and magnetism allow us to use black hole accretion phenomena to quantitatively probe strong-field gravity and constrain black hole physics in various astrophysical contexts.

• on Thursday morning we first discussed populations and statistics of radio galaxies, motivated by a review from Elaine Sadler (University of Sydney, Australia) focusing on results from multi-wavelength radio surveys.

• This was followed by a session about future prospects. Lindy Blackburn (Harvard-Smithsonian Center for Astrophysics, USA) started the discussion with a presentation on the goals and status of the EHT, which has already revealed structure on the scale of the Schwarzschild radius in Sagittarius A*, the supermassive black hole at the centre of our galaxy, and in Messier 87 in the Virgo Cluster.

• A fifth session dealt with the interaction of radio galaxies with their environments. Andy Fabian (Institute of Astronomy, Cambridge University, UK) discussed AGN feedback in clusters of galaxies and explained how energy can be transported and dissipated throughout the cluster core.

In addition to the invited reviews, 20 high-profile contributed talks reviewed the state of the art within the field, and 20 posters had been selected for one-minute/one-slide presentations. The sessions were accompanied by dedicated discussions, giving the audience ample opportunities to help us obtain a wide and complete view of what is driving radio galaxies and what we can learn from them about physical processes in the universe.

Finally, Annalisa Celotti (International School for Advanced Studies (SISSA), Italy) wrapped up FM3 by giving a summary of the results presented during the 1.5 days of the meeting.

The following ~ 60 contributions are representative of the presentations given at the meeting. The articles are sorted in alphabetical order. Photos of the focus meeting can be found on Twitter under `https://twitter.com/iau18radiogalax`

Acknowledgments

We would like to thank the local organisers of the IAU general assembly and the IAU Executive Committee for their efficient support! The Scientific Organizing Committee of this focus meeting put together the program, gave the meeting its scientific direction, and edited these proceedings: Loredana Bassani (IASF / INAF, Italy), Volker Beckmann (chair, CNRS / IN2P3, France), Markus Böttcher (North-West University, South Africa), Chris Done (Durham University, UK), Melanie Johnston-Hollitt (Victoria University, New Zealand), Anne Lähteenmäki (Aalto University, Finland), Raffaella Morganti (ASTRON, The Netherlands), Rodrigo Nemmen (Sao Paolo University, Brazil), Paolo Padovani (ESO, Germany), Claudio Ricci (co-chair, UDP, Chile), Yoshihiro Ueda (Kyoto University, Japan), Sylvain Veilleux (University of Maryland, USA), and Diana Worrall (co-chair, Bristol University, UK).

References

Schwartz, D. 2018, *Astronomy in Focus* 1 (these proceedings)

Astronomy in Focus, Volume 1
XXXth IAU General Assembly, August 2018
Volker Beckmann & Claudio Ricci, eds.

DOI: 00.0000/X000000000000000X

The nature of radio and optically variable radio sources

H. V. Abrahamyan, A. M. Mickaelian, G. M. Paronyan, G. A. Mikayelyan, M. V. Gyulzadyan

NAS RA V. Ambartsumian Byurakan Astrophysical Observatory (BAO), Byurakan 0213, Aragatzotn Province, Armenia
email: abrahamyanhayk@gmail.com

Abstract. We have cross-correlated the NVSS and FIRST radio catalogues having radio flux measurements at the same 1.4 GHz frequency to benefit from repeated observations from both catalogues, which gives more accurate positions and fluxes and more important, in a number of cases reveals large differences between the two measured fluxes, thus allowing to establish radio variability. 79,382 radio variables have been revealed, including 6301 with flux differences at 1.4 GHz larger than 15 mJy, 1917 with flux differences 45 mJy and 260 with flux differences 200 mJy. By using a special technique (Mickaelian & Sinamyan 2010, Mickaelian et al. 2011) we have revealed 2425 optically variable objects out of 6301 radio sources. We have divided 2425 radio sources with both high radio and optical variability into four categories. 1206 (19%) out of 6301 radio sources have activity types from available catalogues and 619 (25.5%) out of 2425 radio sources with at the same time radio and optical variability have activity types from available catalogues. In addition, 279 radio sources out of 2425 have high variability in optical range. We have established their activity types when available. We have studied the IR fluxes and colours for the 6301 variable radio sources. Colour-colour diagrams show that most of the "unknown" sources are galaxies. We also have retrieved the activity types for 110 (42%) out of 260 extremely high variable radio sources.

Keywords. surveys – catalogs – galaxies: active – BL Lacertae objects: general – quasars: general – galaxies: Seyfert – radio continuum: galaxies.

1. Introduction

We use for our investigation FIRST and NVSS catalogues. The FIRST catalogue covers 10,000 deg^2 of the North and South Galactic Caps, to a sensitivity of about 1 mJy with an angular resolution of about 5" and includes 946,432 radio sources. To have large sky coverage, we jointly use the two biggest radio catalogues, NVSS and FIRST, having measurements at the same radio frequency, 1.4 GHz and giving opportunity of repeated observations for achieving better positions and fluxes, as well as investigating radio variability. The NVSS is a radio survey covering the sky north of -40° declination at 1.4GHz. The principal data products of the NVSS are a set of 2326 4°x4° continuum "cubes" with three planes containing Stokes I, Q, and U images, plus a catalog of almost 2 million discrete sources stronger than flux density of about 2.5 mJy. Comparing these catalogues gives us an opportunity to find radio sources which have variability in radio.

2. Cross-matching of radio catalogues and construction of the sample of radio variable objects

The NVSS and FIRST radio catalogues have been cross-matched. Our principle is to take into account positional errors for individual sources, and we have applied a similar to

our previous research method (Abrahamyan et al. 2015). In the FIRST catalogue there is no information on positional errors for each source, that is why 5 arcsecond as errors for all sources is adopted. In NVSS catalogue, each source is given with its individual positional error. We have created a software (http://arvo.sci.am/crosscorrelation/crosscor.html) through which cross-correlations are done. This software allows considering positional errors for each source individually and we have taken associations having coordinate differences between counterparts not exceeding 3σ (calculated using both σ-s from NVSS and FIRST). As a result, we have obtained 556,282 associations between NVSS and FIRST.

As corrected flux difference ΔF we define

$$\Delta F = |F_{FIRST} - (F_{NVSS} - SS)| - 3\sigma \tag{2.1}$$

where σ is the combined positional error

$$\sigma = \sqrt{Error^2_{FIRST} + Error^2_{NVSS}} \tag{2.2}$$

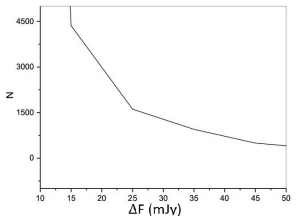

Figure 1. ΔF distribution showing breaks at 15, 25 and 45 mJy.

3. Summary and Conclusions

We have carried out a cross-correlation of the NVSS and FIRST catalogues to distinguish sources which have large differences of fluxes at 1400 MHz. We have selected 6301 radio sources with flux difference of at least 15 mJy. Further investigation of these radio sources led to a new sample of radio sources, which have high optical variability. The main results of our study are the cross-correlation of NVSS and FIRST radio catalogues at 1.4 GHz and the construction of a large sample of 79,382 radio variable sources, including 6301 with radio variability >15 mJy flux differences between NVSS and FIRST, 1699 with flux differences >50 mJy and 260 with flux differences >200 mJy, revelation of 2425 optically variable objects out of 6301 radio sources, revelation of 1206 (19%) active galaxies out of 6301 radio sources, and compilation of a list of 619 (25.5%) out of 2425 radio sources with at the same time optical variability (including many AGN among them).

References

Abrahamyan, H. V., Mickaelian, A. M., & Knyazyan, A. V. 2015, *A&C*, 10, 99
Condon, J. J., Cotton, W. D., Greisen, E. W., et al. 1998, *AJ*, 115, 1693
Helfand, D. J., White, R. L., & Becker, R. H. 2015, *ApJ*, 801, 26
Mickaelian, A. M., Mikayelyan, G. A., & Sinamyan, P. K. 2011, *MNRAS*, 415, 1061
Mickaelian, A. M. & Sinamyan, P. K. 2010, *MNRAS*, 407, 681
Ofek, E. O. & Frail, D. A., 2011, *ApJ*, 737, 45

Astronomy in Focus, Volume 1
XXXth IAU General Assembly, August 2018
Volker Beckmann & Claudio Ricci, eds.

DOI: 00.0000/X000000000000000X

Laboratory simulation of astrophysical jets with Plasma Focus facility

Vasily S. Beskin[1,2], Vyacheslav I. Krauz[1,3], Evgeny P. Velikhov[1,3] Viktor V. Myalton[1,3], Sergey S.Anan'ev[3], Sergey A. Dan'ko[3], Yury G. Kalinin[3], Airat M. Kharrasov[1,3], and K. N. Mitrofanov[4]

[1]Moscow Institute of Physics and Technology (State University), Dolgoprudny, Institutsky per, 9, 141700, Russia
email: krauz_vi@nrcki.ru, myalton_vv@ nrcki.ru, velikhov@mac.com
[2]Lebedev Physical Institute, Moscow, Leninsky prosp., 53, 119991, Russia
email: beskin@lpi.ru
[3]NRC Kurchatov Institute, Moscow, Akademika Kurchatova pl., 1, 123182, Russia
email: ananyev_ss@nrcki.ru, danko_sa@nrcki.ru, kalinin_yg@nrcki.ru
[4]SRC RF TRINITI, Moscow, Troitsk, ul. Pushkovykh, 12, 142190, Russia
email: mitrofan@triniti.ru

Abstract. A new series of experiments has been launched on the Plasma Focus type facility PF-3 in NRC Kurchatov Institute. The experiments with stationary gas filling revealed regimes in which a collimated highly magnetized plasma jet was formed, the head of which was no wider than several centimeters at jet propagation distances of up to 100 cm.

Keywords. methods: laboratory, ISM: jets and outflows

1. Introduction

Laboratory simulation of astrophysical processes is one of the intensively developed areas of plasma physics. Considerable progress in simulating the astrophysical processes has been achieved in recent decades due to new facilities with high energy density, which were developed within the framework of the program of inertial controlled fusion, e.g., the modern Z-pinch systems and high-power lasers (Remington, Drake, & Ryutov, 2006). Here we substantiate the applicability of Plasma Focus (PF) facilities for such modeling and already obtained results. We show that installations of this type have a number of preferences, which allow us to arrange the original experiments aimed at modeling the plasma outflows from compact astrophysical objects.

2. Plasma Focus experiments

Plasma Focus (PF) is a device, the principle of which operating is also based on the Z-pinch effect. It is a source of intense plasma flows, which is widely used in various fields of science and technology. Here we present results of experiments devoted to the astrophysical jets simulation on the PF-3 facility in NRC Kurchatov Institute (Krauz et al. 2015; Krauz, Beskin & Velikhov, 2018). Plasma flow is formed in the stage of pinching, which lasts several hundred ns, in the pinch area with a diameter 1 cm and a length of (3–5) cm and then propagates along the chamber axis.

The PF scheme has a number of advantages. First of all, there is the possibility to investigate the dynamics of the flow propagation in the ambient plasma at sufficiently large distances, more than two orders of magnitude greater than its initial transverse size. For this a new three-section diagnostic drift chamber was designed, which allowed one to

measure the jet and the ambient plasma parameters at distances of up to 100 cm from the flow generation region. Second, the presence of the ambient plasma is an important factor that allows us simulating the interaction of the flow with the external environment. The use of various working gases, including strongly radiating, allows investigating the role of radiation cooling in collimation and confinement of the jet. Finally, sufficiently large spatial dimensions of the flow (in comparison with the laser and Z-pinches experiment) made it possible to use magnetic probe techniques and allowed to investigate the special distribution of magnetic field and its time evolution.

3. Results

One of the main obtained results is finding the regimes with the formation of plasma object, preserving its compact size when spread over large distances (see Fig. 1). It was found that the compact plasma blobs move along the axis with the velocity $V \geqslant 10^7$ cm s^{-1} which is close to that of plasma outflows from young stars. The transverse scale of the flow head does not exceed a few cm at propagation distances more than 100 cm. This implies that there are mechanisms for stabilizing/confining the flow. The flow density determined by the Stark broadening at the distance of 35 cm from the anode was (2–4)$\times 10^{17}$ cm^{-3}, the electron plasma temperature of the jet was (2–8) eV. The concentration of the ambient plasma was (2–4)$\times 10^{16}$ cm^{-3}. The estimations of key dimensionless parameters showed that the PF-type facilities really can be used to simulate the jets from YSO.

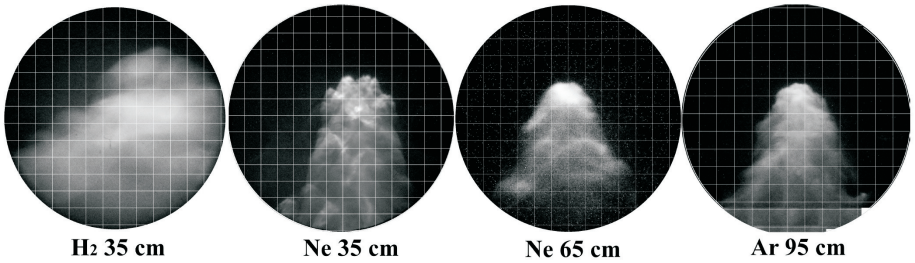

Figure 1. Frame camera pictures of plasma flow front at different distances from the anode plane and at operation with different gases. Scale is 1 cm

Finally, with the help of magnetic probes, the distribution of magnetic fields has been studied. It was shown that the plasma flow moves with the frozen magnetic field of the order (1–10) kG. A complex time-changing spatial configuration of the magnetic field inside the plasma flow was detected, rotation of the magnetic induction vector was found. Obtained radial distribution of the toroidal component of the magnetic field can be explained by the axial current in (1–10) kA flowing in the zone near the axis with the radius of (1–1.5) cm. The observed stability of the plasma flow can be caused by the formation of closed magnetic configurations. In this case, the stable-state duration depends on the decay time of the currents circulating in plasma.

This work was supported by the Russian Science Foundation, project No. 16-12-10051.

References

Remington, B.A., Drake, R.P., & Ryutov, D.D. 2006, *Rev. Mod. Phys.*, 78, 755

Krauz, V., Myalton, V., Vinogradov, V., Velikhov, E., Ananyev, S., Dan'ko, S., Kalinin, Yu., Kharrasov, A., Mitrofanov, K., & Vinogradova, Yu. 2015, in: R. Bingham, W. Suttrop, S. Atzeni, R. Foest, K. McClements (eds.), *Proc. 42nd EPS Conference on Plasma Physics* (Lisbon: Europ. Phys. Soc.), 39E, p. 4.401

Krauz, V.I., Beskin, V.S., & Velikhov, E.P. 2018, *Int. J. Mod. Phys. D*, 27, 1844009

Astronomy in Focus, Volume 1
XXXth IAU General Assembly, August 2018
Volker Beckmann & Claudio Ricci, eds.

DOI: 00.0000/X000000000000000X

Quasar activity in the neighboring Universe

Daniela Bettoni[1], Renato Falomo[1], Riccardo Scarpa[2], Maria Stone[3] and Jari Kotilainen[4]

[1]INAF - Osservatorio Astronomico di Padova
email: daniela.bettoni@inaf.it, renato.falomo@inaf.it

[2] GTC - IAC, Spain
email: riccardo.scarpa@gtc.iac.es

[3]Department of Physics and Astronomy , University of Turku, Finland
email: maria.b.stone@utu.fi

[4] Finnish Centre for Astronomy with ESO (FINCA), University of Turku, Finland
email: jarkot@utu.fi

Abstract. We analyzed the properties of the close environments of a sample of low redshift quasars to investigate the role of interactions for triggering and fueling the QSO phenomenon. We present the results of an extensive spectroscopic campaign at GTC and NOT telescopes in La Palma aimed at deriving the properties of companion galaxies of quasars and detecting signatures of recent star formation both in the host galaxies and in the companion galaxies. The sources are drawn from a large (∼400) sample of (z<0.4) quasars extracted from the SDSS "Stripe 82" for which we previously investigated the host galaxies and the large scale environments properties. We found that the close (<100 kpc) companion galaxies are often associated to the QSO but only a modest recent star formation is present. The implications for the mechanisms of nuclear activity are briefly discussed.

Keywords. galaxies: active, quasars: general, quasars: emission lines

1. Introduction

The role of environment in triggering the AGN activity is still a puzzling subject. At low-redshift, quasars follow the large-scale structure traced by galaxy clusters but they eschew the very centre of clusters (Marziani et al. 2017). On the other hand, on small scales (projected distance < 1 Mpc) the quasar environment appears overpopulated by blue disc galaxies having a strong star formation rate (Coldwell & Lambas 2006). However at Mpc scale comparing the environments of quasars to those of galaxies has given conflicting results. Early studies on scales of 10Mpc suggest that quasars are more strongly clustered than galaxies (e.g. Shanks et al. 1988), while later studies based on surveys such as the Two Degree Field (2dF) and the SDSS have found that the galaxy densities of quasars and inactive galaxies are comparable (e.g. Matsuoka et al. 2014). To better clarify this scenario we are carrying out a program to analyze the properties of the close environments of a sample of low redshift quasars to investigate the role of the interactions for triggering and fueling the QSO phenomenon.

2. Results

To this aim we secured optical spectra of close (<100 kpc) companion galaxies to the QSO in order to probe their physical association and to find signature of recent star formation. The observations were collected using the NOT and GTC telescopes at La Palma (Canary Islands).

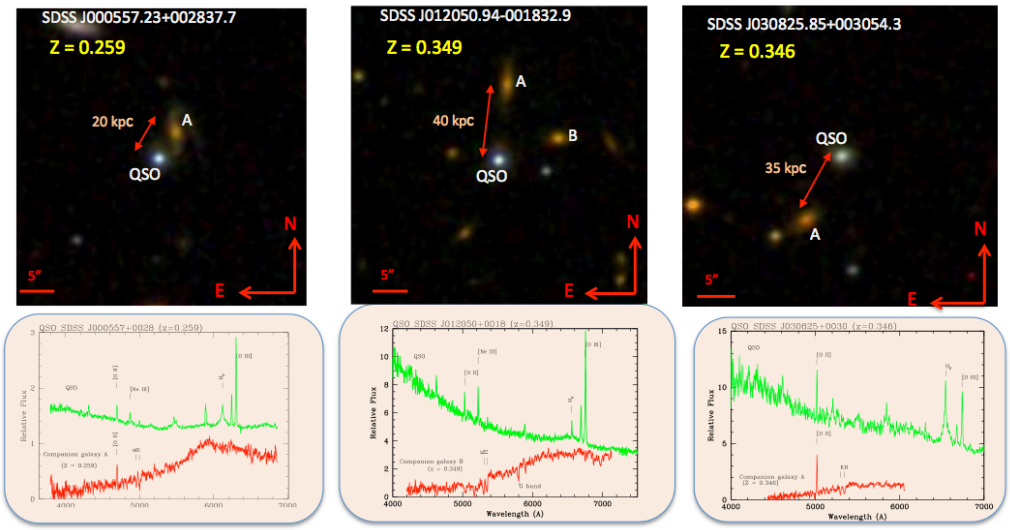

Figure 1. Some examples of QSO and companion galaxies

Galaxy environment of low z QSO was compared with that of inactive galaxies at same redshift and luminosity. Quasars are on average found associated with small groups of galaxies. No statistically significant difference is found between the overdensities around the quasars and the inactive galaxies (Karhunen et al. 2014, Bettoni et al. 2017).

At low redshift (z <0.5) QSO are hosted in a variety of galaxies including a significant fraction containing a disc although the spheroidal component is in most cases dominant. QSO hosts are dominated by luminous galaxies of absolute magnitude $M^* - 2 < M(R) < M^*$. The black hole mass of the quasar are poorly correlated with the total luminosity of the host galaxy. A significant correlation is found with the bulge luminosity of the host (Falomo et al. 2014).

We obtained so far optical spectroscopy of ∼30 companion galaxies to low redshift QSO. The companion galaxies were selected for being at a projected distance < 100 kpc from the QSO. These close companion galaxies are often (more than 50% of those investigated till now) associated to the QSO. In spite of that the star formation rate of the companion galaxies, as derived from [O II] 3727 line luminosity appears modest (on average ∼1 $M_{\odot} yr^{-1}$). In Fig 1 we show some examples of QSO environment and of the spectra o the associated galaxies.

References

Bettoni, D., Falomo, R., Kotilainen, J. K., Karhunen, K., & Uslenghi, M. 2015, *MNRAS*, 454, 4103

Bettoni, D., Falomo, R., Kotilainen, J. K., & Karhunen, K.2017 *MNRAS*, 466, 3600

Coldwell, G. V., & Lambas, D. G. 2006, *MNRAS*, 371, 786

Falomo, R. Bettoni,D., Karhunen,K, Kotilainen, J. K., & Uslenghi, M. 2014 *MNRAS*, 440 476

Karhunen, K, Kotilainen, K., Falomo, R., & Bettoni, D. 2014 *MNRAS*, 441 1802

Marziani, P., D'Onofrio, M., Bettoni, D. Poggianti, B. M., Moretti, A., Fasano, G., Fritz, J., Cava, A., Varela, J., & Omizzolo, A. *A&A*, 599A, 83

Matsuoka, Y., Strauss, M. A., Price, T. N., III, & DiDonato, M. S. 2014 *ApJ*, 780, 162

Shanks, T., Boyle, B. J., & Peterson, B. A. 1988, *ASP Conf. Ser. Vol. 2,The Spatial Clustering of QSOs. Astron. Soc. Pac., San Francisco*, 244

Astronomy in Focus, Volume 1
XXXth IAU General Assembly, August 2018
Volker Beckmann & Claudio Ricci, eds.

DOI: 00.0000/X000000000000000X

Multiwavelength intraday variability: what do the studies tell us about blazar jets?

Gopal Bhatta[1]

[1]Astronomical Observatory of the Jagiellonian University,
ul. Orla 171, 30-244 Kraków, Poland
email: gopal@oa.uj.pl

Abstract. In this presentation, we report the results of intraday variability in the optical (BVRI bands) and hard X-ray band (3-79 keV) in a number of blazars. In the optical microvariability studies of the blazars S5 0716+714 and BL Lac, we observed many interesting features such as rapid variability, large variability amplitude, presence of characteristic timescales, bluer-when-brighter achromatic behavior, and single power-law power spectral density. In *NuSTAR* observations of several blazars, using spectral and timing analysis, we found similar features consistent with the optical studies. In addition, in BL Lacs we estimated the Lorentz factor of the population of highest energy electrons emitting synchrotron emission, and whereas in flat-spectrum radio quasars, using external Compton models, we estimated the energy of the lower end of the injected electrons to be a few tens of Lorentz factors. In addition, we find that the low flux state exhibit more rapid variability in contrast to the previously reported results showing high flux states displaying rapid variability. In both the studies, the size of the emission regions estimated using variability timescales turn out to be an order magnitude smaller than the gravitational radius of a typical black-hole masses between $\sim 10^8 - 10^9$ solar masses, believed to be at the center of the radio-loud AGN. The results of the studies suggest that these low-amplitude rapid variability might originate as a result of magnetohydrodynamical instabilities near the base of the jets triggered by the processes modulated by the magnetic field at accretion disc.

Keywords. Galaxies: active, galaxies: jets, BL Lacertae objects: general, radiation mechanisms: nonthermal: methods: statistical

1. Introduction

Blazars are the radio-loud active galactic nuclei (AGN) that have relativistic jets, beamed upon us, producing non-thermal emission covering a wide electromagnetic spectrum - from radio to most energetic γ-rays. The broadband emission possesses a double-peaked feature in the frequency-flux plane. The lower peak, lying between the radio and the X-ray, is associated with the synchrotron emission by the energetic particles accelerating in the jet magnetic field; whereas the high frequency peak, mostly lying between UV to γ-ray, is believed due to inverse-Compton scattering of low-frequency photons by high-energy particles. Blazars consist of flat-spectrum radio quasars (FSRQ) and BL Lacertae (BL Lac) objects. FSQRs, the more powerful sources that show emission lines over the continuum, have the synchrotron peaks in the lower part of the spectrum; and BL Lacs, the less powerful ones which show weak or no emission lines, have their synchrotron peaks in the higher part of the spectrum. Blazars display variability on diverse timescales ranging from a few minutes to decades. In particular, low amplitude intraday variability, most likely originating at the innermost blazar regions, are central to understanding of blazar physical processes in the vicinity of supermassive black holes in AGN.

2. Intraday variability studies

Over past several years, we closely studied several blazar including S5 716+715, BL Lac and Mrk 501. In particular, we studied S5 716+715 in two WEBT campaigns using photo polarimetric observations (see Bhatta et al. 2013, Bhatta et al. 2015 and Bhatta et al. 2016b); and similarly we investigated blazar BL Lac with multi-band observations for several nights (Bhatta & Webb 2018). In addition, several blazars from the *NuSTAR* data archive were studied (see Bhatta et al. 2018). The studied were conducted with an aim to characterize the flux and spectral variability in blazar in hour-like timescales. In particular, we searched for characteristic timescales, including minimum variability timescales, employing a number of time series methods e.g., power spectral density (PSD), structure function and auto-correlation function. Furthermore, the spectral analysis were carried out exploring intra-day spectral evolution and flux spectra correlation. In hard X-ray observations we studied spectral fitting and evolution of hardness ratio. Besides, multi-band cross-correlations were explored.

3. Conclusion

The optical studies revealed that the statistical nature of the intra-day variability can be characterized by a single power-law PSD in the Fourier space; and that the multi-band observations are strongly correlated with an occasional lead/lag of a few tens of minutes between the wave bands. The results suggests that rapid variability most likely originates in highly magnetized compact substructure of the blazar jets, and the rapid particle acceleration and cooling mechanisms can be associated with either *shock-in-jet* model or magnetic reconnection in turbulent jets. From the distribution of the emission sizes derived from the minimum timescales, we found that some of the emission regions were smaller than the gravitational radius (r_g) of an AGN with a typical black hole mass of $\sim 10^9$ $M_\odot$. This can be possible either if the flux modulations occur at a fraction of the entire black hole region or in the scenario where the fluctuations reflect small-scale magnetohydrodynamic instabilities with the turbulent structures moving relativistically in random directions. Alternatively, high bulk Lorentz factors (e.g., $\Gamma \sim 100$) associated with the emitting regions, such as in *jets-in-a-jet* model, can make the size of these regions appear comparable to r_g. In BL Lacs, hard X-ray emission might represent the synchrotron emission from the high energy tail of the power-law distribution of the electrons. In such a case, the Lorentz factors for the highest energy electrons can be constrained as $\sim 10^6$, and the variability timescales can be directly linked to the particle acceleration and cooling timescales. Whereas in FSRQs, the emission could be result of the inverse-Compton of the circum nuclear photon field (e.g. from dusty torus and broad-line region) by the low energy end of the distribution. In such a scenario, the energy of the particle turns out to be a few tens of Lorentz factors.

We acknowledge the financial support by the Polish National Science Centre through the grants UMO-2017/26/D/ST9/01178 and 2018/09/B/ST9/02004

References

Bhatta, G., Mohorian, M., &, Bilinsky, I., 2018, *A&A* in press, (arXiv:1710.09910v2)
Bhatta, G., & Webb, J. 2018, *Galaxies*, 6, 2
Bhatta, G., Stawarz, Ł., Ostrowski, M., et al. 2016b, *ApJ*, 831, 92
Bhatta, G., Goyal, A., Ostrowski, M., et al. 2015, *ApJL*, 809, L27
Bhatta, G., Webb, J. R., Hollingsworth, H., et. al. 2013, A&A, 558A, 92B

Astronomy in Focus, Volume 1
XXXth IAU General Assembly, August 2018
Volker Beckmann & Claudio Ricci, eds.

DOI: 00.0000/X000000000000000X

Extreme jet distortions in low-z radio galaxies

Mark Birkinshaw[1] Josie Rawes[2] and Diana Worrall[3]

[1]HH Wills Physics Laboratory, University of Bristol,
Tyndall Avenue, Bristol BS8 1TL, U.K.
email: Mark.Birkinshaw@bristol.ac.uk

[2]HH Wills Physics Laboratory, University of Bristol,
Tyndall Avenue, Bristol BS8 1TL, U.K.
email: J.Rawes@bristol.ac.uk

[3]HH Wills Physics Laboratory, University of Bristol,
Tyndall Avenue, Bristol BS8 1TL, U.K.
email: D.Worrall@bristol.ac.uk

Abstract. Jets often display bends and knots at which the flows change character. Extreme distortions have implications for the nature of jet flows and their interactions. We present the results of three radio mapping campaigns. The distortion of 3CRR radio galaxy NGC 7385 is caused by a collision with a foreground magnetised gas cloud which causes Faraday rotation and free-free absorption, and is triggered into star formation. For NGC 6109 the distortion is more extreme, creating a ring-shaped structure, but no deflector can be identified in cold or hot gas. Similar distortions in NGC 7016 are apparently associated with an X-ray gas cavity, and the adjacent NGC 7018 shows filaments drawn out beyond 100 kpc. Encounters with substructures in low-density, magnetised, intergalactic gas are likely causes of many of these features.

Keywords. Galaxies:active, galaxies:jets, radio continuum:galaxies, intergalactic medium

1. NGC 7385

NGC 7385 is radio-bright and a member of the complete 3CRR sample (Laing, Riley & Longair 1983) despite failing to be in the 3C catalogue because of its low redshift ($z = 0.0243$) and consequent large angular size. In low-resolution radio maps (e.g., Schilizzi & Ekers 1975) NGC 7385 appears as a radio trail source, with two distinct tails appearing about 300 kpc southwest of the core. The higher-resolution study by Simkin & Ekers (1979) found that the northeastern side of the source encounters an optically-bright, line-emitting cloud about 10 kpc from the nucleus of NGC 7385. The radio structure seems to disrupt at this point.

We have undertaken new radio, optical, and X-ray imaging of NGC 7385. An L-band radio map constructed from archival VLA data is shown in Fig. 1 superimposed on a galaxy-subtracted HST image (Rawes, Worrall & Birkinshaw 2015). The main jet extends to the southwest and is seen in the optical and X-ray in its inner regions. The wide bandwidth of our new data (Rawes, Worrall & Birkinshaw 2018b), allows spectral indices and Faraday rotation to be mapped at high angular resolution. Prominent features are associated with the gas cloud, showing that it lies on the near side of the counter-jet plume. The free-free optical depth and rotation measure through the cloud can be reconciled with a gas density of about 5 cm^{-3} and a magnetic field of order 1 μG provided that the cloud is strongly clumped.

The strength of the cloud/counter-jet interaction causes the flow to turn through about 180 degrees, with the expanded, post-encounter, flow running back almost along the

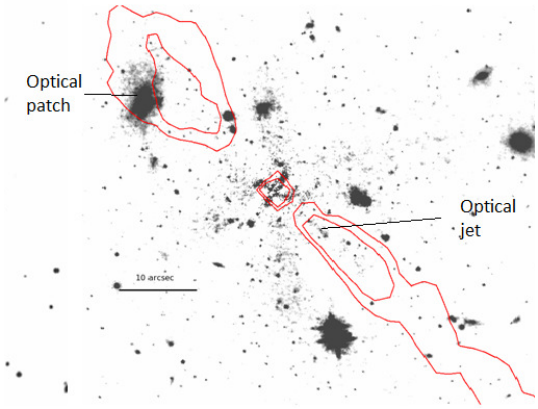

Figure 1. The centre of NGC 7385. At $z = 0.0243$ 10 arcsec corresponds to a projected scale of 4.9 kpc. Galaxy-subtracted HST F160W image with superimposed radio contours, from Rawes, Worrall & Birkinshaw (2015). An optical/X-ray jet extends southwest from the core. To the northeast the counter-jet is deflected and disrupted by the optical patch of Simkin & Ekers (1979), but retains enough integrity to flow back behind the main jet. We detect free-free absorption and Faraday rotation from the optical patch (Rawes, Birkinshaw & Worrall 2018b).

projected main jet, so that low-resolution maps show only a one-sided flow until different environmental conditions cause the projected structure to separate into two tails. This is likely due to gas flows and substructures on 100-kpc scales in the intergalactic medium of Zwicky cluster Zw 2247.3+1107, of which NGC 7385 is a member.

A high signal/noise IFU study of the cloud interaction might provide information about the momentum flux down the jet, and so potentially the jet composition, in the same way as has been possible for other jet/cloud interactions (e.g., PKS 2152-699; Worrall et al. 2012, Smith et al. 2018). While such interactions are rare, they can provide the kinematic information that cannot be obtained from jet synchrotron (or synchrotron plus inverse-Compton) emission alone.

2. NGC 6109

NGC 6109, another neglected member of the 3CRR sample, exhibits a striking example of a radio ring. This low-redshift ($z = 0.0296$) galaxy appears, at low angular resolution, to be a radio trail source. O'Dea & Owen (1985) remarked that the source exhibited a small circular component to one side of the core, and a long tail to the other, and noted that this might indicate that the jet on one side was stopped by external gas, to create an FR II-like lobe, while it was drawn out into a long tail on the other.

Our high-resolution radio map (Fig. 2), shows that the southeastern feature is not a lobe but a circular loop (Rawes, Birkinshaw & Worrall 2018a). No excess or deficit of X-ray emission is seen in the neighbourhood of the loop, and there is no optical or infra-red emission, so the mechanism causing the loop is not like the interaction in NGC 7385.

The brightness contrast between the jet and counter-jet on sub-kpc scales can be interpreted in terms of a relativistic Doppler factor that associates the loop with the jet brightening 12-24 arcsec northwest of the core, so that both could arise from a single event in the AGN. However, relativistic flow and simple precession models cannot explain the structure: there must be asymmetrical acceleration/deceleration of the jet/counter-jet flow by the external medium. Although *Chandra* imaging shows little structured gas in the neighbourhood of NGC 6109, the galaxy is embedded in the large-scale atmosphere of a poor cluster, and our new polarisation data shows a Faraday rotation feature across

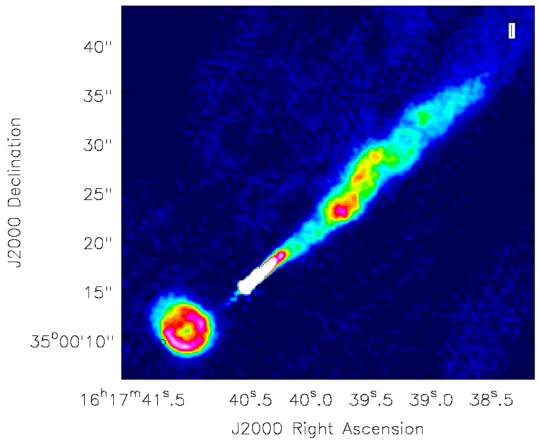

Figure 2. The centre of NGC 6109. At $z = 0.0296$ 5 arcsec corresponds to a projected scale of 3.0 kpc. S-band radio surface brightness image from Rawes, Worrall & Birkinshaw (2018a). The main jet extends northwest of the core for about 5 arcsec before fading, and then re-brightening in a less collinear structure 12-24 arcsec from the core. The counter-jet is faintly detected to about 5 arcsec, then develops a bright loop structure with radius 5 arcsec that lies outside the flattened X-ray emitting atmosphere detected by *Chandra*.

the loop that could suggest interaction with a magnetic substructure such as a galactic wake in the intracluster medium.

3. Abell 3744

NGC 7016 and 7018 lie in Abell 3744, a moderately rich ($kT \approx 3$ keV) cluster of galaxies at $z = 0.0381$. Both galaxies host bright radio sources. The heating effects of the sources should combine to cause significant changes in the intracluster medium. Strong temperature and density structures are, indeed, seen across the cluster though these may be a consequence of a merger (Worrall & Birkinshaw 2014). Both radio sources are highly distorted (Cameron 1988; Bicknell, Cameron & Gingold 1990; Fig. 3), confirming that their interactions with the intracluster medium are strong.

The brightest parts of NGC 7018 show it to be of FR II character, with prominent hot spots at the ends of the lobes, a compact core, and a jet extending from the core towards the NE hot spot. Faint filamentary structures extend from both lobes and lie *around* a prominent cavity in the cluster's X-ray emission (Worrall & Birkinshaw 2014). One filament, < 2 kpc in diameter, can be traced to > 150 kpc, where it seems to end in a faint radio source that might have punctured one lobe of NGC 7018 (Birkinshaw, Worrall & Rawes 2018).

NGC 7016 shows a bent, twin-sided, FR I structure in its inner parts. However, to the north the jet appears to reverse direction and expand, and then to create a radio ring (Worrall & Birkinshaw 2014), before disrupting into a faint array of radio filaments and flowing back parallel to the southern jet (Birkinshaw, Worrall & Rawes 2018). This is seen as a broad structure around the jet in low-resolution maps. The sequence of structures, with the ring downstream of the reversal, might indicate that the reversal is a younger version of the ring, and will develop into a full ring in a few Myr.

The X-ray cavity would collapse rapidly without internal pressure support. This can arise from the repository of electrons within the cavity that produce the diffuse radio emission mapped by Cameron (1988). The irregular X-ray structure suggests that

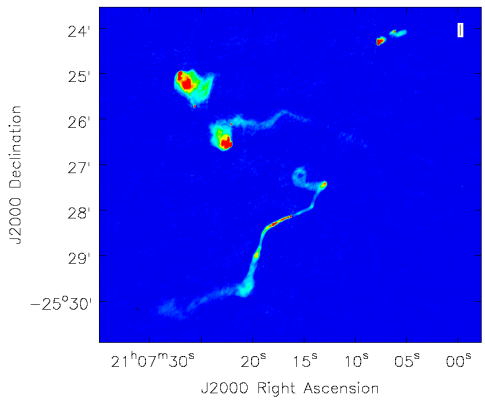

Figure 3. Abell 3744 from Birkinshaw, Worrall & Rawes (2018). At $z = 0.0381$ 5 arcmin corresponds to a projected scale of 230 kpc. The image is dominated by NGC 7016 to the southwest and NGC 7018 to the notheast. An unusual (background?) radio source lies to the northeast.

Abell 3744 is dynamically young (Worrall & Birkinshaw 2014), so that rapid gas motions are likely and could cause some of the radio distortions, though the ring and reversal features seem surprisingly compact unless they are short-lived.

4. Generalisation

The extreme distortions in Figs. 1−3 were detected in arcsec-resolution, high dynamic-range, low-frequency mapping. High resolution is necessary, even at low redshift, to detect the kpc-scale substructures we are reporting. Extreme distortions cannot be rare, since we have two examples (NGC 6109 and NGC 7385) in the low-redshift 3CRR sample of only 35 radio galaxies, so the SKA should find many such structures in the future, as its sub-arcsec capabilities reveal them at redshifts beyond $z = 1$.

While some distortions arise from interactions with optically-emitting gas, where there is the potential for obtaining important dynamical information about the jet flows (e.g., NGC 7385, PKS 2152-699), sometimes there is no clear deflecting gas (NGC 7016, NGC 6109). The evolution of dynamical activity in clusters and groups around low-thrust radio sources could be studied by future radio mapping.

References

Bicknell, G. V., Cameron, R. A., & Gingold, R. A. 1990, *ApJ*, 357, 373
Birkinshaw, M., Worrall, D. M., & Rawes, J. 2018, in preparation
Cameron, R. A. 1988, PhD thesis, ANU
Laing, R. A., Riley, J. M., & Longair, M. S. 1979, *MNRAS*, 204, 151
O'Dea, C., & Owen, F. 1985, *AJ*, 90, 927
Rawes, J., Worrall, D. M., & Birkinshaw, M. 2015, *MNRAS*, 452, 3064
Rawes, J., Birkinshaw, M., & Worrall, D. M. 2018a, *MNRAS*, 480, 3644
Rawes, J., Birkinshaw, M., & Worrall, D. M. 2018b, *MNRAS*, in preparation
Schilizzi, R., & Ekers, R. 1975, *A&A*, 40, 221
Simkin, S. M., & Ekers, R. D. 1979, *AJ*, 84, 56
Smith, D. P., Young, A. J., Worrall, D. M. & Birkinshaw, M. 2018, *MNRAS*, submitted
Worrall, D. M., & Birkinshaw, M. 2014, *ApJ*, 784, 36
Worrall, D. M., Birkinshaw, M., Young, A. J, et al. 2012, *MNRAS*, 424, 1346

Astronomy in Focus, Volume 1
XXXth IAU General Assembly, August 2018
Volker Beckmann & Claudio Ricci, eds.

DOI: 00.0000/X000000000000000X

OJ287: stationary jet components following precession & nutation

Silke Britzen,[1] C. Fendt,[2] G. Witzel,[1] S.-J. Qian,[4] I.N. Pashchenko,[5] O. Kurtanidze,[6,7] M. Zajacek,[1,8,10] G. Martinez,[3] V. Karas,[8] M. Aller,[9] H. Aller,[9] A. Eckart,[10,1] K. Nilsson,[11] P. Arévalo,[12] J. Cuadra,[13] M. Subroweit,[10] and A. Witzel[1]

[1]Max-Planck-Institut für Radioastronomie, Auf dem Hügel 69, 53121 Bonn, Germany
email: sbritzen@mpifr.de

[2]MPI for Astronomy, Heidelberg, Germany

[3]UCLA, Department of Physics and Astronomy, LA, CA 90095, USA

[4]National Astronomical Observatories, Chinese Academy of Sciences, Beijing 100012, China

[5]Astro Space Center, Lebedev Physical Institute, Russian Academy of Sciences

[6]Abastumani Observatory, Mt Kanobili, 0301 Abastumani, Georgia

[7]Engelhardt Astronomical Observatory, Kazan Federal University, Tatarstan, Russia

[8]Astronomical Institute, Academy of Sciences, Boční II 1401, CZ-14131 Prague, Czech Republic

[9]University of Michigan, Ann Arbor, MI 48109, USA

[10]I. Physikalisches Institut der Universität zu Köln, Zülpicher Str. 77, 50937 Köln, Germany

[11]Tuorla Observatory, Department of Physics and Astronomy, University of Turku, 20500, Turku, Finland

[12]Instituto de Física y Astronomía, Facultad de Ciencias, Universidad de Valparaíso, Gran Bretaña No. 1111, Playa Ancha, 2360102 Valparaíso, Chile

[13]Instituto de Astrofísica, Pontificia Universidad Católica de Chile, 782-0436 Santiago, Chile

Abstract. Recently, we proposed that the pc-scale radio jet motion of OJ287 (between Apr. 1995 and Apr. 2017) is consistent with a jet source that is precessing and nutating. In addition to the jet components moving with apparent superluminal speeds, the OJ287 jet also reveals jet components which remain at similar core separations over time. This phenomenon has been observed before in other AGN jets but the nature of such stationary features remained unclear. We show that the stationary features move in fact perpendicular to the jet axis. The apparent rotation of the jet axis can be explained by precession. On top of the precession we find an additional motion that could be explained by a nutation of the jet axis. Strikingly, our results yield a very similar scaling for the time scales of precession and nutation compared to what is indicated for the microquasar SS 433 - with a factor of roughly 50 times longer for OJ287.

Keywords. techniques: interferometric, galaxies: jets, BL Lacertae objects: individual (OJ 287)

1. Summary

The low synchrotron peaked BL Lac object OJ287 (z=0.306, Stickel et al. (1989)) and "Rosetta stone of blazars" (Takalo (1994)) has been studied by many authors. The light-curve in the optical V-band observed since 1890 for this object (Sillanpää et al. (1988)) has revealed repeated outbursts at ∼11.65 yr intervals. Sillanpää et al. (1988) proposed OJ287 to be a supermassive binary black hole (SMBBH) with an orbital period of 9 yr (in the rest frame of OJ287). Further works by Lehto & Valtonen (1996), Valtonen & Wiik (2012), and Valtonen et al. (2016) have explored the binary BH nature of this AGN,

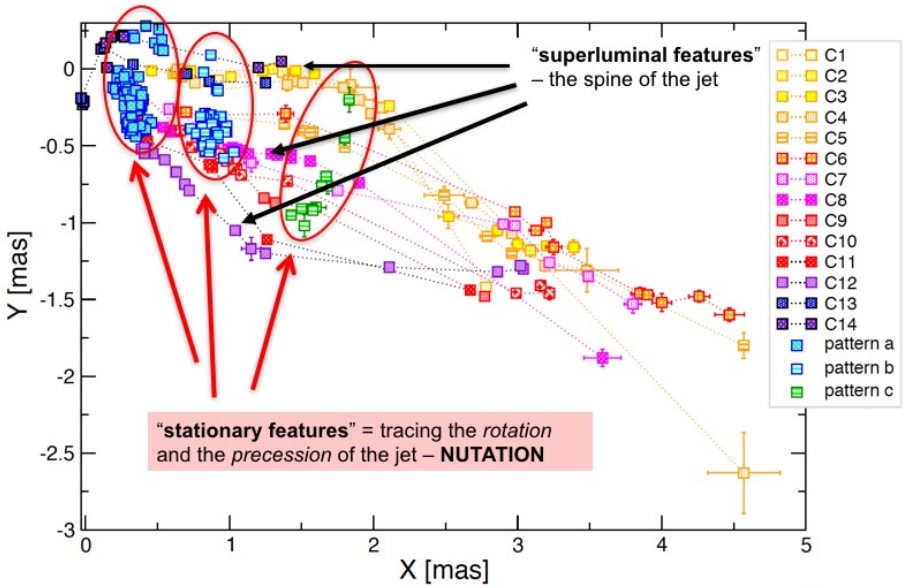

Figure 1. Jet component motion in the pc-scale jet of OJ287 (Britzen et al. (2018)). Yellow to indigo indicate the paths of the superluminal features (black arrows). The blue and green squares indicate the positions and paths of the "stationary" features (red arrows, encircled in red).

in particular possible disturbances of the accretion disc caused by a plunging secondary BH.

In Britzen et al. (2018) we investigated 120 VLBA observations (15 GHz) to search for influences of the plunging black hole on the jet and to test the stability of the jet. As a result we find that the jet is remarkably stable. Despite several claims, the jet is not wobbling in an erratic way, but, instead, reveals a smooth and continuous motion in the plane of the sky. The jet is precessing on a time-scale of about 22yr. This precession is deduced from the motion observed for twelve jet components at apparent superluminal speeds moving along a precession cone.

Superposed to this long time-scale motion, the jet axis seems to be rotating on an additional shorter time-scale. It is this additional jet axis rotation which we trace by the "stationary" components. Their motion is perpendicular to the jet axis and occurs on a time-scale of about one year. In Britzen et al. (2018) we show that the "stationary" components in BL Lac objects reveal a motion perpendicular to the jet axis (Fig. 1). In the case of OJ287 this kind of motion is most likely produced by a combination of precession and nutation. The jet precession and nutation as deduced from both the jet component motion and their "stationary" location along the jet eventually causes and thus explains the variability in the radio flux. The latter can be explained by Doppler beaming due to a change in the viewing angle during precession and nutation. The radio variability on long time scales ($\sim$ two decades) can best be explained and modeled via jet precession, whereas the short term variability on timescales of a year can best be explained and modeled by jet nutation.

References

Britzen, S., Fendt, C., Witzel, G., Qian, S.-J., et al. 2018, *MNRAS*, 478, 3199
Lehto H.J., & Valtonen M.J. 1996, *ApJ*, 460, 207
Sillanpää A., Haarala S., Valtonen M.J., et al., 1988, *ApJ*, 325, 628
Stickel, M., Fried, J.W., & Kühr, H. 1989, *A&AS*, 80, 103
Takalo L. 1994, *Vistas in Astronomy*, 38, 77
Valtonen M.J., & Wiik K. 2012, *MNRAS*, 421, 1861
Valtonen M.J., Zola S., Ciprini S., et al. 2016, *ApJL*, 819, L37

Astronomy in Focus, Volume 1
XXXth IAU General Assembly, August 2018
Volker Beckmann & Claudio Ricci, eds.

DOI: 00.0000/X000000000000000X

Probing restarting activity in hard X-ray selected giant radio galaxies

G. Bruni[1]†, F. Ursini[2], F. Panessa[1], L. Bassani[2], A. Bazzano[1], A. J. Bird[3], E. Chiaraluce[1], D. Dallacasa[4,5], M. Fiocchi[1], M. Giroletti[5], L. Hernández-García[6], A. Malizia[2], M. Molina[2], L. Saripalli[7], P. Ubertini[1], and T. Venturi[5]

[1]INAF - Istituto di Astrofisica e Planetologia Spaziali
via del Fosso del Cavaliere 100, 00133 Roma, Italy
email: gabriele.bruni@inaf.it

[2]INAF - Osservatorio di Astrofisica e Scienza dello Spazio
via Piero Gobetti 93/3, 40129 Bologna, Italy
email: francesco.ursini@inaf.it

[3]School of Physics and Astronomy, University of Southampton, SO17 1BJ, UK

[4]DIFA - Dipartimento di Fisica e Astronomia
Università di Bologna, via Gobetti 93/2, 40129 Bologna, Italy

[5]INAF - Istituto di Radioastronomia, via Piero Gobetti 101, 40129 Bologna, Italy

[6]IFA - Instituto de Física y Astronomía
Universidad de Valparaíso, Gran Bretaña 1111, Playa Ancha, Valparaíso, Chile

[7]Raman Research Institute, C. V. Raman Avenue, Sadashivanagar, Bangalore 560080, India

Abstract.
With their sizes larger than 0.7 Mpc, Giant Radio Galaxies (GRGs) are the largest individual objects in the Universe. To date, the reason why they reach such enormous extensions is still unclear. One of the proposed scenarios suggests that they are the result of multiple episodes of jet activity. Cross-correlating the INTEGRAL+Swift AGN population with radio catalogues (NVSS, FIRST, SUMSS), we found that 22% of the sources are GRG (a factor four higher than those selected from radio catalogues). Remarkably, 80% of the sample shows signs of restarting radio activity. The X-ray properties are consistent with this scenario, the sources being in a high-accretion, high-luminosity state with respect to the previous activity responsible for the radio lobes.

Keywords. galaxies: active, galaxies: evolution, galaxies: jets, radio continuum: galaxies, X-rays: galaxies

1. Introduction

A relatively small fraction of powerful radio galaxies (∼6% in the 3CR catalogue, Ishwara-Chandra & Saikia 1999) exhibits rather large linear extents, i.e. above 0.7 Mpc, making them the largest individual objects in the Universe. These sources are usually referred to as Giant Radio Galaxies (GRG), and can exhibit both Fanaroff-Riley type I and type II radio galaxies (FRI and FRII respectively, Fanaroff & Riley 1974). While FRI GRGs are associated with early type galaxies, those with FRII morphology are hosted both in early type galaxies and quasars. The samples of GRGs available in the literature, mainly drawn from all sky radio surveys such as NVSS, SUMSS, WENSS, have been used to test models for radio galaxy evolution and investigate the origin of

† website: http://gral.iaps.inaf.it

such incredibly extended structures (i.e. Blundell et al. 1999). Despite the dynamical ages typically overestimate the radiative age of the radio source by a factor 2-4 (see Fig. 5 in Parma et al. 1999), the general correlation observed between size and age in radio galaxies (Fig. 6 in Parma et al. 1999) suggests that GRGs represent the oldest tail of the age distribution for radio galaxies. Beyond the source age, the main intrinsic parameters that allow a radio galaxy to reach a linear size of the order of a Mpc during its lifetime are still unclear. The medium must play a role in the overall jet expansion, but its effects remains difficult to evaluate, not to mention that the density of the medium explored by the radio jet during its life/development may change considerably over the large scales considered here. Some GRGs are associated with the dominant member of a galaxy group (e.g. the FRI-GRG NGC 315, Giacintucci et al. 2011), while others have been detected at high redshift in a likely less dense environment (Machalski et al. 2004). Those authors also concluded that the jet power and the central density of the galaxy nucleus seem to correlate with the size of radio galaxies. Yet another study, based on optical spectroscopy of galaxies in a large-scale environment around the hosts of 19 GRGs (Malarecki et al. 2004) finds a tendency for their lobes to grow to giant sizes in directions that avoid dense galaxy on both small and large scales. Finally, other authors suggested that GRG could reach their size thanks to more than one activity episode, being restarting radio sources (Subrahmanyan et al. 1996). More recently, progress in the study of this class of sources has been achieved thanks to the use of low frequency facilities - such as LOFAR, JVLA and GMRT - where old relativistic plasma is better seen (e.g. Orrù et al. 2010; Clarke et al. 2017; Sebastian et al. 2018). All in all, however, the origin and evolution of GRGs remains until now very much unconstrained.

2. Hints of restarting activity

Starting from 2002, the hard X-ray and γ-ray sky has been surveyed by *INTEGRAL*/IBIS and *Swift*/BAT in the spectral range from 10-200 keV. Up to now many catalogues have been released, the most recent ones comprising more than 1000 high energy sources (Bird et al. 2016; Oh et al. 2018), with a large fraction of objects unambiguously associated with AGN. Our group is carrying out a multi-wavelength study of a sample of hard X-ray selected GRG extracted from these high energy catalogues. Bassani et al. (2016) undertook a radio/γ-ray study of the combined *INTEGRAL*+*Swift* AGN populations, and found 64 sources associated with extended radio galaxies with measured redshift. They belong to both the FRI and FRII morphological classes. Interestingly, inspection of NVSS and SUMSS revealed that 14 of them are GRG, i.e. $\sim$22% of the sample. Considered the classical fraction of giant sources in radio-selected samples of radio galaxies (1-6%), this fraction is impressive, and suggests a tight link between the nuclear/accretion properties of the AGN and the radio source size.

In order to better characterize the GRG in this sample and to study their evolutionary history, we are collecting multi-band high sensitivity observations for the fraction of sample observable from the Northern hemisphere (12 targets). Remarkably, 10 over 12 sources ($\sim$80%) of the sample show signs of restarting radio activity from previous studies in the literature or our radio campaign (Bruni et al. 2018), with one even showing an extreme reorientation from radio-galaxy to BL Lac (Hernández-García et al. 2017). This large fraction suggests that multiple radio phases could justify the large size, and be responsible for the strong hard X-ray emission coming from a possible refueled radio core - as suggested from X-ray data (Ursini et al. 2018). Our aim is to confirm the restarting activity for these sources, and possibly understand whether this scenario is a distinctive property of hard X-ray selected GRGs, or rather a general property of GRGs. In 2014,

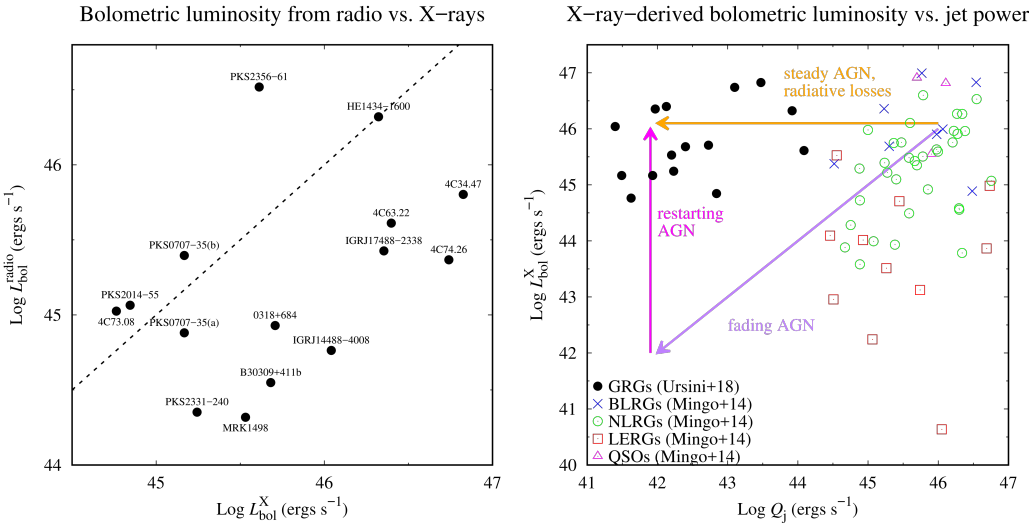

Figure 1. *Left panel:* Bolometric luminosity estimated from the radio luminosity of the lobes versus that estimated from the 2–10 keV luminosity. The dashed line represents the identity $y = x$. *Right panel:* Bolometric luminosity estimated from the 2–10 keV luminosity versus jet power estimated from the relation of Willott et al. (1999). Black dots denote the GRGs of our sample, overlayed in the plot of Mingo et al. (2014). The colored arrows represent two putative evolutionary paths of radio galaxies. Both panels are adapted from Ursini et al. (2018).

we have collected GMRT deep observations at 325 and 610 MHz for a pilot sample of 4 sources from our GRG sample. Those GMRT data allowed our group to identify the second known giant X-shaped radio galaxy (IGR J14488-4008: Molina et al. 2015), and a newly discovered GRG (IGR J17488-2338: Molina et al. 2014).

3. X-ray properties

The bulk of the X-ray emission of GRGs in our sample is consistent with originating from a Comptonizing corona coupled to a radiatively efficient accretion flow (Eddington ratio > 0.02) (Ursini et al. 2018), like in normal-size FR II radio galaxies. This indicates that the nuclei are currently active, despite the likely old age of the radio lobes. The peculiar morphology makes it possible to study the relation between the X-ray emission and the radio emission in detail, separating the contribution from the core and from the lobes. We find that:

- The X-ray luminosity $L_{2-10\rm keV}$ correlates with the radio core luminosity $L_{1.4\rm GHz}^{\rm core}$, as expected from the so-called fundamental plane of black hole activity (Merloni et al. 2003). The slope of the correlation is consistent with the 'radiatively efficient' branch of the fundamental plane rather than the 'standard/inefficient' branch (Coriat et al. 2011).

- In most sources, the X-ray luminosity yields an estimate of the bolometric luminosity ($L_{\rm bol}^{\rm X}$) an order of magnitude larger than the corresponding estimate from the radio lobes luminosity ($L_{\rm bol}^{\rm radio}$), from the relation of van Velzen et al. (2015) (Fig. 1, left panel).

- The time-averaged kinetic power of the jets, as estimated from the radio luminosity using the relation of Willot et al. (1999), is much lower than in the radio luminous AGNs studied by Mingo et al. (2014). This discrepancy is up to 3 orders of magnitude, while the bolometric luminosity is perfectly consistent with high-excitation radio galaxies (Fig. 1, right panel).

These results are consistent with a restarting activity scenario, i.e. the sources are currently highly accreting and in a high-luminosity state compared with the past activity that produced the old and extended radio lobes. GRGs could start their life with high nuclear luminosities and high jet powers; with time, the central engine gradually fades while the radio lobes expand. Eventually, the nuclear activity can be triggered again following a new accretion episode, resulting in a strong increase of the core luminosity. Alternatively, the nuclei would need to sustain a steady activity during their lifetime, with a nearly constant accretion rate and core luminosity; radiative losses would produce the observed dimming of the radio lobes as they grow in size and interact with the environment. In this case, however, the nuclei are required to stay active for at least 100–250 Myrs (Machalski et al. 2004).

4. Future work

Triggered by these results, we are collecting more data both in radio and X-ray bands, in order to connect the nuclear accretion status to the Mpc-scale structure of these objects. The cores have been observed in single-dish mode (Effelsberg-100m telescope) in June 2018, with the aim of reconstructing the radio SED and test the fraction of young radio components. In the X-ray band, a *Swift*/XRT campaign has been planned to build a complete comparison sample of radio-selected GRG (Schoenmakers et al. 2000), and highlight the different properties with respect to the hard X-ray selected ones. Indeed, radio selected GRGs are not necessarily X-ray bright, thus allowing us to explore new portions of the parameter space in luminosity-luminosity diagrams such as those in Fig. 1.

References

Bassani, L., Venturi, T., Molina, A. et al. 2016, *MNRAS*, 461, 3165
Bird, A. J., Bazzano, A., Malizia, A. et al. 2016, *MNRAS*, *ApJS*, 223, 15
Blundell, K. M., Rawlings, S., & Willott, C. J. 1999, *AJ*, 117, 677
Bruni, G., Panessa, F., Bassani, G. et al. 2018, *MNRAS*, in prep.
Clarke, A.O., Heald, G., Jarrett, T. et al. 2017, *A&A*, 601, A25
Coriat M., Corbel, S., Prat, L. et al. 2011, *MNRAS*, 414, 677
Fanaroff, B. L. & Riley, J. M. 1974, *MNRAS*, 167, 31
Giacintucci, S., O'Sullivan, E., Vrtilek, J. et al. 2011, *ApJ*, 732, 95
Hernández-García, L., Panessa, F., Giroletti, M. et al. 2017, *A&A*, 603, A131
Ishwara-Chandra, C.H. & Saikia, D.J. 1999, *MNRAS*, 309, 100
Machalski, J., Chyzy, K. T. & Jamrozy, M. 2004, *Acta Astronomica*, 54, 249
Malarecki, J. M., Jones, D. H., Saripalli, L. et al. 2015, *MNRAS*, 449, 955
Merloni A., Heinz S., di Matteo T. et al. 2003, *MNRAS*, 345, 1057
Mingo, B., Hardcastle, M. J., Croston, J. H. et al. 2014, *MNRAS*, 440, 269
Molina, M., Bassani, L., Malizia, A. et al. 2014, *A&A*, 565, A2
Molina, M., Venturi, T., Malizia, A. et al. 2015, *MNRAS*, 451, 3
Oh, K., Koss, M., Markwardt, C.B. et al. 2018 *ApJS*, 234, 4
Orrù, E., Murgia, M., Feretti, L., et al. 2010, *A&A*, 515, A50
Parma, P., Murgia, M., Morganti, R. et al. 1999, *A&A*, 344, 7
Schoenmakers, A. P., Mack, K.-H., de Bruyn, A. G., et al. 2000, *A&AS*, 146, 293
Sebastian, B., Ishwara-Chandra, C. H., Joshi, R. et al. 2018, *MNRAS*, 473, 4
Subrahmanyan, R., Saripalli, L., Hunstead, R.W. 1996, *MNRAS* 279, 257
Ursini, F., Bassani, L., Panessa, F. et al. 2018, *MNRAS*, in press
van Velzen S., Falcke H., Körding E. et al. 2015, *MNRAS*, 446, 2985
Willott, C. J., Rawlings, S., Blundell, K. M. et al. 1999, *MNRAS*, 309, 1017

Astronomy in Focus, Volume 1
XXXth IAU General Assembly, August 2018
Volker Beckmann & Claudio Ricci, eds.

DOI: 00.0000/X000000000000000X

Thermal wind from low-luminosity active galactic nucleus

De-Fu Bu[1] and Xiao-Hong Yang[2]

[1]Key Laboratory for Research in Galaxies and Cosmology, Shanghai Astronomical Observatory, Chinese Academy of Sciences,
80 Nandan Road, Shanghai 200030, China
email: dfbu@shao.ac.cn

[2]Department of physics, Chongqing University,
Chongqing 400044, China
email: yangxh@cqu.edu.cn

Abstract. We carry out simulations of hot accretion flow at parsec scale irradiated by a low luminosity active galactic nucleus (LLAGN). The LLAGN emits X-ray photons. The Compton temperature of the X-ray photons is 10^8K. We find that due to the Compton heating by the central X-ray photons, the gas around Bondi radius can be heated up to temperature higher than Virial temperature. Gas can escape from the black hole gravitational potential to form wind. Wind can take away mass. Due to the presence of wind, the real black hole accretion rate can be significantly smaller than the Bondi rate.

Keywords. accretion, accretion discs, black hole physics, hydrodynamics, galaxies: active.

1. Introduction

Hot accretion flow operates in LLAGNs (e.g. Ho 2008; Qiao et al. 2013; Li & Xie 2017) and the hard/quiscient states of black hole X-ray binaries (Wu et al. 2013; Yuan & Narayan 2014). The properties of hot accretion flow have been studied intensively by numerical simulations (Tchekhovskoy et al. 2011; McKinney et al. 2012; Bu et al. 2016a, 2016b; Inayoshi et al. 2018).

The simulation works mentioned above focus on the flow very close to the black hole. The outer boundary of the simulation is several hundreds of Schwarzschild radius (r_s). The hot accretion flow at sub-parsec and parsec scales has not been studied. The sub-parsec and parsec accretion flow connects the flow in AGNs and the flow beyond Bondi radius. The feeding gas of the central black hole comes from this region. It is important to study the flow in this region.

In this paper, we set the black hole mass to be $10^8\,M_\odot$. Our computational domain covers a range from $500\,r_s$ to 10 pc. The mass accretion rate of the central black hole is calculated based on the accretion rate at the inner boundary (we refer to Bu & Yang 2018 for details). After obtaining the black hole accretion rate, we calculate the luminosity of the black hole. In this work, we study hot accretion flow. We take $2\%\,L_{Edd}$ (L_{Edd} is the Eddington luminosity) to be the upper limit of the luminosity of the central LLAGN. We assume the central LLAGN only emits X-ray photons. The Compton temperature of the photons is 10^8 K. The X-ray photons from the central LLAGN can Compton heating/cooling the accretion flow. In addition, we also take into account bremsstrahlung cooling, photoionization heating, and line and recombination cooling.

2. Thermal wind

When gas falls to the black hole, X-ray photons will be generated and the accretion flow will be heated by the X-ray irradiation. When the gas temperature is increased to be above the Virial value, a wind will be formed. Fig. 1 shows a snapshot of properties of the accretion flow. A wind forms in the region beyond the Compton and Bondi radius. The right panel of Fig. 1 shows the ratio between the thermal energy and the gravitational energy of the flow. It is clear that the thermal energy of the wind is larger than the gravitational energy. The wind is thermally driven and the Bernoulli parameter of the wind is positive and it can escape from the black hole's gravitational potential.

3. Implications

The thermal wind generated around the Bondi radius has a positive Bernoulli parameter. The wind can easily flow to the region outside Bondi radius and can interact with the interstellar medium. The wind may push away the interstellar medium, which may affect the star formation rate.

Due to the presence of the wind, the real black hole accretion rate is much smaller than the Bondi value (Yang & Bu 2018). In large scale cosmological simulations studying galaxy formation and evolution, the Bondi radius can at most be marginally resolved. In these simulations, the Bondi formula is usually used to estimate the black hole accretion rate. Our work shows that the real accretion rate is much smaller than the Bondi value. Therefore, in the future, calculating the real black hole accretion rate will have to take the described effects into account.

References

Bu, D., & Yang, X. 2018, *MNRAS*, 476, 4395
Bu, D., Yuan, F., Gan, Z., & Yang, X. 2016a, *ApJ*, 818, 83
Bu, D., Yuan, F., Gan, Z., & Yang, X. 2016b, *ApJ*, 823, 90
Ho, L. C. 2008, *ARA&A*, 46, 475
Inayoshi, K., Ostriker, J. P., Haiman, Z., & Kuiper, R. 2018, *MNRAS*, 476, 1412
Li, S., & Xie, F. 2017, *MNRAS*, 471, 2848
McKinney, J. C., Tchekhovskoy, A., & Blandford, R. 2012, *MNRAS*, 423, 3083
Qiao, E., Liu, B., Panessa, F., & Liu, J. 2013, *ApJ*, 777, 102
Tchekhovskoy, A., Narayan, R., & McKinney, J. C. 2011, *MNRAS*, 418, L79
Wu, Q., Cao, X., Ho, L. C., & Wang, D. 2013, *ApJ*, 770, 31
Yang, X., & Bu, D. 2018, *MNRAS*, 476, 954
Yuan, F., & Narayan, R. 2014, *ARA&A*, 52, 529

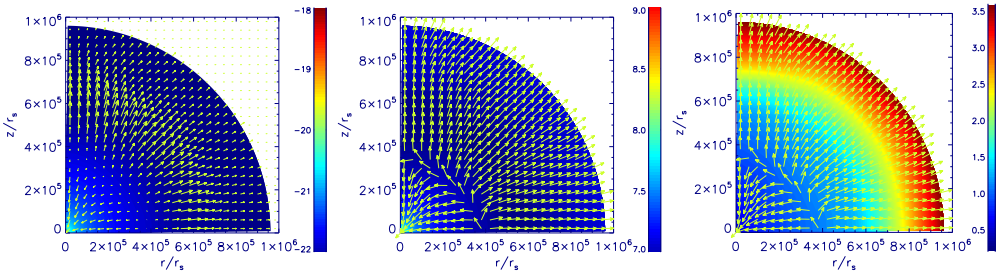

Figure 1. Snapshot of the accretion flow properties. Left: logarithm density (colour) overplotted by the poloidal velocity vector (arrows). Middle: logarithm temperature (colour) overplotted by the direction of the velocity vector. Right: the ratio of thermal energy to the gravitational energy.

Astronomy in Focus, Volume 1
XXXth IAU General Assembly, August 2018
Volker Beckmann & Claudio Ricci, eds.

DOI: 00.0000/X000000000000000X

Molecular gas in radio galaxies at $z = 0.4 - 2.6$ in (proto-)cluster environment

G. Castignani[1,2,3], F. Combes[2,3], P. Salomé[2], C. Benoist[4], M. Chiaberge[5,6], J. Freundlich[7], and G. De Zotti[8]

[1] Laboratoire d'astrophysique, École Polytechnique Fédérale de Lausanne (EPFL), Observatoire de Sauverny, 1290 Versoix, Switzerland
email: gianluca.castignani@epfl.ch

[2]Sorbonne Université, Observatoire de Paris, PSL, CNRS, LERMA, F-75014, Paris, France
[3]Collège de France, 11 Place Marcelin Berthelot, 75231 Paris, France
[4]Université Côte d'Azur, Observatoire de la Côte d'Azur, CNRS, Laboratoire Lagrange, Blvd de l'Observatoire, CS 34229, 06304 Nice cedex 4, France
[5]Space Telescope Science Institute, 3700 San Martin Dr., Baltimore, MD 21210, USA
[6]Johns Hopkins University, 3400 N. Charles Street, Baltimore, MD 21218, USA
[7]Centre for Astrophysics and Planetary Science, Racah Institute of Physics, The Hebrew University, Jerusalem 91904, Israel
[8]INAF-Osservatorio Astronomico di Padova, Vicolo dell'Osservatorio 5, I-35122 Padova, Italy

Abstract. We investigate the role of the environment in processing molecular gas in radio galaxies (RGs). We observed five RGs at $z = 0.4 - 2.6$ in dense Mpc-scale environment with the IRAM-30m telescope. We set four upper-limits and report a CO(7→6) detection for COSMOS-FRI 70 at $z = 2.63$, which is the most distant brightest cluster galaxy (BCG) candidate detected in CO. We speculate that the cluster environment might have played a role in preventing the refueling via environmental mechanisms such as galaxy harassment, strangulation, ram-pressure, or tidal stripping. The RGs of this work are excellent targets for ALMA as well as next generation telescopes such as the *James Webb Space Telescope.*

Keywords. Galaxies: active; Galaxies: clusters: general; Molecular data.

---

1. Introduction. Molecules in galaxies can help to trace star forming regions, even close to an active galactic nucleus (AGN, Omont 2007). Radio galaxies (RGs) are a precious tool to discover distant galaxy groups and (proto-)clusters at high-z, since they are often the brightest cluster galaxies (BCGs, Zirbel 1996).

We consider two RGs at $z = 0.39$ and 0.61 within the DES SN deep fields (DES collaboration 2015) and three additional COSMOS-FRI RGs from the Chiaberge et al. (2009) sample, at $z = 0.97$, 0.91, and 2.63. They have been selected since they show evidence of significant star formation, $\mathrm{SFR}_{24\mu m} \sim (20 - 250)\,\mathrm{M}_\odot/\mathrm{yr}$, based on their emission at $\sim 24\mu$m in the observer frame (WISE or Spitzer-MIPS). All five sources are found in (proto-)cluster candidates by using the Poisson Probability Method (PPM, Castignani et al. 2014ab) that searches for overdensities using photometric redshifts.

2. Methods and Results. We observed the five targets with the IRAM-30m telescope targeting several CO(J→J-1) lines, one for each source, at ∼(1.2-1.4) mm in the observer frame (Castignani et al. 2018). Data reduction and analysis were performed using the CLASS software of the GILDAS package.† Our observations yielded four CO upper limits and one CO(7-6) detection for COSMOS-FRI 70, which makes it the most distant BCG candidate detected in CO. There are in fact pieces of evidence that the radio source is the BCG of one of the most distant proto-clusters hosting a RG. i) The stellar mass is

† https://www.iram.fr/IRAMFR/GILDAS/

exceptionally high ($\log(M_\star/\mathrm{M}_\odot) \simeq 11$, Baldi et al. 2013). ii) By applying Galfit (Peng et al. 2002) to the archival high-resolution HST ACS F814W (I-band) image a Sèrsic index 4.3 ± 0.6 is found, consistently with that of early type galaxies. iii) Color-color and color-magnitude plots further suggest that COSMOS-FRI 70 is indeed a star forming massive elliptical, $\sim$ 0.3mag brighter than all photometrically selected (proto-)cluster members (Castignani et al. 2018). Our results are reported in Table 1 and Fig. 1.

3. Conclusions. All target RGs have molecular gas properties that are consistent with the predictions for main sequence (MS) field galaxies. However they also show that high-z BCGs i) tend to be gas poor and ii) have a relatively short depletion time scale. We thus speculate that the cluster environment might have played a role in preventing the refueling via environmental mechanisms such as galaxy harassment, strangulation, ram-pressure, or tidal stripping.

Galaxy ID	z_{spec}	CO(J→J-1)	$S_{\mathrm{CO(J\to J-1)}}$ (Jy km s^{-1})	$M(\mathrm{H_2})$ (10^{10} M$_\odot$)	τ_{dep} (10^9 yr)	$\frac{M(\mathrm{H_2})}{M_\star}$ (10^8 M$_\odot$)	$\tau_{\mathrm{dep,MS}}$ (10^9 yr)
(1)	(2)	(3)	(4)	(5)	(6)	(7)	(8)
DES-RG 399	0.388439	3→2	< 1.5	<1.0	<0.91	<0.16	$1.10^{+0.16}_{-0.14}$
DES-RG 708	0.60573	3→2	< 1.5	<2.6	<0.36	<0.14	$1.12^{+0.21}_{-0.17}$
COSMOS-FRI 16	0.9687	4→3	< 5.5	<18.8	<0.58	<2.29	$0.91^{+0.16}_{-0.14}$
COSMOS-FRI 31	0.9123	4→3	< 5.2	<15.8	—	<2.71	$0.90^{+0.15}_{-0.13}$
COSMOS-FRI 70	2.625	7→6	0.69 ± 0.31	5.0 ± 2.2	$0.20^{+0.13}_{-0.19}$	$0.22^{+0.15}_{-0.16}$	$0.66^{+0.17}_{-0.13}$

Table 1: (1) galaxy name; (2) spectroscopic redshift; (3-4) CO(J→J-1) transition and flux; (5) molecular gas mass; (6) depletion time scale $\tau_{\mathrm{dep}} = M(\mathrm{H_2})/\mathrm{SFR}_{24\mu\mathrm{m}}$; (7) molecular gas to stellar mass ratio; (8) τ_{dep} predicted for MS field galaxies by Tacconi et al. (2018).

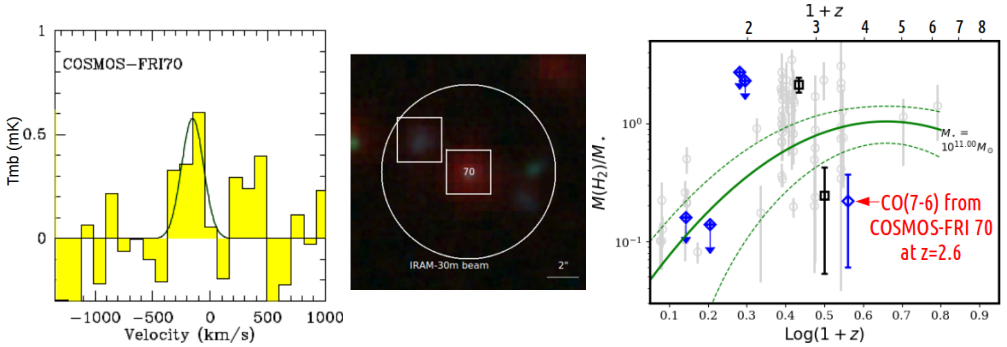

Figure 1: Left: CO(7-6) spectrum of COSMOS-FRI 70 taken with IRAM-30m. Center: RGB image of COSMOS-FRI 70 and its nearby companions, North is up, East is left. Right: molecular gas properties of BCG candidates from our IRAM-30m campaign are highlighted as blue diamonds, BCGs from other studies are shown as black squares (Emonts et al. 2013, Webb et al. 2017), gray circles denote normal cluster galaxies, model predictions from Tacconi et al. (2018) for MS galaxies and their uncertainties are shown as green solid and dashed lines, respectively.

References

Baldi, R. et al. 2013, *ApJ*, 762, 30
Castignani, G., et al. 2014a, *ApJ*, 792, 113
Castignani, G., et al. 2014b, *ApJ*, 792, 114
Castignani, G., et al. 2018, submitted to *A&A*
Chiaberge, M., et al. 2009, *ApJ*, 696, 1103
DES Collaboration 2016, *MNRAS*, 460, 1270
Emonts, B. et al. 2013, *MNRAS*, 430, 3465
Omont, A., 2007, *RPPh*, 70, 1099O
Peng, C. Y. et al. 2002, *AJ*, 124, 266
Tacconi, L. et al. 2018, *ApJ*, 853, 179
Webb, T. M. A. et al. 2017, *ApJ*, 844, 17
Zirbel, E. L. 1996, *ApJ*, 473, 713

Astronomy in Focus, Volume 1
XXXth IAU General Assembly, August 2018
Volker Beckmann & Claudio Ricci, eds.

DOI: 00.0000/X000000000000000X

Extended parameter study of the self-similar relativistic MHD equations for black hole outflows

Chiara Ceccobello[1], Y. Cavecchi[3,4], M. H. M. Heemskerk[2], S. Markoff[2], P. Polko[5], and D. Meier[6]

[1]Department of Space, Earth and Environment, Chalmers University of Technology, Onsala Space Observatory, 439 92 Onsala, Sweden
email: chiara.ceccobello@chalmers.se

[2]"Anton Pannekoek" Instituut voor Sterrekunde, Universiteit van Amsterdam, Science Park 904, 1098 XH Amsterdam, The Netherlands

[3] Department of Astrophysical Sciences, Princeton University, Peyton Hall, Princeton, NJ 08544, USA

[4] Mathematical Sciences and STAG Research Centre, University of Southampton, SO17 1BJ, UK

[5] University of Maryland at College Park, Dept. of Physics, Joint Space-Science Institute, 3114 Physical Sciences Complex, College Park, MD 20742, USA

[6] Jet Propulsion Laboratory, California Institute of Technology, Pasadena, CA 91109, USA

Abstract. Jets are ubiquitous and reveal themselves at different scales and redshifts, showing an extreme diversity in energetics, shapes and emission, in objects such as X-ray binaries (XRBs) and active galactic nuclei (AGN), as well as young stellar objects (YSOs) and gamma-ray bursts (GRBs). Observations suggest that jets are an energetically important component, not only to the systems that host them, but also their larger surrounding environments, where they deposit a significant amount of energy that has been extracted from the accretion flow. Therefore, understanding the mechanisms responsible for the formation and emission of jets is a fundamental problem to be addressed. We developed a new integration scheme to solve scale-invariant, relativistic and non-relativistic MHD equations describing collimated disk-driven outflows. For the first time, jet solutions can be reconstructed from the disk mid-plane to downstream of the modified magnetosonic fast point, while smoothly crossing the three singular surfaces (modified slow/fast and Alfven surfaces). Relativistic solutions show a wide range of jet dynamics (jet Lorentz factor 1-10) and geometric properties (i.e. shock height $\sim 10^3 - 10^7 R_g$), which is even more broadened by the inclusion of the non-relativistic solutions grid. Such diversity makes our model suitable for application to many different systems in which relativistic jets are launched.

Keywords. MHD, methods: analytical, methods: numerical, galaxies: jets, X-rays: binaries

1. Introduction

Jets are a common but not well-understood feature in the universe, manifesting themselves in a variety of systems, such as accreting stellar-mass and supermassive black holes, neutron stars, young stellar objects, etc. They are associated with accretion of matter into a compact object or a star. Magnetic fields play a crucial role in extracting material from the disk and accelerating and collimating the flow (e.g. Pudritz et al. 2007). However the exact mechanism, or combination of mechanisms, responsible for launching jets from black holes is highly debated (Blandford & Znajek 1977, Blandford & Payne 1982).

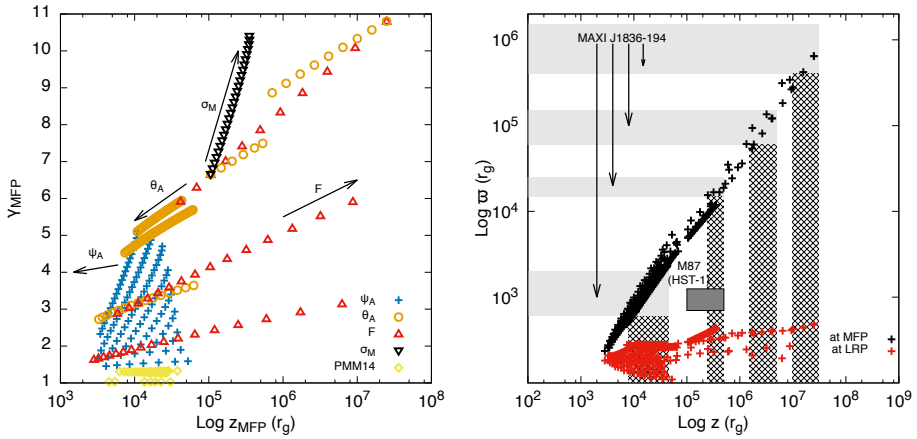

Figure 1. *Left panel:* Lorentz factors at MFP of the solutions presented in Ceccobello et al. (2018), as a function of the height of the MFP. The blue crosses solutions are obtained with a 2-dimensional search varying ψ_A for given values of σ_M. The other symbols correspond to solutions found by varying θ_A (orange hollow circles), σ_M (black hollow downward triangles), F (red hollow triangles) and Polko et al. (2014) with correct gravity terms (yellow hollow diamonds). The arrows mark the direction of increasing values of the given parameter. *Right panel:* Same solution sample shown in the the left panel with respect to cylindrical radius versus height of the MFP (black crosses) and of the last recollimation point (LRP, red crosses). The shaded light grey areas corresponds to the radial extent of the jet at the location of the jet spectral break during a state transition, including error bars reported by Russell et al.(2014) for the X-Ray Binary MAXI J1836-194. Solutions in the grey areas are suited to describe the jet configurations at the different stages. The areas with the pattern denotes the predicted heights for the jet break. The dark grey rectangle is the height/radius of the knot HST-1 in the jet of M87 as estimated by Asada & Nakamura (2012).

2. Results

The model presented in Ceccobello et al. (2018) describes a magnetohydrodynamics (MHD) disk- driven jet including the effect of gravity. In Ceccobello et al. (2018), we discuss the details of the numerical algorithm we developed to solve the r-self-similar, stationary, axisymmetric MHD equations describing collimated, relativistic outflows crossing smoothly all the singular points (Alfven point and modified slow/fast points; Vlahakis & Königl 2003, Polko et al. 2014). We studied the properties of a large set of solutions, distributed over an extended volume of the parameter space (Fig. 1). Recently, we adapted the algorithm to solve the non-relativistic MHD equations formulated in Vlahakis et al. (2000) and the new results will be discussed in a forthcoming paper (Ceccobello et al. in preparation).

References

Asada K., & Nakamura M. 2012, *ApJ*, 745, L28
Blandford, R.D., & Payne, D.G. 1982, *MNRAS*, 199, 883
Blandford, R.D., & Znajek, R.L. 1977, *MNRAS*, 179, 433
Ceccobello, C., Cavecchi, Y., Heemskerk, M. H. M., *et al.* 2018, *MNRAS*, 473, 4417
Polko, P., Meier, D. L., Markoff, S., *et al.* 2014, *MNRAS*, 438, 959
Pudritz, R.E., Ouyed, R., Fendt, Ch., & Brandenburg, A. 2007, *Protostars and Planets V*, 277
Russell, T.D., Soria, R., Miller-Jones, J. C. A., *et al.* 2014, *MNRAS*, 439, 1390
Vlahakis, N., Königl, A. 2003, *ApJ*, 596, 1080
Vlahakis, N., Tsinganos, K., Sauty, C., & Trussoni, E. 2000, *MNRAS*, 318, 417

Astronomy in Focus, Volume 1
XXXth IAU General Assembly, August 2018
Volker Beckmann & Claudio Ricci, eds.

DOI: 00.0000/X000000000000000X

BCGs radio analysis from EGMRT and CLASH samples of galaxy clusters

B. Terni de Gregory[1,2], T. Venturi[1], D. Dallacasa[1,2], and M. Nonino[3]

[1]INAF-Istituto di Radio Astronomia, Via P. Gobetti 101, Bologna, Italy
[2]DIFA-UniBO, Via P. Gobetti 93/2, Bologna, Italy
[3]INAF-Osservatorio Astronomico di Trieste, Via G. Tiepolo 11, Trieste, Italy

Abstract. We started the 'radioCLASH-GCAV' project to address some important questions concerning galaxy clusters and galaxy evolution in different environments at redshift $z > 0.2$. The occurrence of AGN feedback, ram pressure and tidal stripping, harassment and starvation as a function of mass, environment and redshift are at present day still largely unexplored. In the broad context aiming at studying galaxy evolution in clusters, we focused the first part of our research on a sample of eleven Brightest Cluster Galaxies selected mainly from the optical CLASH (Postman et al. 2012) and the radio EGMRT (Kale et al. 2015) surveys. Among the radio galaxy hosts, the BCGs witness special conditions, being large objects at the center of a deep potential well. The aim was to properly evaluate the contributions of Star Formation (Fogarty 2015, Donahue 2015) and of their active nucleus to the radio emission.

Keywords. Galaxies: clusters : general – intergalactic medium – Radio continuum: general – X-rays: general

1. Introduction

Brightest Cluster Galaxies are the most massive and luminous elliptical galaxies in the present-day Universe. They are typically located at the center of clusters, often found at the bottom of their gravitational potential well (Donahue et al. 2015). If BCGs are special it is likely to be because their formation and evolution is tied to physical mechanisms unique to rich galaxy clusters (see Lauer & Postman 2014 for a review). BCGs provide an excellent opportunity to study the relationships between star formation, the circumgalactic medium (CGM), and feedback from a central active galactic nucleus (AGN). Multiwavelength observational programs have shown that BCGs are not quiescent systems and exhibit high activity such as radio emission, extended emission-line nebulae, significant excess blue or UV light, far-infrared emission from warm dust, and vibrationally excited molecular hydrogen (see Donahue 2015). This enhanced activity in the BCGs is strongly related with the environmental conditions. In the most rich relaxed clusters all such active BCGs are embedded in a "cool-core", a coronae of dense, low-entropy, high-pressure gas.

2. The research and results

Our sample is composed by ten clusters in different dynamical stages: A209, A1300, A2744 are merging and A611, A1423, MACS J1931, MACS J0429, MACS J1206, RXC J1115, RXC J1532 are relaxed. The total number of galaxies for our analysis is eleven BCGs in a redshift range between $0.2 < z < 0.44$ (A2744 has two BCGs). From the radio point of view the merging clusters host diffuse emission (i.e. giant radio halo); some of the cool

core clusters host a central mini-halo (i.e. MACS J1206, RXC J1115, RXC J1532). We performed a detailed radio analysis from reprocessed VLA archival data at 1.4 GHz and from GMRT data at 325 MHz and 610 MHz and we exploited also a lot of ancillary data in other bands already available. We compared our results with previous observations in the Optical and UV bands from Fogarty 2015 and Donahue 2015. Radio emission is clearly detected and characterized for six BCGs for the VLA data and seven for the GMRT. For the remaining ones we considered an upper limit of 3σ. We found radio powers in the range from $10^{21} < \log P_{1.4}\ \mathrm{GHz} < 10^{25}\ \mathrm{W\,Hz^{-1}}$ for the VLA and from $10^{22} < \log P_{325\div600}\ \mathrm{MHz} < 10^{26}\ \mathrm{W\,Hz^{-1}}$ for the GMRT. These results are in agreement with the hypothesis that BCGs are intermediate between FRI and FRII radio galaxies. The spectral indices (defined as the slope at 1.4 GHz and 610 MHz or 325 MHz for GMRT data) are distributed from 0.08 to 1.3 with the $S_\nu \propto \nu^{-\alpha}$. We found that the trend is not homogeneous but consistent with being all powered by an AGN. The radio emission was unresolved in the most cases. To discriminate between the AGN or Star Formation contribution to the radio emission detected we used the Condon et al. 2002 relation where they defined the q parameter as:

$$q = \log \frac{(FIR/3.75 \times 10^{12}\ \mathrm{Hz})}{S_{1.4}(\mathrm{W\,Hz^{-1}\,m^{-2}})} \tag{2.1}$$

where FIR is defined as

$$FIR(\mathrm{W\,m^{-2}}) = 1.26 \times 10^{-14}[2.58\mathrm{S}_{60\mu\mathrm{m}}(\mathrm{Jy}) + \mathrm{S}100_{\mu\mathrm{m}}(\mathrm{Jy})] \tag{2.2}$$

If q is < 1.8 the AGN dominates the radio emission (Condon et al. 2002). We calculated it for all targets except A1300, A1423 and A2744 because of the lack of FIR emission from catalogues (Herschel & Spitzer). We derived the FIR luminosity $L_{60_{\mu m}} = 4\pi D_L^2 S_\nu (1+z)^{1-\alpha}$ taking into account the k-correction $(1+z)^{1-\alpha}$, where α is the spectral index. D_L is the luminosity distance accordingly with the cosmology adopted $H_0 = 70\ \mathrm{km\ s^{-1}\ Mpc^{-1}}$. We found values from $2 \times 10^9 < L_{60\mu m} < 6 \times 10^{11} L_\odot$, they are all below $10^{12} L_\odot$, which is the limit up to that they are Ultra Luminous Infra-Red Galaxies (ULIRG). We calculated the FIR SFR by the following relation and then we compared it with the SFR in the UV band from Donahue 2015 and with optical and H_α from Fogarty 2015:

$$SFR_{FIR} = \frac{L_{60\mu m}}{5.1 \times 10^{23}\ \mathrm{W\,Hz^{-1}}} \tag{2.3}$$

Not all the values are consistent with what is available in literature, but all of them have the same trend. Only A209, which is merging and the BCG is undetected, stands on the radio-FIR correlation. MACS J0429 and A611, both relaxed, have SFR lower than 30 $\mathrm{M_\odot yr^{-1}}$. MACS J1931, MACS J1206, RXC J1115 and RXC J1532 have SFR higher than 30 $\mathrm{M_\odot yr^{-1}}$. With our analysis, we confirmed that the environmental conditions are related to the enhanced activity in BCGs. In relaxed clusters, the presence of the mini-halo strongly influences the Star Formation activity.

References

Postman, M., Coe, D., Benitez, N., et al. 2012, *AJS*, 199, 25P
Kale, R., Venturi, T., Cassano, R., et al. 2015, *A&A*, 581, A23
Fogarty, K., Postman, M., Connor, T., et al. 2015, *ApJ*, 813, 117F
Lauer, T.R., Postman, M., Strauss, M.A., et al. 2014, *ApJ*, 797, 82L
Donahue, M., Connor, T., Fogarty, K., et al. 2015, *ApJ*, 805, 177D
Condon, J. J., Cotton, W. D., & Broderick, J.J. 2002, *AJ*, 124, 675C

Astronomy in Focus, Volume 1
XXXth IAU General Assembly, August 2018
Volker Beckmann & Claudio Ricci, eds.

DOI: 00.0000/X000000000000000X

The QUOCKA Survey: Overview

George Heald[1] and the QUOCKA Team[2]

[1]CSIRO Astronomy and Space Science, PO Box 1130, Bentley WA 6102, Australia
email: george.heald@csiro.au
[2]https://research.csiro.au/quocka/team/

Abstract. We introduce the QUOCKA project: a new polarimetric radio survey aimed at understanding detailed magnetoionic properties of radio galaxies, and enabling the science goals of modern broadband surveys to be carried out with Square Kilometre Array (SKA) pathfinders and precursors. The QUOCKA survey employs the broadband correlator available at the Australia Telescope Compact Array (ATCA), primarily to build on and supplement Early Science observations with the Australian Square Kilometre Array Pathfinder (ASKAP) telescope.

Keywords. magnetic fields, polarization, surveys, radio continuum: galaxies

1. Introduction

Radio astronomy is entering a golden era for broadband polarimetry. Projects like ASKAP's POSSUM, MeerKAT's MIGHTEE, the VLA Sky Survey (VLASS), and future all-sky surveys with the SKA are poised to throw open a new window on the magnetised Universe. We know that Faraday complexity carries a tremendous amount of astrophysical information, and that wider frequency spans permit constraints on increasingly complicated models (Gaensler et al. 2015). Yet we still have an incomplete picture of how observational properties reflect detailed magnetoionised features of emitting and foreground media. In this contribution, we introduce a Large Program aimed at bridging this gap that is being carried out with the Australia Telescope Compact Array (ATCA): *QU Observations at Cm wavelength using Km baselines with the ATCA* (the QUOCKA survey). The QUOCKA survey has two primary scientific aims:

- **Reveal the magnetoionic structure of radio galaxies** on multiple scales and link those properties to the evolution of the galaxies themselves, through QUOCKA observations and associated modelling. Linearly polarized synchrotron radiation is a sensitive tracer of magnetic fields in distant radio galaxies, and a delicate probe of material co-located with the emitting regions or in the foreground. Broadband data are required to uncover the properties and distribution of the gas and magnetic fields.
- **Jet magnetic fields** are powerfully traced by circular polarization emitted by radio galaxies, which has not been comprehensively studied. QUOCKA will provide unique information about how many radio galaxies produce circular polarization, allow further understanding of the emission mechanism, and motivate follow-up with the SKA.

2. QUOCKA sample selection

Here we describe the procedure that we have employed to construct the QUOCKA sample. The underlying philosophy is to leverage and complement the observations of linearly polarized sources as determined from ASKAP Early Science data.

For the first semester of QUOCKA observations, we processed and analysed data from six 30-square degree ASKAP fields following polarization calibration. Details of the calibration procedure will be published separately (Anderson et al., in prep), but

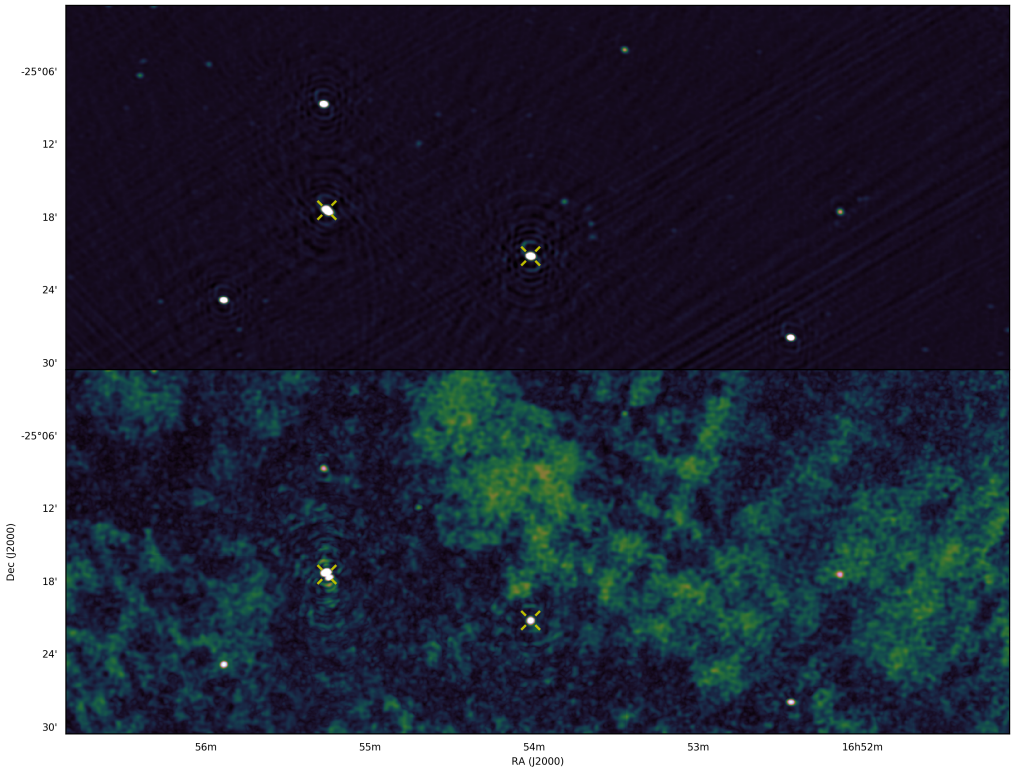

Figure 1. Representative region of an ASKAP mosaic used to identify sources for inclusion in the QUOCKA sample. Top: total intensity; bottom: linear polarization amplitude (see text). Sources matching the QUOCKA selection criteria are indicated with yellow crosses. S-shaped artifacts in the images are the result of incomplete deconvolution. The diffuse structure filling the field of view in the bottom panel is real and reflects Galactic polarized foreground emission.

the technique currently relies on an artificially induced polarization leakage signal to calibrate the XY phase difference.

Following bandpass and polarization calibration of the ASKAP data, a self-calibration procedure was employed using the standard ASKAPsoft strategy. Stokes Q and U were imaged in 1-MHz channels and used to perform RM Synthesis (Brentjens & de Bruyn 2005). The resulting peak polarized flux density per pixel was mapped. Source finding using BANE and Aegean (Hancock et al. 2018) identified sources in both Stokes I and linear polarization. Reliable sources were found by cross-matching these catalogs. Then, sources for QUOCKA observations were selected with the following criteria:

- Fractional polarization $P/I > 1\%$ (to avoid instrumental polarization); and
- $P > 2.5\,\mathrm{mJy/beam}$ (to provide high broadband S/N using snapshot ATCA scans).

Following these considerations, we observed 201 sources in the first semester. Double sources were combined. Early results are presented by Heald et al. (2018b, this volume).

References

Brentjens, M. A. & de Bruyn, A. G. 2005, *A&A*, 441, 1217

Gaensler, B., Agudo, I., Akahori, T., et al. 2015, proc. *Advancing Astrophysics with the Square Kilometre Array (AASKA14)*, 103

Hancock, P. J., Trott, C. M., & Hurley-Walker, N. 2018, *PASA*, 35, 11

Astronomy in Focus, Volume 1
XXXth IAU General Assembly, August 2018
Volker Beckmann & Claudio Ricci, eds.

DOI: 00.0000/X000000000000000X

A detailed view of the tailed radio galaxy 3C 31 with LOFAR

Volker Heesen,[1] Judith H. Croston,[2] Raffaella Morganti,[3] Martin J. Hardcastle,[4] and Jeremy J. Harwood[4]

[1]University of Hamburg, Hamburger Sternwarte, Gojenbergsweg 112, 21029 Hamburg, Germany

[2]School of Physical Sciences, The Open University, Walton Hall, Milton Keynes, MK6 7AA, UK

[3]ASTRON, Netherlands Institute for Radio Astronomy, PO 2, 7990 AA, Dwingeloo, The Netherlands

[4]School of Physics, Astronomy and Mathematics, University of Hertfordshire, Hatfield AL10 9AB, UK

Abstract. We present new low-frequency radio continuum observations of the nearby Fanaroff–Riley class I (FR I) radio galaxy 3C 31 using the Low-Frequency Array (LOFAR; 115–178 MHz). Our new LOFAR 145-MHz map shows that 3C 31 has a largest physical size of 1.1 Mpc in projection, which means 3C 31 now falls in the class of giant radio galaxies. We model the radio continuum intensities with advective cosmic ray transport, evolving the cosmic ray electron population and magnetic field strength in the tails as functions of distance to the nucleus. We find that if there is no in-situ particle acceleration in the tails, then decelerating flows are required that depend on radius r as $v \propto r^{\beta}$ ($\beta = 1$). This then compensates for the strong adiabatic losses due to the lateral expansion of the tails. We are able to find self-consistent solutions in agreement with the entrainment model of Croston & Hardcastle, where the magnetic field provides $\approx$1/3 of the pressure needed for equilibrium with the surrounding intracluster medium. We obtain an advective time-scale of $\approx$190 Myr, which, if equated to the source age, would require an average expansion Mach number $M \approx 5$ over the source lifetime.

Keywords. radiation mechanisms: non-thermal – cosmic rays – galaxies: individual: 3C 31 – galaxies: active – radio continuum: galaxies.

1. Introduction

The jets of low-luminosity radio galaxies (class I of Fanaroff & Riley 1974, hereafter FR I) are thought to be relativistic decelerating flows that emanate from active galactic nuclei. Progress with modelling of FR I sources has been possible by combining radio and X-ray observations, where the latter are a tracer for the hot intracluster medium (ICM). This allows one to constrain the density, temperature and pressure without having to rely on the assumption of energy equipartition between cosmic rays and the magnetic field (Burbidge 1956). Interestingly, most FR I sources are under-pressured when one considers the contribution from electrons, positrons, and the magnetic field only. The most promising avenue out of this, since the sources clearly have to be in pressure equilibrium, is to postulate the entrainment of the surrounding ICM into the jet. Here, we present a low-frequency study using the Low-Frequency Array (LOFAR) of the prototypical FR I radio galaxy 3C 31 to test the applicability of these models. This source is particularly well suited for jet modelling studies, because it is large, bright and nearby ($D = 73.3$ Mpc), and these properties of the source have enabled some of the most detailed studies of radio-galaxy physics to date.

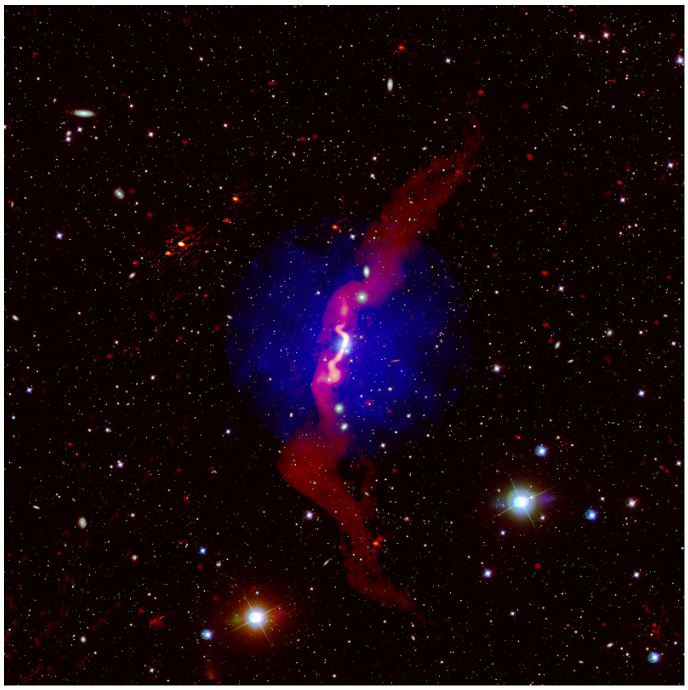

Figure 1. LOFAR 145-MHz radio continuum emission ($1.5 \ldots 700$ mJy beam^{-1}), shown in heat-scale, overlaid on an optical rgb-colour (r, g, and u bands) image from SDSS. In blue, we show *Chandra* X-ray emission. The image shows a 1 deg^2 area (corresponding to 1.2×1.2 Mpc^2). The angular resolution of 145-MHz map is 16.5×11.8 arcsec^2 (PA $= 73°$) FWHM.

2. Results and conclusions

Figure 1 presents our new 145-MHz map of 3C 31 (Heesen et al. 2018). The low-frequency radio continuum emission is sensitive to the oldest cosmic ray electrons (CRe), so we can now expand significantly on the previously known source size. We modelled the radio continuum emission with a CRe advection model for which we used the magnetic field strengths of the entrainment model by Croston & Hardcastle (2014) as a constraint. The LOFAR data are in good agreement with the entrainment model if we assume that the advection speed decelerates as function of the tail radius with $v \propto r^{-1}$. This then compensates for the strong adiabatic losses caused by the expansion of the tails. Using the spectral ageing information by the means of radio spectral indices, we could estimate that the advection speed in the tails drops from 20.000–45.000 km s^{-1} in the vicinity of the nucleus (15 kpc distance) to a few 1000 km s^{-1} at 500 kpc distance from the nucleus. This means an advective time-scale of ≈190 Myr, which equates to a mean mach number of $M \approx 5$ over the source lifetime. Dynamical arguments suggest that instead either the outer tail material does not represent the oldest jet plasma or else the particle ages are underestimated due to the effects of particle acceleration on large scales.

References

Burbidge, J. R. 1956, *ApJ*, 124, 416
Croston, J. H., & Harcastle, M. J. 2014, *MNRAS*, 438, 3310
Fanaroff, B. L. & Riley, J. M. 1974, *MNRAS*, 167, 31
Heesen, V., Rafferty, D. A., Horneffer, A., et al. 2018, *MNRAS*, 474, 5049

Astronomy in Focus, Volume 1
XXXth IAU General Assembly, August 2018
Volker Beckmann & Claudio Ricci, eds.

DOI: 00.0000/X000000000000000X

Restarting activity in the nucleus of PBC J2333.9-2343

Lorena Hernández-García[1], Francesca Panessa[2], Marcello Giroletti[3], Gabriele Ghisellini[4], Loredana Bassani[3], Nicola Masetti[3,5], Mirjana Pović[6,7], Angela Bazzano[2], Pietro Ubertini[2], Angela Malizia[3], Vahram Chavushyan[8], Giustina Vietri[9,10,11], Enrico Piconcelli[9], Eric Faustino Jiménez-Andrade[12,13], Sara Cazzoli[7], Lorenzo Monaco[5], and Ivo Saviane[14]

[1]IFA-UV, Universidad de Valparaíso, Valparaíso, Chile
email: lorena.hernandez@uv.cl

[2]IAPS-INAF, Roma, Italy

[3] IRA-INAF, Bologna, Italy

[4] INAF-Osservatorio Astronomico di Brera, Merate, Italy

[5] Departamento de Ciencias Físicas, Universidad Andrés Bello, Las Condes, Santiago, Chile

[6] ESSTI, EORC, Astronomy and Astrophysics Research Division, Addis Ababa, Ethiopia

[7] IAA-CSIC, Granada, Spain

[8] INAOE, Puebla, Mexico

[9]OAR-INAF, Monte Porzio Catone, Italy

[10]Excellence Cluster Universe, Technische Universität München, Garching, Germany

[11] ESO, Garching b. München, Germany

[12] Argelander Institute for Astronomy, University of Bonn, Bonn, Germany

[13] International Max Planck Research School of Astronomy and Astrophysics

[14] ESO, Santiago, Chile

Abstract. Under unification schemes, active galactic nuclei (AGN) can be explained by orientation effects. However, some sources cannot be explained by such unification scheme. This is the case of PBC J2333.9-2343; non-simultaneous data shows that its optical spectrum is of a type 2 AGN but its X-ray spectrum does not show signs of absorption, and in the radio it has many features typical of a blazar but it is a giant radio galaxy. Our simultaneous multiwavelength data shows that these classifications cannot be attributed to variability. We propose that PBC J2333.9-2343 is a blazar that has undergone a restarting activity episode in its nucleus, showing an exceptional change in the direction of the jet and changing from being a radio galaxy to become a blazar. It also shows a change in the broad line region (BLR) clouds and increasing variability at all observed wavelengths and we have detected an outflow in its optical spectra.

Keywords. galaxies: active, galaxies: jets,

1. Introduction

About 10% of the active galactic nuclei (AGN) population shows strong biconical relativistic jets (Panessa et al. 2016). When the jet points towards the line of sight the AGN is classified as a blazar and only one jet is visible, whereas at larger angles it is a radio galaxy and its morphology is characterized by two extended lobes.

2. Data and results

We have analyzed simultaneous data of PBC J2333.9–2343 ($z = 0.0475$) from the Very Long Baseline Array (VLBA), San Pedro Martir Telescope, and *XMM–Newton*, plus complementary Very Long Array (VLA), ESO -New Technology Telescope, and *Swift* data. These data reveal that:

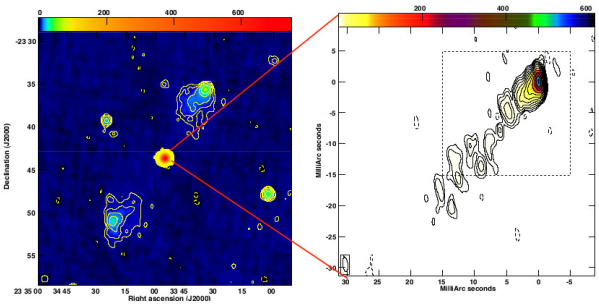

Figure 1. *Left panel*: VLA image of PBC J2333.9–2343, where the powerful nucleus and the old lobes can be observed (the apparent size of the large scale structure is 22 arcmin or 1150 kpc), and *Right panel*: VLBA image of PBC J2333.9–2343, where a jet pointing towards us can be observed. The red lines represent the zoom-in part of the nucleus (not at scale).

• At Mpc scales, the VLA map shows two jets (see left panel in Fig. 1), while at mas scales the VLBA data shows only one jet (right panel in Fig. 1). The modelling of the simultaneous spectral energy distribution (SED) requires the angle between the small scale jet and the observer to be smaller than 6 degrees.

• The source is strongly variable in the broad Balmer optical lines (Hα and Hβ), at X-rays, optical, and UV continuum.

• A broadened, blueshifted component is confirmed in high and low ionization lines, compatible with outflowing material.

3. Discussion and summary

The most plausible explanation is that about 10^4-10^6 yr ago the activity of the nucleus was restarted, and the jets changed the direction in the plane of the sky, so that a new jet is now pointing towards us, making this source from being a radio galaxy in the past to become a blazar, a very exceptional case of restarting activity (Hernández-García et al. 2017). In this scenario the extended lobes are explained by reservoirs of plasma from the old jets.

Its optical spectra revealed a change in the broad lines, which are thought to be created in the broad line region (BLR). The BLR in PBC J2333.9–2343 has a velocity width of $v = 16700\,\mathrm{km\,s^{-1}}$ and might be redshifted by more than $1000\,\mathrm{km\,s^{-1}}$ (Hernández-García et al. 2018). On the other hand, the spectra show a blueshifted ($350\,\mathrm{km\,s^{-1}}$) broadened component in all the emission lines associated with a possible variable outflow (Fiore et al. 2017). The spectral X-ray and broad Hα component variations are of the same order, they occur during the same timescale and they show the same trend. Because X-rays are interpreted as emission from the jet, we propose that the BLR is at least in part responsible for the ionization of the AGN. Moreover, the extreme kinematics of the broadened component in [OIII] and its low bolometric luminosity suggest that the outflow is induced by the interaction between the jet and the ambient gas.

References

Fiore, F., Feruglio, C., Shankar, F., et al. 2017, *A&A*, 601, A143
Hernández-García, L., Panessa, F., Giroletti, M., et al. 2017, *A&A*, 603, A131
Hernández-García, L., Vietri, G., Panessa, F., et al. 2017, *MNRAS*, 478, 4634
Panessa, F., Bassani, L., Landi, R., et al. 2016, *MNRAS*, 461, 3153

Astronomy in Focus, Volume 1
XXXth IAU General Assembly, August 2018
Volker Beckmann & Claudio Ricci, eds.

DOI: 00.0000/X000000000000000X

Double irony in XXL-North: A giant radio galaxy in a supercluster

Cathy Horellou[1], H.T. Intema[2], V. Smolčić[3], A. Nilsson[1], F. Karlsson[1], C. Krook[1]. L. Tolliner[1], C. Adami[4], C. Benoist[5], M. Birkinshaw[6], C. Caretta[7], L. Chiappetti[8], J. Delhaize[3], C. Ferrari[5], S. Fotopoulou[9], V. Guglielmo[10,17], K. Kolokythas[11], F. Pacaud[12], M. Pierre[13,14], B.M. Poggianti[10], M.E. Ramos-Ceja[12], S. Raychaudhury[11], H.J.A. Röttgering[2], and C. Vignali[15,16]

[1]Chalmers Univ. of Technology, Dept of Space, Earth and Environment, 43992 Onsala, Sweden
[2] Leiden Observatory, Leiden University, Niels Bohrweg 2, 2333 CA, Leiden, The Netherlands
[3] Department of Physics, Faculty of Science, University of Zagreb, 10000 Zagreb, Croatia
[4] Aix Marseille Université, CNRS, LAM, UMR 7326, 13388, Marseille, France
[5] Labo. Lagrange, Univ. Côte d'Azur, Obs. de la Côte d'Azur, 06304 Nice Cedex 4, France
[6] H.H. Wills Physics Laboratory, University of Bristol, Tyndall Avenue, Bristol BS8 1TL, U.K.
[7] Departamento de Astronomía, Universidad de Guanajuato; 36240, Guanajuato, Gto., Mexico
[8] INAF, IASF Milano, via Bassini 15, I-20133 Milano, Italy
[9] Centre for Extragalactic Astronomy, Dept of Physics, Durham Univ., U.K.
[10] INAF – Astronomical Observatory of Padova, I-35122 Padova, Italy
[11] Inter-University Centre for Astronomy and Astrophysics, Pune 411007, India
[12] Argelander-Inst. für Astronomie, Univ. Bonn, Auf dem Hügel 71, D-53121 Bonn, Germany
[13] IRFU, CEA, Univ. Paris-Saclay, F-91191 Gif sur Yvette, France
[14] Univ. Paris Diderot, AIM, Sorbonne Paris Cité, CEA, CNRS, 91191 Gif sur Yvette, France
[15] Dipartimento di Fisica e Astronomia, Univ. degli Studi di Bologna, 40129 Bologna, Italy
[16] INAF – Osservatorio di Astrofisica e Scienza dello Spazio, 40129 Bologna, Italy
[17] Max-Planck-Institut f. Extraterrestrische Physik, D-85748 Garching b. München, Germany

Abstract. We present a giant radio galaxy of peculiar shape identified in XXL-North.

Keywords. X-rays: galaxies: clusters, radio continuum: galaxies, galaxies: clusters: general.

The XXL multiwavelength survey† is well suited to investigate AGN and galaxy clusters. We have recently discussed two of the most prominent radio galaxies in XXL-North (Horellou et al. 2018). Both are in a supercluster at $z \approx 0.14$. The Double Irony radio galaxy‡ is in a galaxy group with no detected extended X-ray emission (Fig. 1). Its large size ($\approx$ 1.1 Mpc) and particular shape suggest that it is located in a low-density environment with which it interacts. The analysis of new data is in progress.

References

Adami, C. et al. 2018, *A&A*, in press
Horellou, C., Intema, H. T., Smolčić, V., et al. 2018, arXiv:1807.08653
Pierre, M., Pacaud, F., Adami, C., et al. 2016, *A&A*, 592, A1
Pierre, M., Adami, C., Birkinshaw, M., et al. 2017, *Astronomische Nachrichten*, 338, 334
Smolčić , V., Intema, H., Slaus, B., et al. 2018, *A&A*, in press, arXiv:1803.06142
Tasse, C., Röttgering, H. J. A., Best, P. N., et al. 2007, *A&A*, 471, 1105

† Pierre et al. (2016), Pierre et al. (2017); `http://xxlmultiwave.pbworks.com`
‡ The percontation point (a reversed question mark, ⸮) was invented in the sixteenth century to mark the end of a rhetorical question and was later used to denote irony.

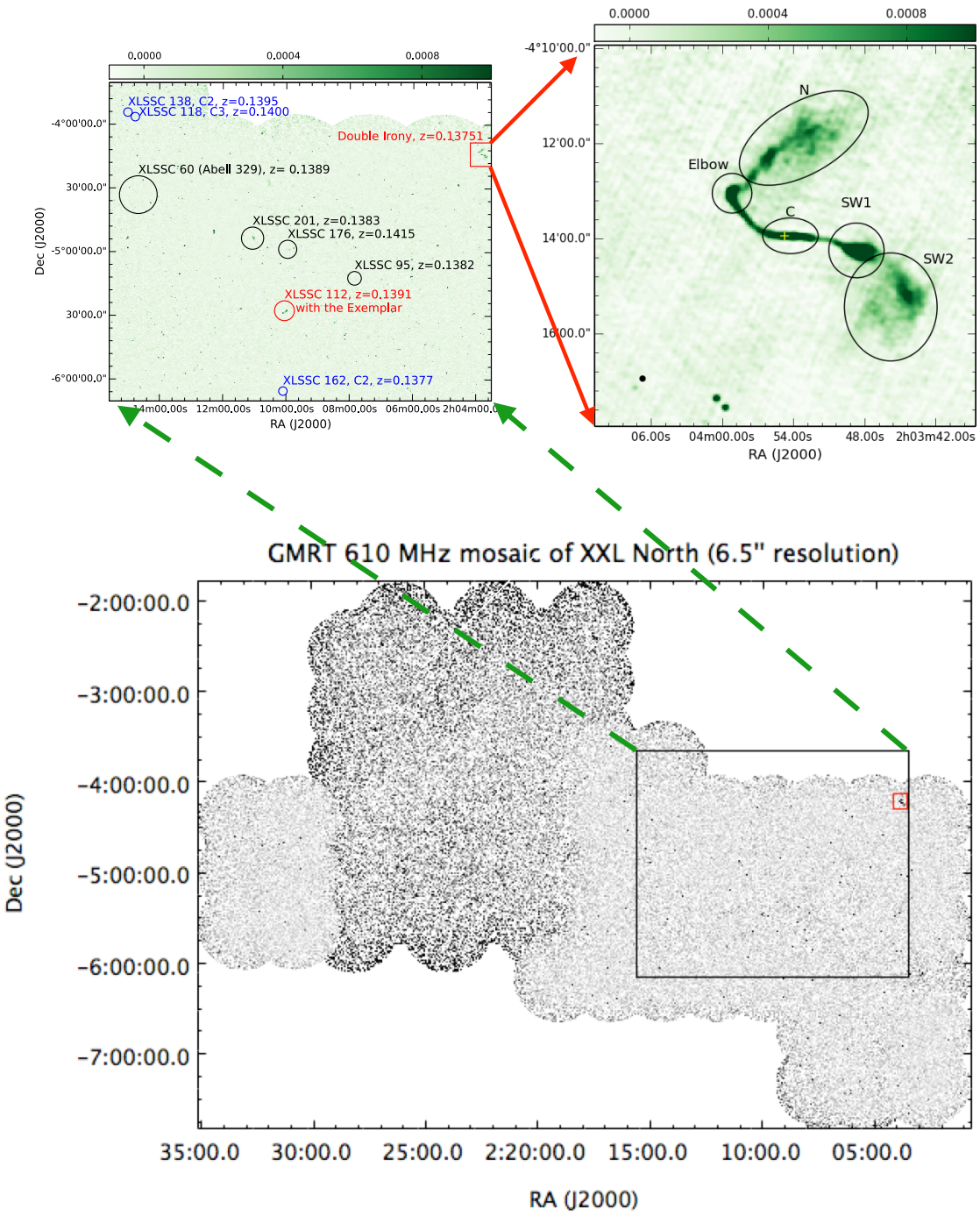

Figure 1. *The bottom panel* shows the ∼30 deg^2 GMRT (Giant Meterwave Radio Telescope) 610 MHz mosaic of XXL-North, at a resolution of 6.5″. The noisier central region is the XMM-LSS field covered earlier (Tasse et al. 2007). The new area of 12.7 deg^2 has a noise of about 45 μJy/beam (Smolčić et al. 2018). *The top left panel* shows the NW region that contains the supercluster XLSSsC N03 with eight X-ray-detected clusters (Adami et al. 2018). The Double Irony radio galaxy, shown in the *top right panel*, was discovered in the GMRT data, and it was found to lie in a galaxy cluster/group that is detected in the optical but not in X-rays. A new friends-of-friends analysis showed that the Double Irony's cluster is the ninth member of the supercluster (Horellou et al. 2018).

Astronomy in Focus, Volume 1
XXXth IAU General Assembly, August 2018
Volker Beckmann & Claudio Ricci, eds.

DOI: 00.0000/X000000000000000X

Growth of massive black holes in dusty clouds: impacts of relative velocity between dust and gas

Shohei Ishiki[1], Takashi Okamoto[2], and Hidenobu Yajima[3]

[1]Department of Cosmoscience, Hokkaido University,
N10 W8, Kitaku, Sapporo, 060-0810 Hokkaido, Japan
email: ishiki@astro1.sci.hokudai.ac.jp

[2]Department of Cosmoscience, Hokkaido University,
N10 W8, Kitaku, Sapporo, 060-0810 Hokkaido, Japan
email: okamoto@astro1.sci.hokudai.ac.jp

[3]Center for Computational Sciences, University of Tsukuba,
1-1-1 Tennodai, Tsukuba, 305-8577 Ibaraki, Japan
email: yajima@ccs.tsukuba.ac.jp

Abstract. We here investigate the impacts of the relative motions of dust and gas on the accretion rate onto intermediate-mass black holes (IMBHs) with the mass of 10^5 $M_\odot$ by using one-dimensional radiation hydrodynamic simulations. To investigate the effect of grain size on the gas accretion, we introduce two additional fluid components which describe large (0.1 μm) and small (0.01 μm) dust grains in the simulations as we did in Ishiki *et al.* (2018). Our simulations show that the decoupling motion of dust from gas reduces the dust-to-gas mass ratio significantly. As a result, the accretion rate increases to $\sim$1% of Bondi accretion rate which is ten times higher than the case of complete coupling between dust and gas. Thus, we suggest that the effect of the relative motion can allow moderate growth of black holes even in dusty clouds.

Keywords. accretion, accretion disks, black hole physics, radiative transfer, dust, extinction

1. Introduction

Recent observations have suggested the existence of a large amount of dust around supermassive black holes (SMBHs) in the early universe (e.g. Maiolino *et al.* 2004). In dusty clouds, the gas accretion proceeds under the influence of radiation feedback on dust. Yajima *et al.* (2017) recently showed that the accretion rate onto IMBHs in dusty clouds are significantly suppressed. They, however, assumed that the dust and gas are completely coupled. This assumption might be invalid in the vicinity of black holes. In this work, we investigate the growth of IMBHs in dusty clouds by one-dimensional radiation hydrodynamics simulations taking the relative motion of dust into account.

2. Methods

We place a BH with the mass of 10^5 $M_\odot$ at the centre of a spherically symmetric gas cloud. The species included in our simulations are H_I, H_{II}, He_I, He_{II}, He_{III}, electrons, and dust. We assume that the dust-to-gas mass ratio is proportional to metallicity as the correlation in local galaxies (e.g., Spitzer 1978): $M_{\rm dust}/M_{\rm gas} = 6.0 \times 10^{-3}(Z/Z_\odot)$.

In order to study spatial dust distribution, we solve gas and dust motion self-consistently as we did in our previous work (Ishiki *et al.* 2018). The inner and outer boundaries are set to 10^{-2} and 10^{3} pc, respectively.

3. Results, Discussions, and Conclusions

Fig. 1 shows the time averaged Eddington ratio ($f_{\rm Edd}$) as a function of initial gas density under the fixed conditions of the metallicity $Z = 1.0\ Z_{\odot}$ and the radiative efficiency $\eta = 0.3$. As shown in Yajima *et al.* (2017), in the case of assuming the complete coupling between dust and gas, $f_{\rm Edd}$ is regulated to $\sim 10^{-4}$–10^{-3} due to the strong radiation pressure on dust. On the other hand, in the case of considering the relative motion of dust, $f_{\rm Edd}$ increases to $\sim 10^{-3}$–10^{-2}.

We present the radial density profiles of gas and dust at $t = 5.0$ Myr as shown in Fig. 2. We find that the radiation force induces the decoupling of dust from accreting gas near the BH, resulting in the lower dust-to-gas mass ratio.

Thus, we suggest the relative motion between dust and gas alleviates the suppression of BH growth, which can be a key factor for understanding the formation of SMBH in the early Universe.

References

Ishiki S., Okamoto T., & Inoue A. K. 2018, *MNRAS*, 474, 1935
Spitzer L. 1978, Physical processes in the interstellar medium, Wiley-Interscience, New York
Yajima H.,, Ricotti M., Park K., & Sugimura K. 2017, *ApJ*, 846, 3
Maiolino, R., Schneider, R., & Olivia, E., *et al.* 2004, *Nature*, 431, 533

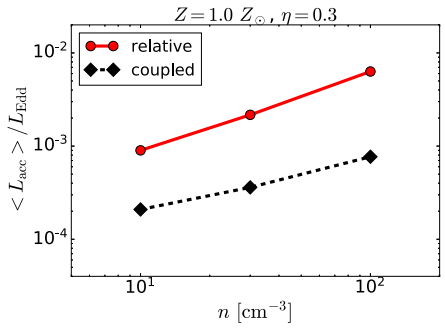

Figure 1. Time averaged Eddington ratio. The red solid lines with filled circles represents the results of simulations that allow relative motion between dust and gas. The black dashed lines with filled diamond represents the results of simulations that assume dust and gas move together.

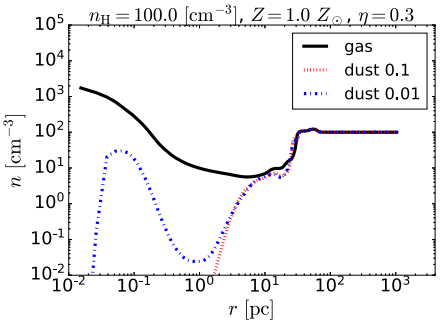

Figure 2. Density profile at $t = 5.0$ Myr. The black solid line shows the hydrogen number density profile. The red dashed line represents the large dust number density. The blue dot–dashed line shows the small dust number density profile. The dust number density profiles are normalized by hydrogen number density.

Astronomy in Focus, Volume 1
XXXth IAU General Assembly, August 2018
Volker Beckmann & Claudio Ricci, eds.

DOI: 00.0000/X000000000000000X

Prevalence of radio jets associated with quasar outflows and feedback

Miranda E. Jarvis[1,2]

[1]Max-Planck Institut fûr Astrophysik, Karl-Schwarzschild-Str. 1, 85741 Garching, Germany
email: mjarvis@eso.org

[2]European Southern Observatory, Karl-Schwarzschild-Str. 2, 85748 Garching, Germany

Abstract.
We have identified that radio jets are commonly associated with "radiative mode" feedback in quasars. By performing a systematic multi-wavelength study of $z < 0.2$ quasars, we have found that 70–80% of our sample of 'radio-quiet' type 2 quasars, which host kpc-scale ionized gas outflows, exhibit radio jet structures. Here, we discuss our results on the pilot sample of 10 objects that combine high resolution (∼0.25-1 arcsec) radio imaging at 1-7 GHz with optical IFU observations. Our results demonstrate that it is extremely common for jets to be spatially and kinematically linked to kpc-scale ionized gas kinematics in such quasars. Therefore, radio jets may be an important driver of outflows during 'radiative mode' feedback, apparently blurring the lines between the traditional divisions of feedback modes.

Keywords. galaxies: active –galaxies: evolution – galaxies: jets – quasars: emission lines

1. Introduction

The mechanisms by which AGN influence the gas of their host galaxies (feedback) are often split into two categories: the 'quasar' or 'radiative' mode, where radiation pressure dominates the feedback, and the 'jet' or 'radio' mode, where the majority of the AGN's energy is in a relativistic jet (see e.g., Heckman & Best 2014; Fabian 2012). In particular, the exact mechanism by which 'quasar' mode AGN interact with their host galaxies has been widely studied with little consensus, with radiative winds, compact jets and star formation all suggested (see e.g. Condon et al. 2013; Mullaney et al. 2013; Zakamska & Greene 2014). However, much of the previous observational work has lacked the spatial resolution to unambiguously distinguish between these possibilities. Our current work seeks to shed additional light on this problem by using high spatial resolution (∼1kpc) radio images of 10 'radio-quiet' quasars, and in so doing we have found that the division between quasar and jet mode feedback might not be as sharp as has previously been believed. This work will be presented in full in Jarvis et al. (in prep).

2. Sample properties

The ten quasars discussed here were selected from our parent sample of 24 264 $z < 0.4$ AGN, that were spectroscopically identified as AGN from SDSS (DR7; Abazajian et al. 2009). We selected type 2 ('obscured') AGN with $z < 0.2$, with 'quasar' like luminosities ($\log L_{\rm AGN} = 45$–$46[\,{\rm erg\,s^{-1}}]$), and a luminous broad [O III] component, indicative of a powerful ionised outflow (i.e., a broad component that contributes $\geqslant$30% of the total flux and has a full width at half-maximum FWHM>700 $\rm km\,s^{-1}$; Mullaney et al. 2013). In Harrison et al. (2014), we found large scale ($\gtrsim$kpc) ionised outflows in all 10 AGN, using Gemini-South GMOS (Gemini Multi-Object Spectrograph) IFS data.

All of our targets were detected by the FIRST survey (Becker et al. 1995) with moderate radio luminosities ($\log L_{1.4\,\mathrm{GHz}}$ =23.2–24.4[$\mathrm{W\,Hz^{-1}}$]) and are either unresolved or marginally resolved at FIRST's $\sim$5″ resolution (see Harrison et al. 2014). They are all classified as 'radio-quiet' using the separation criteria of Xu et al. (1999) (see Figure 1) and 'star formation dominated' by the separation criteria of Best & Heckman (2012). However, we find that all but one of our targets have a radio excess from what would be expected from their star formation alone. We determined this by using the infrared–radio correlation for normal star forming galaxies from Bell (2003) and UV-FIR SED fitting to isolate the infrared luminosity due to star formation from the AGN contribution (see Figure 1; Jarvis et al. in prep.). This provides initial evidence for non star formation processes (likely AGN) producing the majority of the radio emission in our sources.

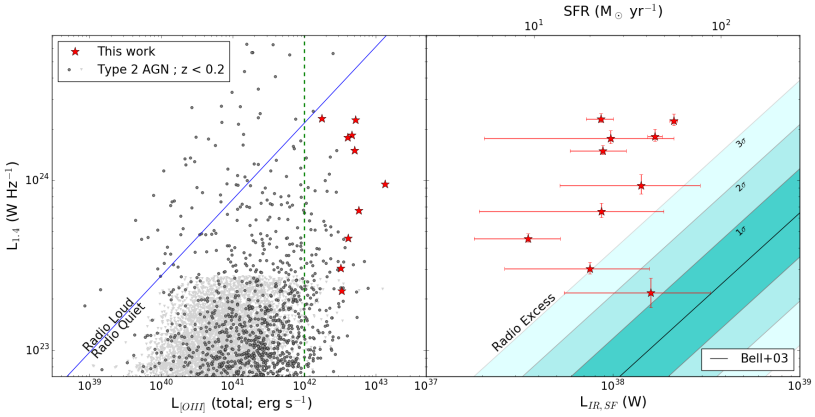

Figure 1. Left: Radio versus [O III] luminosity for our galaxies (red stars), with the division between "radio-loud" and "radio-quiet" from Xu et al. (1999) (blue line) and our parent sample of type 2 AGN with $z < 0.2$ (black points, grey for upper limits; Mullaney et al. 2013). Our selection criterion of $L_{[\mathrm{OIII}]} > 10^{42}$ erg s^{-1} is shown by a dashed green line. Right: The FIR-radio correlation of Bell (2003) compared to the values for our primary sample. We take $L_{IR,SF}$ from the luminosity of the dust component from UV-FIR SED fitting. The solid black line is the average correlation from Bell (2003), with the cyan regions marking 1, 2 and 3σ regions respectively. Although all of our targets are classified as radio-quiet by most traditional methods, all but one appear to have excess radio emission above what is predicted from star formation.

3. Observations

We present radio images from our observing campaigns with the Karl G. Jansky Very Large Array (VLA) in the L and C-bands with A and B configurations and the enchanced Multi-Element Radio Linked Interferometer Network (*e*MERLIN) that were designed to obtain high resolution (i.e., $\approx$0.3–1″; $\approx$ 600 pc at a representative redshift of $z = 0.1$) 1–7 GHz radio images of these targets. We compared the radio images to the ionized gas outflow properties traced by [O III] in our GMOS (Harrison et al. 2014) and VIMOS observations (Harrison et al. 2015 and Jarvis et al. in prep.). We fit the [O III] line profile with multiple Gaussians to reduce the effect of noise and measure the kinematic properties of the ionized gas in all pixels (Harrison et al. 2014). Specifically, in Figure 2 we show the signal-to-noise ratio (S/N) of [O III] with radio contours from our VLA C-band A configuration data (0.3″ beam) and where needed to show additional morphological features the *e*MERLIN (0.3″ beam) and VLA C-band B-configuration data (1″ beam)†.

† For J1338+1503 we only have VLA C-band B configuration data

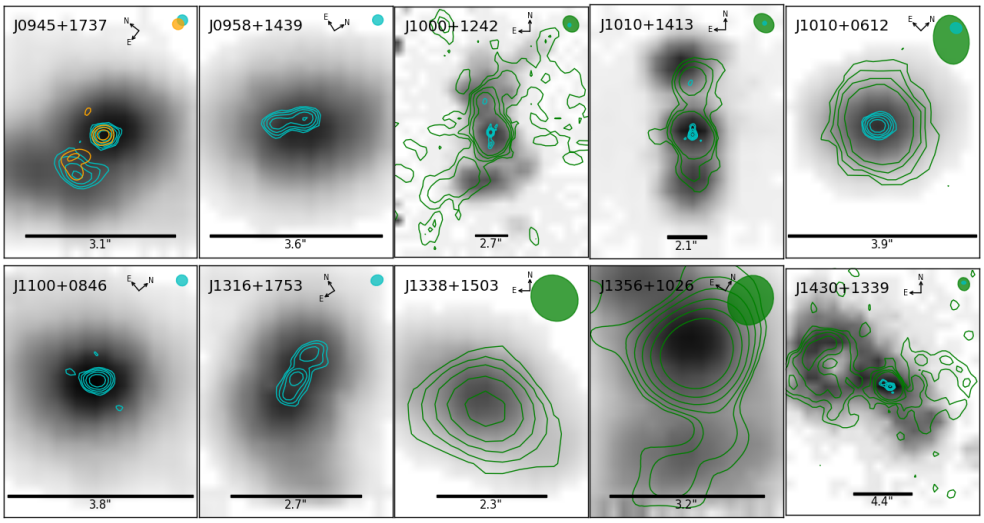

Figure 2. The distribution of [O III] emission (S/N maps) with contours overlaid from our radio images. Specifically, our VLA C-band B-configuration data is shown in green, VLA C-band A-configuration data in cyan and *e*MERLIN in orange. The beam for each radio image is shown as an appropriately coloured ellipse in the top right corner. The scale bar in each is 7kpc long. We observe a close connection between the radio and ionised gas morphologies.

4. Results and Conclusions

Perhaps surprisingly for a 'radio-quiet' sample, 70–80% show distinct, collimated morphological features in the radio on 1–25 kpc scales (for one target, J1338+1503, we cannot rule out the presence of ∼kpc scale features due to the lack of high resolution radio images). For three sources in particular (J0945+1737, J1000+1242 and J1010+1413) the high resolution images reveal elongated jet like components and flat spectrum ($\alpha > -0.2$) compact components. These latter structures, identified in the high-resolution images, are embedded in low resolution lobes, and we suggest that the most viable interpretation is that they are hot-spots from a jet. Furthermore, the sizes and lumionsities of our sources in the radio are comparable to the low luminosity population of compact steep spectrum (CSS) and Fanaroff-Riley type I (FRI) radio galaxies (see e.g. An & Baan 2012), suggesting a possible continuity between radio-loud and radio-quiet populations and supporting our interpretation that the collimated structures we identify are due to jets. Finally, these jets are in all cases coincident with kinematically disturbed ionised gas, an example of which can be seen in Figure 3. The combination of ionized gas kinematics and radio morphologies suggests that the jets and gas are interacting with each other, with the jet possibly driving outflows and the gas possibly deflecting the jets (see e.g. Leipski & Bennert 2006; Jarvis et al. in prep.). We note that shallow, low-resolution radio images such as those from the FIRST survey are insufficient to unambiguously determine the origin of the radio emission or the driving mechanism of the outflows in typical quasars, even at these low redshifts. Our observations support a scenario where compact radio jets, with modest radio luminosities, are a crucial feedback mechanism for massive galaxies during the quasar phase. In our future work, we will explore the impact of these jets on the molecular (star forming) gas through a recently accepted ALMA proposal and extend the sample to 42 objects, through newly acquired VLA images.

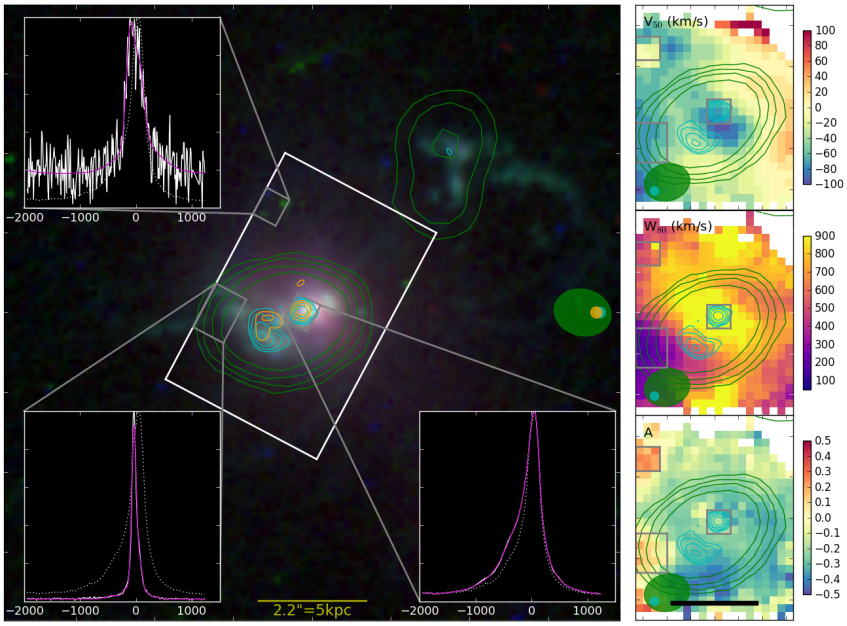

Figure 3. A comparison of the ionized gas and the radio features for J0945+1737. Left: contours from our radio data colour coded as they are in Figure 2 with the beams shown in the middle right, over-layed on HST data with continuum emission in red, [O III] and Hβ in green and H-alpha in blue (proposal id.13741; Cui et al. 2001). The FOV of the GMOS IFS is shown in white. [O III]5007 emission line profiles from the grey regions are shown each corner. The weighted average in the box is shown in white, the fit in magenta and the total over the cube as a dotted white line, all normalised to 1 and with the velocity given in km/s. Right: maps of the median velocity (v_{50}), line width (w_{80}) and asymmetry (A; see Harrison et al. 2014) with the boxes from the main panel overlayed. The scalebar is the same as in the main panel. The interactions between the radio jet features and the ionised gas are clearly visible.

References

Abazajian, K. N., Adelman-McCarthy, J. K., Agueros, M. A., et al. 2009, *ApJS*, 182, 543
An, T. & Baan, W. A. 2012, *ApJ*, 760, 77
Becker, R. H., White, R. L., & Helfand, D. J. 1995, *ApJ*, 450, 559
Bell, E. F. 2003, *ApJ*, 586, 794
Best, P. N. & Heckman, T. M. 2012, *MNRAS*, 421, 1569
Condon, J. J., Kellermann, K. I., Kimball, A. E., Ivezic, ., & Perley, R. A. 2013, *ApJ*, 768, 37
Cui, J., Xia, X.-Y., Deng, Z.-G., Mao, S., & Zou, Z.-L. 2001, *AJ*, 122, 63
Fabian, A. C. 2012, *ARAA*, 50, 455
Harrison, C. M., Alexander, D. M., Mullaney, J. R., Swinbank, A. M. 2014, *MNRAS*, 441, 3306
Harrison, C. M., Thomson, A. P., Alexander, D. M., et al. 2015, *ApJ*, 800, 45
Heckman, T. M., & Best, P. N. 2014, *ARAA*, 52, 589
Leipski, C. & Bennert, N. 2006, *A&A*, 448, 165
Mullaney, J. R., Alexander, D. M., Fine, S., et al. 2013, *MNRAS*, 433, 622
Noll, S., Burgarella, D., Giovannoli, E., et al. 2009, *A&A*, 507, 1793
Xu, C., Livio, M., & Baum, S. 1999, *AJ*, 118, 1169
Zakamska, N. L. & Greene, J. E. 2014, *MNRAS*, 442, 784

Astronomy in Focus, Volume 1
XXXth IAU General Assembly, August 2018
Volker Beckmann & Claudio Ricci, eds.

DOI: 00.0000/X000000000000000X

Swift and *XMM-Newton* monitoring of the ISP blazar ON 231 in outburst state

Nibedita Kalita[1] and Utane Sawangwit[1]

[1]National Astronomical Research Institute of Thailand (NARIT), Chiang Mai, 50180, Thailand
email:nibedita@narit.or.th

Abstract. We present a detailed temporal and spectral study of the intermediate type blazar, ON 231 with observations taken by *Swift* and *XMM-Newton* satellites during an outburst phase in June 2008. The source shows multiple X-ray flares in that period when the flux amplitude varies in the range of $27-38\%$. The X-ray spectra are well fitted with a broken power-law model indicating the presence of both synchrotron and inverse Compton components. We find that the source shows strong and variable emission in the soft energy bands (below $3-4$ keV), where the hard band emission is weak and stable. All the soft X-ray bands show correlated variability with zero lag, while a soft lag of -600s between the $0.3-0.5$ and $4-10$ keV bands is observed with DCF analysis. A time-resolved spectral study of the flares gives a positive relation between the total fluxes and the break energies of the two emission components.

Keywords. galaxies: active − BL Lacertae objects: individual: ON 231 (W Comae)

1. Introduction

ON 231, also known as W Comae ($z = 0.102$) was the 1st intermediate type synchrotron peaked (ISP) blazar detected in TeV $\gamma-ray$ range by *VERITAS* in March, 2008 when the source went to an outburst phase (Acciari et al. 2008). The source entered into a second outburst state in June in the same year, which triggered a multi-frequency campaign to observe the source in different wavelengths. This time the gamma-ray flux was higher than the previous flare by a factor of 3. The observations that we have used in this work were taken as part of the multi-wavelength campaign. Assuming that the photons are emitted due to shocks in the jet during the outburst state, Sorcia et al. (2014) estimated the polarization degree, $\sim 33.3\%$ and the jet angle, $\sim 2^{\circ}$. They also reported that the optical gamma-ray emitting regions could be co-spatial. The source has not much studied in the X-ray bands as compared to other blazars (LSPs or HSPs). However, a previous study reported the presence of variable soft and stable hard X-ray emission in the source with *BeppoSAX* observations (Tagliaferri et al. 2000).

The motivation behind this work is to investigate thoroughly the variability nature of the ISP blazar in flaring state. It is important to note that the ISPs are the connecting link between the high synchrotron peaked (HSPs) and the low synchrotron peaked (LSPs) blazars, so their study might unfold interesting information to understand the blazar phenomenon as a whole.

2. Results: Timing and spectral analysis

Swift and *XMM-Newton* satellites monitored the blazar in consecutive periods between 7−18 June 2008. We extract all the background subtracted light curves in the energy range 0.3-10 keV using the data processing method described in Kalita et al. 2015 for *XMM-Newton*'s EPIC-pn observations and the online Build-XRT-products for *Swift-XRT*

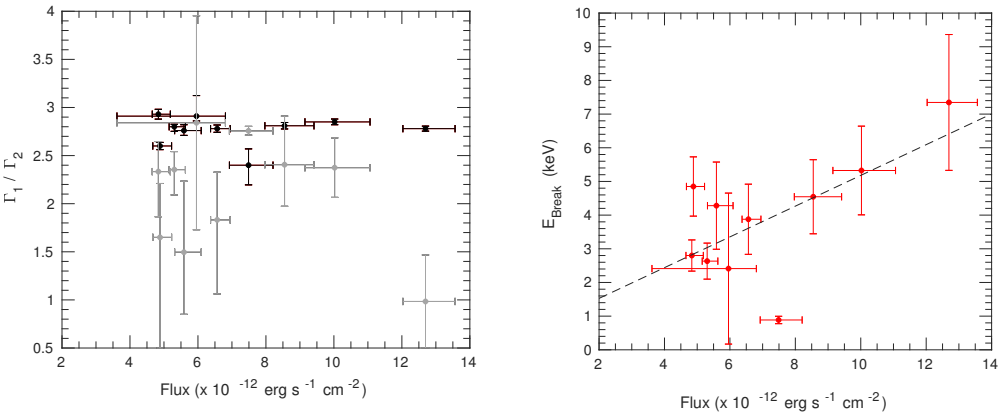

Figure 1: The left plot shows the relationship between the two spectral indices and the 0.6-10 keV total fluxes derived from the BPL fit. The black and grey points represent Γ_1 and Γ_2, respectively. The plot for the break energies vs. the total fluxes is shown in the right panel of the figure.

observations. The fractional rms variability amplitude (F_{var}), estimated using the method given in Edelson et al. (2002) indicates high flux variation ($\sim 27-38\%$) on timescales of hours with 100% duty cycle.

In order to study the energy-dependent variability properties of the event, we divide the 0.3-10 keV LCs into different energy bands and find that the emission in soft bands is strong and more variable than that in hard bands. To search for correlated variation among these energy bands, we have used Discrete Co-correlation Function (DCF) given by Edelson et al. 1988. The result of DCF analysis is the same for all the soft bands where the peak appeared at DCF=1 with zero time lag. However, a soft lag of -600s is detected between the 0.3−0.5 and 4−10 keV bands.

For all of the spectra when fitted with a simple power-law model with Galactic absorption due to the hydrogen column density, give positive residuals above 3-4 keV. This indicates that the spectra are intrinsically curved. So, we tried to fit the spectra with a log-parabolic model, but the residuals remain the same as in the previous case. However, a broken power-law (BPL) model gives an acceptable fit to all of the spectra with break energy (E_{break}) ranging between 2.6−5.4 keV and the two photon indices, Γ_1 and Γ_2 ranging from 2.74±0.01−3.03±0.1 and 1.74±0.35−2.4±0.15, respectively. To understand the evolution of the X-ray flares, we perform a time-resolved spectral analysis where all the spectra are split into several time intervals. We repeat spectral fits for each time episode with the best fit model and estimate the model parameters. The results of the time-resolved spectral fits are shown in Figure 1.

References

Acciari, V. A., Aliu, E., Beilicke, M., et al. 2008, *ApJ*, 684, L73
Edelson, R. A., & Krolik, J. H. 1988, *ApJ*, 333, 646
Edelson, R., Turner, T. J., Pounds, K., et al. 2002, *ApJ*, 568, 610
Kalita N., Gupta A. C., Wiita P. J., Bhagwan J., & Duorah K. 2015, *MNRAS*, 451, 1356
Sorcia, M., Benítez, E., Hiriart, D., et al. 2014, *ApJ*, 794, 54
Tagliaferri, G., Ghisellini, G., Giommi, P., et al. 2000, *A&A*, 354, 431

Astronomy in Focus, Volume 1
XXXth IAU General Assembly, August 2018
Volker Beckmann & Claudio Ricci, eds.

DOI: 00.0000/X000000000000000X

Direct evidence of a few to tens of parsecs torus in 3C84

Nozomu Kawakatu[1], Kiyoaki Wajima[2] and Motoki Kino[3]

[1]National Astronomical Observatory of Japan,2-21-1 Osawa, Mitaka, Tokyo 181-8588, Japan
email: kawakatsu@kure-nct.ac.jpl

[2]Korea Astronomy and Space Science Institute, 776 Daedeokdae-ro, Yuseong, Daejeon 34055, Korea
email: wajima@kasi.re.kr

[3] Academic Support Center, Kogakuin University,2665-1 Nakano, Hachioji, Tokyo 192-0015, Japan
email: motoki.kino@nao.ac.jp

Abstract. The optically thick free-free absorption (FFA) features of a parsec scale northern lobe in a nearby bright radio galaxy 3C 84 at 43 and 86 GHz shed light on the nature of structure surrounding active galactic nuclei (AGNs). The dependence of FFA optical depth on frequency is weaker than the form $\tau_{\rm ff}^{-2}$ expected for uniform absorbing matter, indicating that the absorbers are highly clumpy. In addition, a newly-detected feature in the northern lobe suggests a column density of $N_{\rm H} = 3 \times 10^{23}\,{\rm cm}^{-2}$ for an inclination angle of 40 deg. Our results provide evidence for a parsec scale clumpy torus.

Keywords. galaxies: active — radio continuum: galaxies — techniques: interferometric

1. Introduction

Multi-wavelength observations have indicated the existence of an active galactic nucleus (AGN) obscuring structure near a central supermassive black hole (SMBH), a well known component of AGN unified models (e.g., Antonucci 1993). With ALMA, dense molecular gas in a 10pc-scale torus have been found around nearby AGNs (e.g., Imanishi 2016) However, the parsec scale structure has not been revealed so far because of the lack of an angular resolution. NGC 1275 (a.k.a. 3C 84) is a nearby giant elliptical galaxy at the center of the Perseus cluster. A newborn lobe (C3) was discovered by Nagai et al.(2010), but the counter lobe (N1) was not detected until 2015 (Fujita & Nagai 2017). By conducting quasi-simultaneous VLBI observations at 43 GHz and at 86 GHz, we examine properties of the parsec scale structure and circumnuclear environment in 3C84. We use the FFA features to probe the structure of the obscuring structure.

2. Results

The source consists of two bright components, the central core (C1) and the southern lobe (C3). We also detect a weak component (N1), which is a part of counter lobe of C3 (Fig. 1). The detection level of N1 is about 6 times the off-source rms noise at both frequencies. In addition, the flux ratios between C3 and N1 are $\sim$ 40 at 43 GHz and $\sim$ 11 at 86 GHz. Note that these large ratios cannot be interpreted as due to relativistic beaming. We estimate the spectral index α of each component. Both C1 and C3 show an optically thin feature at the peak intensity position with its spectral index of -0.11 ± 0.02 and -0.54 ± 0.03, respectively. On the other hand, N1 has an optically thick spectral feature with $\alpha = +1.19 \pm 0.43$. The spectral indices of C1 and C3 are typical

of synchrotron emission, which means these components are unlikely to be affected by absorption. On the other hand, N1 has an inverted spectrum, and thus may suffer strong absorption. Combining the observation of an optically thick spectral feature with the large flux ratio, the most likely interpretation is free-free absorption (FFA). From the observed intensity ratios, we found $\tau_{\rm ff} = 3.6$ at 43 GHz, $\tau_{\rm ff}$=2.4 at 86 GHz. Moreover, the ratio of the observed optical depths at 43 GHz and at 86 GHz indicates $\tau_{\rm ff} \propto \nu^{-0.57}$. This is quite different from $\tau_{\rm ff} \propto \nu^{-2}$ for a uniform absorbing medium. Thus, it may suggest that the absorbing matter is highly inhomogeneous and consists of optically thick clouds ($\tau_{\rm ff} > 1$) and an optically thin ($\tau_{\rm ff} < 1$) uniform defuse region, i.e., the covering factor for N1 is less than unity. In addition, assuming the gas temperature $T = 10^4$ K and path length $L = 1$ pc, the column density derived from FFA is found to be $N_{\rm H} = 3\times10^{23}\,{\rm cm}^{-2}$.

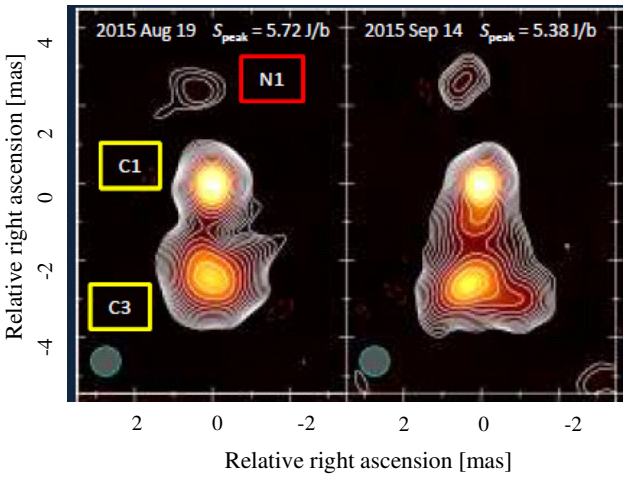

Figure 1. Two epoch images of 3C 84 at 43 GHz

3. Summary

We newly discovered a parsec-scale counter lobe (N1) in a nearby bright radio galaxy 3C 84 at 43 GHz and at 86 GHz. From its spectral index, N1 can be interpreted as providing evidence for the existence of a dense medium, which is responsible for the FFA of the northern lobe with column density, $N_H \sim 10^{23}\,{\rm cm}^{-2}$. In addition, the optical depth of FFA is less dependent on frequency than the case for uniform absorbers, i.e, $\tau_{\rm ff} \propto \nu^{-0.57}$. Thus, it suggests that the dense absorbing medium may be a highly inhomogeneous structure.

References

Antonucci, R. 1993, *ARA&A*, 31, 473
Fujita, Y., & Nagai, H. 2017, *MNRAS*, 465, L94
Imanishi, M., Nakanishi, K., & Izumi, T. 2016, *ApJ* (Letters), 822, L10
Kino, M., Wajima, K., Kawakatu, N., et al. 2018, arXiv:1808.08855
Nagai, H., Haga, T., Giovannini, G., et al. 2014, *ApJ*, 785, 53
Nagai, H., Suzuki, K., Asada, K., et al. 2010, *PASJ*, 62, L11

Astronomy in Focus, Volume 1
XXXth IAU General Assembly, August 2018
Volker Beckmann & Claudio Ricci, eds.

DOI: 00.0000/X000000000000000X

The New Variability Phase of OJ 287 and Emergence of New Components in NIR to X-ray Region

P. Kushwaha[1], E. M. de Gouveia Dal Pino[1], A. C. Gupta[2], and P. J. Wiita[3]

[1]Department of Astronomy (IAG-USP), University of Sao Paulo, Sao Paulo 05508-090, Brazil
email: pankaj.kushwaha@iag.usp.br
[2]Aryabhatta Research Institute of Observational Sciences (ARIES), Manora Peak, Nainital 263002, India
[3]Department of Physics, The College of New Jersey, P.O. Box 7718, Ewing, NJ 08628-0718, USA

Abstract. We present a multi-wavelength (MW) spectral and temporal study of the recent activity of the claimed super-massive binary black hole system OJ 287 since December 2015. The overall MW activity can be divided into two durations: December 2015 – April 2016 (MJD: 57360 – 57500), showing strong activity from near-infrared (NIR) to γ-rays and September 2016 – June 2017 (MJD: 57650 – 57930), showing intense NIR to X-ray variability concurrent with detection at very high energies (VHE) by VERITAS, but without any signatures of variability in the Fermi-LAT band. In the first duration, the variations are almost simultaneous and the SEDs show new components in NIR-optical and optical-UV region. The NIR-optical bump is consistent with standard accretion-disk (AD) description while the optical-UV appears consistent with contributions from the broad-line region. The extracted broadband SEDs also show a clear shift in gamma-ray SED peak and can be explained with inverse Compton scattering of photons from broad line region. In the second period, the variations are also simultaneous except for one duration during which X-ray leads the optical/UV by $\sim$ 5-6 day. The broadband SEDs, on the other hand, show mixture of a typical OJ 287 SED and an HBL SED, consistent with an origin from two different zones, one located at sub-parsec scales and other at parsec scales.

Keywords. BL Lac objects: individual: OJ 287, radiation mechanisms: non-thermal

1. Introduction

Blazar are radio-loud active galactic nuclei (AGNs) with their jet align at a close angle to the observer's line of sight. They are characterized by a rapid variability with emission spanning the entire accessible electromagnetic (EM) spectrum, high and variable polarization, and frequent detection of superluminal motion. Temporally, the variability is consistent with stochastic variation while the in the spectral domain, they exhibit a characteristic broad double hump spectral energy distributions (SEDs). The lower energy hump is well understood be synchrotron emission from relativistic non-thermal electron population while high energy hump can arise from inverse Compton (IC) scattering of photons within the jet and/or surrounding photons depending on the location of emission region e.g. broad line region and torus IR photons at sub-parsec scales, torus IR photons at parsec scales etc (e.g. see Kushwaha et al. 2013). In this scenario, the emission at different wavelengths is highly correlated, both in the spectral and temporal domain, due to being generated from the same underlying particle population. Thus, any change in lower energy hump of SED should be reflected at the higher energy hump as well.

2. OJ 287 & Recent Multi-wavelength Activity

OJ 287 is an optically bright BL Lac object with optical record available since 1890. It shows regular quasi-periodic outbursts of $\sim$ 12 years in the optical band in addition to the typical stochastic variability of blazars. The regular feature has been suggested to be a result of precessing, binary supermassive black hole (SMBH) system (Valtonen et al. 2016, and references therein). The model, with many improvements since its inception, has been relatively successful in predicting the timing of these regular outbursts and predicted the latest of next outburst around December 2015 – January 2016.

As per prediction, an increase in NIR-optical emission was observed at November 2015 end. The predicted impact outburst was observed on December 5, 2016 (MJD 57361) with a relatively low optical polarization ($< 10\%$, Valtonen et al. 2016). However, a systematic rotation of $\sim 200^\circ$ in optical polarization was observed (Gupta et al. 2017), untypical for a dominant thermal emission as argued in the above model. Further, outburst at X-rays and γ-rays was also seen. Following this till mid-2017, the source has been very active across the entire EM spectrum which is the focus of our report here.

Temporally and spectrally, the overall MW activity can be clubbed into two durations: December 2015 – April 2016 (MJD $\sim$ 57300 – 57500) and June 2016 – September 2017 (MJD $\sim$ 57650 – 57930), as is originally presented in Kushwaha et al. 2018a and Kushwaha et al. 2018b. The first duration showed activity from NIR to Fermi-LAT γ-ray energies while the second duration showed a historic NIR to X-ray activity but lacks variability at Fermi-LAT γ-ray energies. The historic phase coincided with the first ever detection of OJ 287 at VHE energies by VERITAS (O'Brien et al. 2017).

Correlation study shows that the variations are simultaneous except for one period during the second duration which shows a systematic variation with optical/UV lagging X-ray by $\sim$ 5-6 days. In the spectral domain, the first duration revealed two new features: a bump at NIR-optical interface and a hardened Fermi-LAT γ-ray spectrum with a shift in its peak location (e.g. Kushwaha et al. 2013 for comparison). The NIR-optical bump is consistent the standard Shakura-Sunyaev accretion disk description of the primary SMBH (1.8×10^{10}M$_\odot$) while the γ-ray spectral hardening and peak shift can be naturally produced if it originates as a result of IC scattering of BLR photons as reported in Nilsson et al. 2010 for previous impact periods. This explanation resonates with the fact that NIR-optical SED shows no sign of a shift in its peak location. The IC/BLR constraining the emission region location at sub-parsec scales. The SEDs during the second duration, on the other hand, show an additional non-thermal component peaking at X-ray energies during high activity states while the X-ray spectra show curved spectrum with departure consistent with the level of X-ray emission during the quiescent state of the first duration. The location of X-ray peak and coincident VHE detection is consistent with properties of HBL blazars and can be reproduced by an addition emission region at parsec scales if emission is related with peak escape events of the binary SMBH model.

PK acknowledges FAPESP support grant 2015/13933-0.

References

Gupta, A. C., Agarwal, A., Mishra, A., et al. 2017, *MNRAS*, 465, 4423
Kushwaha, P., Gupta, A. C., Wiita, P. J., et al. 2018b, *MNRAS*, 479, 1672
Kushwaha, P., Gupta, A. C., Wiita, P. J., et al. 2018a, *MNRAS*, 473, 1145
Kushwaha, P., Sahayanathan, S., & Singh, K. P. 2013, *MNRAS*, 433, 2380
O'Brien, S., for the VERITAS Colloboration 2017, *arXiv*, arXiv:1708.02160
Nilsson, K., Takalo, L. O., Lehto, H. J., & Sillanpää, A. 2010, *A&A*, 516, A60
Valtonen, M. J., Zola, S., Ciprini, S., et al. 2016, *ApJL*, 819, L37

Astronomy in Focus, Volume 1
XXXth IAU General Assembly, August 2018
Volker Beckmann & Claudio Ricci, eds.

DOI: 00.0000/X000000000000000X

NGC 4869 in the Coma cluster: Its collimated radio jet and the role of Kelvin-Helmholtz instabilities

Dharam V. Lal

National Centre for Radio Astrophysics – Tata Institute of Fundamental Research,
Post Box 3, Ganeshkhind PO, Pune 411007, India
email: dharam@ncra.tifr.res.in

Abstract. The GMRT upgrade, an SKA pathfinder instrument, has begun operations. Here, we present radio and X-ray imaging of NGC 4869 in the Coma cluster, an important 'laboratory' to study the role of cluster environment on the properties of radio sources, and demonstrate the importance of multi-wavelength imaging. We report flaring of a straight collimated jet at approximately the position where it crosses the surface brightness edge seen in the hot gas.

Keywords. galaxies: clusters, individual: Coma, galaxies: NGC 4869, galaxies: active

1. Introduction

Complex, unusual structures in radio sources are often associated with a number of 'events' in which radio-emitting plasma clouds have been created. Depending on the several theories of radio galaxies, these 'events' may be regarded as truly separate or as continuous; for example, when the radio galaxy is moving through the intra-cluster medium, as is obviously the case with the head-tail radio sources, a history of activity is traced in the tail of radio-emitting plasma left behind the parent host galaxy.

Radio and X-ray observations of clusters of galaxies can be interpreted in terms of a diffuse hot intra-cluster gas, and several important effects have been predicted. One such effect is that a Kelvin-Helmholtz instability is likely to develop at the boundary, a.k.a. the surface-brightness edge, and a straight, collimated radio jet of the moving radio galaxy apparently flares-up (Livio et al 1980) when it crosses the edge.

2. Observations and Results

We have mapped NGC 4869 in the Coma cluster (Venturi et al. 1990) using the Giant Metrewave Radio Telescope in several frequency bands, from 150 MHz to 610 MHz. Below we list the observational results from these observations:

– NGC 4869 is the most interesting radio source in the Coma cluster of galaxies. The elliptical host galaxy shows a weak radio core, two oppositely directed radio jets, and a long low-surface brightness tail which begins after sharp bends in the jets.

– The large-scale structure of the source is given in Fig. 1 and is characterised by a bend towards north at 3.5 arcmin from the position of the host galaxy.

– The radio jet is inclined by $\sim 70^\circ$ with respect to the radio-tail direction. This indicates that projection effects are important in the radio jets, in particular the host galaxy velocity does not seem to be perpendicular to the projected radio jets.

– The spectral structure in NGC 4869 across 300 MHz and 500 MHz shows the presence of a clear steep-spectrum sheath on a flat-spectrum radio spine (Feretti et al. 1990).

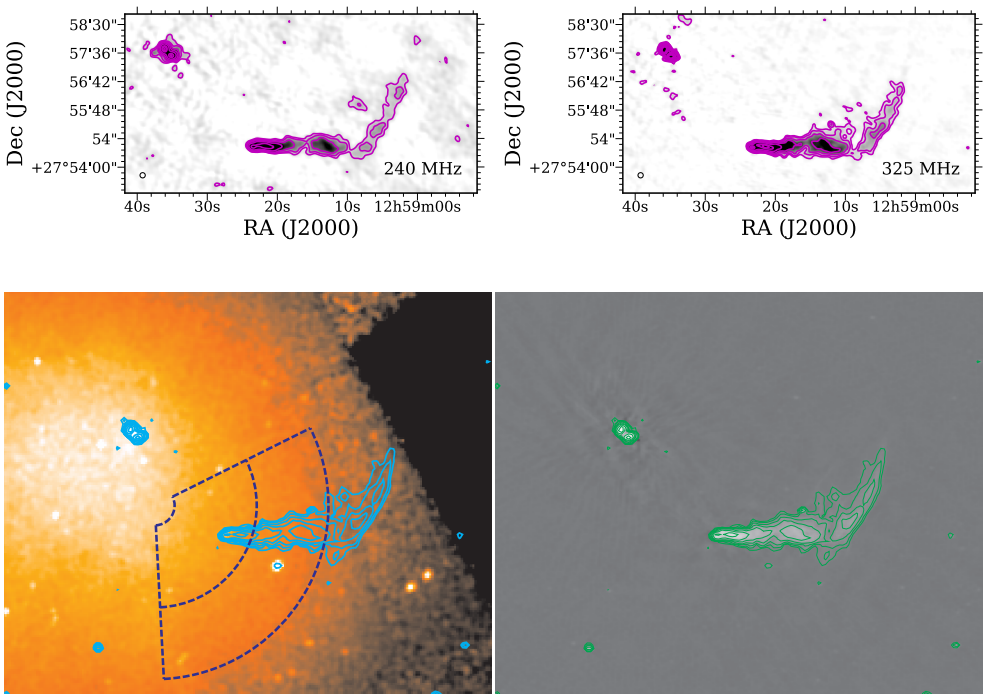

Figure 1. GMRT images of NGC 4869 at 240 MHz (upper left-panel) and 325 MHz (upper right-panel). The broadband X-ray flux image, showing the presence of several surface brightness edges (lower left-panel) with the blue contours from the radio image at 300–500 MHz band using the upgraded GMRT (lower right-panel, Gupta et al. 2017).

– Fig. 1 (lower left-panel) shows the presence of a surface brightness edge, exactly at the location where the collimated radio jet has bent.

Interpretation Hydrodynamic simulations (Loken et al. 1995) of the motion of radio galaxies through the hot intra-cluster gas show that a Kelvin-Helmholtz instability develops at the interface between the moving radio source and the surface-brightness edge in the gas. This suggests that host galaxies always retain their gas in their motion through the intra-cluster gas and thus always exhibit a large drag at the location where they cross the surface brightness edge, causing a straight, collimated radio jet to flare. Alternatively, the bend of the jets occurs at the transition surface of the inter-stellar and inter-galactic medium. Furthermore, since the distance from the core is small, ∼3 kpc, the amount of inter-stellar medium in the galaxy is small; suggesting that a gas stripping mechanism on this galaxy must be at play (Livio et al. 1980).

References

Feretti, L., Dallacasa, D., Giovannini, G., & Venturi, T. 1990, *A&A*, 232, 337
Gupta, Y., Ajithkumar, B., Kale, H. S., et al. 2017, *Current Science*, 113, 707
Livio, M., Regev, O., & Shaviv, G. 1980, *ApJL*, 240, L83
Loken, C., Roettiger, K., Burns, J. O., & Norman, M. 1995, *ApJ*, 445, 80
Venturi, T., Giovannini, G., & Feretti, L. 1990, *AJ*, 99, 1381

Astronomy in Focus, Volume 1
XXXth IAU General Assembly, August 2018
Volker Beckmann & Claudio Ricci, eds.

DOI: 00.0000/X000000000000000X

Radio Properties of AGN in the GAMA 23 Field

Denis Leahy[1] and the ASKAP and GAMA collaborations

[1]Dept. of Physics & Astronomy, University of Calgary, Calgary, Canada
email: leahy@ucalgary.ca

Abstract. The GAMA 23 Field, a region of about 6 degrees by 7degrees, was observed by the Australia Square Kilometer Array Pathfinder (ASKAP) during its commissioning phase. We utilize the radio data from ASKAP in conjuntion with the optical data from the GAMA survey, and infrared data from the WISE survey to investigate the properties of AGN over this large field. A number of well-known properties of the AGN population are confirmed but we find some new properties because of the large area and sensitivity of the radio and optical data, which allows low mass galaxies to be identified out to a redshift of about 0.5.

Keywords. galaxies: general, radio continuum: galaxies, galaxies: active

1. Summary

We have observed the G23 field of the Galaxy And Mass Assembly (GAMA) survey using the Australian Square Kilometre Array Pathfinder (ASKAP) in its commissioning

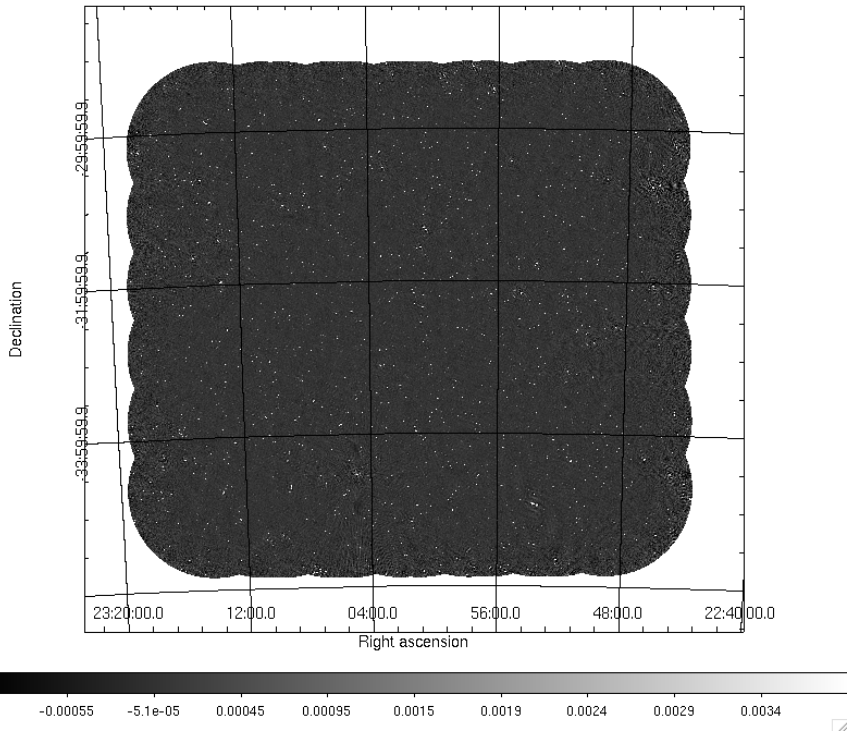

Figure 1. ASKAP image of the GAMA 23 field at 936 MHz.

phase, to validate the performance of the telescope and to characterize the detected galaxy and radio galaxy populations. This observation covers ∼48 square degrees with synthesized beam of 32.7" by 17.8" at 936 MHz, and ∼39 square degrees with synthesized beam of 15.8" by 12.0" at 1320 MHz. Figure 1 shows the 936 MHz image. At 1320 MHz ∼3600 radio sources are detected and at 936 MHz, ∼5800 radio sources are detected. At both frequencies, the RMS (root-mean-square) noise is ≃0.1 mJy/beam. Figure 2 shows a close up image of one region illustrating the image quality.

We combine these radio observations with the GAMA galaxy data, which includes spectroscopy of galaxies that are i-band selected with a magnitude limit of 19.2.Wide-field Infrared Survey Explorer (WISE) infrared photometry is used to determine which galaxies host an active galactic nucleus (AGN). We compare redshifts and stellar masses for galaxies with and without radio counterparts and for different categories of galaxies based on their optical emission and absorption lines. Optical line and infrared colour diagnostic are used to distinguish AGN from star forming galaxies (SFG), but we find that the different methods disagree on the classification for many galaxies. We find that AGN and radio-emitting galaxies have higher stellar mass and luminosity in infrared, optical and UV than other galaxies. Radio-emitting galaxies are more likely (∼6%) to have an AGN than normal galaxies (∼1%), but the majority of AGN are not detected in radio at this sensitivity. Details of this work are given in Leahy et al. (2018).

References

Leahy, D., Hopkins, A.M, Norris, R.P., et al. 2018, *MNRAS*, submitted

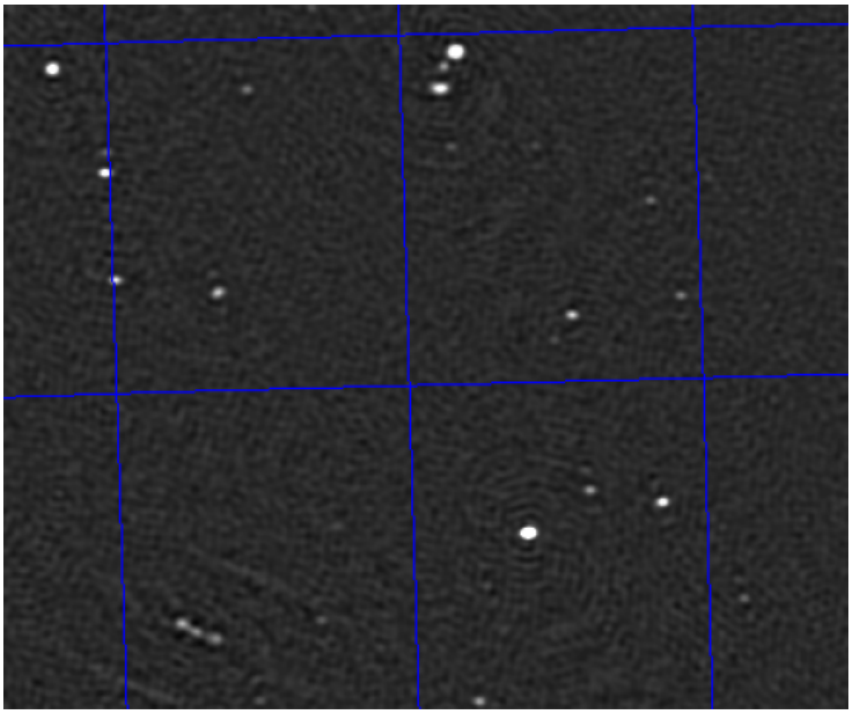

Figure 2. Image of a small region at 1320 MHz with single, double and triple radio sources. The grid spacing is 0.2 degrees in R.A. and in Dec.

Astronomy in Focus, Volume 1
XXXth IAU General Assembly, August 2018
Volker Beckmann & Claudio Ricci, eds.

DOI: 00.0000/X000000000000000X

The radio-loud fraction of high-z low-luminosity Subaru/HSC quasars

Kianhong Lee[1], Kotaro Kohno[1], Yoshiki Matsuoka[2], Tohru Nagao[2], Bunyo Hatsukade[1], Hideki Umehata[3], Takuma Izumi[4], Malte Schramm[4], Yoshiki Toba[5,6], Takuji Yamashita[2], Chien-Hsiu Lee[7,8], Masafusa Onoue[4,9,10], Kazushi Iwasawa[11], Masatoshi Imanishi[4,9], Toshihiro Kawaguchi[12] and Michael A. Strauss[13]

[1]Institute of Astronomy, The University of Tokyo, Mitaka, Tokyo 181-0015, Japan
email: cflee@ioa.s.u-tokyo.ac.jp

[2]Research Center for Space and Cosmic Evolution, Ehime University, Matsuyama, Ehime 790-8577, Japan

[3]RIKEN Cluster for Pioneering Research, 2-1 Hirosawa, Wako-shi, Saitama 351-0198, Japan

[4]National Astronomical Observatory of Japan, Mitaka, Tokyo 181-8588, Japan

[5]Department of Astronomy, Kyoto University, Sakyo-ku, Kyoto, Kyoto 606-8502, Japan

[6]Institute of Astronomy and Astrophysics, Academia Sinica, Taipei, 10617, Taiwan

[7]National Optical Astronomy Observatory, 950 North Cherry Avenue, Tucson, AZ 85719, USA

[8]Subaru Telescope, Hilo, HI 96720, USA

[9]Department of Astronomical Science, Graduate University for Advanced Studies (SOKENDAI), Mitaka, Tokyo 181-8588, Japan

[10]Max Planck Institut für Astronomie, Königstuhl 17, D-69117, Heidelberg, Germany

[11]ICREA and Institut de Ciències del Cosmos, Universitat de Barcelona, IEEC-UB, Martí i Franquès, 1, 08028 Barcelona, Spain

[12]Department of Economics, Management and Information Science, Onomichi City University, Onomichi, Hiroshima 722-8506, Japan

[13]Princeton University Observatory, Peyton Hall, Princeton, NJ 08544, USA

Abstract. We conducted JVLA 1.4 GHz observations of 22 low-luminosity (rest-frame ultraviolet luminosity $M_{1450} > -25$ mag) quasars at $z \sim 6$ discovered with Subaru/HSC, which are more representative compared to the known luminous quasars at similar redshifts. With a typical sensitivity of $\sim 10 - 50$ μJy (1σ), we constrain 20 of 22 quasars' radio-loudness to $R < 100$, and the stacked image ($1\sigma \sim 7\mu$Jy) implies a lower radio-loud fraction of this sample compared with luminous quasars at $z \sim 6$.

Keywords. radio continuum: galaxies, galaxies: high-redshift, quasars: general

1. Introduction

In spite of the fact that quasars are historically discovered due to their strong radio emission, only about $10\% - 20\%$ of quasars show such feature and have been classified as 'radio-loud' (e.g., Ivezić et al. 2002). To understand the physical origins of this dichotomy, people tried to figure out whether there is any differential evolution between these two populations by studying the radio-loud fraction of quasars. In the local or lower redshift universe, some studies showed that the radio-loud fraction tend to depend on both the redshift and the optical luminosity (e.g., Jiang et al. 2007), while it has been argued that the result is biased by the apparent magnitudes (Kratzer & Richards 2015). Such potential bias can become more significant at higher redshifts, and in fact, the previous study

of radio-loudness of high-z ($z > 5.5$) quasars (Bañados et al. 2015) is focused on the very luminous ones which likely host heavy super-massive black holes (SMBHs) (Izumi et al. 2018). However, recently, a sample of high-z ($z \sim 6$) low-luminosity quasars is discovered by the Subaru High-z Exploration of Low-Luminosity Quasars (SHELLQs; Matsuoka et al. 2016) project with the Hyper Suprime-Cam (HSC) on Subaru 8-m telescope. Most of these newly discovered quasars have lower rest-frame ultraviolet luminosity ($M_{1450} > -25$ mag) and thus fall near the break of the quasar luminosity function at $z \sim 6$, which means that their properties are more representative compared to the known luminous ones in the early universe. We checked the FIRST survey data (Becker et al. 1995) and found no detections at their optical positions.

2. Observations and results

We conducted the radio follow-up observations of SHELLQs quasars with JVLA at L-band (1.4 GHz). 22 targets were observed during 18A semester (project code: VLA/18A-316, PI: K. Lee) from March to June 2018. Data reduction was carried out with CASA (McMullin et al. 2007) version 5.3.0 by using the standard VLA pipeline and imaging with the task `CLEAN`. The synthesized beam is $\sim 2''$ and the rms noise is ranging from $\sim 10 - 50$ μJy beam^{-1}.

Given the assumption of the spectral indices (radio: -0.75; optical: -0.5), we adopt the conventional definition of radio-loudness which is the radio/optical flux density ratio, $R = f_{\nu,5\mathrm{GHz}}/f_{\nu,4400\mathrm{A}}$ (Kellermann et al. 1989), and thus constrain 20 of 22 SHELLQs quasars to $R < 100$ (3σ). The rms noise of stacked image is only $\sim 7\mu$Jy which is close to the boundary between radio-loud and radio-quiet, $R = 10$ (Fig. 1). This may imply a lower radio-loud fraction of normal quasars than luminous ones in the early universe (Bañados et al. 2015).

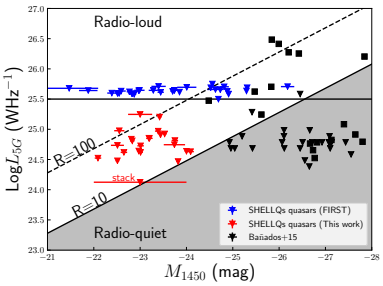

Figure 1. Rest-frame 5 GHz luminosity versus 1450 Å absolute magnitude for SHELLQs quasars (Blue for the FIRST survey and red for this work) and luminous quasars in Bañados et al. 2015 (Black). The downward triangle symbols represent the 3σ upper limit of the rest-frame 5 GHz luminosity and the square symbols represent the detections. The dashed lines indicate the R of 100 and 10. The horizontal black line located at Log$L_{5G} = 25.5$ (WHz^{-1}) indicates the absolute division of radio-loud and radio-quiet quasars employed by Jiang et al. (2007).

References

Bañados, E., Venemans, B. P., Morganson, E., et al. 2015, *ApJ*, 804, 118
Becker, R. H., White, R. L., & Helfand, D. J. 1995, *ApJ*, 450, 559
Ivezić, Ž., Menou, K., Knapp, G. R., et al. 2002, *AJ*, 124, 2364
Izumi, T., Masafusa, O., Shirakata, H., et al. 2018, *PASJ*, 70, 36
Jiang, L., Fan, X., Ivezić, Ž., et al. 2007, *ApJ*, 656, 680
Kellermann, K. I., Sramek, R., Schmidt, M., Shaffer, D. B., & Green, R. 1989, *AJ*, 98, 1195
Kratzer, R. M., & Richards, G. T. 2015, *AJ*, 149, 61
Matsuoka, Y., Onoue, M., Kashikawa, N., et al. 2016, *ApJ*, 828, 26
McMullin, J. P., Waters, B., Schiebel, D., Young, W., & Golap, K. 2007, *Astronomical Data Analysis Software and Systems XVI*, 376, 127

Astronomy in Focus, Volume 1
XXXth IAU General Assembly, August 2018
Volker Beckmann & Claudio Ricci, eds.

DOI: 00.0000/X000000000000000X

A New Generation of AGN Feedback Models in Simulations of the Turbulent Intracluster Medium

Yinghe Lü[1]and Paul M. Ricker[2]

Dept. of Astronomy, University of Illinois,
Urbana, Illinois, 61801, USA
email: ylv4@illinois.edu

Abstract. We propose a new model to treat AGN feedback in hydrodynamical simulations of an isolated cluster environment. Under the new model we perform a set of kiloparsec scale simulations with the numerical code FLASH to study the interaction of AGN jets and driven turbulence in the intracluster medium. We aim to determine the amount of turbulence produced by jet feedback versus other sources and whether it can help regulate accretion and feedback. Our analysis shows that precessing jets coupled with strong turbulent driving can enhance accretion onto the SMBH and thus affect the feedback process.

Keywords. hydrodynamics, turbulence, galaxies: clusters: general, galaxies: jets

1. Introduction

Observations have shown that the cold gas formation rate at the centers of some galaxy clusters is much smaller than expected based on X-ray luminosity, a discrepancy called the 'cool-core problem' (Peterson et al. 2003). Active galactic nuclei (AGNs) are considered to be a major feedback source that prevents the hot gas from cooling and reduces star formation (Sijacki et al. 2007). However, with the large range of spatial and temporal scales involved in the problem, feedback models are usually included via a phenomenological prescription, using relatively arbitrary parameters and little information about black hole accretion physics. Often, they fail to capture the actual interplay between cooling and feedback, and variation of these parameters can lead to strong differences in feedback power and energy propagation (Yang et al. 2012).

To improve the AGN feedback modeling, we have developed a new technique to incorporate AGN feedback in numerical simulations which includes more realistic prescriptions for accretion, the jet and its interaction with turbulent ICM, and radiative cooling. With the new model we carried out several small-box (kiloparsec scale) simulations and addressed questions concerning the details of the AGN feedback process, especially how the feedback energy is deposited into the ICM. The results and subsequent findings will be valuable in translating our subgrid model into one suitable for the coarser resolutions achievable in cosmological simulations.

2. The Simulation

The Sink Particle Model . Sink particles are commonly used in star formation simulations to solve the problem of large scale differences, which introduce regions of flow that accrete incoming material but have no internal structure on resolved scales. Following a similar methodology, in our model we calculate accretion rate using the flux across a spherical control surface. Picking N random points on the surface, we can sum the mass flow at these points. We remove the accreted gas from the grid to avoid the development of back pressure using a normalized weighting kernel. After the accretion rate is calculated, we reset the density and pressure within this region using the kernel.

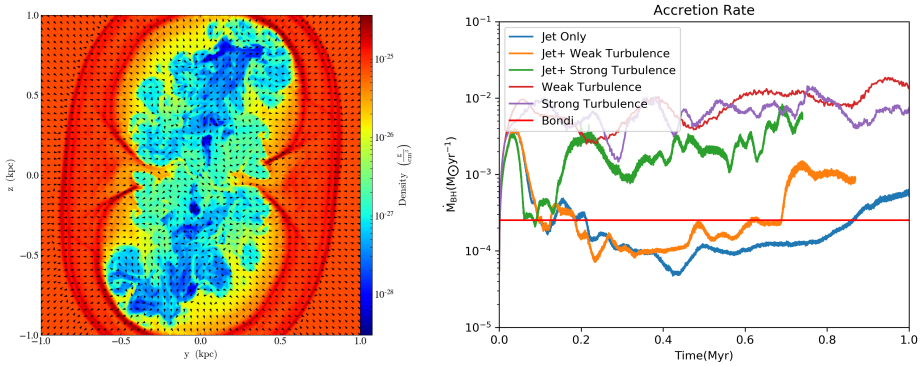

Figure 1. Left: density slices for a simulation with precessing jets in turbulence-driven ICM. Here we use precessing angle $\theta = 10^{\circ}$ and precessing period P = 1 Myr. Right: accretion rate onto the black hole with varying turbulent driving and precessing jet feedback, here weak turbulence has a turbulence velocity of 50 km/s while strong turbulence 150 km/s.

Driving Turbulence in the ICM. We initialize the grid with a uniform gas having quantities that resemble the Perseus cluster (Fabian et al. 2006). The ICM is treated as fully ionized gas with an adiabatic equation of state. We impose turbulent stirring that follows a Kolmogorov-like spectrum by adding a divergence-free, time-correlated velocity evolved by an Ornstein-Uhlenbeck (OU) random process (Uhlenbeck & Ornstein 1930). We use recent Hitomi observations (Hitomi collaboration et al. 2018), which provide direct measurement of turbulent velocities, to set our stirring energy.

Jet Feedback . We performed three-dimensional hydrodynamic simulations with radiative cooling and AGN feedback in a 2 kpc box using the adaptive mesh refinement (AMR) code FLASH 4 (Fryxell et al. 2000). The supermassive black hole is placed at the center of the grid, while the jet model is implemented by treating injection rates of mass, momentum and energy onto the grid as source terms in the hydrodynamic equations. Precessing jets are launched from a cylinder with a window function and the direction of the cylinder precesses about the grid z-axis. Feedback from the jet is both thermal and kinetic.

3. Interaction of Jets with the Turbulent ICM

We have performed preliminary runs with stationary and precessing jets as well as without turbulence, and with weak or strong turbulence that corresponds to different turbulent velocity dispersion values. An example is shown in Figure 1. While turbulent driving itself enhances the kinetic energy of the ICM and triggers accretion, we see that with precessing jets, the gas is primarily blown away and cavity-like structures are formed. However, with strong turbulence, the accretion process is enhanced, and more energy is thus deposited in the ICM. In summary, coupling between precessing jets and turbulent driving helps to regulate AGN feedback. Further discussion will be present in a paper in preparation.

References

Peterson, J. R., Kahn, S. M., Paerels, F. B. S., et al. 2003, *ApJ*, 590, 207
Sijacki, D., Springel, V., Di Matteo, T. & Hernquist, L. 2007, *MNRAS*, 380, 877
Yang, H. Y. K., Sutter, P. M., & Ricker, P. M. 2012, *MNRAS*, 427, 1614
Fryxell, B., Olson, K., Ricker, P., et al. 2000, *ApJS*, 131, 273
Uhlenbeck, G. E., & Ornstein, L. S., 1930, *Phys. Rev.*, 36, 823
Fabian, A. C., Sanders, J. S., Taylor, G. B., et al. 2006, *MNRAS*, 366, 417
Hitomi Collaboration, et al. 2018, *PASJ*, 70.2, 9

Astronomy in Focus, Volume 1
XXXth IAU General Assembly, August 2018
Volker Beckmann & Claudio Ricci, eds.

DOI: 00.0000/X000000000000000X

The mass-metallicity relation of high-z type-2 AGNs

Kenta Matsuoka[1,2,3], Tohru Nagao[3], Alessandro Marconi[1,2], Roberto Maiolino[4,5], Filippo Mannucci[2], Giovanni Cresci[2], Koki Terao[3] and Hiroyuki Ikeda[6]

[1]Dipartimento di Fisica e Astronomia, Universitá degli Studi di Firenze, Via G. Sansone 1, I-50019 Sesto Fiorentino, Italy

[2]INAF – Osservatorio Astrofisico di Arcetri, Largo Enrico Fermi 5, I-50125 Firenze, Italy

[3]Research Center for Space and Cosmic Evolution, Ehime University, 2-5 Bunkyo-cho, Matsuyama 790-8577, Japan
email: matsuoka@arcetri.astro.it

[4]Cavendish Laboratory, University of Cambridge, 19 J. J. Thomson Avenue, Cambridge CB3 0HE, UK

[5]Kavli Institute for Cosmology, University of Cambridge, Madingley Road, Cambridge CB3 0HA, UK

[6]National Astronomical Observatory of Japan (NAOJ), 2-21-1 Osawa, Mitaka, Tokyo 181-8588, Japan

Abstract. The mass-metallicity relation (MZR) of type-2 active galactic nuclei (AGNs) at $1.2 < z < 4.0$ is investigated by using high-z radio galaxies (HzRGs) and X-ray selected radio-quiet AGNs. We focus on rest-frame ultraviolet (UV) emission lines, i.e., C IVλ1549, He IIλ1640, and C III]λ1909, of a sample of 11 HzRGs and four additional X-ray selected type-2 AGNs, whose host stellar masses have been estimated in literature. We divided our sample in three stellar mass bins and estimated their averaged gas metallicities in the narrow-line region (NLR) by using the emission lines. In the results, we found that there is a positive correlation between NLR metallicities and stellar masses of type-2 AGNs at $z \sim 3$. This is the first indication that AGN metallicities are related to their hosts, i.e., stellar mass (see Matsuoka et al. 2018).

Keywords. galaxies: active – galaxies: evolution – quasars: emission lines – quasars: general

1. Introduction

Metallicity provides one of the most important clues in understanding galaxy formation and evolution since metal formation and enrichment are closely connected with the past star formation history in galaxies. The relationship between mass of galaxies and their metal (the so-called mass-metallicity relation, MZR) has been investigated for about forty years not only for local galaxies (e.g., Lequeux et al. 1979; Tremonti et al. 2004) but in high-redshift, up to $z \sim 3$, universe (e.g., Maiolino et al. 2008; Mannucci et al. 2009), and a clear evolution with cosmological time has been reported. However, since the emission lines for the metallicity diagnostics shift out of the K-band atmospheric window for galaxies at $z > 3.5$, studies are more challenging for higher-z galaxies requiring space-based spectrograph. An alternative approach to investigate the metallicity in the early universe is to focus on active galactic nuclei (AGNs) instead of star-forming galaxies. Thanks to their high luminosity and strong emission lines in the wide wavelength range from the ultraviolet (UV) to the infrared, it is possible to measure the metallicity even in high-z universe. Especially, to investigate the metallicity on the scale of AGN host galaxies, the narrow line region (NLR) has been studied (e.g., Matsuoka et al. 2009),

since the typical NLR size is comparable to their hosts. In this study, we focus on 11 high-z radio galaxies (HzRGs) and four X-ray selected type-2 AGNs at $1.2 < z < 4.0$, whose UV emission lines of C IVλ1549, He IIλ1640, and C III]λ1909 have been detected. By collecting their stellar masses ($M_\star$) derived by spectral energy distribution fits in the recent literature, we divided our sample in three stellar mass bins and estimated their averaged NLR metallicities by adopting a diagnostic diagram of C IVλ1549/He IIλ1640 and C III]λ1909/C IVλ1549 (see Nagao et al. 2006 for more details).

2. Result and Discussion

The left-top panel in Figure 1 shows $M_\star$-averaged emission-line flux ratios of our sample on the diagnostic diagrams. Comparing photoionization model predictions (shown as grid lines) with these flux ratios we estimated mean NLR metallicities ($Z_{\rm NLR}$) for each stellar mass bin. In the result, we found there is a positive correlation between NLR metallicities and stellar masses of type-2 AGNs (see the left-bottom panel). This is the first direct evidence that AGN metallicities are related to their host properties. Moreover, we found that the MZR of type-2 AGNs are compatible with that of star-forming galaxies at similar redshifts (see the right-hand panel), indicating that NLR metallicity is connected with host metallicities (see Matsuoka et al. 2018 for more details).

References

Lequeux, J., Peimbert, M., Rayo, J. F., et al. 1979, *A&A*, 80, 155
Maiolino, R., Nagao, T., Grazian, A., et al. 2008, *A&A*, 488, 463
Mannucci, F., Cresci, G., Maiolino, R., et al. 2009, *MNRAS*, 398, 1915
Matsuoka, K., Nagao, T., Maiolino, R., et al. 2009, *A&A*, 503, 721
Matsuoka, K., Nagao, T., Marconi, A., et al. 2018, *A&A*, 616, L4
Nagao, T., Maiolino, R., & Marconi, A. 2006, *A&A*, 447, 863
Tremonti, C. A., Heckman, T. M., Kauffmann, G., et al. 2004, *ApJ*, 613, 898

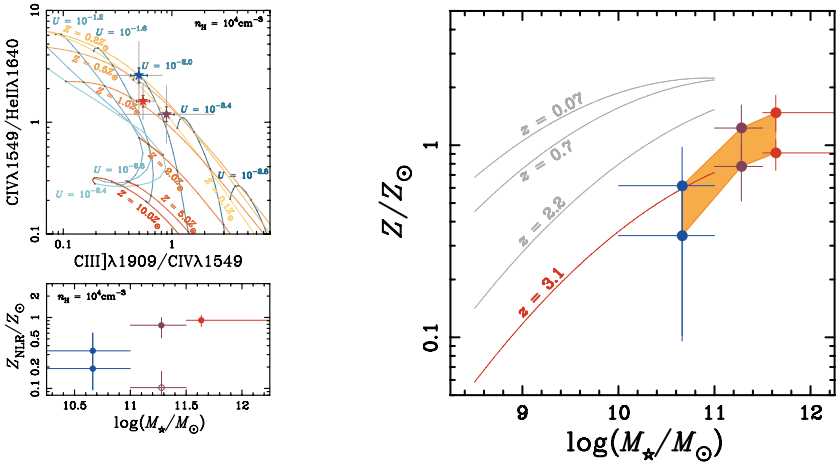

Figure 1. Averaged emission-line flux ratios of low (blue), middle (purple), and high (red) mass subsamples plotted on the diagnostic diagram (*left-top* panel). Constant metallicity and constant ionization parameter sequences are denoted by orange and blue solid lines, respectively. The *left-bottom* panel shows the NLR metallicities as a function of stellar masses, estimated with $\log n_{\rm H} = 4$. Open circle would be a less-likely solution. The *right-hand* panel shows the mass-metallicity relation of type-2 AGNs at $z \sim 3$ comparing with MZR of star-forming galaxies at $z = 0.07$, 0.7, 2.2, and 3.1 in Mannucci et al. (2009). Filled circles denote our type-2 AGNs with metallicity estimates with plausible $n_{\rm H}$ models, i.e., $\log n_{\rm H} = 4$ and 5.

Astronomy in Focus, Volume 1
XXXth IAU General Assembly, August 2018
Volker Beckmann & Claudio Ricci, eds.

DOI: 00.0000/X000000000000000X

Morphological study of a large sample of extragalactic radio sources for revelation of radio jets

A. M. Mickaelian, H. V. Abrahamyan, G. A. Mikayelyan, and G. M. Paronyan

NAS RA V. Ambartsumian Byurakan Astrophysical Observatory (BAO), Byurakan 0213, Aragatzotn Province, Armenia
email: aregmick@yahoo.com

Abstract. With an improved cross-correlation technique, we have matched two largest radio catalogs at 1.4 GHz (21 cm), NVSS and FIRST to improve positions and photometry, to reveal radio variability and check with optical variability, to study the radio structure and optical morphology of sources, to classify radio sources into FRI and FRII types, and to reveal jets and additional features.

Keywords. surveys – catalogs – galaxies: active – quasars: general – radio continuum: galaxies.

1. Introduction

The most powerful extragalactic sources of radio waves are double-lobed sources (or dumbbells) in which two large regions of radio emission are situated in a line on diametrically opposite sides of an optical galaxy. The parent galaxy is usually a giant elliptical, sometimes with evidence of recent interaction. The classic example is Cygnus A, the strongest radio source in the direction of the constellation Cygnus. Cygnus A was once thought to be two galaxies of comparable size in collision, but more recent ideas suggest that it is a giant elliptical whose body is bifurcated by a dust lane from a spiral galaxy that it recently swallowed. The collisional hypothesis in its original form was abandoned because of the enormous energies found to be needed to explain the radio emission.

2. Cross-correlation of NVSS and FIRST

NVSS (Condon et al. 1998) contains 1,773,484 sources and FIRST (Helfand et al. 2015) contains 946,432 sources and have better positional and photometric accuracy (5 arcsec and 1 mJy, respectively). As a preliminary result, we obtained 556,282 common sources. 6301 of them show obvious signs of variability having >50 mJy differences between fluxes in NVSS and FIRST. For these sources we have made multiwavelength (MW) investigations in all wavelength ranges aimed at finding relations between the radiation fluxes in different bands for different types of sources (blazars, QSOs, other AGN, and starbursts).

Table 1. NVSS and FIRST catalogues

Catalogues	Year	Coverage	Number of sources
NVSS	1998	82% of the celestial sphere	1,773,484
FIRST	2015	10,575 deg^2	946,432

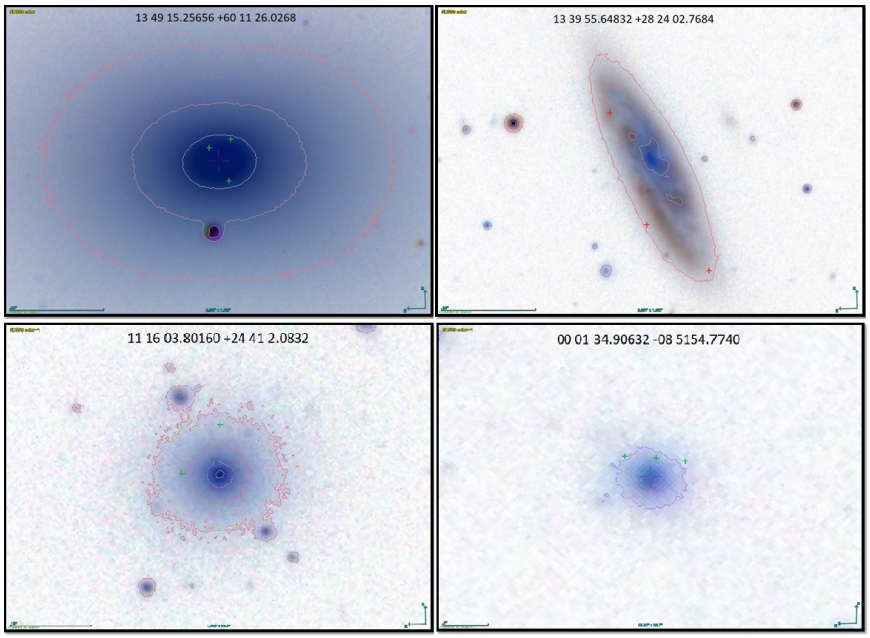

Figure 1. Radio sources associated with galaxies in optical image with overlapped radio contours.

3. Sources with several radio and optical components

Another possibility that appeared after having cross-correlated NVSS/FIRST sources, is the study of radio morphology. Given that FIRST resolution is higher, very often we have 2-4 FIRST associations within 30 arcsec corresponding to 1 NVSS source. In such cases the central source is considered as the core, and 2 farther bright sources are considered as radio lobes. Depending on the flux ratio of the central source and the lobes, we have preliminarily classified sources to FRI and FRII. On the other hand, the 4th component, when available, may be regarded as a jet, and very often it appears not far from the core. We match these results with radio contours to verify candidate jets, as well as we check these sources for radio variability. We identify NVSS/FIRST sources having 4 FIRST components and radio variability, a highly reliable sample for revelation of radio jets.

References

Condon, J. J., Cotton, W. D., Greisen, E. W., et al. 1998, *AJ*, 115, 1693
Helfand, D. J., White, R. L., & Becker, R. H. 2015, *ApJ*, 801, 26

Astronomy in Focus, Volume 1
XXXth IAU General Assembly, August 2018
Volker Beckmann & Claudio Ricci, eds.

DOI: 00.0000/X000000000000000X

The parsec-scale structure of jet-driven H I outflows in radio galaxies

Raffaella Morganti[1,2], Robert Schulz[1], Kristina Nyland[3], Zsolt Paragi[4], Tom Oosterloo[1,2], Elizabeth Mahony[5], and Suma Murthy[1,2]

[1]ASTRON, the Netherlands Institute for Radio Astronomy, Oude Hoogeveensedijk 4, 7991 PD Dwingeloo, The Netherlands. email: morganti@astron.nl

[2]Kapteyn Astronomical Institute, University of Groningen, P.O. Box 800, 9700 AV Groningen, The Netherlands;
[3] National Radio Astronomy Observatory, Charlottesville, VA 22903, USA;
[4] Joint Institute for VLBI ERIC, Oude Hoogeveensedijk 4, 7991 PD Dwingeloo, Netherlands;
[5] CSIRO Astronomy and Space Science, PO Box 76, Epping NSW 1710, Australia

Abstract. Radio jets can play multiple roles in the feedback loop by regulating the accretion of the gas, by enhancing gas turbulence, and by driving gas outflows. Numerical simulations are beginning to make detailed predictions about these processes. Using high resolution VLBI observations we test these predictions by studying how radio jets of different power and in different phases of evolution affect the properties and kinematics of the surrounding H I gas. Consistent with predictions, we find that young (or recently restarted) radio jets have stronger impact as shown by the presence of H I outflows. The outflowing medium is clumpy with clouds of with sizes up to a few tens of pc and mass $\sim 10^4 M_\odot$) already in the region close to the nucleus (< 100 pc), making the jet interact strongly and shock the surrounding gas. We present a case of a low-power jet where, as suggested by the simulations, the injection of energy may produce an increase in the turbulence of the medium instead of an outflow.

Keywords. ISM: jets and outflows, radio lines: galaxies, galaxies: active

---

The impact of active galactic nuclei (AGN) on the surrounding medium can be due to either winds and radiation from the nuclear region, or to plasma jets. Both these mechanisms are known to play a role and, depending on the situations and on the physical conditions, one can dominate via a strong coupling with the surrounding medium (e.g. Cielo et al. 2018). However, quantifying the actual impact of these phenomena is still a challenging task. Radio jets play a particularly important role in the feedback process, providing the best examples of AGN-driven feedback seen in action by preventing the cooling of the X-ray gas on cluster scales. However, radio jets can also provide an effective mechanism on *galaxy scales*. Their impact manifests itself in different ways: by counterbalancing the cooling of the hot coronae present around even isolated galaxies (e.g. Croston et al. 2008; Ogorzalek et al. 2017); by driving fast outflows traced by different gas phases or by injecting turbulence in the ISM, e.g. Alatalo et al. (2015), Guillard et al. (2015). All these mechanisms are relevant and need to be quantified.

Particularly interesting are the results from recent numerical simulations (Wagner et al. 2012, Mukherjee et al. 2018a, 2018b, Cielo et al. 2018). These show that radio jets can couple more strongly to the ISM if that is modelled to be clumpy (Wagner et al. 2012). Furthermore, a connection is expected with the cycle of activity of radio galaxies: given their small size, young (and recently restarted) radio jets have the highest impact on the gas. A dependence is also expected with jet power: powerful jets can drive faster outflows while low power jets can be "trapped" for longer times and induce more turbulence in

the galactic ISM (Mukherjee et al. 2018b). Finally, the orientation of the jet with respect to the distribution of gas in the host galaxy is also relevant for the impact of the jet.

AGN-driven and jet-driven outflows are known to be multi-phase and can be traced also by atomic neutral hydrogen. This has opened the possibility to test the impact of plasma jets using radio data and, in particular, 21-cm H I observed in absorption (see Morganti & Oosterloo 2018 for an overview). The advantage of this is that the gas can be traced down to very small scales and the location of the outflow and their properties can be studied. This can be done using (sub-)arcsec down to milli-arcsec data (i.e. down to pc scales) as shown by the global Very Long Baseline Interferometry (VLBI) data described below and obtained by arrays including telescopes from the European VLBI Network, the Very Long Baseline Array (VLBA), as well as Arecibo. The results allow us to investigate not only the impact of radio jets, but also whether the predictions from the simulations are confirmed.

1. Where and how often do we see jet-driven outflows?

Jet-driven outflows are long known from ionised gas, but more recent work has not only shown that also atomic neutral hydrogen (H I) and molecular gas can be associated with these outflows and also that they may carry a significant (possibly the largest) fraction of the outflowing gas mass. The jet-driven origin of outflows of cold gas has been confirmed in a number of cases traced by molecular gas (see e.g. Alatalo et al. 2011, Dasyra et al. 2012, Combes et al. 2013, Morganti et al. 2015, Garcia-Burillo et al. 2014, Oosterloo et al. 2017, Runnoe et al. 2018) and by H I see Morganti & Oosterloo (2018) for a review. The H I outflows have typically velocities between a few hundred to $\sim$1300 $\mathrm{km\,s^{-1}}$.

In addition to this, a relation between the occurrence of H I outflows and the evolutionary status of the radio jet has been found by observations of a relatively large sample (248 objects) presented in Geréb et al. (2015). They find that at least 5% of all sources (15% of H I detections) show H I outflows. These numbers represent lower limits, given that absorption measurements are sensitive only to gas (and outflows) located in front of the radio continuum. Particularly interesting is that the vast majority of the H I outflows are detected in sources with newly born (or reborn) radio jets. This supports the idea that these phases in the evolution are those where the jet has most of its impact on the surrounding medium. This is in agreement with predictions from the simulations of Wagner et al. (2012) and Cielo et al. (2018). The recurrent nature of radio sources (see e.g. Morganti 2017) would ensure that this impact is repeated during the life of the host galaxy. A similar effect was also seen in the ionised gas (see Holt et al. 2008). However,

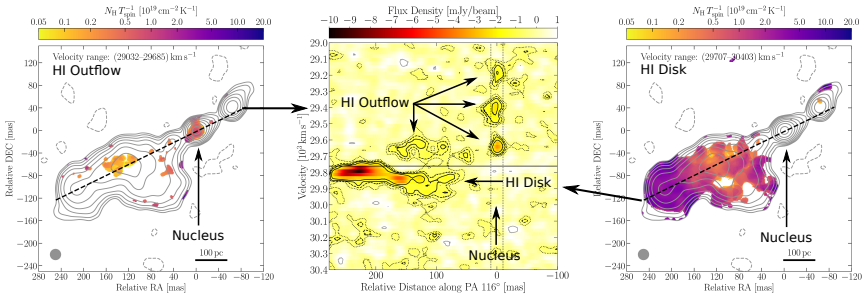

Figure 1. Radio continuum superposed on the H I absorption column density of the H I outflow (left) and of the H I disk (right) of the radio galaxy 3C236 obtained with VLBI. Position-velocity plot (centre) along the jet showing the outflowing clouds. From Schulz et al. (2018).

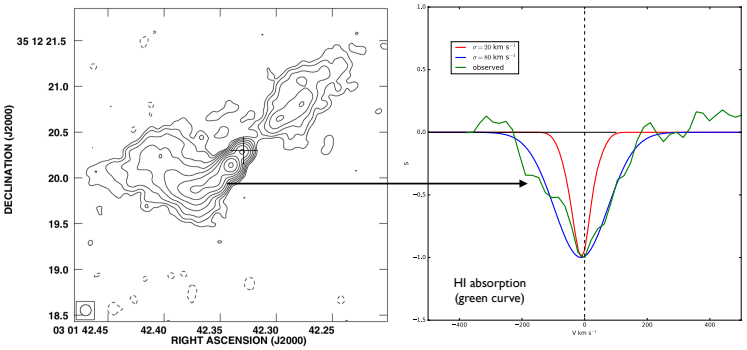

Figure 2. Left: Radio continuum image from Giroletti et al. (2005). **Right:** H I absorption profile (green) from VLA observations with superposed (red) the model from the H I disc observed in emission in this object by Struve et al. (2010) and in blue the model adding a component of turbulence due to the interaction of the jet with the H I in the disk (Murthy et al. in prep).

this phase of the gas was found to show mass outflow rates reaching at most 1 $M_\odot$ yr^{-1}, while mass outflow rates up to 50 $M_\odot$ yr^{-1} have been found for the H I outflows.

2. Do we see the interaction of the jet with a clumpy medium?

For a small number of objects we have used VLBI observations to trace the properties of the H I outflows down to pc scales. The results show that a clumpy distribution of the gas is seen in all observed objects. Fig. 1 illustrates the distribution of H I absorption in the central region of the restarted radio galaxy 3C 236, Schulz et al. (2018). Interestingly, in this and other targets observed so far, fast outflowing clouds (many hundred km s^{-1}) are detected already in the very inner region, at distances $< 50 - 100$ pc from the core. The clouds have masses of a few $\times 10^4$ $M_\odot$, and are unresolved on VLBI scales (< 40 pc). The presence of a clumpy medium (see also Oosterloo et al. 2017) is of key importance and confirms the prediction of the numerical simulations. A clumpy medium can make the impact of the jet much larger than previously considered: because of the clumpiness of the medium, the jet is meandering through the ISM to find the path of minimum resistance and so creating an overpressured cocoon of outflowing and shocked gas, as suggested by Wagner et al. (2012), Mukherjee et al. (2018a).

Furthermore, for the smaller (and perhaps younger) sources in the sample (4C 12.50, Morganti et al. 2013 and 4C 52.37, Schulz et al. in prep) the VLBI observations not only spatially resolve the outflows, but they also recover all the H I flux observed at low resolution. This suggests that these outflows are mostly made up by relatively compact structures, easy to be detected at the very high resolution of VLBI observations. In the largest (and likely more evolved) sources, like 3C 293 (Schulz et al. in prep) and 3C 236 (Schulz et al. 2018), we also find evidence of a clumpy structure but the H I outflows in these sources are only partly recovered by VLBI. This suggests the additional presence of a diffuse component in which the clumps are embedded. This could be due to the expansion of the jet in the medium changing the structure of the outflows, the fraction of diffuse component increasing with time.

3. Do the low power jets have also an impact?

Interestingly, a growing number of cases (among which some listed above e.g. NGC1433, IC 5063, NGC1068, PG1700+518) show that, despite being classified as *radio quiet*, the

power of the jet is sufficient to be the driving mechanism of their outflows. However, the simulations also show that an other effect expected from low power jets (Mukherjee et al. 2018b) is to increase the turbulence of the gas. Figure 2 shows the H I absorption detected against the kpc-scale jet of the low-luminosity radio source B2 0258+35. The width of the absorption ($\sim$ 400 km s^{-1}) is too large to be explained by the rotation of the large scale H I disk known to be present in this object. The most likely hypothesis is that the jet enters the disk and, being trapped there, disturbs the kinematics of the gas without being able to produce a fast outflow, but injects energy increases the turbulence of the gas (Murthy et al. in prep). As already suggested for the low-power radio source NGC 1266 (Alatalo et al. 2015), jet-induced turbulence may play a role in preventing star formation despite the large reservoir of cold gas observed in these objects.

4. Implications

The observations are showing evidence - in a growing number of sources - of interaction between the radio jets and the surrounding ISM. The properties appear to be, to first order, consistent with the predictions from some of the recent numerical simulations. This supports the idea that also on galactic scales the role of radio jets should not be neglected. However, the impact of outflows may not always be as large as required by models of galaxy evolution. A relatively small fraction of the outflowing gas may actually leave the galaxy. This is also seen in more AGN-driven outflows, i.e. those driven by winds or radiation. Thus, the likely main effect of jet-ISM interactions and their injection of energy could be on the redistributing the gas and possibly in keeping it turbulent for longer periods of time. This has been now seen in particular for (much more common) low luminosity radio jets. Thus, in addition to the search for violent processes like outflows, other more subtle effects needs to be searched for and investigated.

References

Alatalo, K., Blitz, L., Young, L. M., et al. 2011, *ApJ*, 735, 88
Alatalo, K., Lacy, M., Lanz, L., et al. 2015, *ApJ*, 798, 31
Cielo, S., Bieri, R., Volonteri, M., Wagner, A. Y., & Dubois, Y. 2018, *MNRAS*, 477, 1336
Combes, F., García-Burillo, S., Casasola, V., et al. 2013, *A&A*, 558, A124
Croston, J. H., Hardcastle, M. J., Kharb, P., Kraft, R. P., & Hota, A. 2008, *ApJ*, 688, 190
Dasyra, K. M., & Combes, F. 2012, *A&A*, 541, L7
García-Burillo, S., Combes, F., Usero, A., et al. 2014, *A&A*, 567, A125
Geréb, K., Maccagni, F. M., Morganti, R., & Oosterloo, T. A. 2015, *A&A*, 575, A44;
Giroletti, M., Giovannini, G., & Taylor, G. B. 2005, *A&A*, 441, 89
Guillard, P., Boulanger, F., Lehnert, M. D., et al. 2015, *A&A*, 574, A32
Holt, J., Tadhunter, C. N., & Morganti, R. 2008, *MNRAS*, 387, 639
Morganti, R., Fogasy, J., Paragi, Z., Oosterloo, T., & Orienti, M. 2013, Science, 341, 1082
Morganti, R., Oosterloo, T., Oonk et al. 2015, *A&A*, 580, A1
Morganti, R. 2017, Nature Astronomy, 1, 596
Morganti, R., & Oosterloo, T. 2018, *A&ARev.* in press,arXiv:1807.01475
Mukherjee, D., Wagner, A. Y., Bicknell, G. V., et al. 2018a, *MNRAS*, 476, 80;
Mukherjee, D., Bicknell, G. V., Wagner, A. Y. et al. 2018b, *MNRAS* , 479, 5544
Ogorzalek, A., Zhuravleva, I., Allen, S. W., et al. 2017, *MNRAS*, 472, 1659
Oosterloo, T., Raymond Oonk, J. B., Morganti, R., et al. 2017, *A&A*, 608, A38
Runnoe, J. C., Gültekin, K., & Rupke, D. S. N. 2018, *ApJ*, 852, 8
Schulz, R., Morganti, R., Nyland, K., et al. 2018, *A&A* in press, arXiv:1806.06653
Struve, C., Oosterloo, T., Sancisi, R., Morganti, R., & Emonts, B. H. C. 2010, *A&A*, 523, A75
Wagner A. Y., Bicknell G. V., Umemura M. 2012, *ApJ*, 757, 136

Astronomy in Focus, Volume 1
XXXth IAU General Assembly, August 2018
Volker Beckmann & Claudio Ricci, eds.

DOI: 00.0000/X000000000000000X

Multi-frequency study of a large sample of double-double radio galaxies

S. Nandi[1], D.J. Saikia[2], R. Roy[2], P. Dabhade[2], Y. Wadadekar[3], J. Larsson[4], M. Baes[5], H.C. Chandola[6] and M. Singh[7]

[1] Indian Institute of Astrophysics, Bangalore 560034, India
email: sumana.nandi@iiap.res.in

[2] Inter-University Centre for Astronomy and Astrophysics (IUCAA), Ganeshkhind, Pune 411007, India

[3] National Centre for Radio Astrophysics, TIFR, Ganeshkhind, Pune 411 007, India

[4] KTH, Department of Physics, and the Oskar Klein Centre, AlbaNova, SE-106 91 Stockholm, Sweden

[5] Sterrenkundig Observatorium, Universiteit Gent, Krijgslaan 281 S9, B-9000 Gent, Belgium

[6] Department of Physics (UGC Centre of Advanced Study), DSB Campus, Kumaun University, Nainital-263001, India

[7] Aryabhatta Research Institute of Observational Sciences (ARIES), Manora Peak, Nainital, 263 129, India

Abstract. Striking examples of episodic jet activity in active galactic nuclei (AGN) are the double-double radio galaxies (DDRGs) with two pairs of lobes emerging from the same central engine. The mechanism for multiple jet activity in DDRGs is still unclear. Several ideas were proposed to explain this phenomenon and the most likely scenario is the merging of the two black holes. The number of DDRGs reported so far is very limited, and it is important to identify more of these to provide a significant statistical overview of the conditions to trigger the jets and the role of jets in terms of feedback mechanisms that affect the host galaxies. A significant number of smaller sized candidate DDRGs have been identified in our recent study. We started low-frequency observation of this sample to confirm that the sources are related to distinct epochs of nuclear activity. For a few sources in this sample, we noticed instability in jet direction. Radio galaxies with a rapid change of jet axis are the prime candidates to detect binary black hole systems. Interestingly, we identified one candidate which shows not only restarted jet activity with an axis reorientation but also generates double-peaked emission lines from the central AGN. The split in emission lines are the possible out come of a bound pair of supermassive black holes, moving with their own characteristic velocity. Here, I will highlight the main results from our observations and discuss on the possible scenarios responsible for the episodic activity in DDRGs.

Keywords. galaxies: active, galaxies: nuclei, galaxies: jets, radio continuum: galaxies

1. Introduction

The best observational confirmations of episodic jet activity in the active galactic nuclei (AGN) are double-double radio galaxies (DDRGs) (Saikia & Jamrozy 2009). In DDRGs the steep-spectrum, diffuse pair of lobes represent the early epoch of jet activity. A new pair of lobes with prominent hotspot form closer to the nucleus and before the old diffuse lobes through the recent jet activity. Usually, in DDRGs two pairs of lobes and the central AGN of are aligned along a common axis and maintain a steadiness in jet direction for both epochs. However, the jet direction of two epochs may not be the same for all DDRGs. The new restarting jet does not follow the previous jet direction in case of misaligned DDRGs. To enlarge the sample of DDRGs we identified 23 new sources

from FIRST (Faint Images of the Radio Sky at Twenty centimeters) survey (Nandi & Saikia 2012). We performed GMRT (Giant Metrewave Radio Telescope) observations for this sample at 610 MHz to confirm their episodic nature. Here we present the results of our GMRT observations.

2. Observational results and discussions

High-sensitivity GMRT observations reveal more diffuse emission for the outer fossil lobes for most of the sources. Three examples are shown in Fig. 1, upper panel. From GMRT images we note that the median value of projected linear size of these DDRGs is $\sim$ 685 kpc. Using GMRT data and available FIRST data we estimated spectral indices for each source. The steeper spectral indices for outer lobes than the inner ones confirm the episodic jet activity in these sources (Nandi et al. 2018). In this sample, we identified two episodic radio loud quasar and three misaligned DDRGs. One quasar J0746+4526, shows significantly red-continuum-dominated optical host spectrum with reddening $E(B-V)_{host} = 0.70\pm0.16$ mag (Nandi et al. 2014). High extinction is often related to massive starbursts and galaxy merger. One of the misaligned DDRGs J1328+2752, shows the axis rotation of new jet of about $\sim$30°. The optical spectrum also shows the double-peaked line profiles for this source (Fig. 1, lower panel). The estimated velocity separation between two components is 235 ± 10.5 kms^{-1}. Inconstancy of jet out flow and double-peaked emission lines give an indication that it is associated with a merging system (Nandi et al. 2017).

References

Nandi, S., Saikia, D. J., Roy, R., et al. 2018, *MNRAS*, (submitted)
Nandi, S., Jamrozy, M., Roy, R., et al. 2017, *MNRAS*, 467, L56
Nandi, S., Roy, R., Saikia, D. J., et al. 2014, *ApJ*, 789, 16
Nandi, S., & Saikia, D. J. 2012, *Bulletin of the Astronomical Society of India*, 40, 121
Saikia, D. J., & Jamrozy, M. 2009, *Bulletin of the Astronomical Society of India*, 37

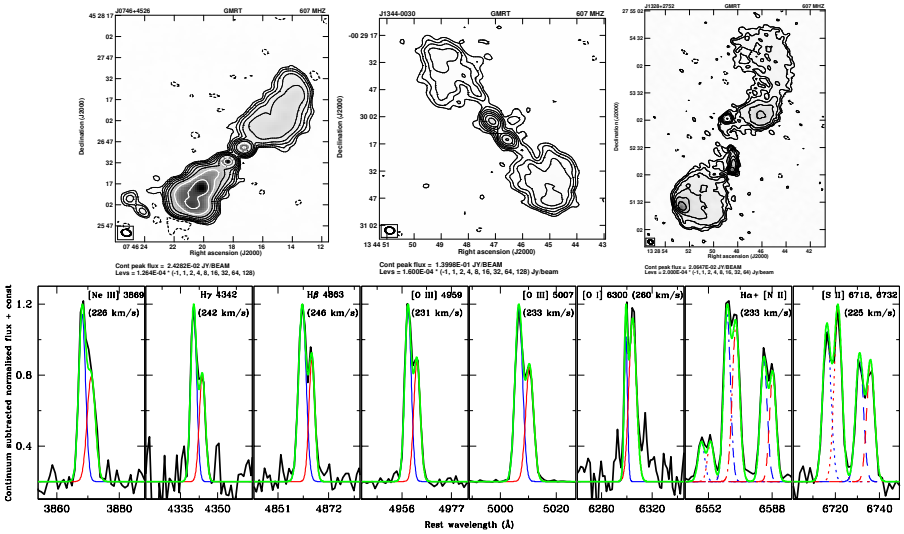

Figure 1. Upper panel: GMRT 610 MHz images of DDRGs. **Lower panel:** The Sloan Digital Sky Survey (SDSS) spectrum of misaligned DDRG J1328+2752.

Astronomy in Focus, Volume 1
XXXth IAU General Assembly, August 2018
Volker Beckmann & Claudio Ricci, eds.

DOI: 00.0000/X000000000000000X

AGN Feedback and its Importance to Galaxy Evolution in the Era of the ngVLA

Kristina Nyland[1]

[1]National Radio Astronomy Observatory
520 Edgemont Rd.
Charlottesville, VA 22903
United States
email: knyland@nrao.edu

Abstract. Energetic feedback by Active Galactic Nuclei (AGN) plays an important evolutionary role in the regulation of star formation (SF) on galactic scales. However, the effects of this feedback as a function of redshift and galaxy properties such as mass, environment and cold gas content remain poorly understood. The broad frequency coverage (1 to 116 GHz), high collecting area (about ten times higher than the Karl G. Jansky Very Large Array), and superb angular resolution (maximum baselines of at least a few hundred km) of the proposed next-generation Very Large Array (ngVLA) are uniquely poised to revolutionize our understanding of AGN and their role in galaxy evolution.

Keywords. galaxies: active, galaxies: jets, galaxies: evolution

1. Introduction

A key missing element in our understanding of cosmic assembly is the nature of energetic feedback from supermassive black holes (SMHBs) and the impact of active galactic nuclei (AGN) on galaxy evolution. Energetic feedback produced by Active Galactic Nuclei (AGN) is believed to play an important role in galaxy evolution through the regulatory effect it may have on the star formation rate and efficiency of the host galaxy. Despite its importance, identifying AGN-driven feedback in action is observationally challenging and requires high sensitivity, high angular resolution, and broad frequency coverage. As a result, large-scale studies of jet-driven AGN feedback using existing radio telescopes, such as the Karl G. Jansky Very Large Array (VLA) and Atacama Large Millimeter and Submillimeter Array (ALMA), have not been feasible. With its unprecedented current reference design consisting of $\sim$214 $\times$ 18m antennas operating from 1 to 116 GHz with baselines out to several hundred km, the next-generation Very Large Array (ngVLA) will overcome current observational limitations and enable significant advancements in our understanding of the impact of jet-driven feedback on galaxy evolution.

2. Observing Jet-ISM Feedback with the ngVLA

The most well-studied population of sources exhibiting radio jet-driven feedback consists of massive elliptical galaxies residing at the centers of galaxy clusters with powerful jets capable of influencing galaxy evolution through the regulation of cooling flows. Jet-ISM feedback may also occur on sub-galactic scales in lower-mass and/or gas-rich galaxies, which typically have less massive SMBHs and much weaker radio jets. However, the prevalence of low-power ($L_{1.4\,\mathrm{GHz}} < 10^{24}$ W Hz^{-1}), $\sim$kpc-scale radio jets, and their impact on galaxy evolution, remain poorly constrained. The ngVLA will be an ideal instrument for studying sub-galactic-scale radio jets and their impact on the interstellar

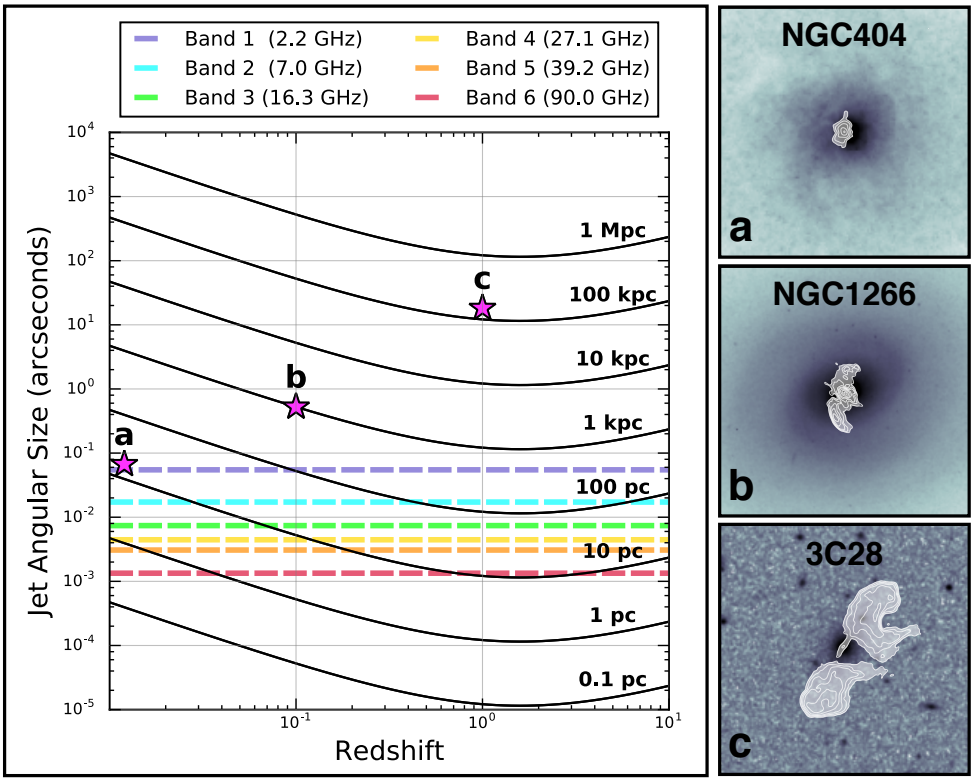

Figure 1. Jet angular size as a function of redshift. The black solid lines trace the redshift dependence of the angular extent of a jetted AGN for intrinsic jet sizes (measured from end to end along the major axis of the jet) from 0.1 pc to 1 Mpc. The maximum angular resolution of the ngVLA at the center of each of the ngVLA bands as defined in (Selina et al. 2017) is denoted by the dashed colored lines. The magenta stars and thumbnails to the right of the main figure indicate three jetted radio AGN representing a wide range of jet size scales: **a)** the dwarf galaxy NGC 404 with a jet extent of 10 pc, **b)** the jet-driven feedback host NGC 1266 with a jet extent of 1 kpc, and **c)** the radio galaxy 3C28 with a jet extent of 150 kpc. The redshifts of the representative sources correspond to simulated ngVLA maps from Nyland et al. (2018) at $z \approx 0$ ($D = 10$ Mpc), $z = 0.1$, and $z = 1.0$, respectively.

medium (ISM), particularly for sources with extents of a few pc to a few kpc such as young radio AGN, jetted AGN hosted by low-mass galaxies, and radio jets that are interacting strongly with the interstellar medium of the host galaxy. Figure 1 illustrates the redshift dependence of the angular jet extent as observed by the ngVLA for a wide range of radio jet size scales ranging from sub-parsec jets to giant radio galaxies with Mpc-scale lobes. Thus, future ngVLA studies of radio jets with intrinsic extents of a few pc to a few kpc will be able to fully utilize the unique combination of angular resolution, collecting area, and frequency coverage of the ngVLA over a wide range of redshifts.

ISM Content and Conditions. The ngVLA will link source morphologies and energetics from deep, high-resolution continuum observations with spectral line data that encode information on the ISM content and conditions. The combination of broadband continuum and spectral line imaging will allow the ngVLA to uniquely probe the energetic impact of radio jets on the cold gas reservoirs of their hosts. In particular, spectral line measurements of both the molecular (Figure 2) and atomic gas may be used to identify AGN-driven outflows, perform detailed kinematic studies to estimate the amount of en-

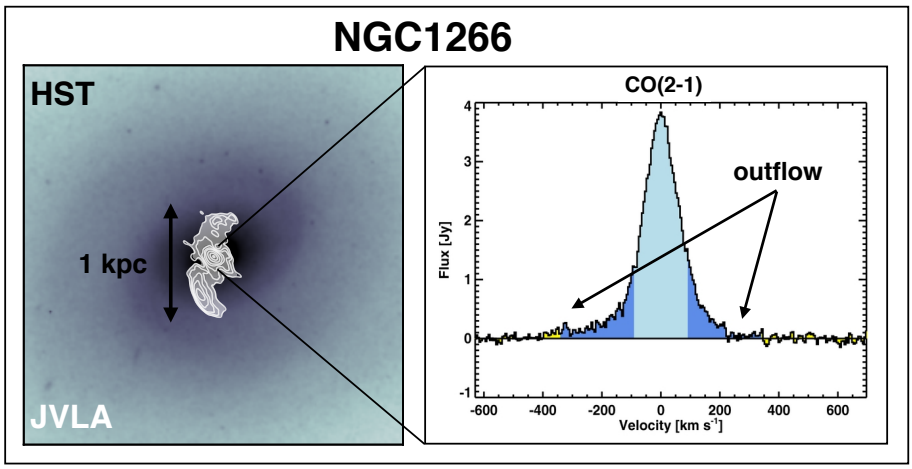

Figure 2. The radio jet and outflow of the nearby galaxy NGC 1266. **Left:** The background colorscale image illustrates the *HST J*-band data (WFC3, F140W; Nyland et al. 2013) and the filled white contours trace VLA 5 GHz continuum data from Nyland et al. (2016). **Right:** The CO(2–1) data from CARMA highlights the molecular outflow originally identified in Alatalo et al. (2011) based on the presence of excess emission in the wings of the spectrum (dark blue).

ergy injected into the ISM via feedback, and address the future evolutionary impact on the star formation efficiency on local/global scales caused by the AGN feedback (e.g., negative vs. positive feedback; Gaibler et al. 2012). Through comparisons with state-of-the-art jet-feedback simulations (e.g., Mukherjee et al. 2016), these continuum + cold gas ngVLA studies would place direct constraints on the prevalence and energetic importance of jet-ISM feedback as a function of redshift, galaxy mass, and environment.

Radio Spectral Ages. The ngVLA will uniquely excel at studies of radio AGN spanning a wide range of ages at low redshift, as well as radio AGN that are young or embedded in dense environments at higher redshifts (Figure 3). As shown by results from the Australia Telescope 20 GHz (AT20G) survey, continuum measurements in the tens of GHz range are needed to adequately model the radio spectral energy distributions (Sadler et al. 2006). This is particularly important for modeling the ages of young, low-redshift sources less than 10 Myrs old (Patil et al. 2018). Lower frequency continuum data in the MHz range will be important for constraining the ages of high-z sources; however, the inclusion of the lowest-frequency ngVLA bands down to ∼1 GHz would provide sufficient frequency coverage for measuring ages of sources as old as 30–40 Myrs at $z \sim 1$.

AGN Hosted by Low-mass Galaxies. Recent studies suggest that accreting SMBHs with masses in the range of $10^3 \lesssim M_{\rm BH} \lesssim 10^6$ M$_\odot$ may commonly reside in the nuclei of nearby low-mass ($M_* < 10^{10}\,M_\odot$) galaxies (Mezcua 2017, and references therein), thus motivating deep searches for their radio continuum signatures. However, identifying SMBHs in this population of galaxies is inherently difficult due to their faint accretion signatures. An ngVLA survey of accreting SMBHs hosted by nearby low-mass galaxies (e.g., analogs to NGC 404; Nyland et al. 2017) would offer new insights into the occupation fraction of SMBHs analogous to the SMBH seeds that formed at high redshift, thus profoundly impacting our understanding of the origin of SMBHs. Deep, high-angular-resolution observations with the ngVLA will both help constrain the SMBH seed mass distribution and also provide new constraints on the energetic impact of AGN feedback associated with sub-million-solar-mass SMBHs.

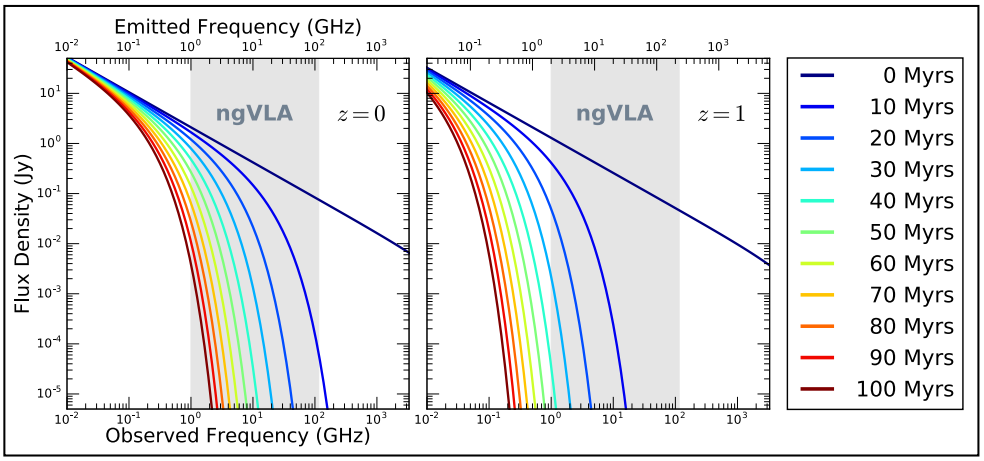

Figure 3. Example of JP model (Jaffe & Perola 1973) spectral ages calculated using the BRATS software (Harwood et al. 2013) demonstrating the need for ngVLA observations spanning a wide range of frequencies. The left and center panels correspond to redshifts of 0 and 1, respectively. The flux density values shown on the y-axis have been arbitrarily scaled. Because of its advantages of wide frequency range and angular resolution compared to the SKA, the ngVLA will uniquely excel in studies of low-redshift radio AGN that are young, or higher-redshift AGN that are embedded in dense environments.

3. Opportunities for Multiwavelength Synergy

The unique capabilities of the ngVLA will facilitate exciting advancements in our understanding of AGN feedback and its broader connection to galaxy evolution, particularly when combined with multiwavelength data from other current and next-generation instruments. In terms of synergy with current radio telescopes, observations with ALMA at frequencies above the ngVLA's limit of 116 GHz will provide key insights into the energetic and chemical impact of jet-driven feedback on the dense gas phase of the ISM. In the low radio frequency regime, the Square Kilometre Array (SKA) and its pathfinders will probe the 21 cm line out to higher redshifts (though at lower spatial resolution) than the ngVLA (Morganti 2017). The combination of constraints on both the atomic and molecular gas conditions from ngVLA and SKA observations will be important for studying the full impact of energetic jet-driven feedback on the ISM.

References

Alatalo, K., Blitz, L., Young, L. M., Davis, T. A., et al. 2011, *ApJ*, 735, 88
Mukherjee, D., Bicknell, G. V., Sutherland, R., & Wagner, A. 2016, *MNRAS*, 461, 967
Harwood, J. J., Hardcastle, M. J., Csoton, J. H., Goodger, J. L. 2013, *MNRAS*, 435, 3353
Jaffe, W. J. & Perola, G. C. 1973, *A&A*, 26, 423
Mezcua, M. 2017, *IJMPD*, 26, 1730021
Morganti, R. 2017, *AN*, 338, 165
Mukherjee, D., Bicknell, G. V., Sutherland, R., & Wagner, A. 2016, *MNRAS*, 461, 967
Nyland, K., Alatalo, K., Wrobel,J. M., Young, L. M., et al. 2013, *ApJ*, 779, 173
Nyland, K., Young, L. M., Wrobel, J. M., Sarzi, M., et al. 2016, *MNRAS*, 859, 23
Nyland, K., Davis, T. A., Nguyen, Dieu D., Seth, A., et al. 2017, *ApJ*, 845, 50
Nyland, K., Harwood, J.J., Mukherjee, D., Jagannathan, P., et al. 2018, *ApJ*, 458, 2221
Patil, P., Nyland, K., Whittle, M., Lonsdale, C., & Lacy, M. 2018, *Astronomy in Focus*, 1
Sadler, E. M., Ricci, R., Ekers, R. D., Ekers, J. A., et al. 2006, *MNRAS*, 371, 898

Astronomy in Focus, Volume 1
XXXth IAU General Assembly, August 2018
Volker Beckmann & Claudio Ricci, eds.

DOI: 00.0000/X000000000000000X

JVLA Imaging of Heavily Obscured, Luminous Quasars at $z \sim$ 1-3

Pallavi Patil[1,2,3], Kristina Nyland[2], Mark Whittle[1], Carol Lonsdale[2] and Mark Lacy[2]

[1]Department of Astronomy, University of Virginia,
530 McCormick Road, Charlottesville, VA, USA - 22904
email: pp3uq@virginia.edu, dmw8f@virginia.edu

[2]National Radio Astronomy Observatory,
520 Edgemont Road, Charlottesville, VA, USA - 22904
email: knyland@nrao.edu, clonsdal@nrao.edu, mlacy@nrao.edu

[3] Grote Reber Pre-Doctoral Fellow

Abstract. We present high-resolution Jansky Very Large Array (JVLA) imaging of 156 hyper-luminous and heavily obscured quasars found at redshifts from z $\sim$ 0.4-3. These galaxies were selected to have extremely red mid-infrared (MIR) colors in *Wide-field Infrared Survey Explorer* (WISE) and bright, compact radio emission in NVSS/FIRST. JVLA snapshot observations at 10 GHz with sub-arcsecond-scale angular resolution revealed that 115 out of 156 sources are indeed compact, radio-loud, and have structures on scales $\leqslant$ 2 kpc (at z $\sim$ 2). We performed a detailed analysis of the radio sepctral energy distributions (SEDs) of our sample sources. A few sources have peaked radio spectra, and thus belong to the class of High Frequency Peakers (HFP), Gigahertz Peaked Spectrum (GPS) and Compact Steep Spectrum (CSS) radio sources. This suggests that the radio jets could be recently triggered and are clearing their way out of the dense ISM of the host. We discuss implications of this study for our understanding of the impact of young jets on the evolution of the host galaxy.

Keywords. radio continuum: galaxies, (galaxies:) quasars: general , galaxies: evolution

1. Introduction

Through processes of radiative and mechanical energy transfer to the surrounding interstellar and intergalactic media, Active Galactic Nuclei (AGN) profoundly influence the formation and subsequent evolution of galaxies and their constituent stars, gas, and dust. A direct view of such galactic scale interactions is often limited due to the presence of obscuring dust, particularly for the population of young, luminous quasars during the peak epoch of galaxy assembly. However, these obscured nuclear regions are transparent at radio wavelengths. Thus, radio observations with high-spatial resolution are crucial to study the role and importance of jet related feedback mechanisms in the obscured AGN population. Here we present preliminary results from a high-resolution JVLA imaging survey of heavily obscured, luminous, z $\sim$ 2 quasars with compact radio jets.

2. Sample

The 156 quasars in our sample were selected by cross-matching luminous WISE sources with extremely red MIR colors and compact 1.4 GHz radio emission in the NVSS and/or FIRST surveys (Lonsdale et al. 2015). The luminous ($L_{\rm MIR} = 10^{12.5-13.5}$ L$_\odot$) quasars in our sample lie in the redshift range of $0.4 < z < 3$. Our sample galaxies are believed to

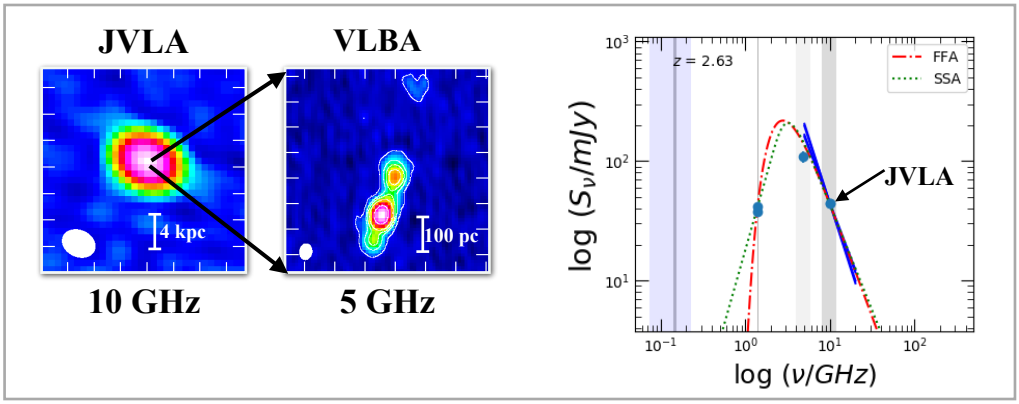

Figure 1. The left-hand image shows an example of our new X-band JVLA observations. The image in the middle is the VLBA C-band follow-up of the same target. This source shows a core-jet morphology on scales of ∼200 pc. The plot on the right illustrates an example radio SED from our sample with clear spectral turnover. We also show best-fit curves for the free-free absorption (FFA) and synchrotron self-absorption (SSA) models.

be in a unique evolutionary stage just after the (re)ignition of the radio AGN, but while the host galaxy is still experiencing substantial starburst activity.

3. High-resolution Radio Survey

We performed broadband JVLA imaging of our sample at X-band (8-12 GHz) in the A and B configurations. A forthcoming paper will discuss the radio properties of the sample (Patil *et al.* in prep.). Although the original radio selection in Lonsdale et al. (2015) used low-resolution survey data (45″ and 5″ for NVSS and FIRST, respectively), our new high-resolution (0.2″) observations confirmed that 72% of the quasars included in our study are compact at sub-arcsecond scales, which correspond to linear sizes of $\leqslant$ 2 kpc. For a subset of these sources, we performed follow-up imaging using the VLBA and e-MERLIN (Figure 1). The compact jets have typical luminosities in the range of $10^{24} \lesssim L_{5\,\mathrm{GHz}} \lesssim 10^{28}\,\mathrm{WHz^{-1}}$, which results in high calculated pressures ($\mathrm{P_{min}} \gtrsim 10^{-9} - 10^{-6}\,\mathrm{dyne\,cm^{-2}}$) for our radio sources. Future comparison of the radio source pressures with information on the ISM conditions will provide new insights into jet-ISM feedback in our sample of obscured, young quasars. We also combined our new JVLA observations with archival radio surveys from 74 MHz to 10 GHz in order to analyze the radio SEDs of our sources. As shown in Figure 1, we found a high incidence of curved or peaked spectral shapes among our target sources. The radio SED properties of our sources, as well as their compact morphologies, suggests a high prevalence of young radio AGNs (e.g., HFP, GPS, and CSS sources; O'Dea 1998) with jets confined within their host galaxies. A detailed radio SED analysis will be presented in Patil et al. (in prep.).

References

Becker, R. H., White, R. L., & Helfand, D. J. 1995, *ApJ*, 450, 559
Condon, J. J., Cotton, W. D., Greisen, E. W., et al. 1998, *AJ*, 115, 1693
Lonsdale, C. J., Lacy, M., Kimball, A. E., et al. 2015, *ApJ*, 813, 45
O'Dea, C. P. 1998, *PASP*, 110, 493

Astronomy in Focus, Volume 1
XXXth IAU General Assembly, August 2018
Volker Beckmann & Claudio Ricci, eds.

DOI: 00.0000/X000000000000000X

The relationship between the radio core-dominance parameter and spectral index in different classes of extragalactic radio sources (II)

Zhi-Yuan Pei[1,2,3,4] †, Jun-Hui Fan[1,2], Denis Bastieri[1,3,4], Utane Sawangwit[5] and Jiang-He Yang[6]

[1]Center for Astrophysics, Guangzhou University, Guangzhou 510006, China

[2]Astronomy Science and Technology Research Laboratory of Department of Education of Guangdong Province, Guangzhou 510006, China

[3]Dipartimento di Fisica e Astronomia "G. Galilei", Università di Padova, I-35131 Padova, Italy

[4]Istituto Nazionale di Fisica Nucleare, Sezione di Padova, I-35131 Padova, Italy

[5]National Astronomical Research Institute of Thailand (NARIT), Chiang Mai, 50200, Thailand

[6]Department of Physics and Electronics Science, Hunan University of Arts and Science, Changde 415000, China

Abstract. Active galactic nuclei (AGNs) can be divided into two major classes, namely radio loud and radio quiet AGNs. A small subset of the radio-loud AGNs is called blazars, which are believed to be unified with Fanaroff & Riley type I/II (FRI/II) radio galaxies. Following our previous work (Fan et al. 2011), we present a sample of 2400 sources with measured radio flux densities of the core and extended components. The sample contains 250 BL Lacs, 520 quasars, 175 Seyferts, 1178 galaxies, 153 Fanaroff & Riley type I and type II galaxies and 104 unidentified sources. We then calculate the radio core-dominance parameters and spectral indices and study their relationship. Our analysis shows that the core-dominance parameters and spectral indices are quite different for different types of sources. We also confirm that the correlation between core-dominance parameter and spectral index exists for a large sample presented in this work.

Keywords. galaxies: active-galaxies: general-galaxies: jets-quasars: general

1. Introduction

Active galactic nuclei (AGNs) are interesting extragalactic sources. Blazars are an extreme subclass of AGNs, that show rapid and large variability, high and variable polarization, superluminal motions in their radio components, and strong γ-ray emissions etc. There are two subclasses of blazars, namely flat spectrum radio quasar (FSRQ) and BL Lacertae objects (BL Lac) with the former showing strong emission line features and the latter showing very weak to no emission lines at all.

In a relativistic beaming model, the emission is assumed to be produced by two components, namely the beamed (core, $S_{\rm core}$) and the unbeamed ones (extended, $S_{\rm ext.}$). The ratio of the two components, $R = \frac{S_{\rm core}}{S_{\rm ext.}}$ is called the core-dominance parameter (Fan et al. 2011; Pei et al. 2016; Pei et al. 2018).

† Corresponding author: matt.pui.astro@gmail.com

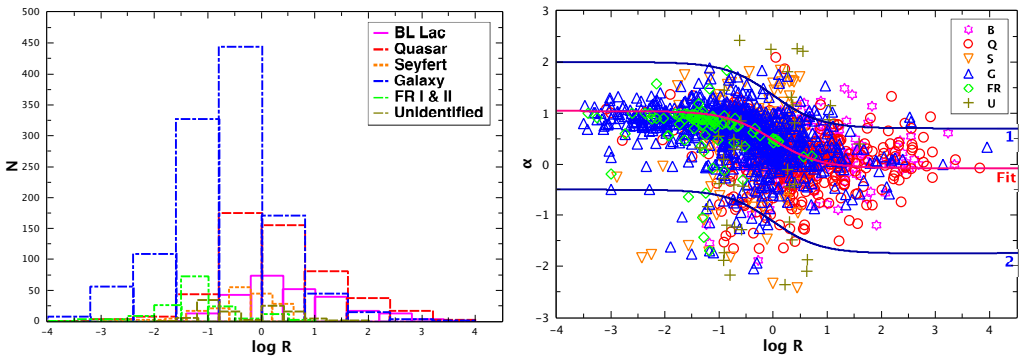

(a) (b)

Figure 1. Distribution of core-dominance parameter, log R (a) and plot of the the radio spectral index, $\alpha_{\rm R}$, against log R (b) for the whole sample.

2. Calculations and Results

We calculate the core dominance parameter using (Fan et al. 2011; Pei et al. 2016; Pei et al. 2018)

$$S_{\rm core}^{5\,{\rm GHz}} = S_{\rm core}^{\nu,\,{\rm obs}},\ S_{\rm ext.}^{5,\,{\rm GHz}} = S_{\rm ext.}^{\nu,\,{\rm obs}}(\frac{\nu}{5\,{\rm GHz}})^{\alpha_{\rm ext.}},$$

$$R = \frac{S_{\rm core}}{S_{\rm ext.}}(1+z)^{\alpha_{\rm core}-\alpha_{\rm ext.}}.$$

In our calculation we adopted $\alpha_{\rm core} = 0.00$ and $\alpha_{\rm ext.} = 0.75$ (Fan et al. 2011). We collected 250 BL Lacs, 520 quasars,175 Seyferts, 1178 galaxies, 153 FRIs & FRIIs and 104 unidentified sources. Figure 1 (a) shows that the distributions of core-dominance parameter, log R and the cumulative probability for the whole sample and the subclasses.

Fan et al. (2011) gives a interesting correlation between core-dominance parameter log R and radio spectral index $\alpha_{\rm R}$,

$$\alpha_{\rm Total} = \frac{R}{1+R}\alpha_{\rm core} + \frac{1}{1+R}\alpha_{\rm ext.},$$

and we adopt this relation on our present sample and shown in Figure 1 (b). The fitting curve corresponds to $\alpha_{\rm core} = -0.08$ and $\alpha_{\rm ext.} = 1.04$ (Pei et al. 2018).

3. Conclusions

From the discussions above, we can draw the following conclusions:

1. Core-dominance parameters (log R) are quite different for different subclasses of AGNs: $\log R|_{\rm BL\,Lac} > \log R|_{\rm quasar} > \log R|_{\rm Seyfert} > \log R|_{\rm galaxy} > \log R|_{\rm FRI} > \log R|_{\rm FRII}$.

2. A correlation between core-dominance parameter (log R) and radio spectral index ($\alpha_{\rm R}$) is adopted, which means the spectral index is dependent on the core-dominance parameter. $\alpha_{\rm core} = 0.08$ and $\alpha_{\rm ext.} = 1.04$ are obtained.

References

Pei, Z. Y., Fan, J. H., Liu, Y., et al. 2016, *Ap&SS*, 361, 237
Pei, Z. Y., Fan, J. H., D. Bastieri, et al. 2018, *RAA*, Submitted
Fan, J. H., Yang, J. H., Pan, J., & Hua, T. X. 2011, *RAA*, 11, 1413

Astronomy in Focus, Volume 1
XXXth IAU General Assembly, August 2018
Volker Beckmann & Claudio Ricci, eds.

DOI: 00.0000/X000000000000000X

An interferometric quest to reveal the true nature of the core in the radio galaxy 3C 411

Krisztina Perger[1,2], Sándor Frey[2], and Krisztina É. Gabányi[3,2]

[1] Department of Astronomy, Eötvös Loránd University
Pázmány Péter sétány 1/A, H-1117 Budapest, Hungary
email: k.perger@astro.elte.hu

[2]Konkoly Observatory, MTA Research Centre for Astronomy and Earth Sciences
Konkoly Thege Miklós út 15-17, H-1121 Budapest, Hungary

[3]MTA-ELTE Extragalactic Astrophysics Research Group, Eötvös Loránd University
Pázmány Péter sétány 1/A, H-1117 Budapest, Hungary

Abstract. X-ray spectral energy distribution model fitting of the classical radio galaxy 3C 411 raised the possibility of the presence of a blazar-like component in its centre. We investigated the pc-scale radio structure of the galaxy core with sub-milliarcsec resolution very long baseline interferometry (VLBI) imaging, using archival Very Long Baseline Array (VLBA) data and new European VLBI Network (EVN) observations at multiple frequencies. The data do not confirm the presence of a blazar-like nucleus in the radio galaxy, and provide evidence for a change in the jet inclination angle with respect to the line of sight between pc and 100 kpc scales.

Keywords. galaxies: active, galaxies: individual (3C 411), galaxies: jets, radio continuum: galaxies

1. Introduction

The 100 kpc scale view of the radio continuum emission of 3C 411 (PKS J2022+1001, $z = 0.467$) shows a classical double-lobed morphology, placing the object in the class of Fanaroff-Riley type II radio galaxies (Fanaroff & Riley 1974). Examination of the X-ray spectrum of 3C 411 by Bostrom et al. (2014) resulted in two equally well-fitting models. One of the models was consistent with those known for radio galaxies, but the other one was a combination of two components: one similar to those found for Seyfert nuclei and another blazar-like, hard X-ray component.

To reveal the true nature of the central 10 pc in the active galactic nucleus (AGN) we applied the technique of very long baseline interferometry (VLBI). For the analysis we used archival Very Long Baseline Array (VLBA) data at 4.3 and 7.6 GHz obtained from the Astrogeo VLBI database† (L. Petrov, in preparation) and new observations at 1.6 and 5 GHz with the European VLBI Network (EVN).

2. Data reduction and results

Inner structure. The EVN data were calibrated in the US National Radio Astronomy Observatory (NRAO) Astronomical Image Processing System‡ (AIPS; Greisen 2013), while imaging with a prior amplitude and phase calibration was done in DIFMAP program (Shepherd 1997) for all four datasets. We fitted multiple circular Gaussian model components to the calibrated visibility data. We found that the radio emission of the

† http://astrogeo.org/vlbi_images/
‡ http://www.aips.nrao.edu/index.shtml

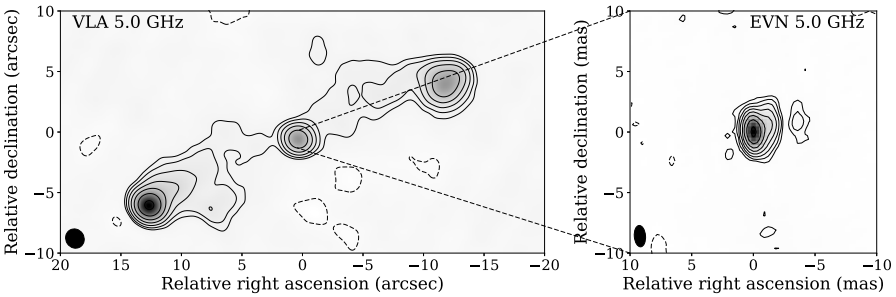

Figure 1. Clean maps of 3C 411 at 5 GHz. The arcsec resolution VLA image (Neff et al. 1995) has a peak intensity of 220.4 mJy beam^{-1}, the first contours are drawn at ±3.0 mJy beam^{-1}. The mas resolution EVN map has a peak of 27.3 mJy beam^{-1}, the first contours are drawn at ±0.18 mJy beam^{-1}. In both images, the positive contour levels increase by a factor of 2.

source does not exhibit Doppler boosting (i.e. it is not relativistically enhanced). Based on the values of the Doppler factor ($\delta < 1$), the possible range of jet inclination angles was derived ($24^\circ \leqslant \varphi \leqslant 55^\circ$).

Outer structure. We estimated the angle to the line of sight of the large-scale structure of 3C 411 using an archival 5 GHz Very Large Array (VLA) map by Neff et al. (1995). Based on the flux density and the arm-lengths ratios of the hot spots, the angle to the line of sight is between $77^\circ \leqslant \Phi \leqslant 87^\circ$.

Comparing the pc and 100 kpc scale radio structure (Fig. 1) we found that the inclination angles differ by $\gtrsim 30^\circ$. The absence of the Doppler enhancement in the radio jet did not confirm a blazar nucleus.

Acknowledgement

The EVN is a joint facility of independent European, African, Asian and North American radio astronomy institutes. Scientific results from data presented in this publication are derived from the EVN project code EP104. This research made use of data from the astrogeo.org website, and we thank Leonid Petrov for making results of 3C 411 observations online prior to publication. This publication has received funding from the European Union's Horizon 2020 research and innovation programme under grant agreement No 730562 (RadioNet). KP is grateful for the IAU grant supporting her to attend the General Assembly. We thank the Hungarian National Research, Development and Innovation Office (OTKA NN110333) for support. KÉG was supported by the János Bolyai Research Scholarship of the Hungarian Academy of Sciences.

References

Bostrom, A., Reynolds, C. S., & Tombesi, F. 2014, *ApJ*, 791, 119

Fanaroff, B. L., & Riley, J. M. 1974, *MNRAS*, 167, 31P

Greisen, E. W. 2003, in Heck A., ed, *Astrophysics and Space Science Library Vol. 285, Information Handling in Astronomy – Historical Vistas*. Kluwer, Dordrecht, p. 109

Neff, S. G., Roberts, L., & Hutchings, J. B. 1995, *ApJS*, 99, 349

Shepherd, M. C. 1997, in Hunt, G., Payne, H., eds, *ASP Conf. Ser. Vol. 125, Astronomical Data Analysis Software and Systems VI, Astron. Soc. Pac.*, San Francisco, p. 77

Astronomy in Focus, Volume 1
XXXth IAU General Assembly, August 2018
Volker Beckmann & Claudio Ricci, eds.

DOI: 00.0000/X000000000000000X

The code Pégase.3 for distant radiogalaxies with the future JWST

Brigitte Rocca-Volmerange[1] **and Michel Fioc** [1]

[1] Institut d'Astrophysique de Paris, CNRS and Sorbonne Université,
98bis Bd Arago, F-75014, Paris France
email: rocca@iap.fr, fioc@iap.fr

Abstract. The physical link of the star formation-AGN activities is analyzed from multiwavelength energy distributions of distant radiogalaxies (RG) with the help of two models: the new evolutionary code PÉGASE.3 with dust predictions and the Siebenmorgen's AGN model, with the aim to to disentangle the farIR dust emissions from respectively interstellar medium and torus of RGs. Best-fits of the HST-Spitzer-Herschel (UV-to-IR) observations of the 3CR RGs with libraries of hybrid SED templates identify three components (AGN, old galaxy and young starburst) tracing the relation of starburst-AGN luminosities. To confirm this relation at higher resolutions, the JWST/NIRCam, MIRI and NIRspec instruments are needed, SED libraries and evolving colors of galaxy hosts adapted to the JWST instruments are in preparation with PÉGASE.3.

Keywords. galaxies:evolution, infrared: galaxies, (ISM:) dust, emission

1. The 3 components of RG: AGN, starburst and old galaxy

Multiwavelength hybrid SEDs for distant radiogalaxies are built by associating the evolution of a massive host galaxy and of a short intense starburst from the code PÉGASE.3, with the constant far-IR emission of a clumpy AGN torus model (Drouart & et al.(2016)). PÉGASE.3 (Fioc & Rocca-Volmerange, submitted to Astronomy & Astrophysics Journal, see also www2.iap.fr/pegase) predicts from 0 to 20 Gyrs, the stellar and nebular emissions, corrected for metallicity dependent dust attenuation, updated from Fioc & Rocca-Volmerange (1997), extended to the coherent dust emission of the same source respecting the energy balance by radiative transfer MonteCarlo simulations. The best-fit procedures of these multiple synthetic libraries on UV-to-far-IR observations of 3CR galaxies (Fig. 1) identify the three components (AGN, old and young stellar populations).

2. The 3CR catalog: a star formation-AGN link?

Podigachoski et al.(2016) applied the hybrid method to galaxies of the 3CR catalog at various z. The three components are found in all cases (Fig. 2), even at higher redshifts. From the 3CR galaxies, an interesting relation is observed between the luminosities $L_{\rm starburst}$ and $L_{\rm AGN}$, respectively from the dusty starburst and the AGN torus (Fig. 3), suggesting a relation between star formation and AGN activities hinted by the different thermal peaks in the far-IR. In the mid-IR, these components deserve to be analyzed with better spatial and spectral resolutions of the *JWST/NIRcam, MIRI, NIRspec* instruments. We plan to build PÉGASE.3 template libraries and corresponding synthetic colors to help the community to analyze future JWST data.

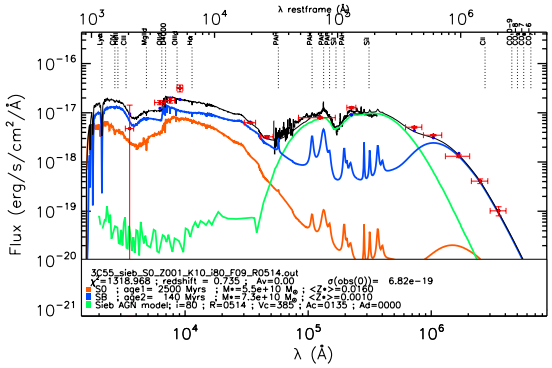

Figure 1. Best-fits of the HST-Spitzer-Herschel observations of the radio galaxy 3C 368 show three components: the old (orange) population of early-type galaxy, a recent starburst (blue) and the AGN torus (green). The library of hybrid templates is built with PÉGASE.3 and the clumpy Siebenmorgen's AGN model. The disentangling is consistent with the Spitzer/IRS spectra within the error bars.

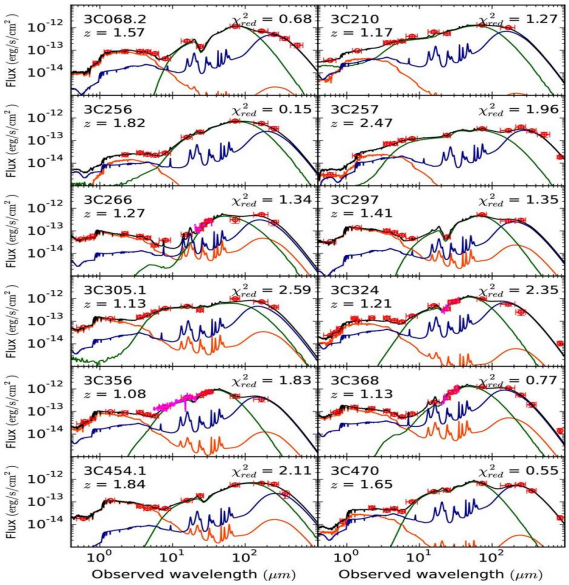

Figure 2. 3CR radiogalaxies show the same distribution of the three components (AGN, old and recent) at various redshifts.

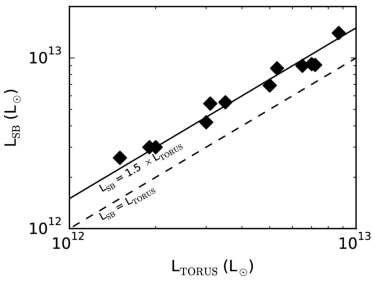

Figure 3. The luminosity relation of $L_{\rm starburst}$ with $L_{\rm AGN}$ for the analyzed 3CR galaxies.

References

Drouart, G., Rocca-Volmerange, B., De Breuck, C., Fioc, M., Lehnert, M., Seymour, N., Stern, D., & Vernet, J. 2016, *A&A*, 593, 109

Fioc, M., & Rocca-Volmerange, B. 1997, *A&A* 326, 950

Podigachoski, P., Rocca-Volmerange, B., Barthel, P., Drouart, G., & Fioc, M., 2016, *MNRAS*, 462, 4183

Siebenmorgen, D., Kruegel, E., 2007, *A&A*, 461, 445

Astronomy in Focus, Volume 1
XXXth IAU General Assembly, August 2018
Volker Beckmann & Claudio Ricci, eds.

DOI: 00.0000/X000000000000000X

Probing black hole axis perturbations using low axial ratio radio galaxies

Lakshmi Saripalli[1]

[1]Raman Research Institute, Sadashivanagar, Bangalore, India
email: lsaripal@rri.res.in

Abstract. With the unique advantage that radio galaxies have in delineating the central supermassive black hole axis along their radio axes they make useful probes for unseen central engine processes. In this paper I bring to attention the remarkable power of low axial ratio radio galaxy samples in opening up for examination this hard-to-probe regime of active galaxies. I present results from our recent EVLA observations of a large radio source sample originally selected on the basis of shapes. The observations have revealed a plethora of radio sources that potentially show signatures of axis changes of various types suggesting such samples as effective means for probing black hole axis perturbations and hence such samples to be effective means in searches for binary black hole pairs in radio galaxies.

Keywords. galaxies: active, radio continuum: galaxies, stars: black holes

1. Introduction

Already in the early years when radio galaxies were being imaged and their basic twin-lobe morphologies recognised and studied occurrence of deviant structures as in S, Z and X-shaped radio galaxies (XRGs) were noted and models examined as to how they developed their morphologies (e.g. Ekers 1978). Over the years several such sources were found, serendipitously, and their morphologies of striking inversion symmetry were mostly modelled as arising due to jet axis precession (e.g. Begelman et al. 1980, Gower et al. 1982, Cox et al. 1991). XRGs came in for separate attention given their structures, which exhibited two lobe pairs vastly separated in position angle. Initial models included the backflow deflection model (Leahy & Williams 1984) in which, as backflows in powerful lobes flow towards the central regions they get deflected in opposite directions in the density gradients in an asymmetric host atmosphere and thereby create the transverse 'wings'. Also suggested was a model where a black hole associated with a radio source undergoes an axis precession and renews its activity in the new direction with backflows from the new lobes energising the older relic lobes (also Leahy & Parma 1992). In later years in the backdrop of growing interest in binary black hole systems and gravitational waves (Merritt & Ekers 2002) suggested what became known as spin-flip model where the black hole associated with a radio source undergoes a rapid large-angle spin axis flip and continues its activity in the new direction. Over time these two quite contrasting models, the backflow deflection model and the rapid spin-flip model became the main contending scenarios for XRG formation.

Despite both XRG formation models enjoying support in observational and simulation realms, e.g. requirement within the backflow deflection model of asymmetry and main lobes to be of FR-II type are both met (Capetti et al. 2002, Saripalli & Subrahmanyan 2009, Hodges-Kluck et al. 2010, Hodges-Kluck et al. 2011) and separately, black hole spin-flips are clearly found to occur in simulations of binary black hole systems (Campanelli et al. 2007), neither model is devoid of serious drawbacks. For example, subsonically

advancing wings in XRGs that have extents same as or larger than the supersonically advancing main lobes are a problem within the backflow scenario, whereas prevalence of relic radio sources in the form of wings in XRGs when relics are known to be rare is difficult to understand within the spin-flip model (besides central emission gaps, smooth continuity between a wing and associated main lobe, main lobes needing to be of FR-II type, and wings forming along the host minor axis (Saripalli & Subrahmanyan 2009 and Saripalli & Roberts 2018).

It was with the motivation of obtaining clarity in this regard that we embarked on EVLA observations (Roberts et al. 2018) of a large sample of 100 candidate XRGs (Cheung 2007), originally selected on the basis of their shapes from the FIRST survey. The multi-band and multi-array total intensity and polarization continuum observations were carried out over a year and (including our analysis of archival VLA data of a large subset of 55 sources) resulted in 95 sources being imaged in multiple frequencies and resolutions. This allowed a thorough characterisation of the sample sources (Saripalli & Roberts 2018), an analysis that draws attention to the immense opportunity that low axial ratio radio sources provide us for probing black hole axis behaviour and perturbations to black hole axes in radio galaxies.

2. Source morphologies in low axial ratio radio source samples

Our EVLA observations of a sample selected on the basis of low axial ratios has revealed the sample to be dominated by inversion symmetric radio morphologies. Strikingly, the inversion symmetry is bimodal with off-axis emission features originating from two strategic locations, the outer ends of lobes (Outer-deviation sources or O-devs) and inner ends of lobes (Inner-deviation sources or I-devs). Remarkably, the more dominant I-devs are invariably of FR-II type. Nearly one-third of I-devs have at least one wing extent same or larger than their main lobes. Trends are also seen of longer wings likely associated with lobes having stronger hotspots and of sources with fractionally longer wings having physically smaller sizes (also reported in a separate study of XRGs by (Saripalli & Subrahmanyan 2009). We identify a separate class of sources as XRGs, where there is a central swathe of emission that cannot be clearly linked to any individual lobe. Two-thirds of O-dev sources are either of S- or Z-shape. A large fraction, nearly one-third of sources in the entire sample, exhibit inner-S shape in their main radio axes. Sources with double hotspots in both lobes are seen where the hotspots appear to lie along two separate axes through the core. The imaged sample includes a small subset with evidence of two separate radio sources along separate axes through the core.

3. Inner-deviation sources and XRGs

In the literature the term 'XRG', besides referring to the classic X-structure, includes X-shaped sources with central emission gaps where each of the wings is separately associated with a main lobe. We choose to separate the two types using instead 'XRG' for the classic X-shaped sources and I-dev for the group with emission gaps. The present study allowed us to address the original motivation for the project, that of the formation scenario for XRGs. In revealing I-devs to invariably be associated with FR-II morphologies the present work shows that backflows cannot be ignored in the formation of central distortions. However, as pointed out above, there remain areas where both models encounter problems. Combining the main aspects of the two models, namely, black hole spin-flip and backflow deflection in a central asymmetric environment (Leahy & Williams 1984, Leahy & Parma 1992 and suggested for NGC 326 by Hodges-Kluck & Reynolds 2012),

we suggested the following scenario for formation of XRGs and I-devs, where after suffering a large-angle axis flip from the host minor axis direction and leaving behind a relic radio source the central engine continues activity in the new direction where any ensuing backflows in the new source would energise the respective parts of the relic after being deflected by density gradients in the asymmetric host halo distribution. With fractionally longer wings likely associated with physically smaller sources as found in the present study, such a combined model has no difficulty in accounting for wings larger than main sources. The central emission gaps seen in several XRGs (called I-devs here) may develop as the source evolves, affected by age and buoyancy effects in the host atmosphere. Interestingly, we find the average linear size of I-devs is more than twice (354 kpc) that of XRGs (151 kpc) for the sample we studied.

4. Low axial ratio radio sources as probes for black hole axis perturbations

Our EVLA observations of the large sample of low axial ratio radio galaxies have revealed source structures that exhibit a variety of signs of axis change. At least 4% of radio galaxies in radio source samples are found to likely suffer axis perturbations. Black hole axis precession is a favourite mechanism to explain S- or Z-shaped sources and also those with double hotspots as in Cygnus-A (Cox et al. 1991), where precession can arise in situations of re-aligning black holes or tilted or warped accretion disks or binary black hole systems, which also give rise to large-angle spin axis-flips (Natarajan & Pringle 1998; Liu 2004, Begelman et al. 1980, Campanelli et al. 2007). Given the variety of conditions in which such processes could occur, large samples of low axial ratio radio sources with the variety of source morphologies such as what we have characterised, which between them would include a range of precession parameters, are ideal for investigating the variety in physical conditions likely involved.

5. Implications

The implications of such a study described here are immense for galaxy merger evolution studies, particularly in the final stages. Efforts in this area have included searches

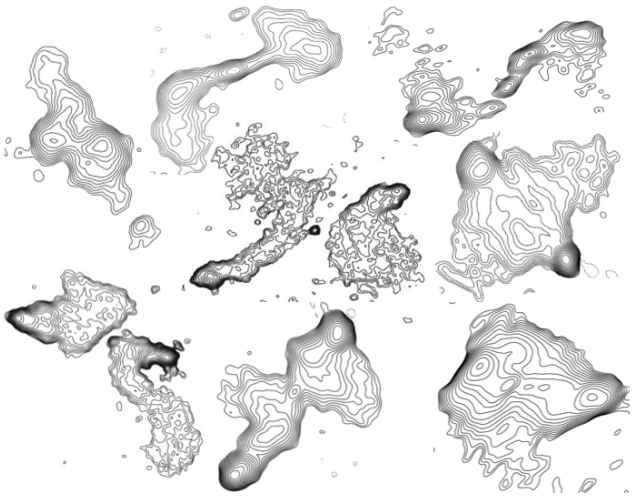

Figure 1. Montage of radio galaxy morphological types in the low axial ratio source sample

for dual and binary black holes that allow to identify individual galaxies and to study the conditions that prevail at the particular stage of merger and also study of the evolution of the merger from tens of kiloparsec separations to the final stages of binary black holes. The workhorse in this effort has been the strategy of using double-peaked emission line galaxies as markers for dual AGN (Müller-Sánchez et al. 2015), although this approach is recognised for the tedious effort involved. A newer technique of using mid-IR selected galaxy merger candidates has recently found several dual AGN candidates, promising to be a more efficient method (Satyapal et al. 2017). Even so, binary AGN have been difficult to find. They require high resolution and with radio observations capable of providing the highest resolution through VLBI and with availability of abundant target populations as shown in this study, it appears that using low axial ratio radio samples may be an effective method. With two-thirds of our sample sources possibly candidates for axis perturbation, low axial ratio radio samples may be a strong search method for binary black holes as well as recoiling black holes.

6. Conclusions and Future work

With the present work showing a way to generate large samples of sources with signatures of axis change, low axial ratio radio sources are shown to be potentially effective and useful resource for searching for binary black holes and recoiling black holes as well as in capturing the wide parameter space in study of galaxy mergers into extreme gravity regimes. Having isolated candidates for perturbed black holes, follow up studies of the host galaxy, radio spectra, VLBI observations, axis precession modelling etc are needed towards examining S-, Z-, XRG and I-dev formation scenarios and towards gaining clues to prevailing conditions as galaxy merger progresses. A few are presently in progress.

References

Begelman, M. C., Blandford, R. D. & Rees, M. J. 1980, *Nature*, 287, 307
Campanelli, M., Lousto, C., Zlochower, Y., & Merritt, D., 2007, *ApJ*, 659, L5
Capetti, A., Zamfir, S., Rossi, P., Bodo, G., Zanni, C., & Massaglia, S. 2002, *AA*, 394, 39
Cheung, C.C. 2007, *AJ*, 133, 2097
Cox, C. I., Gull, S. F., & Scheuer, P. A. G. 1991, *MNRAS*, 252, 558
Ekers, R.D.. 1978, *Nature*, 276, 588
Gower, A. C., Gregory, P. C., Unruh, W. G., & Hutchings, J. B. 1982, *ApJ*, 262, 478
Hodges-Kluck, E. J., Reynolds, C. S., Cheung, C. C., & Miller, M. C. 2010, *ApJ*, 710, 1205
Hodges-Kluck, E.J. & Reynolds, C.S. 2011, *ApJ*, 733, 58
Hodges-Kluck, E.J. & Reynolds, C.S. 2012, *ApJ*, 746, 167
Leahy, J.P., & Williams, A.G. 1984, *MNRAS*, 210, 929
Leahy, J.P. & Parma, P. 1992, *Extragalactic Radio Sources. From Beams to Jets*, (CUP), 307
Liu, F.K. 2004, *MNRAS*, 347, 1357
Merritt, D. & Ekers, R. D. 2002, *Science*, 297, 1310
Müller-Sánchez, F., Comerford, J. M., Nevin, R., Barrows, R. S., Cooper, M. C., Greene, J. E. 2015, *ApJ*, 813, 103
Natarajan, P. & Pringle, J. E. 1998, *ApJ*, 506, L97
Saripalli, L. & Subrahmanyan, S. 2009, *ApJ*, 695, 156
Saripalli, L. & Roberts, D.H. 2018, *ApJ*, 852, 48
Satyapal, S., Secrest, N. J., Ricci, C., et. al. 2017, *ApJ*, 848, 126

Astronomy in Focus, Volume 1
XXXth IAU General Assembly, August 2018
Volker Beckmann & Claudio Ricci, eds.

DOI: 00.0000/X000000000000000X

High-redshift radio galaxies at low radio frequencies

A. Saxena[1], and H. J. A. Röttgering[1]

[1] Leiden Observatory, Leiden University,
P.O. Box 9513, 2300 RA
Leiden, The Netherlands
email: saxena@strw.leidenuniv.nl

Abstract. High-redshift radio galaxies (HzRGs) are some of the rarest objects in the Universe. They are often found to be the most massive galaxies observed at any epoch and are known to harbour active supermassive black holes that give rise to powerful relativistic jets. Finding such galaxies at high redshifts can shed light on the processes that shaped the most massive galaxies very early in the Universe. We have started a new campaign to identify and follow-up promising radio sources selected at 150 MHz in a bid to identify the most distant radio galaxies and study their properties, both intrinsic and environmental. Here we describe the progress of our campaign so far, highlighting in particular the discovery of the most distant radio galaxy known till date, at $z = 5.72$.

Keywords: galaxies: high-redshift, galaxies: active, radio continuum: galaxies

1. Introduction

Powerful radio galaxies are robust beacons of the most massive galaxies at any epoch. High-redshift radio galaxies (HzRGs) in particular are thought to be the progenitors of the massive elliptical galaxies that are observed in the local Universe. HzRGs contain an old stellar population (Best, Longair & Röttgering 1998), large amounts of dust and gas, are seen to be forming stars intensively (Seymour *et al.* 2008) and are often located in the centre of clusters and proto-clusters of galaxies (Venemans *et al.* 2002). Studying their underlying stellar populations and their environment can shed light into the assembly and evolution of some of the most massive structures in the early Universe, including the evolution of the large scale structure of the Universe. Miley & De Breuck (2008) give an extensive review about the properties of distant radio galaxies and their environments. Since HzRGs host large supermassive black holes (SMBHs) in their centres that power the bright radio synchrotron emission, detailed studies of radio galaxies at the highest redshifts can help test and constrain SMBH growth models and set estimates on the seed SMBH masses in the very early Universe.

Bright radio galaxies at $z > 6$, into the Epoch of Reionisation (EoR), are particularly interesting as they could in principle be used to study the process of reionisation in detail, constraining which remains one of the most important goals of modern cosmology. The redshifted 21cm (1.4 GHz) hyper-fine transition line of neutral hydrogen falls in the low radio frequency regime ($\nu < 200$ MHz) and can be observed as absorption in the spectra of a $z > 6$ radio galaxy (Carilli, Gnedin & Owen 2002). Such absorption signals from patches of neutral hydrogen could in principle be observed by current and next-generation radio telescopes such as the Giant Meterwave Radio Telescope (GMRT), the Low Frequency Array (LOFAR), the Murchinson Widefield Array (MWA) and the Square Kilometer Array (SKA). Detection of even a single bright radio source at $z > 6$ could have profound implications for cosmology.

Motivated by the challenge of finding a HzRG deep in the EoR, we have designed a programme to isolate candidate HzRGs from large area radio surveys that go deeper than before. The shortlisted candidates are then followed up spectroscopically and photometrically, yielding distance measurements and galaxy properties. In the following sections we describe in detail our sample selection and some initial results

2. Sample selection

The sample of HzRGs presented in this paper were initially selected at a frequency of 150 MHz, from the TIFR GMRT Sky Survey Alternative Data Release (TGSS ADR; Intema, Jagannathan, Mooley & Frail 2017) covering ~ 10000 square degrees of overlap with the VLA FIRST survey at 1.4 GHz. To isolate promising HzRG candidates from thousands of radio sources, we employed the ultra-steep spectrum selection ($\alpha_{1400}^{150} < -1.3$, where $S_\nu \propto \nu^\alpha$), which has proven to be very efficient at selecting HzRGs from large surveys (Röttgering *et al.* 1994). Flux limits were introduced so that a completely new parameter space in flux density and spectral index was probed, with all our sources having $50 < S_{150} < 200$ mJy. We then introduced angular size restrictions, as radio galaxies at the highest redshifts are expected to be compact (Saxena, Rottgering & Rigby 2017) and ensured that none of the promising candidates had any counterparts in the available all-sky optical and infrared surveys. Further details about the sample selection can be found in Saxena *et al.* (2018).

The strict selection criteria resulted in a small sample of 32 promising candidates out of ~ 60000 radio sources with spectral index information from TGSS ADR and FIRST. These 32 candidates were first followed up with the VLA at 1.4 GHz in A-configuration, to obtain high-resolution positions that would enable blind spectroscopy and accurate host galaxy identification in deep optical/infrared imaging. The radio maps at 1.4 GHz are presented in Saxena *et al.* (2018).

3. Multi-wavelength follow-up

3.1. *Redshifts*

A sub-sample of the 32 shortlisted sources was observed spectroscopically using GMOS on Gemini North, the William Herschel Telescope (WHT) and the Hobby-Eberly Telescope (HET). A few of these sources were also imaged at near infrared wavelengths in the J and K bands using the Large Binocular Telescope (LBT). Spectroscopic redshifts were obtained for 13 sources, and photometric redshifts were calculated for another two sources thanks to deeper optical and infrared data available in their field. We find redshifts in the range $0.57 < z < 5.72$ in our sample, with 5 newly discovered radio galaxies at $z > 4$. There remain several radio sources from our initial sample of 32 that do not have any spectroscopic information yet and obtaining spectra for these sources is of the highest priority. The overall redshift distribution of the sample is shown in Figure 1 and the detailed analysis of the spectroscopic properties of the spectra is part of a manuscript in preparation.

3.2. *Stellar masses*

Next, we calculate stellar masses for radio galaxies that have a redshift measurement and a K band observation. We use simple stellar population models using SMPY, a PYTHON package that enables creation of synthetic spectra in an easy and flexible manner. To model radio galaxy spectra, we use the assumptions outlined in Saxena *et al.* (2018) to create synthetic stellar population templates, that we then convolve with the broadband

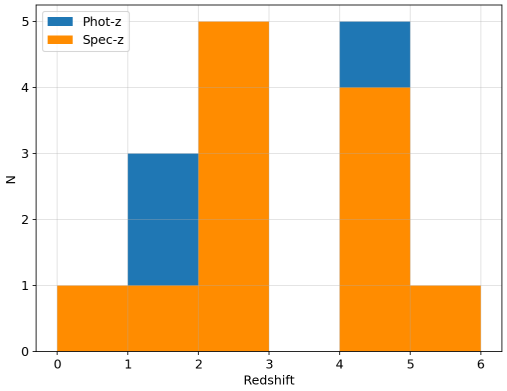

Figure 1. Distribution of spectroscopic and photometric redshift determined for the sample of radio galaxies presented in (Saxena *et al.* 2018).

filter profiles at optical and infrared wavelengths. We then scale the synthetic photometry produced by these models, specifically in the K band, to calculate stellar masses for each radio galaxy. The distribution of tracks on the $K-z$ parameter space and K band magnitudes measured for sources in our sample will be presented in Saxena et al. (in prep). We find that our radio galaxies lie in the stellar mass range $10^{10.5} < M_{\star} < 11.7\ M_{\odot}$, which is a bit lower than the stellar masses measured for powerful radio galaxies currently known across all epochs. Nonetheless, our radio galaxy stellar masses still appear to be representing the more massive end of the galaxy stellar mass function at all epochs, in line with previous studies, such as Overzier *et al.* (2009).

4. Discovery of the highest redshift radio galaxy, at $z = 5.72$

In this section we draw attention to the discovery of the highest redshift radio galaxy discovered to date, TGSS J1530+1049, which was initially part of our sample. The discovery of this galaxy was first reported in Saxena *et al.* (2018). The redshift was determined using the Lyα emission line, which is slightly asymmetric, in line with what is seen for Lyman-alpha emitting galaxies (LAEs) at high-z (Kashikawa *et al.* 2011). Its faint K band magnitude $K > 24.3$ AB is also indicative of a high-redshift nature, owing to the $K-z$ relation that exists for radio galaxies (Willott, Rawlings, Jarvis & Blundell 2003). The Lyα line flux is 1.6×10^{-17} erg s^{-1} cm^{-2} and the FWHM is ~ 370 km s^{-1}, which is closer to that of normal LAEs at $z \sim 5.7$ than other known $z > 4$ radio galaxies. The line emission from TGSS J1530+1049 is shown in Figure 2.

TGSS J1530+1049 has a bright radio luminosity of $L_{150} = 10^{29.1}$ W Hz^{-1} and the deconvolved radio size is measured to be ~ 3.5 kpc, which is very compact. The relatively weak Lyα, bright radio luminosity and a small radio size suggest that TGSS J1530+1049 is a radio galaxy that is at a very early stage in its lifetime. The stellar mass limit, under assumptions highlighted in Saxena *et al.* (2018) are $M_{\star} < 10^{10.5}\ M_{\odot}$, which suggest that the host galaxy of this radio source is still in the process of assembling its stellar mass.

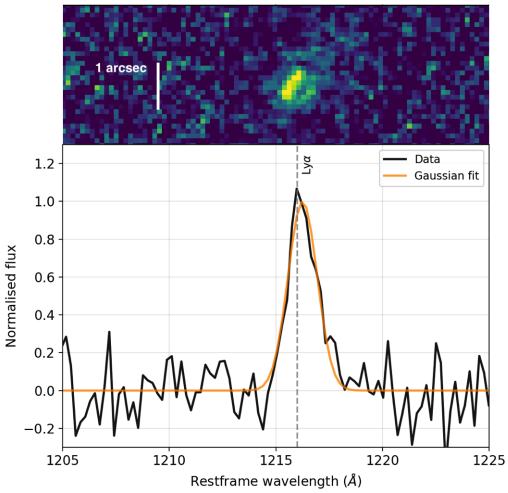

Figure 2. The rest-frame 1D spectrum (bottom) and 2D spectrum (top) for TGSS J1530+1049 at $z = 5.72$ (Saxena *et al.* 2018). The FWHM is narrower than other HzRGs and is closer to that observed for 'non-radio' LAEs at $z \sim 5.7$.

5. Going forward

Having successfully demonstrated that sensitive large area radio surveys can be used to hunt for radio galaxies at record distances, the big challenge facing the field now is to detect a radio galaxy deep in the EoR ($z > 6$). Additionally, statistically significant samples of fainter radio galaxies across all redshifts can shed further light into the role of radio mode AGN feedback in shaping massive galaxies that we observe in the local Universe. Studying the underlying stellar populations and star formation histories for fainter, more 'normal' radio galaxies would go a long way in gaining a complete picture about the formation and evolution of massive (radio) galaxies in the Universe.

References

Best, P.N., Longair, M.S., & Röttgering, H.J.A. 1998, *MNRAS*, 295, 549

Carilli, C.L., Gnedin, N.Y., & Owen, F. 2002, *ApJ*, 577, 22

Intema, H.T., Jagannathan, P., Mooley, & K.P., Frail, D.A. 2017, *A&A*, 598, A78

Kashikawa, N., Shimasaku, K., Matsuda, Y., Egami, E., Jiang, L., Nagao, T., Ouchi, M., Malkan, M.A., Hattori, T., Ota, K., Taniguchi, Y., Okamura, S., Ly, C., Iye, M., Furusawa, H., Shioya, Y., Shibuya, T., Ishizaki, Y., & Toshikawa, J. 2011, *ApJ*, 734, 119

Miley, G.K., & De Breuck, C. 2008, *A&AR*, 15, 67

Overzier, R.A., Shu, X., Zheng, W., Rettura, A., Zirm, A., Bouwens, R.J., Ford, H., Illingworth, G.D., Miley, G.K., Venemans, B., & White, R.L. 2009, *ApJ*, 704, 548

Röttgering, H.J.A., Lacy, M., Miley, G.K., Chambers, K.C., & Saunders, R. 1994, *A&AS*, 108, 79

Saxena, A., Röttgering, H.J.A., & Rigby E.E., 2017, *MNRAS* 469, 4083

Saxena, A., Jagannathan, P., Röttgering, H.J.A.; Best, P.N., Intema, H.T., Zhang, M., Duncan, K.J., Carilli, C.L., & Miley, G.K. 2018, *MNRAS* 475, 5041

Saxena, A., Marinello, M., Overzier, R.A., Best, P.N., Röttgering, H.J.A., Duncan, K.J., Prandoni, I., Pentericci, L., Magliocchetti, M., Paris, D., Cusano, F., Marchi, F., Intema, H.T., & Miley, G.K. 2018, *MNRAS* 480, 2733

Seymour, N., Ogle, P., De Breuck, C., Fazio, G.G., Galametz, A., Haas, M., Lacy, M., Sajina, A., Stern, D., Willner, S.P., & Vernet, J. 2008, *ApJ*, 681, L1

Venemans, B.P., Kurk, J.D., Miley, G.K., et al. 2002, *ApJ*, 569, L11

Willott, C.J., Rawlings, S., Jarvis, M.J., & Blundell, K.M. 2003, *MNRAS* 322, 536

Astronomy in Focus, Volume 1
XXXth IAU General Assembly, August 2018
Volker Beckmann & Claudio Ricci, eds.

DOI: 00.0000/X000000000000000X

The High-energy emission of jetted AGN

Daniel A. Schwartz[1]

[1]Smithsonian Astrophysical Observatory,
60 Garden St.,Cambridge, MA 02138, USA
email: das@cfa.harvard.edu

Abstract. Quasars with flat radio spectra and one-sided, arc-second scale, ≈ 100 mJy GHz radio jets are found to have similar scale X-ray jets in about 60% of such objects, even in short 5 to 10 ks *Chandra* observations. Jets emit in the GHz band via synchrotron radiation, as known from polarization measurements. The X-ray emission is explained most simply, i.e. with the fewest additional parameters, as inverse Compton (iC) scattering of cosmic microwave background (cmb) photons by the relativistic electrons in the jet. With physics based assumptions, one can estimate enthalpy fluxes upwards of 10^{46} erg s^{-1}, sufficient to reverse cooling flows in clusters of galaxies, and play a significant role in the feedback process which correlates the masses of black holes and their host galaxy bulges. On a quasar-by-quasar basis, we can show that the total energy to power these jets can be supplied by the rotational energy of black holes with spin parameters as low as $a = 0.3$. For a few bright jets at redshifts less than 1, the *Fermi* gamma ray observatory shows upper limits at 10 Gev which fall below the fluxes predicted by the iC/cmb mechanism, proving the existence of multiple relativistic particle populations. At large redshifts, the cmb energy density is enhanced by a factor $(1+z)^4$, so that iC/cmb must be the dominant mechanism for relativistic jets unless their rest frame magnetic field strength is hundreds of micro-Gauss.

Keywords. (galaxies:) quasars: general, galaxies: jets, X-rays: galaxies, radio continuum: galaxies, black hole physics,(cosmology:) cosmic microwave background

1. Introduction

Radio astronomy is intimately related to high energy astronomy. Estimates of magnetic fields in the lobes of radio sources led to the recognition that TeV electrons must be present to radiate via the synchrotron mechanism. This motivated early suggestions (Morrison(1958), Savedoff(1959)) that direct detection of celestial gamma rays might be feasible. Estimates of the energy contents of these radio lobes were extremely large, posing difficulties for explaining the origin and possible relation to the associated galaxy or quasar. The dilemma was solved by theoretical explanations of how collimated beams of particles and fields, i.e. jets, could carry energy to the lobes (Rees(1971), Longair et al.(1973), Scheuer(1974), Blandford & Rees(1974), Begelman, Blandford, & Rees), and by direct imaging of these radio jets (Turland(1975), Waggett et al.(1977), Readhead et al.(1978), Perley et al.(1979), Bridle & Perley(1984)). The existence of X-ray emission from the nearest, brightest jets in Cen A (Feigelson et al.(1981)), 3C273 (Willingale(1981)), and M87 (Schreier et al.(1982)) resulted from observations by the *Rosat* and *Einstein* X-ray telescopes, each with about $5''$ angular resolution. The *Chandra* X-ray observatory (Weisskopf *et al.* (2002), Weisskopf *et al.* (2003), Schwartz(2014)) with its $0\farcs5$ resolution telescope gives a 100-fold increase in 2-dimensional imaging capability. This has led to the discovery of X-ray jets in a wide variety of astronomical systems (Schwartz(2010)), and in particular has exploded the study of X-ray emission from extragalactic radio jets.

1.1. *Importance of jets*

In their 1984 review, Begelman, Blandford, & Rees wrote "...the concept of a jet is crucial to understanding all active nuclei, ..." Jets can carry significant amounts of energy, and since that power is not subject to the Eddington radiation limit jets may allow super-Eddington accretion rates. Such accretion may be relevant to the growth of super-massive black holes in the early universe. High energy observations using the *Chandra* Observatory revealed the effects of jets on the gas filling clusters of galaxies Fabian et al.(2000). This solved a long standing problem that the cooling time of gas in clusters of galaxies was much less than the Hubble time, implying that the cluster gas should collapse catastrophically. Jets on parsec scales in the nuclei of galaxies explain the blazar phenomena of rapid variability and apparent superluminal expansion. It is now known from direct imaging that regions within X-ray jets may be variable even 10's of kpc from the black hole (Marshall et al.(2010), Hardcastle et al.(2016)). From gravitational lensing observations (Barnacka(2018)) of γ-ray blazars it was found that variability could originate from regions many kpc from the black hole (Barnacka et al.(2015)) and that γ-ray flares occur at locations distinct from the radio core (Barnacka et al.(2016)). These X-ray and γ-ray variability cases constrain the mechanisms of particle acceleration.

1.2. *Outline of this review*

This review considers non-thermal jets from extra-galactic sources, and will emphasize X-ray observations of powerful quasars. In the case of FR-I radio sources, the X-ray jet emission can generally be interpreted as an extension of the radio synchrotron spectrum (Worrall(2005), Harris & Krawczynski(2006), Harris & Krawczynski(2007), Worrall(2009)). The subject of this review will be FR-II quasars, in which case an optical flux or upper limit generally shows that the X-rays can not be an extension of the radio synchrotron emission. In section 3 we will see how this gives information on the relativistic parameters of the jet, and/or on multiple distinct populations of relativistic electrons.

2. Application of the minimum energy assumption

The intensity of synchrotron radiation from a power law distribution of relativistic electrons, $\mathrm{dN/d}\gamma{=}\kappa\gamma^{-(2\alpha+1)}$ is proportional to the product of κ and the magnetic field strength B. Here, α is the energy index of the observed radiation, γmc^2 is the electron energy, and the spectrum is usually assumed to extend from a minimum γ_1 to a maximum γ_2. From the radio synchrotron flux density alone, one cannot determine either the magnetic field strength or the relativistic particle density. Another relation between B and κ can be obtained by assuming minimum total energy in particles and fields, which is nearly equivalent to assuming equipartition of energy between those two channels (Burbidge(1956)). This assumption is now widely used for the interpretation of sources emitting synchrotron radiation.

Miley(1980) has previously discussed the assumptions necessary to apply the minimum energy condition. We update that discussion by considering the relativistic particle spectrum to extend from γ_1 to γ_2 instead of fine tuning the γ to extend from the limits of observed radio frequencies, and by considering the application to X-ray jet measurements. This picture allows the equation for the minimum energy magnetic field strength to be written in the form given by Worrall(2009):

$$\boldsymbol{B_{min} = f_{min}[G(\alpha)(1+k)L_\nu \nu^\alpha(\gamma_1{}^{1-2\alpha} - \gamma_2{}^{1-2\alpha})/(\phi l r t)]^{1/(\alpha+3)}},$$

where G($\boldsymbol{\alpha}$) is a combination of physical constants and functions of $\boldsymbol{\alpha}$.

In the on-line version we have color-coded the symbols as follows: green symbols for quantities which can be measured directly, namely the spectral index $\boldsymbol{\alpha}$, the luminosity

density L_ν at frequency ν, and the length of the jet element l. In turn, the luminosity is determined from the flux density and the length is determined from the angular extent by using the measured redshift and a cosmological model. Here we use H_0=67.3 km s^{-1} Mpc^{-1} and Ω_m=0.315 from the Planck Collaboration et al.(2017) results, in a flat universe. Blue symbols are not directly measured, but have some observational limits. These include the extremes of the power law electron spectrum, γ_1 and γ_2, and the width of the jet r. We note that γ_2 has a negligible effect on the calculation, since it is typically orders of magnitude larger than γ_1. Red symbols are based on intuitive or simplifying assumptions, such as the ratio, k, of energy in relativistic protons to the energy in electrons (including positrons), the filling factor, ϕ, of particles and fields in the jet, the line of sight thickness, t, through the jet, and the assumption, f_{min} that the magnetic field strength corresponds exactly to the minimum energy condition. Here we will take the values $k = \phi = f_{min} = 1$ and t=r. In addition to assuming minimum energy, we must transform observed quantities to the jet rest frame using the Doppler factor $\delta = 1/(\Gamma(1 - \beta\cos(\theta)))$ where θ is the angle of the jet to our line of sight and Γ is the Lorentz factor of the jet relative to the cmb frame. The above discussion shows that we must consider possible magnetic field strength uncertainty of a factor of 2 or 3 in any modeling.

The *Lynx* X-ray observatory (Gaskin et al.(2017), Gaskin et al.(2018), Özel(2018), Vikhlinin(2018)), which is being studied for submission to the 2020 Decadal Committee for Astronomy and Astrophysics, would have $0\farcs5$ angular resolution and 2 m^2 effective area. The *Lynx* capabilities will allow significant improvements in the determination of some of the quantities needed to calculate B_{min} for X-ray jets. Currently, the modest photon statistics from *Chandra* observations allow only an upper limit of $\approx 0\farcs5$ for the width, r, and assumed thickness, t, of X-ray jets. With the 30-fold increase in collecting area, *Lynx* should allow measurements of widths down to $0\farcs1$, or of order 700 pc even for the most distant jets. At 200—300 eV, the *Lynx* throughput will be 100 times that of *Chandra*. This should allow direct determination of γ_1 via measurement of the soft X-ray turn-over at those energies. With *Chandra* this measurement could only be applied to PKS0637-752 (Mueller & Schwartz(2009)) due to the build-up of contamination on the filter of the ACIS camera. The improved statistics will also allow precise measurement of the jet X-ray spectral index α. The iC/cmb mechanism assumes this is the same index as the GHz spectrum, although it could be flatter if the radiative lifetime of the GHz emitting electrons is comparable to or less than the age of the jet.

3. The iC/cmb interpretation

The X-ray emission of the luminous jet in PKS 0637-752 could not be explained by reasonable models of synchrotron, inverse Compton, or thermal mechanisms (Schwartz et al.(2000), Chartas et al.(2000)). Tavecchio et al.(2000) and Celotti et al.(2001) provided the insight of invoking relativistic bulk motion of the jet with Lorentz factor Γ, and using the result from Dermer and Schlickeiser(1994) that this increased the energy density of the cosmic microwave background in the rest frame of the jet by the factor Γ^2. Subsequently the iC/cmb model has been widely used to interpret the X-ray emission from the jets of powerful quasars (Siemiginowska et al.(2002), Sambruna et al.(2002), Sambruna et al.(2004), Sambruna et al.(2006), Marshall et al.(2005), Schwartz(2005), Marshall et al.(2011), Marshall et al.(2018), Schwartz et al.(2006), Schwartz et al.(2006b), Worrall(2009), Perlman et al.(2011), Massaro et al.(2011)).

Arguments supporting the iC/cmb model were originally based on the similarity of the X-ray and the radio jet profiles over extended angular distances, with the interpreta-

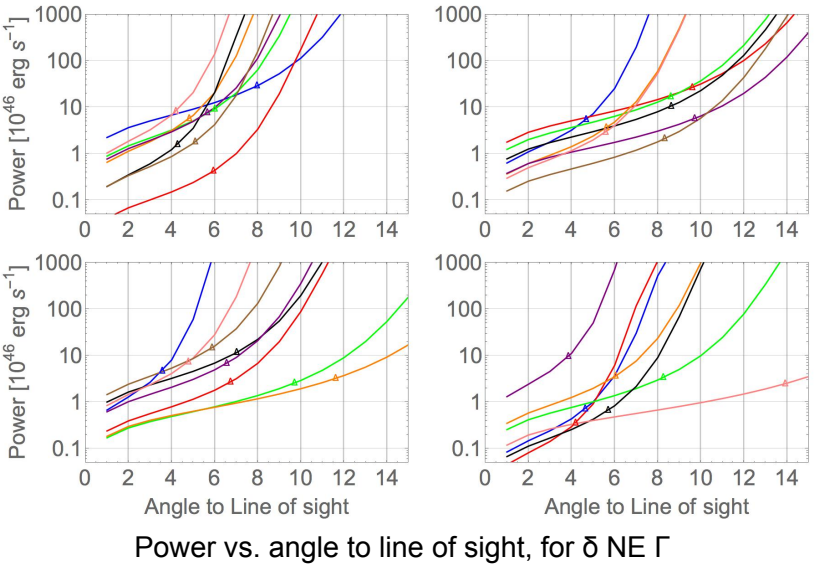

Figure 1. Each curve in one of the panels gives what would be the enthalpy flow in one of the 31 detected jets, calculated as a function of the unknown angle of that jet to our line of sight, and using the iC/cmb model. The triangle on each curve marks the point for which $\boldsymbol{\Gamma = \delta}$, and gives reasonable values for the distribution of parameters of the jet sample.

tion that they therefore originated from a single, broad relativistic electron population. (Schwartz et al.(2000), Schwartz(2005b), Harris et al.(2017)), Further evidence is suggested by the termination of X-ray emission just where the radio jet goes through a large change of direction (Schwartz et al.(2003), Schwartz(2010)). This is naturally explained by the X-ray to radio ratio of $\boldsymbol{\delta^{1+\alpha}}$ discussed by Dermer(1995). However, powerful evidence against the iC/cmb mechanism in the case of PKS 0637-752 was presented by Meyer et al.(2015), and Meyer et al.(2017), while Breiding et al.(2017) presented similar evidence for 3 jets for which the iC/cmb model had not been indicated. They showed *Fermi* upper limits to GeV $\boldsymbol{\gamma}$-ray emission was below the level expected *if* the electron spectrum producing the GHz radio emission also produced the jet emission observed in the *ALMA* and IR/optical regions. In any event, there must be two distinct populations of relativistic electrons, and the X-rays could possibly arise from iC/cmb if the second population produced the *ALMA* and optical emission. The existence of two populations immediately shows that the assumption on the filling factor, $\boldsymbol{\phi = 1}$, is not correct.

In this review we will continue to interpret the X-ray emission as iC/cmb, which we note involves no new parameters for these relativistic jets. In particular, we discuss the results from the systematic survey of Marshall et al.(2005), Marshall et al.(2011), Marshall et al.(2018) and previously presented by Schwartz et al.(2015). Figure 1 shows the deduced enthalpy power (Bicknell(1994)) carried by the 31 detected jets, parameterized as a function of the unknown angle to our line of sight. Qualitatively it is apparent that very small angles imply a very large population of unrecognized sources which lie at larger

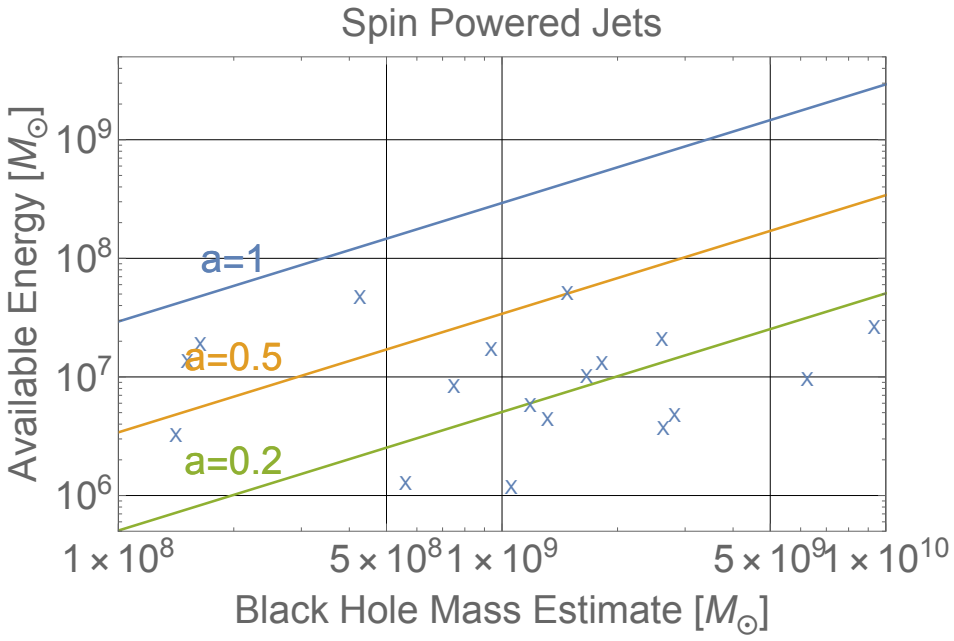

Figure 2. The solid lines show the available rotational energy, in terms of rest mass, which can be recovered by optimal spin-down of a black hole as a function of initial mass. The different spin parameters a=1,0.3,0.2, respectively allow 29%, 1%, and 0.5% of the mass-energy of the black hole to be recovered in principle. The x's plot the amount of energy required to sustain the power of the jets for 10^7 years. The black hole mass estimate here is taken as a median value of estimates in the literature tabulated by Shen et al.(2011), and by Xiong & Zhang(2014) and references therein. Even black holes with only 0.2 to 0.3 of the maximum possible angular momentum, can power the jets we measured for millions of years.

angles. Large angles, greater than 6° to 12° for most of the objects, imply unrealistically large powers; namely, greater than 10^{49} ergs s^{-1}. An assumption is often made that $\boldsymbol{\Gamma = \delta}$. This corresponds to the jet being at the largest possible angle to our line of sight for the given value of $\boldsymbol{\delta}$. Those points are indicated by the triangles on each curve, and we expect they give a reasonable estimate of the distribution of results from the sample.

4. Connection to the super-massive black hole

The rotational energy, E_r of a Kerr black hole manifests as a contribution $E_r/c^2=M_r$ to the total mass of the black hole. The relation is non-linear, with the fraction

$$M_r/M = 1 - \sqrt{0.5(1 + \sqrt{(1 - a^2/M^2)})}$$

being available in principle to be expelled. Here, $\boldsymbol{a}$ is the spin parameter in units of the total black hole mass $\boldsymbol{M}$. The solid lines in Figure 2 show the available mass that can, in principle, be released as a function of the total black hole mass. The $\boldsymbol{x's}$ plot the mass-energy equivalent required to energy to power the jets for 10^7 years, as determined

from the $\boldsymbol{\Gamma = \delta}$ point in Figure 1. We plot those masses against the estimated mass of the given black hole. That black hole mass is taken from the median of values given in the literature for 18 objects where it is available. We see that maximally spinning black holes, $\boldsymbol{a \approx 1}$ can provide more than the required energy, and super-massive black holes with spin parameters even as low as 0.3 could in principle power the observed jets for millions of years. Of course, this consideration does not address the dynamics of actually extracting such energy in a collimated flow.

Numerical calculations of the magnetically arrested disk (MAD) model (Narayan et al.(2003), Igumenshchev(2008), Sądowski et al.(2014), Tchekhovskoy et al.(2011), Zamaninasab et al.(2014)) for a rapidly spinning black hole have had some success showing that jets can be formed, and can extract more than the potential energy of the accreting matter. A magnetic field is advected in with the accreting matter, and is compressed and amplified until its pressure balances the gravitation pull (Narayan et al.(2003)). This results in chaotic variability of the accretion, and the rapidly spinning black hole wraps the magnetic field lines into a tight spiral about the spin axis. Observations of rotation measure gradients across pc-scale radio jets provides evidence for such field geometry (Gabuzda(2014), Gabuzda et al.(2015), Gabuzda et al.(2017)). The magnetic pressure then causes ejection along the spin axis. If we assume that the initial ejection right at the gravitational radius of an extreme Kerr black hole is a pure Poynting flux, then we can obtain a lower limit to that initial magnetic field by assuming 100% efficiency for converting that Poynting flux into the energy flux deduced for the kpc-scale jet. Such initial field strengths are shown in Figure 3. We have taken the mass from fundamental plane relation of Gültekin et al.(2009) to deduce the gravitational radius $\boldsymbol{r_g}$ of each quasar.

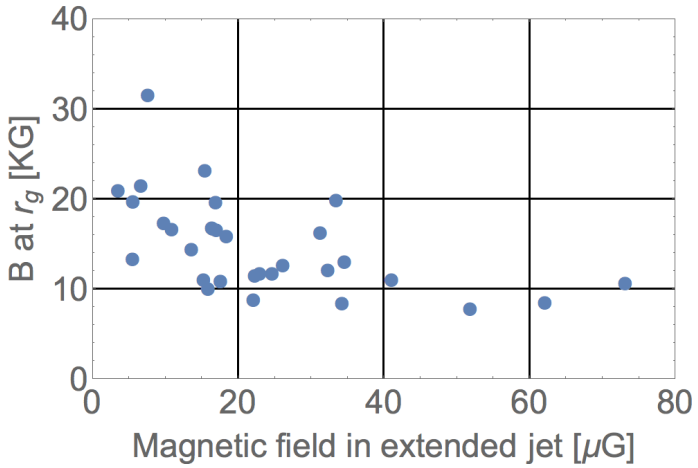

Figure 3. Ordinate: Magnetic field strength at the gravitational radius such that the Poynting vector equals the power deduced for the kpc-scale jet. Abscissa: Mean magnetic field strength in the rest frame of the kpc scale jet, according to the iC/cmb model. Points are the 31 jets detected in the survey discussed in section 3. (In view of numerous uncertainties, we do not consider the possible anti-correlation to be significant.)

5. Summary

We use Chandra X-ray observations to estimate the power of quasar jets, by observing the jet itself. We tie this to the central black hole mass on an individual object basis. The rotational energy of super-massive black holes can power these quasar jets, even with spin parameters as low as a=0.2, for lifetimes longer than millions of years. If the power we observe originates as a pure Poynting flux, we derive initial magnetic field strengths of a few 10's of kilo-Gauss. For models of magnetically arrested disks this inferred magnetic flux is of the order of magnitude of predictions, for Eddington limited accretion onto maximally spinning super-massive black holes.

References

Barnacka, A., Geller, M. J., Dell'Antonio, I. P., & Benbow, W. 2015, *ApJ*, 809, 100
Barnacka, A., Geller, M. J., Dell'Antonio, I. P., & Zitrin, A. 2016, *ApJ*, 821, 58
Barnacka, A. 2018, *arXiv:1810.07265*, https://doi.org/10.1016/j.physrep.2018.10.001
Begelman, M. C., Blandford, R. D., & Rees, M. J. 1984, *Reviews of Modern Physics*, 56, 255
Bicknell, G. V. 1994, *ApJ*, 422, 542
Blandford, R. D., & Rees, M. J. 1974, *MNRAS*, 169, 395
Breiding, P., Meyer, E. T., Georganopoulos, M., et al. 2017, *ApJ*, 849, 95
Bridle, A. H., & Perley, R. A. 1984, *AAR&A*, 22, 319
Burbidge, G. R. 1956, *ApJ*, 124, 416
Celotti, A., Ghisellini, G., and Chiaberge, M. 2001, *MNRAS*, 321, L1
Chartas, G., et al. 2000, *ApJ*, 542, 655
Dermer, C. D. 1995, *ApJL*, 446, L63
Dermer, C. D. and Schlickeiser, R. 1994, *ApJS*, 90, 945
Fabian, A. C., Sanders, J. S., Ettori, S., et al. 2000, *MNRAS*, 318, L65
Feigelson, E. D., Schreier, E. J., Delvaille, et al. 1981, *ApJ.*, 251, 31
Gaskin, J. A., Allured, R., Bandler, S. R., et al. 2017, *SPIE Conference Series*, 10397, 103970S
Gaskin, J. A., Dominguez, A., Gelmis, K., et al. 2018, *SPIE Conference Series*, 10699, 106990N
Gabuzda, D. 2014, *Nature*, 510, 42
Gabuzda, D. C., Knuettel, S., & Reardon, B. 2015, *MNRAS*, 450, 2441
Gabuzda, D. C., Roche, N., Kirwan, A., et al. 2017, *MNRAS*, 472, 1792
Gültekin, K., Cackett, E. M., Miller, J. M., et al. 2009, *ApJ*, 706, 404
Hardcastle, M. J., Lenc, E., Birkinshaw, M., et al. 2016, *MNRAS*, 455, 3526
Harris, D. E., & Krawczynski, H. 2006, *ARAA*, 44, 463
Harris, D. E., & Krawczynski, H. 2007, *Revista Mexicana de Astronomia y Astrofisica*, vol. 27, 27, 188
Harris, D. E., Lee, N. P., Schwartz, D. A., et al. 2017, *ApJ*, 846, 119
Igumenshchev, I. V. 2008, *ApJ*, 677, 317
Longair, M. S., Ryle, M., & Scheuer, P. A. G. 1973, *MNRAS*, 164, 243
Marshall, H. L., Schwartz, D. A., Lovell, J. E. J., et al. 2005, *ApJS*, 156, 13
Marshall, H. L., Hardcastle, M. J., Birkinshaw, M., et al. 2010, *ApJL*, 714, L213
Marshall, H. L., Gelbord, J. M., Schwartz, D. A., et al. 2011, *ApJS*, 193, 15
Marshall, H. L., Gelbord, J. M., Worrall, D. M., et al. 2018, *ApJ*, 856, 66
Massaro, F., Harris, D. E., & Cheung, C. C. 2011, *ApJS*, 197, 24
Meyer, E. T., Georganopoulos, M., Sparks, W. B., et al. 2015, *ApJ*, 805, 154
Meyer, E. T., Breiding, P., Georganopoulos, M., et al. 2017, *ApJL*, 835, L35
Miley, G. 1980, *ARAA*, 18, 165
Morrison, P. 1958, *Nuovo Cimento*, 7, 858
Mueller, M., & Schwartz, D. A. 2009, *ApJ*, 693, 648
Narayan, R., Igumenshchev, I. V., & Abramowicz, M. A. 2003, *PASJ*, 55, L69
Narayan, R., McClintock, J. E., & Tchekhovskoy, A. 2014, in: J. Bičák & T. Ledvinka (eds.), *General Relativity, Cosmology and Astrophysics* (Springer) p. 523

Özel, F. 2018, *Nature Astronomy*, 2, 608
Perley, R. A., Willis, A. G., & Scott, J. S. 1979, *Nature*, 281, 437
Perlman, E. S., Georganopoulos, M., Marshall, H. L., et al. 2011, *ApJ*, 739, 65
Planck Collaboration, Aghanim, N., Akrami, Y., et al. 2017, *A&Ap*, 607, A95
Readhead, A. C. S., Cohen, M. H., & Blandford, R. D. 1978, *Nature*, 272, 131
Rees, M. J. 1971, *Nature*, 229, 312
Sądowski, A., Narayan, R., McKinney, J. C., & Tchekhovskoy, A. 2014, *MNRAS*, 439, 503
Sambruna, R. M., Maraschi, L., Tavecchio, F., Urry, C. M., Cheung, C. C., Chartas, G., Scarpa, R., & Gambill, J. K. 2002, *ApJ*, 571, 20
Sambruna, R. M., Gambill, J.K., Maraschi, L., Tavecchio, F., Cerutti, R., Cheung, C. C., Urry, C. M., & Chartas, G., 2004, *ApJ*, 608, 698
Sambruna, R. M., Gliozzi, M., Donato, D., et al. 2006, *ApJ*, 641, 717
Savedoff, M. P. 1959, *Nuovo Cimento*, 13, 12
Scheuer, P. A. G. 1974, *MNRAS*, 166, 513
Schreier, E. J., Gorenstein, P., and Feigelson, E. D., 1982,*ApJ*, 261, 42
Schwartz, D. A., et al. 2000,*ApJL*, 540, L69
Schwartz, D. A., Marshall, H. L., Miller, B. P., et al. 2003, in: S. Collin, F. Combes and I. Shlosman (eds.) *ASP Conference Series*, 290, 359
Schwartz, D. A. 2005, *EAS Publications Series*, 15, 353
Schwartz, D. A. 2005, in: Pisin Chen, Elliott Bloom, Greg Madejski, and Vahe Patrosian (eds.), *22nd Texas Symposium on Relativistic Astrophysics*, p.38
Schwartz, D. A., Marshall, H. L., Lovell, J. E. J., et al. 2006, *ApJ*, 640, 592
Schwartz, D. A., Marshall, H. L., Lovell, J. E. J., et al. 2006b, *ApJL*, 647, L107
Schwartz, D. 2010, *PNAS*, 107, 7190
Schwartz, D. A. 2014, *Rev. Sci. Inst.*, 85, 061101
Schwartz, D. A., Marshall, H. L., Worrall, D. M., et al. 2015, *IAU Symposium Extragalactic Jets from Every Angle*, 313, 219
Shen, Y., Richards, G. T., Strauss, M. A., et al. 2011, *ApJS*, 194, 45
Siemiginowska, A, Bechtold, J., Aldcroft, T. L., Elvis, M., Harris, D. E., Dobrzycki, A. 2002, *ApJ*, 570, 543
Tavecchio, F.,Maraschi, L., Sambruna, R. M., Urry, C. M. 2000, *ApJL*, 544, L23
Tchekhovskoy, A., Narayan, R., & McKinney, J. C. 2011, *MNRAS*, 418, L79
Turland, B. D. 1975, *MNRAS*, 172, 181
Vikhlinin, A. 2018, *AAS Meeting* #231, 231, 103.04
Waggett, P. C., Warner, P. J., & Baldwin, J. E. 1977, *MNRAS*, 181, 465
Weisskopf, M. C., Brinkman, C., Canizares, C., et al. 2002, *PASP*, 114, 1
Weisskopf, M. C., Aldcroft, T. L., Bautz, M., et al. 2003, *Exp. Astron.*, 16, 1
Willingale, R. 1981 *MNRAS*, 194, 359
Worrall, D. M. 2005, *Highlights of Astronomy*, 13, 685
Worrall, D. M. 2009, *A&ARv*, 17, 1
Xiong, D. R., & Zhang, X. 2014, *MNRAS*, 441, 3375
Zamaninasab, M., Clausen-Brown, E., Savolainen, T., & Tchekhovskoy, A. 2014, *Nature*, 510, 126

Astronomy in Focus, Volume 1
XXXth IAU General Assembly, August 2018
Volker Beckmann & Claudio Ricci, eds.

DOI: 00.0000/X000000000000000X

SKA and the Cosmic Radio Dipole

Dominik J. Schwarz[1*], Carlos A. P. Bengaly[2], Roy Maartens[2,3], and Thilo M.Siewert[1]

[1]Fakultät für Physik, Universität Bielefeld, Postfach 100131, 33501 Bielefeld, Germany
[*]email: dschwarz@physik.uni-bielefeld.de

[2]Department of Physics & Astronomy, University of the Western Cape, Cape Town 7535, South Africa

[3]Institute of Cosmology & Gravitation, University of Portsmouth, Portsmouth PO1 3FX, United Kingdom

Abstract. We study the prospects to measure the cosmic radio dipole by means of continuum surveys with the Square Kilometre Array. Such a measurement will allow a critical test of the cosmological principle. It will test whether the cosmic rest frame defined by the cosmic microwave background at photon decoupling agrees with the cosmic rest frame of matter at late times.

Keywords. Cosmology

The Square Kilometer Array (SKA) will enable the observation of extragalactic radio sources up to large cosmological distances. The SKA's high survey speed offers the unique possibility to survey wide areas and to probe the largest observationally available scales in the Universe. The largest feature on the radio sky is the cosmic radio dipole.

The standard model of cosmology predicts that the radio sky must be isotropic. Deviations from isotropy are expected to arise from the proper motion of the Solar system w.r.t. to the isotropic sky. This kinematic signal is expected to be contaminated by a dipole from the matter distribution in the local large scale structure and from light propagation effects. We show that the SKA will be able to measure the kinematic dipole.

It is expected that this kinematic radio dipole agrees with the cosmic microwave background (CMB) dipole, which is assumed to be caused by the proper motion of the Sun with respect to the cosmic heat bath. The CMB dipole establishes the frame of the comoving observers, a central concept in modern cosmology, i.e. the observers that are at rest with respect to a spatially flat Friedmann-Lemaître space-time.

The CMB dipole has been measured by Planck with high accuracy and allows us to infer a proper motion of the Sun with a speed of $v = (369.82 \pm 0.11)$ km/s towards the Galactic coordinates $l = (264.021 \pm 0.011)^\circ$ and $b = (48.253 \pm 0.005)^\circ$ (Akrami *et al.* (2018)). However, the CMB dipole could also contain other contributions, e.g. a primordial temperature dipole or an integrated Sachs-Wolfe effect. Both effects are expected to be sub-dominant, but the cosmic variance of the dipole is large.

The extragalactic radio sky offers an excellent opportunity to perform an independent test of the proper motion hypothesis. It is expected that the radio dipole is dominated by the kinematic dipole, similar to the CMB. This is not the case for galaxy surveys at visible or infrared wavebands, which probe much lower redshifts.

The kinematic dipole in the radio source counts is due to Doppler and aberration effects and leads to a dipole amplitude of Ellis & Baldwin (1984)

$$A = [2 + x(1 + \alpha)]\beta \,, \tag{0.1}$$

assuming a universal power-spectrum of the flux density $S \propto \nu^{-\alpha}$, a scaling of number counts according to the relation $N(> S) \propto S^{-x}$, and β the dimensionless velocity of our

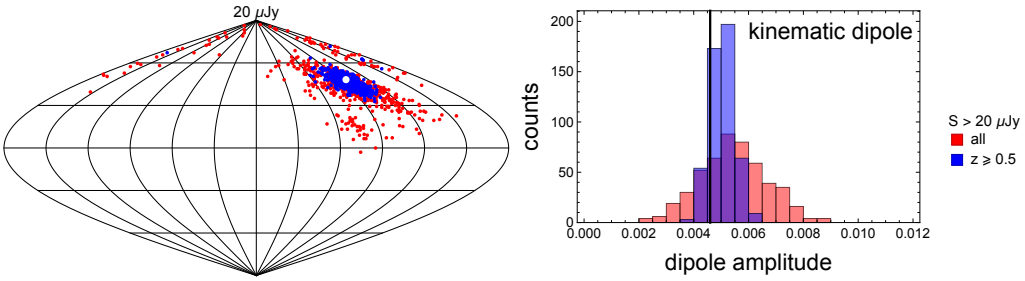

Figure 1. Reconstructed radio dipole direction (left) and amplitude (right) for 500 simulations of an SKA1 wide area continuum survey in frequency band 1. The red points include all radio sources, for the blue points we assume that local sources (at redshift below 0.5) can be identified and excluded from the analysis. The direction and amplitude of the kinematic radio dipole show good agreement with the assumed fiducial values (white point and vertical line).

motion relative to the radio sky. We will assume hereafter $\alpha = 0.76$, $x = 1$ and $\beta \equiv v/c$, hence giving a fiducial kinematic dipole amplitude of $A = 0.0046$.

In order to test the ability to measure the cosmic radio dipole, we create mock catalogues on which we test our dipole estimators. The mock catalogues and our analysis is described in detail in Bengaly *et al.* (2018). Here we present results for a wide area survey with SKA phase 1 by means of the SKA-mid frequency instrument in band 1 (350 MHz to 1050MHz) and assume a continuum flux density limit of $S > 20\mu$Jy (see Fig.1).

The result for the estimated radio dipole from 500 simulations is $l = (260 \pm 20)^\circ$ and $b = (45 \pm 16)^\circ$, when all radio sources are taken into account. The significant scatter is due to the contribution of the local matter dipole, i.e. the inhomogenous distribution of radio objects at small redshifts. This scatter can be reduced when local sources are excluded from the analysis. We assume that we will be able to identify the objects below redshift of 0.5 and exclude them from the analysis. That is likely to be possible by means of redshift measurements based on an SKA HI survey or based on photometric redshifts from surveys in the infrared and visible. Excluding local structures leads to a slight increase of Poisson noise, but the random admixture of the local structure dipole is largely suppressed. The resulting radio dipole points towards $l = (264.9 \pm 5.6)^\circ$ and $b = (46.7 \pm 5.1)^\circ$, in excellent agreement with the CMB dipole direction. Similar improvement is seen in the dipole amplitiude, which reduces from $A = 0.0052 \pm 0.0012$ to $A = 0.0048 \pm 0.0005$, when local radio sources are excluded. The estimate is in excellent agreement with the fiducial value, with an uncertainty on the kinematic radio dipole of 10 per cent.

This analysis goes beyond and complements the results presented in Schwarz *et al.* (2015), where the effects of Poisson noise, survey area, kinematic dipole and declination dependent systematics have been studied. We now included the effects of large scale structure and relativistic light propagation effects.

CB and RM acknowledge support from the South African SKA Project and the National Research Foundation of South Africa (Grant No. 75415). RM was also supported by the UK Science & Technology Facilities Council (Grant No. ST/N000668/1). TMS and DJS acknowledge support from DFG within project RTG 1620 “Models of Gravity”.

References

Akrami, Y. *et al.* [Planck collaboration] 2018, arXiv:1807.06205
Ellis, G.F.R., & Baldwin, J.E. 1984, *MNRAS* 206, 377
Bengaly, C.P.A., Siewert, T.M., Schwarz, D.J., & Maartens, R. 2018, arXiv:1810.04960
Schwarz, D.J., *et al.* 2015, *PoS AASKA* **14**, 032

Astronomy in Focus, Volume 1
XXXth IAU General Assembly, August 2018
Volker Beckmann & Claudio Ricci, eds.

DOI: 00.0000/X000000000000000X

Environmental dependence of radio galaxy populations

Stanislav S. Shabala[1]

[1]School of Natural Sciences, Private Bag 37, University of Tasmania, Hobart, TAS 7001, Australia
email: stanislav.shabala@utas.edu.au

Abstract.
Sensitive continuum surveys with next-generation interferometers will characterise large samples of radio sources at epochs during which cosmological models predict feedback from radio jets to play an important role in galaxy evolution. Dynamical models of radio sources provide a framework for deriving from observations the radio jet duty cycles and energetics, and hence the energy budget available for feedback. Environment plays a crucial role in determining observable radio source properties, and I briefly summarise recent efforts to combine galaxy formation and jet models in a self-consistent framework. Galaxy clustering estimates from deep optical and NIR observations will provide environment measures needed to interpret the observed radio populations.

Keywords. galaxies: jets, galaxies: active, hydrodynamics, radio: continuum

1. Introduction

Properties of radio Active Galactic Nuclei (AGN), their host galaxies and larger-scale environment are closely linked. On the one hand, radio sources are now widely accepted to be responsible for the bulk of the feedback required to restrict gas cooling and star formation in the most massive galaxies and clusters since $z \sim 1$ (e.g. Silk & Rees 1998, Croton et al. 2006). These objects are prevalent in environments where cooling needs to be suppressed, namely massive elliptical galaxies (Sadler et al. 1989) and clusters with short cooling times (Mittal et al. 2009); and there appears to be approximate heating/cooling equilibrium in the hot haloes (Best et al. 2007, Shabala et al. 2008). There is also strong evidence for an environmental dependence of the AGN triggering mechanisms (Sabater et al. 2013, Pimbblet et al. 2013, Poggianti et al. 2017, Marshall et al. 2018), related to two quite different accretion modes: direct cold gas fuelling of the central engine in strong line radio galaxies, and chaotic accretion of gas cooled out of the hot phase in weak line radio galaxies (Hardcastle 2018).

On the other hand, the morphologies of radio galaxies are also strongly influenced by environment. On sub-kpc scales, the jets may be mass-loaded, ultimately determining whether a core (Fanaroff-Riley type I; FR) or edge-brightnened (FR-II) structure emerges. On group and cluster scales of tens and hundreds of kpc, the observed properties of radio lobes and efficiency with which they impart feedback onto the surrounding gas are shaped by their environment (Hardcastle & Krause 2013, Yates et al. 2018).

Dynamical models of radio galaxies provide the framework within which observed radio galaxy properties can be interpreted. In this contribution, I describe recent development of environment-sensitive jet models, and future prospects for studying the energetics and duty cycles of radio galaxies in large continuum surveys.

2. Dynamical modeling of radio sources

Dynamical models of powerful FR-II radio sources date back to work by Scheuer (1974). In the basic picture, the momentum flux of relativistic jets drives expansion along the jet axis, while transverse growth is due to the expansion of an overpressured cocoon of radio plasma inflated by backflow from the jet termination shock. The radio cocoon expands supersonically through the surrounding gas, driving strong bow shocks. The dynamics of lobed FR-Is is similar to FR-IIs, despite differences in jet morphology and lobe particle content (Croston et al. 2018). Jetted FR-Is, on the other hand, are dominated by velocity structure in the sheared jet forward flow, and the surface brightness of the uncollimated jets decreases with distance from the core. Radio emissivity is calculated by making some assumptions about jet particle content and lobe magnetic field strength, the latter typically parametrised in terms of lobe pressure.

A key feature of all these models is their sensitivity to the pressure profile of the atmosphere into which the jets expand. While X-ray observations are the "gold standard" for quantifying jet environments, these are only available for a relatively small fraction of systems, and are biased towards gas-rich haloes. The alternative approach, adopted by Turner & Shabala (2015) in developing the **R**adio **A**GN **i**n **S**emi-analytic **E**nvironments (RAiSE), is to use statistical properties of galaxy haloes inferred from cosmological galaxy formation models. The RAiSE model successfully reproduces a number of key observables, including departure from self-similarity, the relationship between radio luminosity, morphology, and host galaxy mass (Turner & Shabala 2015); and by including broadband radio spectra, lobe magnetic field strengths estimated from Inverse Compton observations (Turner et al. 2018b). Recently, Turner et al. (2018a) combined the RAiSE model with numerical simulations of backflow in FR-IIs, and showed that the discrepancy between spectral and dynamical ages in the powerful radio galaxy 3C436 can be explained by the mixing of electron populations of different ages; this effect is most pronounced in regions far from the hotspots, where a relatively small number of young electrons can skew the broadband radio spectra to younger spectral ages. Combining jet and galaxy formation models within a self-consistent framework also places strong constraints on AGN feedback models: requiring observations of both galaxy *and* radio AGN populations to be matched simultaneously can rule out some feedback models (Raouf et al. 2017).

3. Radio source populations

Application of dynamical models to well-defined radio AGN samples can in principle yield a census of jet energetics and duty cycles. Figure 1 shows the results of applying the RAiSE model (Turner & Shabala 2015) to a volume-limited sample of local ($z < 0.1$) radio AGN. Best-fitting jet power and age are estimated for each observed point in size – luminosity space, after marginalising over all other parameters. The derived mass scaling of jet powers suggests the hot haloes are in heating – cooling equilibrium, and jet generation efficiencies are consistent with predictions of jet production models. The derived jet kinetic luminosity function shows that most of the kinetic energy budget is provided by the low number of bright radio sources.

Figure 1 clearly shows selection effects. The observed dearth of low-luminosity, large sources is simply a consequence of survey surface brightness sensitivity limit. By extrapolating inferred properties of sources just above the detection limit, it is possible to quantify the fraction of sources missed in the survey (see right panel).

The overabundance of compact, low-luminosity sources is more puzzling. Sometimes referred to as FR-0 radio sources (e.g. Baldi et al. 2015), these have been variously

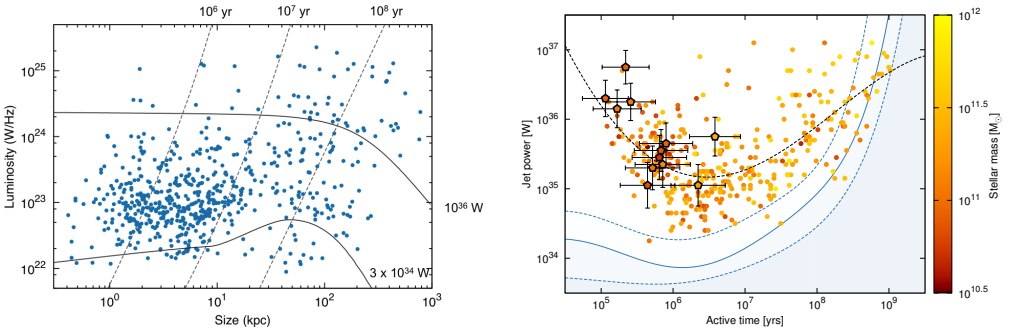

Figure 1. Application of the RAiSE model to a local ($z < 0.1$) sample of radio AGN from Shabala et al. (2008). *Left*: size-luminosity distributions at 1.4 GHz, with two representative tracks. *Right*: inferred jet kinetic power - age distributions (from Turner & Shabala 2015). Lines are detection limits for 50 (solid), 16 and 84 (dashed) percent of low surface brightness sources.

proposed to be young radio sources, or "frustrated" older jets whose expansion has been impeded by a dense atmosphere. The other possibility is that at least some of these objects are cores whose diffuse lobes are below the surface brightness detection threshold. This scenario is supported by the modelling of Shabala et al. (2017), who showed that lobes inflated by VLBI-detected jets will rapidly become too diffuse for detection if the AGN host galaxy is located in a poor environment, consistent with observational evidence for an increased fraction of compact radio AGN in lower-mass haloes (Shabala 2018).

The potential implications of such a population of radio sources could be important. If jets can form lobes which rapidly fade below the detection limit, existing models would be underestimating both the lifetimes and kinetic powers of jets, and hence the energy available for feedback on their hot haloes. If there is sufficient pressure to collimate the jets and form well-defined lobes (Krause et al. 2012), more sensitive observations may constrain jet parameters through measurements of lobe volume and/or spectral ageing. Jetted FR-Is are a more challenging proposition, since the lack of backflow in these objects ensures that the oldest electrons will be located in the most diffuse regions; here, observations sensitive to low surface brightness emission are the best hope, as spectacularly shown by Heesen et al. (2018) for the archetypal jetted radio galaxy 3C31. Environment-sensitive simulations connecting galaxy and hot halo scales will provide the theoretical framework within which observations can be interpreted.

4. Probing environment through asymmetric radio sources

Jet production models predict that the two anti-parallel jets should be intrinsically identical. Hence asymmetric radio sources provide the ideal test bed for both models of jet – environment interaction, and metrics used to quantify environment. Rodman et al. (submitted) used data from the Radio Galaxy Zoo citizen science project (Banfield et al. 2015) to test the hypothesis that any observed asymmetry in the radio continuum emission associated with the two jets is due to interaction with the environment. To minimize the effects of projection and model uncertainties, this analysis was restricted to a sample of straight FR-II lobes; environment associated with each lobe was quantified by counting SDSS galaxies with redshifts consistent with the AGN host. These authors found that the observed correlation between lobe length and galaxy clustering† is in excellent

† Correlations with lobe luminosity are much weaker, in agreement with model predictions of highly non-linear relations with age and environment (e.g. Shabala & Godfrey 2013).

quantitative agreement with model predictions. Galaxy clustering therefore provides an environmental metric which can be used in conjunction with radio source models to extract physical parameters of radio source populations.

5. Conclusions and future prospects

We are fast entering an era of large radio surveys. Dynamical models provide a mechanism for interpreting radio source energetics and lifetimes, yet both these models and inferences about radio source population properties are sensitive to assumptions about the environments into which the jets expand. We have developed a dynamical model in which the adopted measure of environment is halo mass. Studies of asymmetric radio sources suggest that halo masses measured through galaxy clustering will provide an excellent description of jet environments. A combination of sensitive radio surveys with ancillary galaxy clustering data therefore holds much promise. The in-progress GAMA Legacy ATCA Southern Survey (GLASS; Huynh et al. in prep.) will survey 60 deg^2 of the GAMA G23 field; on much larger scales, over the next few years SKA surveys will be complemented by optical catalogues from next-generation optical/IR instruments.

Acknowledgements

This research was supported by the Australian Research Council (grant DE130101399), and an Endeavour Research Fellowship. I am grateful to all my collaborators, past and present, for their insights into the physics of radio galaxies.

References

Baldi, R., Capetti, A., Giovannini, G., 2015, A&A, 576A, 38
Banfield, J. K., et al. 2015, MNRAS, 453, 2326
Best, P. N., et al. 2007, MNRAS, 379, 894
Croston, J. H., Ineson, J., Hardcastle, M J. 2018, MNRAS, 476, 1614
Croton, D. J., et al. 2006, MNRAS, 365, 11
Hardcastle, M. J., Krause, M. G H. 2013, MNRAS, 430, 174
Hardcastle, M. J., 2018, Nature Astronomy, 2, 273
Heesen, V., et al. 2018, MNRAS, 474, 5049
Krause, M. G. H., Alexander, P., Riley, J. M., Hopton, D. 2012, MNRAS, 427, 3196
Marshall, M. A., et al. 2018, MNRAS, 474, 3615
Mittal, R., Hudson, D. S., Reiprich, T. H., Clarke, T. 2009, A&A, 501, 835
Pimbblet, K. A., et al. 2013, MNRAS, 429, 1827
Poggianti, B., et al. 2017, Nature 548, 304
Raouf, M., et al. 2017, MNRAS, 471, 658
Sabater, J., Best, P. N., Argudo-Fernández, M. 2013, MNRAS, 430, 638
Sadler, Elaine M.; Jenkins, C. R.; Kotanyi, C. G. 1989, MNRAS, 240, 591
Scheuer, P. A. G. 1974, MNRAS, 166, 513
Shabala, S. S., Godfrey, L. E. H. 2013, ApJ, 769, 129
Shabala, S. S. 2018, MNRAS, 478, 5074
Shabala, S. S., Ash, S., Alexander, P., Riley, J. M. 2008, MNRAS, 388, 625
Shabala, S. S., et al. 2017, MNRAS, 464, 4706
Silk, J., Rees, M. J. 1998, A&A Lett., 331, 1
Turner, R. J., Shabala, S. S. 2015, ApJ, 806, 59
Turner, R. J., Rogers, J. G., Shabala, S. S., Krause, M. G. H. 2018, MNRAS, 473, 4179
Turner, R. J., Shabala, S. S., Krause, M. G. H. 2018, MNRAS, 474, 3361
Yates, P. M., Shabala, S. S., Krause, M. G. H. 2018, MNRAS, 480, 5286

Astronomy in Focus, Volume 1
XXXth IAU General Assembly, August 2018
Volker Beckmann & Claudio Ricci, eds.

DOI: 00.0000/X000000000000000X

Radio morphology as a probe of the environment: the radio galaxy 3C 382

L. Slavcheva-Mihova and B. Mihov

Institute of Astronomy and NAO, Bulgarian Academy of Sciences,
72 Tsarigradsko Chaussee Blvd., BG-1784 Sofia, Bulgaria
email: lslav@astro.bas.bg, bmihov@astro.bas.bg

Abstract.
We present a study of the optical morphology and its alignment with the radio structures in the radio galaxy 3C 382. The deep images have disturbed appearance with three filaments that match the radio pattern. We suggest that this alignment is related to interaction with the environment rather than to positive jet feedback. The galaxy closely projected to the northern hotspot is a physical companion. The tidal filaments oriented towards it interact with the light jet and deflect it. The southern filament is associated with the opposite lobe offset.

Keywords. Galaxies: active, galaxies: individual (3C 382)

1. Introduction and aims

Some Fanaroff-Riley II (FR II) galaxies show alignment of the major axis with the radio axis that could be associated with the star formation in case the latter has been triggered by the jet (e.g., Roche & Eales 2000). 3C 382 (z=0.05787) is an FR II broad-line radio galaxy. It hosts 1.′68 long jet and two radio lobes with a total extension of 3′ ending with hotspots. The lobe opposite the jet is displaced from the main axis of about 50°.

We present a study of the optical morphology and its alignment with the radio structures in 3C 382 in the framework of both interaction with a companion and jet feedback.

2. Results and discussion

We used spectra and images acquired at the 2-m telescope ($BVRI$ bands) at the Rozhen NAO, as well as archival data from Very Large Array (VLA, 1.5 GHz; Leahy & Perley 1991) and Isaac Newton Telescope (INT, r band). We performed a 2-D structural decomposition of the Rozhen images using GALFIT (Peng *et al.* 2010).

According to the 2-D fitting results and the colour maps, 3C 382 is an early type – E or S0 – galaxy. The residual image has an overall disturbed appearance – an irregular clumpy offset ring-like structure with filaments emerging out of it (Fig. 1). A couple of them extends to the northeast (NE) towards a barred spiral galaxy. There is another, more extended, filament to the south (S) found by us (Slavcheva-Mihova & Mihov 2011). The N lobe manifests a notable match in orientation and curvature with the NE filaments; the S filament probes the location of the opposite lobe displacement (Fig. 1). What is the origin of this alignment?

First, the possibility of positive jet feedback is studied. The velocity of the warm absorber outflow in 3C 382 is of order of 10^3 km s^{-1}, which favours the torus wind scenario (Torresi *et al.* 2012). Given the power of the jet, its Eddington ratio exceeds the critical one, determined by the requirement that the velocity of the outflow driven by the jet equals the velocity dispersion expected from the correlation between the black hole mass

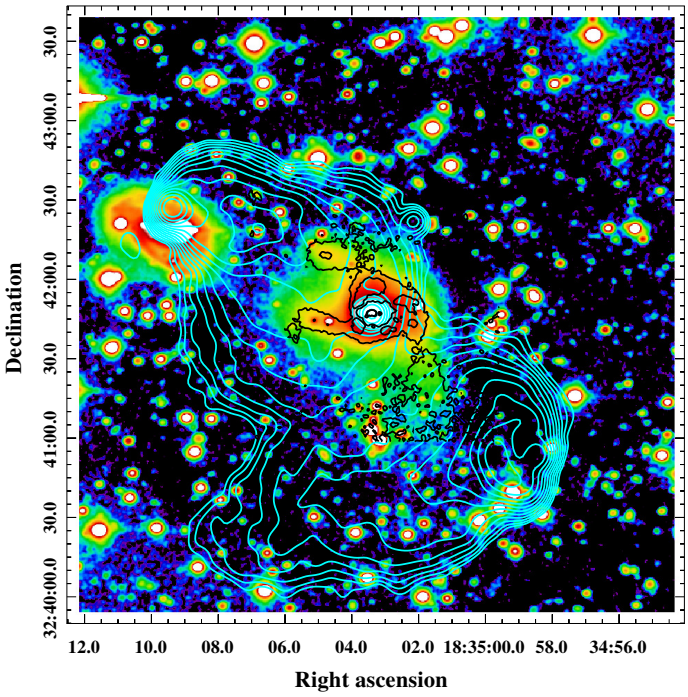

Figure 1. INT image (r band) of 3C 382 with the contours of the decomposition residual (R band, black) and VLA image (1.5 GHz, cyan) overplotted. The galaxy about 1.″4 to the NE (2MASX J18350968+3242162) is a physical companion. The match of the filaments with the relevant radio structure is outstanding.

and the bulge velocity dispersion. Thus, not only positive feedback is hardly expected, but the jet meets the criterion for effective negative feedback (Wagner *et al.* 2012).

Secondly, we explore the 3C 382 environment. The star-like object at the S filament base is most probably a projected star (Slavcheva-Mihova & Mihov 2011). The N hotspot is closely projected to the NE galaxy. The redshift derived from its optical spectrum prompts that this is a physical companion. The filaments are of tidal origin, viz. bridges and a counter-tail. Although the asymmetries in the companion are not major, both its bar and disturbed spiral structure may be induced by the interaction with 3C 382.

The hotspot spectra on both sides of 3C 382 are similar giving rise to the idea of a single injection spectrum (Dennett-Thorpe *et al.* 1999). We suggest the following scenario. The gas associated with the NE filaments interacts with the jet and deflects it; it has been shown that light jets can easily be bent by diffuse medium. The S filament, on its turn, interacts with the back flowing plasma of the opposite lobe and causes its offset. The lifetime of strong visible tidal features is of order of a few 10^8 yr up to 10^9 yr, while FR II jet lifetime is up to about 10^8 yr. Thus, it is reasonable for the filaments to precede the jet, which makes this scenario viable.

This research was partially supported by the Bulgarian National Science Fund of the Ministry of Education and Science under grants DN 08-1/2016 and DN 18/13-2017.

References

Dennett-Thorpe, J., Bridle, A. H., Laing, R. A. & Scheuer, P. A. G. 1999, *MNRAS*, 304, 271
Leahy, J., & Perley, R. 1991, *AJ*, 102, 537
Peng, C. Y., Ho, L. C., Impey, C. D., & Rix, H.-W. 2010, *AJ*, 139, 2097
Roche, N., & Eales, S. 2000, *MNRAS*, 317, 120
Slavcheva-Mihova, L. & Mihov, B. 2011, *A&A*, 526, A43
Torresi, E., Grandi, P., Costantini, E., & Palumbo, G. G. C. 2012, *MNRAS*, 419, 321
Wagner, A. Y., Bicknell, G. V., & Umemura, M. 2012, *ApJ*, 757, 136

Astronomy in Focus, Volume 1
XXXth IAU General Assembly, August 2018
Volker Beckmann & Claudio Ricci, eds.

DOI: 00.0000/X000000000000000X

AGN parameters in the ELAIS field using CIGALE

Nofoz Suleiman[1], Sándor Frey[2], Sándor Pintér[1], Timea Orsolya Kovács[1], and L. Viktor Tóth[1,2]

[1]Astronomy Deptartment, Eötvös Loránd University, 1117 Budapest, Hungary
email: n.suleiman@astro.elte.hu

[2]Konkoly Observatory, MTA CSFK, 1121 Budapest, Hungary

Abstract. We present a sample of AGN galaxies in ELAIS N1 field at various redshifts. We combined the new Herschel point source catalogue data with Sloan Digital Sky Survey (SDSS), 2MASS, Spitzer, WISE and other archival photometry data, creating spectral energy distributions (SEDs) that cover the rest-frame wavelength range from far-UV to far-IR. The SEDs were modeled using the CIGALE software, deriving galaxy properties with a high reliability. The SEDs of the sample were re-fitted once without Herschel data points and another one without AGN module, that to illustrate the effect of Herschel data on the AGN parameters.

Keywords. AGN host galaxy, Spectral Energy Distribution, Herschel data, ELAIS N1, CIGALE.

1. Introduction

There is compelling evidence that the growth of super-massive black holes and the stellar populations of their host galaxies are intricately linked (Torres-Papaqui et al. 2012). At the same time, the exact relationship between the buildup of stellar mass and the growth of super-massive black holes is still not well understood. The radio emission travels through the dusty media and allows a study of the active nucleus and its physical processes. Molecular line emission on the other hand indicates the physical properties of the interstellar medium. A statistical sample of galaxies should be investigated sampling all evolutionary phases and a range of galaxy masses. For that purpose, this research started to uncover parameters of the AGN host galaxies in ELAIS N1 field. The ELAIS (European Large Area ISO Survey) was the biggest open-time project of ISO (Infrared Space Observatory). Measurements were taken in four different bands (in a wavelength range of 6.7–175 μm) of multiple regions on the sky (12 square degrees in total) (Olivier et al. 2000). Multiple follow-up surveys were carried out in different wavelength ranges. This way the ELAIS N1 became one of the most known regions on the sky.

2. Framework & Results

To solve and to analyze the physical properties of AGN host galaxies in ELAIS N1 field, a catalogue was constructed including 43 AGN host galaxies with strict conditions. The new Herschel point source catalogue data are combined with Sloan Digital Sky Survey (SDSS), Two Micron All Sky Survey (2MASS), Spitzer, Wide-field Infrared Survey Satellite (WISE) and other archival photometry data, creating spectral energy distributions (SEDs) that cover the rest-frame wavelength range from far-UV to far-IR (from 0.15 to 160 μm). The new Herschel catalogues were used to add data points in the far infrared, where the dust surrounding young stars radiate, to constrain star formation better. The SEDs were modelled using the CIGALE (Code Investigating GALaxy

Table 1. The properties of the AGN host galaxy (ID:10) from the sample.

ID	Case	SFR ($M_\odot$/yr)	AGN Luminosity ($\times 10^{37}$ W)	Stellar Luminosity ($\times 10^{37}$ W)	Dust Luminosity ($\times 10^{37}$ W)	Stellar Mass ($\times 10^{9}$ $M_\odot$)
10	(1)	41.9	5.7	1.9	8.7	7.8
	(2)	78.1	5.9	2.0	8.9	8.0
	(3)	12.2	-	49.9	4.2	29.7

Emission) software (Noll et al. 2009), deriving galaxy properties with a high reliability by fitting the attenuated stellar emission and the related dust emission at the same time. The aimed galaxies in the sample were found in HerMES catalogue (Bussmann et al. 2015) and WISE AGN catalogue (Assef et al. 2018). The data were collected from the VizieR catalogue access tool and SIMBAD database, operated at CDS, Strasbourg, France. As well as Hershel data from NASA/IPAC Infrared Science Archive and SDSS magnitudes which were transformed to flux densities, taking into account the extinction yields by the dust. After fitting for all of that data (1), we refitted for the same object once without Herschel data (2) and once without AGN module (3), to see how the main properties change and to know the effectiveness of Herschel data and the AGN module on the SEDs and the AGN parameters.

The results of SED fitting of the AGN host galaxies in three cases show significant differences in the total flux density in the far-IR region, as illustrated with an example in Fig. 1. The fitted AGN parameters vary substantially in the different scenarios, as shown in Table 1.

References

Assef, R.J., Stern, D., Noirot, G., et al. 2018, *ApJS*, 234, 23
Bussmann, R.S., Riechers, D., Fialkov, A., et al. 2015, *ApJ*, 812, 43
Noll, S., Burgarella, D., Giovannoli, E., et al. 2009, *A&A*, 507, 1793
Oliver, S., Rowan-Robinson, M., Alexander, D.M., et al. 2000, *MNRAS*, 316, 749
Torres-Papaqui, J.P., Coziol, R., Ortega-Minakata, R.A., & Neri-Larios, D.M. 2012, *ApJ*, 754, 144

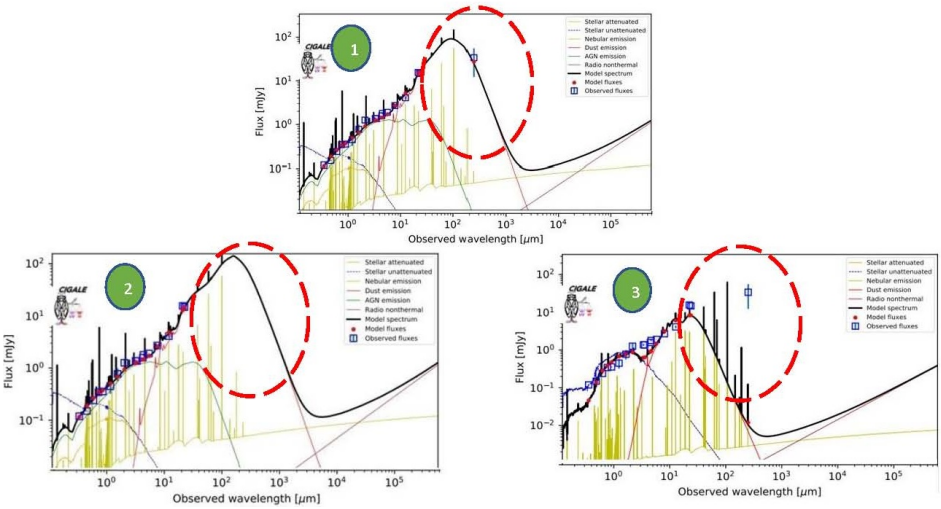

Figure 1. The SEDs for galaxy ID:10 (1) with Herschel data (2) without Herschel data (3) without AGN module

Astronomy in Focus, Volume 1
XXXth IAU General Assembly, August 2018
Volker Beckmann & Claudio Ricci, eds.

DOI: 00.0000/X000000000000000X

Physical and chemical properties of narrow-line regions in $z \sim 3$ radio galaxies through multi-line analysis

Koki Terao[1], Tohru Nagao[2], Kenta Matsuoka[3], Takuji Yamashita[2], Kyoko Onishi[2], and Yoshiki Matsuoka[2]

[1]Graduate School of Science and Engineering, Ehime University, Bunkyo-cho 2-5, Matsuyama, Ehime 790-8577, Japan email: terao@cosmos.phys.sci.ehime-u.ac.jp

[2]Research Center for Space and Cosmic Evolution, Ehime University, Bunkyo-cho 2-5, Matsuyama, Ehime 790-8577, Japan

[3]Dipartimento di Fisica e Astronomia, Universit di Firenze, Via G. Sansone 1, I-50019 Sesto Fiorentino, Italy

Abstract. The diagnostic studies for NLR clouds in high-z AGNs have been carried out by using only strong rest-UV emission lines, but such diagnostics require some assumptions due to the limited number of available emission lines. In this study, we focus on relatively faint rest-UV lines in some high-z radio galaxies, that may tell us details about gas properties. We diagnose the physical and chemical properties of the ISM for each object through the comparison between the measured emission-line fluxes and detailed photoionization models with Cloudy. We confirm that the metallicity of NLRs in AGNs at $z \sim 3$ is higher than the solar metallicity, without assuming the gas density and ionization parameter thanks to the newly detected faint emission lines. This result suggests that high-redshift radio galaxies have already matured chemically at $z \sim 3$.

Keywords. galaxies: active, galaxies: nuclei, (galaxies:) quasars: emission lines

1. Introduction

Physical and chemical properties of the interstellar medium (ISM) in galaxies and their redshift evolution are important to understand the formation and evolution of galaxies. The ISM properties of massive galaxies at $z > 2$ are particularly interesting, because the evolution of massive galaxies had been already completed at such high redshift. However, normal massive-galaxies at $z > 2$ are too faint to be examined spectroscopically in detail. On the other hand, emission-line spectra of narrow-line regions (NLRs) in active galactic nuclei (AGNs) offer an alternative approach to investigate the ISM properties of high-z massive galaxies (e.g., Nagao et al. 2006).

Numerous rest-UV emission lines are generally seen with optical spectroscopy for NLRs in $z \sim 3$ AGNs (e.g., Matsuoka et al. 2009). However, only strong UV lines (such as C IVλ1549, He IIλ1640, and C III]λ1909) have been used for diagnostic studies so far. Thus, some assumptions are required for examining the ISM properties (e.g., the gas density, ionization parameter, and so on). Here we focus on the high-sensitivity rest-UV spectra of 10 $z \sim 3$ radio galaxies to measure the flux of several emission lines including relatively faint ones (Humphrey et al. 2008; Matsuoka et al. 2009). Then, we diagnose the physical and chemical properties of the ISM in NLRs for each object through the comparison between the measured emission-line fluxes and detailed photoionization models with Cloudy version 13.03. The parameter ranges in our models are as follows; ionization parameter $\log U = -3.0$ - -0.5, gas density $\log n = 2.0$-6.0 cm^{-3}, and metallicity

$Z = 0.1 - 5.0\,Z_{\odot}$. The chemical composition is fixed to be solar elemental abundance ratios except for nitrogen. Nitrogen relative abundance is assumed to scale with the metallicity since N is a secondary element. The best-fit parameters are determined by searching for minimum reduced χ^2. From these procedures, we determine physical and chemical properties in NLRs using many emission lines. The detail methods are given in Terao et al. (in prep.).

2. Results and Conclusion

The best fit parameters are shown in Fig. 1 as a function of the He II luminosity. Most objects show a higher gas metallicity than the solar metallicity ($Z \sim 1.5 Z_{\odot}$). The inferred metallicity is consistent with earlier works for high-z radio galaxies, and these results indicate that the NLR metallicity shows no redshift evolution for $1 < z < 4$ (e.g., Nagao et al. 2006; Matsuoka et al. 2009). These results suggest that the NLRs of $z \sim 3$ radio galaxies had been already chemically evolved. We also compare $z \sim 3$ radio galaxies with low-z type 2 AGN taken from the SDSS and literature (Snijders et al. 1986; Evans et al. 1999). The density and ionization parameter of NLRs in $z \sim 3$ radio galaxies tend to be higher than those of low-z samples. This result infers that the ISM properties of AGN host galaxies show systematic redshift evolution.

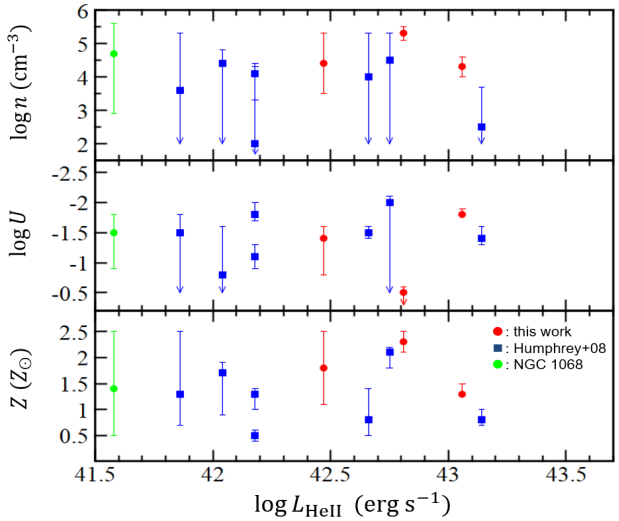

Figure 1. The best-fit parameters as a function of the He II luminosity. Red circles denote our targets. Blue filled squares denote the sample of Humphrey et al. (2008). Green circle denotes NGC 1068 (Snijders et al. 1986). Arrows indicate the cases reaching the upper/lower limit of parameter ranges in our model runs.

References

Evans, I., Koratkar, A., Allen, M., Dopita, M., & Tsvetanov, Z. 1999, *ApJ*, 521, 531
Humphrey, A., Villar-Martín, M., Vernet, J., et al. 2008, *MNRAS*, 383, 11
Matsuoka, K., Nagao, T., Maiolino, R., Marconi, A., & Taniguchi, Y. 2009, *A&A*, 503, 721
Nagao, T., Maiolino, R., & Marconi, A. 2006, *A&A*, 447, 863
Snijders, M. A. J., Netzer, H., & Boksenberg, A. 1986, *MNRAS*, 222, 549
Terao, K., Nagao, T., Matsuoka, K., et al. in prep.

Astronomy in Focus, Volume 1
XXXth IAU General Assembly, August 2018
Volker Beckmann & Claudio Ricci, eds.

DOI: 00.0000/X000000000000000X

The Nature of Blazar Radio Cores from Multi-Frequency Polarization Observations with the Korean VLBI Network

Sascha Trippe, Jongho Park, and Minchul Kam

Seoul National University, Gwanak-gu, Seoul 08826, South Korea
email: trippe@astro.snu.ac.kr

Abstract. We study the linear polarization of the radio cores of eight blazars simultaneously at 22, 43, and 86 GHz with observations obtained by the Korean VLBI Network (KVN) in three epochs between late 2016 and early 2017 in the frame of the Plasma-physics of Active Galactic Nuclei (PAGaN) project. We investigate the Faraday rotation measure (RM) of the cores; the RM is expected to increase with observing frequency if core positions depend on frequency due to synchrotron self-absorption. We find a systematic increase of RMs at higher observing frequencies in our targets. The RM–ν relations follow power-laws with indices distributed around 2, indicating conically expanding outflows serving as Faraday rotating media. Comparing our KVN data with contemporaneous optical polarization data from the Steward Observatory for a few sources, we find indication that the increase of RM with frequency saturates at frequencies of a few hundreds GHz. This suggests that blazar cores are physical structures rather than simple $\tau = 1$ surfaces. A single region, e.g. a recollimation shock, might dominate the jet emission downstream of the jet launching region. We detect a sign change in the observed RMs of CTA 102 on a time scale of ≈1 month, which might be related to new superluminal components emerging from its core undergoing acceleration/deceleration and/or bending. We see indication for quasars having higher core RMs than BL Lac objects, which could be due to denser inflows/outflows in quasars.

Keywords. BL Lacertae objects: individual (OJ 287, BL Lac, 1749+096) — qusars: individual (3C 273, 3C 279, 3C 345, 3C 454.3, CTA 102, 0235+164, 1633+38) — galaxies: active — galaxies: jets — polarization

---

The nature of blazar radio cores is a matter of ongoing debate. On the one hand, the standard Blandford & Königl jet model describes the core as the upstream region where the conical jet becomes optically thin, i.e., at unity optical depth. On the other hand, astrometric VLBI observations suggest that the core is a stationary, optically thin physical structure.

The Korean VLBI Network (KVN) has the unique capability of observing simultaneously at four frequencies, 22, 43, 86, and 129 GHz, or at two of these frequencies in dual polarization mode (Lee et al. 2014). Thanks to the simultaneous observation at multiple frequencies, one can overcome rapid phase variations at high frequencies caused by tropospheric delay that reduce the coherence time by applying the fringe solutions obtained at lower frequencies to higher ones, i.e., frequency phase transfer (FPT; Zhao et al. 2018). In early 2017, we launched a KVN large program, the Plasma-physics of Active Galactic Nuclei (PAGaN) project (J.-Y. Kim et al. 2015, Oh et al. 2015), for monitoring about 14 AGNs at the four KVN frequencies in dual polarization mode almost every month. Here we present the results from three observation epochs located between late 2016 and early 2017. Our main results were as follows:

(*a*) We found that RMs increase with frequency, with median values of 2.62×10^3 rad/m^2 and 1.42×10^4 rad/m^2 for the frequency pairs 22/43 GHz and 43/86 GHz, respectively.

These values are also higher than those obtained by Hovatta et al. (2012) at 8.1–15.4 GHz for the same sources. The median values are described well by a power-law function with $|\mathrm{RM}| \propto \nu^{\mathrm{a}}$ with $a = 2.42$. When a values are obtained separately for each source, they are distributed around $a = 2$ with mean and standard deviation of $a = 2.25 \pm 1.28$. This agrees with the expectation from core-shift (Jorstad et al. 2007) for many blazars at the KVN frequencies. This finding implies that the geometry of Faraday rotating media in blazar cores can be approximated as conical.

(*b*) We compared our KVN data with contemporaneous (within $\approx$ 1 week) optical polarization data from the Steward Observatory for a few sources. When we assume that the direction of EVPA rotation at radio frequencies is the same at optical wavelengths and that there is no $n\pi$ ambiguity, the optical data show a trend of EVPA rotation similar to that of the radio data. The RM values obtained with the optical data indicate that the power-law increase of RM with frequency continues up to a certain frequency, ν_{trans}, and then saturates, with $|\mathrm{RM}| \approx 10^{5-6}$ rad/m^2 at $\approx$ 250 GHz, depending on source and flaring activity. We suggest that this saturation is due to the absence of core shift above ν_{trans}; instead, radio cores are standing recollimation shocks. This is in agreement with other studies which concluded that the radio cores of blazars cannot purely be explained as the unity optical depth surface of a continuous conical jet but are physical structures at least in some cases.

(*c*) We detected a sign change in the observed RMs of CTA 102 over $\approx$ 1 month, while the magnitudes of RM were roughly preserved. Since this source showed strong flaring at the time of our observations, we suggest that new relativistic jet components emerging from the core undergo acceleration/deceleration and/or jet bending, thus leading to a change in the direction of the line-of-sight component of helical magnetic fields in the jet because of relativistic abberation.

(*d*) We found indication that the absolute values of the core RMs of FSRQs are larger than those of BLOs at 22–86 GHz, which is consistent with results found at cm wavelengths. This difference might arise from FSRQs having higher accretion rates than BLOs, resulting in larger amounts of material in the central engine.

(*e*) For those sources which show non-linear EVPAs–λ^2 relations, the RM-corrected (intrinsic) EVPAs might be different at different frequencies and thus at different locations of the jets. A recent ultra-high resolution image of BL Lac observed with space VLBI shows that its intrinsic EVPAs in the core region vary with different locations indeed.

(*f*) We suggest that the systematic increase of RM as function of observing frequency appears only when covering sufficiently large ranges in frequency, with different λ^2 laws at different frequency ranges connecting smoothly. Combining this with the fact that linear EVPA–λ^2 relations are commonly observed over narrow frequency ranges suggests that blazars cores might consist of multiple recollimation shocks such that polarized emission from one of the shocks is dominant in a given narrow frequency range.

References

Hovatta, T., Lister, M. L., Aller, M. F., et al. 2012, *ApJ*, 144, 105
Jorstad, S. G., Marscher, A. P., Stevens, J. A., et al. 2007, *AJ*, 134, 799
Kim, J.-Y., Trippe, S., Sohn, B. W., et al. 2015, *JKAS*, 48, 285
Lee, S.-S., Petrov, L., Byun, D.-Y., et al. 2014, *AJ*, 147, 77
Oh, J., Trippe, S., Kang, S., et al. 2015, *JKAS*, 48, 299
Zhao, G.-Y., Algaba, J. C., Lee, S. S., et al. 2018, *AJ*, 155, 26

Astronomy in Focus, Volume 1
XXXth IAU General Assembly, August 2018
Volker Beckmann & Claudio Ricci, eds.

DOI: 00.0000/X000000000000000X

ALMA observations at 1mm towards the starburst NGC 253: a tentative detection of propynal

Villicaña-Pedraza I.[1], Martin S. [2], Zapata L. [3], Thelen A.[4], Walterbos R. [4], Carreto-Parra F. [1], Binette L. [5], Armijos- Abendaño J. [6], and Saucedo Julio [7]

[1]New Mexico State University, 88003, Las Cruces, New Mexico, USA
email: ilhui7@nmsu.edu

[2]European Southern Observatory join ALMA, Santiago, Chile.

[3] Instituto de Radioastronomia, UNAM campus Morelia, Mexico.

[4] Astronomy dpt., New Mexico State University, Las Cruces, New Mexico, USA.

[5] Instituto de Astronomia, Universidad Nacional Autonoma de Mexico, Mexico.

[6] Observatorio Astronomico de Quito, Ecuador.

[7] Dpt. de Investigacion en Fisica, Universidad de Sonora, Hermosillo, Sonora. Mexico

Abstract. NGC 253, is one of the brightest extragalactic molecular line source with a star formation rate of about 3 $M_{\odot}$/yr. We report ALMA observations using an array of 38 antennas in band 7 at 1mm of the starburst galaxy NGC 253. The galaxy was mapped with an angular resolution of 0.26 arcsec, according to the map header. We detected HNCO, CH_3OH, H_3O^+, CH_3C_2H, and tentatively detection of C_3H_2O (propynal). We determined the flux density for each spatial component for each transition of the observed molecules. We analyze the spatial distribution and present the corresponding integrated maps.The flux of the clumps is consistent with that found in previous studies. We compare our results with those of the same sources obtained by other authors using ALMA at other frequencies. We observed less clumps than Ando et al. due to higher resolution. Their measured isotopic ratios extracted from the continuum present similarities to some of our clumps and molecules.The position of our clumps are in agreement with Sakamoto et al. We did the first extragalactic detection of Propynal.

Keywords. galaxies:evolution, galaxies: NGC253, ALMA, astrochemistry: ISM

1. Introduction

Using ALMA with a wide spectral band at 3mm, Meier *et al.* (2015) studied the chemical composition of NGC 253 and tentatively detected molecules not reported before. Ando *et al.* (2017) studied NGC 253 from 340 GHz to 365 GHz (0.85mm). They could resolve the nuclear starburst into 8 Clumps and detected complex organic molecules. Furthermore, they found that the hot and chemically rich environment is located within a 10pc region. In this Paper, we present ALMA observations to complete band 7 of NGC 253, focussing primarily on observational results.

2. Observations and Data Reduction

The ALMA cycle 2 data for the project No. 2013.1.00973 (PI:Villicaña-Pedraza) for NGC 253 were obtained on June 10th of 2015 using 38 Antennas of the main array in band 7. The data were imaged and analyzed using CASA. A water vapor of 0.9309mm

was measured. The peak flux position was determined to be at RA = 00h 47' 33.17" and DEC = −25° 17' 17.1". A 3344 seconds integration was carried out at a single point location. The continuum emission has a flux density of approximately 1 Jy (Fig. 1 top-left image) in the entire region. The setup presented here covers the 306.02 to 307.89 GHz frequency range.

3. Results and Conclusions

On the continuum map we identify four clumps. We measured differences in molecular line intensities between each clump. The molecules identified (see Fig. 1 Left- bottom) are HNCO ($14_{0,1}$- 13 $_{0,1}$ and 14 $_{1,1}$- $13_{1,1}$) with two transitions, CH_3OH (4_1-4_0), H_3O^+ (1_1 - 2_1), CH_3CCH (18_1-17_1), and for first time outside the Galaxy the tentative detection of Propynal (C_3H_2O) with two transitions ($22_{3,19}$- $22_{2,20}$ and $23_{3,20}$- $23_{2,21}$). Only in the second clump we cannot resolve CH_3CCH from HCNO. We derive the flux density of each molecule for the observed transitions. We analyze the spatial distribution and present the corresponding integrated maps. Our data are in agreement with the clumps observed by Sakamoto *et al.* (2011). Furthermore, comparing our ratios with the ones obtained by Ando *et al.* (2017), we get similar results for the central clumps but not for the external ones. The two transitions of Propynal that we detected are in agreement with Zhou et al. Zhou *et al.* (2008) showed for the first time that C_3H_2O, an isomer of cyclopropenone observed in the Galaxy, can be formed at low-temperature. It explains the gas phase abundances of cyclopropenone in star forming regions via sublimation of c-C_3H_2O formed on icy grains in the cold molecular cloud stage.

References

Ando, R., Nakanishi, K., Kohno, K., et al. 2017, *ApJ*, 81, 849
Meier, D. S., Walter, F., Bolatto, A.D., et al., 2015, *ApJ*, 63, 801
Sakamoto, K., Mao, R.Q., Matsushita, S., et al., 2011, *ApJ*, 19, 735
Zhou, L., Kaiser, R.I., Gao, L.G., et al., 2008, *ApJ*, 1493, 686

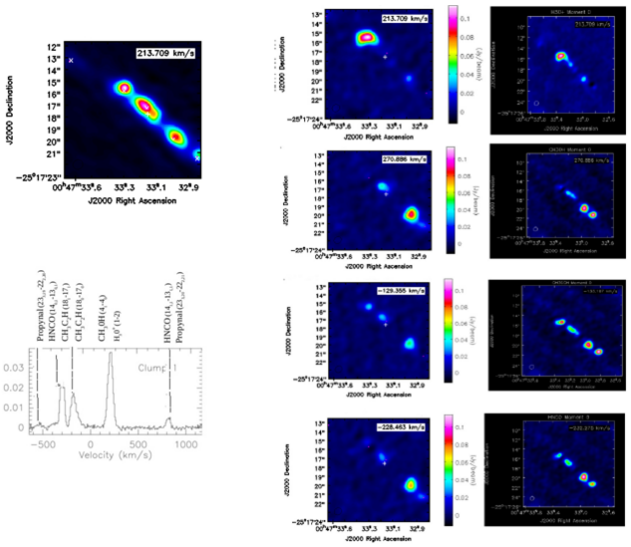

Figure 1. Top: continuum map. Bottom: molecular line identification. Rightmost figure: left panels: flux maps, and right panel: integrated maps.

Astronomy in Focus, Volume 1
XXXth IAU General Assembly, August 2018
Volker Beckmann & Claudio Ricci, eds.

DOI: 00.0000/X000000000000000X

Discovery of a dying, giant radio galaxy in the distant Universe

Yogesh Wadadekar[1]

[1]National Centre for Radio Astrophysics
Postbag 3, Ganeshkhind, Pune 411007, India
email: yogesh@ncra.tifr.res.in

Abstract.
We report the discovery of an intriguing relic Giant Radio Galaxy (GRG) J021659-044920 at redshift $z \sim 1.3$ that exhibits large-scale extended, nearly co-spatial, radio and X-ray emission from radio lobes, but without detection of Active Galactic Nuclei core, jets and hotspots. The total angular extent of the GRG at the observed frame 0.325 GHz, using Giant Metrewave Radio Telescope observations is found to be ∼2.4 arcmin, which corresponds to a total projected linear size of ∼1.2 Mpc. The integrated radio spectrum between 0.240 and 1.4 GHz shows high spectral curvature with sharp steepening above 0.325 GHz, consistent with relic radio emission that is $\sim 8 \times 10^6$ yr old. The radio spectral index map between observed frame 0.325 and 1.4 GHz for the two lobes varies from -1.4 to -2.5 with the steepening trend from outer–end to inner–end, indicating backflow of plasma in the lobes. The extended X-ray emission characterized by an absorbed power law with photon index $\Gamma \sim 1.86$ favours inverse Compton scattering of the Cosmic Microwave Background (ICCMB) photons as the most plausible origin. Using both X–ray and radio fluxes under the assumption of ICCMB we estimate the magnetic field in the lobes to be 3.3 μG. The magnetic field estimate based on energy equipartition is ∼3.5 μG. Our work presents a case study of a rare example of a GRG caught in dying phase in the distant Universe. This work is described in detail in Tamhane et al. 2015

Keywords. galaxies: high redshift, galaxies: magnetic fields, radio continuum: galaxies, galaxies: nuclei

1. The Giant Radio Galaxy J021659-044920

The relic GRG J021659-044920 centred at RA 02h 16m 59s and Dec. 04 49 20.6 (J2000) is located in a smaller subfield of the XMM-LSS field, known as the Subaru X-ray Deep Field. We combined radio data at 325 MHz from our own GMRT observations, with archival observations at 240 MHz, 610 MHz (both with GMRT) and 1.4 GHz (VLA). Archival X-ray observations with XMM-Newton consisted of 25.63 ks EPIC PN and 27.35 ks of EPIC MOS data. Our X-ray analysis shows that the observed X-ray emission is non-thermal in origin and most likely originates due to inverse Compton scattering of the CMB photons (ICCMB). The optical counterpart of the relic GRG was identified using ultradeep *BRiz* Suprime-Cam/Subaru images. The identified host galaxy is very red ($R-z = 2.0$) and resides almost exactly mid-way between the radio lobes. There is no radio emission seen from the core of the radio galaxy even in an image with r.m.s. of 10 μJy at 610 MHz (Russ Taylor, private communication). The host galaxy is also detected in near-IR (J, H and K bands) and mid-IR (3.6, 4.5, 5.8 and 8 μm) respectively by the UKIDSS and SpUDS surveys. The spectroscopic redshift of the optical counterpart ($z = 1.325$) is based on a low S/N spectrum from FOCAS/Subaru. However, two different photometric redshift estimates are consistent with the spectroscopic redshift measurement. The total

angular extent at 0.325 GHz (within the 5σ contour) is 2.4 arcmin and corresponds to a projected linear size of ∼1.2 Mpc.

2. Magnetic field estimates in the lobes

Together with radio observations, the ICCMB X-ray fluxes can be used to constrain the magnetic field strength in the lobes of radio galaxies. This analysis requires the observed X-ray and radio fluxes to be co-spatial. To get the co-spatial flux, we extracted the source spectrum in a region matching the 5σ contours of the 0.325 GHz image. Using this technique, we estimate $B \sim 3.3\mu$G in the lobes.

It is also possible to compute the magnetic field in the lobes under equipartition between CREs and the magnetic field. Assuming a typical spectral index for synchrotron losses as 1.0, the equipartition magnetic field is $B_{eq} \sim 3.5\mu$G in the lobes. The equipartition magnetic field strength and the magnetic field strength derived using the X-ray and radio emission agree well with each other indicating the energy equipartition to be valid in the lobes of the GRG. For our estimated value of magnetic field strength of $\sim 3.3\mu$G and $\nu_{br,rest} = 1.32$ GHz, we find the age of the relativistic electrons in the lobes and hence the age of the relic to be 8×10^6 yr, which is typical for relic GRGs.

3. Summary of results

We have discovered a relic GRG J021659-044920 at redshift $z = 1.325$ with extended diffuse ICCMB X-ray emission, nearly co-spatial with the radio lobes.

- The radio lobes are best detected at low radio frequencies observed using the GMRT at 0.325 GHz. The total angular extent at 0.325 GHz is 2.4 arcmin that corresponds to a projected linear size of ~ 1.2 Mpc at the redshift of the source.
- The host galaxy is identified in deep optical (Subaru), near- IR (UKIDSS) and mid-IR (SpUDS). It is a very red ($R - z = 2.0$) and dusty galaxy that brightens in mid-IR bands.
- The relic nature of the radio galaxy is evident as the AGN core, jets and/or hotspots remain undetected and the lobes exhibit a very steep radio spectral index, $\alpha \sim 1.4 - 2.5$. The $0.24 - 1.4$ GHz radio spectrum of the lobe emission is convex and steepens sharply above 0.325 GHz due to radiative losses. The spectral index of the lobes, estimated between 0.325 and 1.4 GHz, varies from 1.4 in the outer edges to 2.5 in the inner regions, suggesting backflow of plasma.
- The X-ray spectrum between 0.3 and 10 keV is best fitted by an absorbed power-law model with photon index $\Gamma = 1.86$ for a fixed absorbing column density similar to the Galactic value. The comparison of radio and X-ray spectral and morphological properties suggests that X-ray emission is likely due to inverse Comptonization of CMB photons by low-energy electrons compared to electrons radiating at 0.325-1.4 GHz frequencies. Using the ICCMB X-ray emission, we estimate the lower limit for the total energy in relativistic electrons to be $\sim 4.2 \times 10^{59}$ erg (for $\gamma_e \sim 10^3$), implying significant feedback from the GRG into the surrounding IGM.
- The magnetic field strength estimated using X-ray and radio emission and by energy equipartition yield consistent field strengths of $\sim 3.5\mu$G. This suggests that the energy equipartition between magnetic field and relativistic electrons is valid in this GRG.

References

Tamhane, P., Wadadekar, Y., Basu, A., et al. 2015, *MNRAS*, 453, 2438

Astronomy in Focus, Volume 1
XXXth IAU General Assembly, August 2018
Volker Beckmann & Claudio Ricci, eds.

DOI: 00.0000/X000000000000000X

The MWA GLEAM 4-Jy (G4Jy) Sample

Sarah V. White (SVW)[1,2], Thomas M.O. Franzen[3], O. Ivy Wong[4], Anna D. Kapińska[5,4], Chris Riseley[6], Paul Hancock[1], Joseph Callingham[3,7], Richard Hunstead[7], Natasha Hurley-Walker[1], Chen Wu[4], Nick Seymour[1], Jesse Swan[8], Randall Wayth[1], John S. Morgan[1], Rajan Chhetri[1], Carole Jackson[3,1], Stuart Weston[9], and Tom Mauch[2]

[1]International Centre for Radio Astronomy Research (ICRAR), Curtin University, Bentley, WA 6102, Australia
email: sarah.white@icrar.org

[2]South African Radio Astronomy Observatory (SARAO), 2 Fir Street, Black River Park, Observatory, 7925, South Africa
[3]ASTRON, PO Box 2, 7990 AA Dwingeloo, The Netherlands
[4]ICRAR, University of Western Australia M468, 35 Stirling Highway, WA 6009, Australia
[5]National Radio Astronomy Observatory, 1003 Lopezville Rd, Socorro NM 87801, USA
[6]CSIRO Astronomy and Space Science, PO Box 1130, Bentley, WA 6102, Australia
[7]Sydney Institute for Astronomy (SIfA), University of Sydney, NSW 2006, Australia
[8]School of Physical Sciences, University of Tasmania, Hobart, Tasmania, 7001 Australia
[9]Institute for Radio Astronomy and Space Research (IRASR), Auckland University of Technology, Auckland 1010, New Zealand

Abstract. Powerful radio-galaxies feature heavily in our understanding of galaxy evolution. However, when it comes to studying their properties as a function of redshift and/or environment, the most-detailed studies tend to be limited by small-number statistics. During Focus Meeting 3, on "Radio Galaxies: Resolving the AGN phenomenon", SVW presented a new sample of nearly 2,000 of the brightest radio-sources in the southern sky (Dec. < 30 deg). These were observed at low radio-frequencies as part of the GaLactic and Extragalactic All-sky MWA (GLEAM) Survey, which is a continuum survey conducted using the Murchison Widefield Array (MWA). This instrument is the precursor telescope for the low-frequency component of the Square Kilometre Array, and allows us to select radio galaxies in an orientation-independent way (i.e. minimising the bias caused by Doppler boosting, inherent in high-frequency surveys). Being brighter than 4 Jy at 151 MHz, we refer to these objects as the GLEAM 4-Jy (G4Jy) Sample. The G4Jy catalogue is close to being finalised, with SVW describing how multi-wavelength data have been used to determine the morphology of the radio emission, and identify the host galaxy. In addition, the MWA's excellent spectral-coverage and sensitivity to extended/diffuse emission were highlighted. Both of these aspects are important for understanding the physical mechanisms that take place within active galaxies, and how they interact with their environment.

Keywords. galaxies: active, radio continuum: galaxies, galaxies: evolution, galaxies: jets.

1. The brightest sources at low radio-frequencies

Low-frequency radio observations allow us to probe older emission from an active galactic nucleus (AGN) than is traced at higher radio-frequencies, thereby providing information on the timescale over which an AGN may influence its host galaxy and surroundings. Moreover, this low-frequency emission is dominated by radio lobes. These are unaffected by Doppler boosting (also known as relativistic beaming), unlike the radio jets, hotspots, and core that dominate at high frequencies. As such, the angle at which we view the AGN has no bearing on the observed flux-density, and so selecting radio sources at low frequencies results in a sample that is free from orientation bias.

Currently, the most prominent, low-frequency radio-source sample that is optically complete is the revised Third Cambridge Catalogue of Radio Sources (3CRR; Laing et al. 1983). However, its flux-density limit (10 Jy at 178 MHz) restricts the detection of radio-bright galaxies to 173 sources. Requiring additional criteria, Wang & Kaiser (2008) note that there is an insufficient number of objects for studying their cosmological evolution in detail, in terms of age or environmental density. A larger sample would also aid further investigation into the accretion modes of radio galaxies (Best & Heckman 2012), and modelling of their dynamical behaviour (e.g. Turner & Shabala 2015).

We create such a sample using new observations at low radio-frequencies, obtained via the Murchison Widefield Array (MWA). Thanks to its location in a protected, radio-quiet zone, we have excellent spectral-coverage, with 20 flux-density measurements spanning a frequency range of 72–231 MHz. In addition, the large number of short baselines (< 200 m) makes the MWA very sensitive to large-scale, diffuse radio emission. The data collected over the entire southern sky compose the GaLactic and Extragalactic All-sky MWA (GLEAM; Wayth et al. 2015) Survey, and the extragalactic component is publicly available in the form of a catalogue and images at multiple frequencies (Hurley-Walker et al. 2017)†. Using all radio sources with $S_{151\,\mathrm{MHz}} > 4$ Jy in this catalogue, we construct the GLEAM 4-Jy Sample (Jackson et al. 2015). This complete sample contains 1,860 sources and is over 10 times larger than 3CRR, due to its lower flux-density limit (4 Jy at 151 MHz) and larger survey area (24,831 square degrees). Like 3CRR, the majority of these sources are galaxies with an active black-hole at the centre, and many have radio jets associated with them. By using this larger sample to study radio-bright active galaxies, we can gain a better understanding of their fuelling mechanism, their connection with their environment, and how these radio sources evolve over cosmic time.

2. The G4Jy catalogue: determining the morphology and host galaxy

The spatial resolution of MWA data ($\sim$2 arcmin) means that we need to use other radio surveys for determining the morphology of the G4Jy sources. This involves visually inspecting overlays that use the TIFR GMRT Sky Survey (TGSS) alternative data release (ADR1; Intema et al. 2017), providing 25-arcsec resolution, and either the NRAO VLA Sky Survey (NVSS; Condon et al. 1998) or the Sydney University Molonglo Sky Survey (SUMSS; Mauch et al. 2003, Murphy et al. 2007), both of which provide 45-arcsec resolution. An example overlay is shown in Figure 1, and demonstrates how only the GLEAM Survey reveals the extended distribution of relativistic plasma associated with the radio lobes. Spanning 40 arcmin across, this radio galaxy is resolved into multiple GLEAM components by the MWA, as are a further 60 radio sources in our sample.

A crucial part of our careful visual inspection is to identify, where possible for each G4Jy source, the galaxy that hosts the radio emission. For this we use data from the mid-infrared AllWISE survey (Cutri et al. 2012), so that we are not biased against dust-obscured AGN. This is in contrast to many historical radio-source identifications, where radio contours were only overlaid onto *optical* images. Hence, we have completed thorough checks against the literature; reassessing 'well-known' radio sources in light of relatively-new mid-infrared information, and searching for follow-up observations at high radio-frequencies (which may confirm the position of the radio core). The G4Jy catalogue will provide flags to highlight which sources would most-greatly benefit from further follow-up observations, due to there being multiple, candidate host-galaxies, or the AllWISE data having insufficient sensitivity. Meanwhile, our entire sample has been

† https://gleam-vo.icrar.org/gleam_postage/q/form

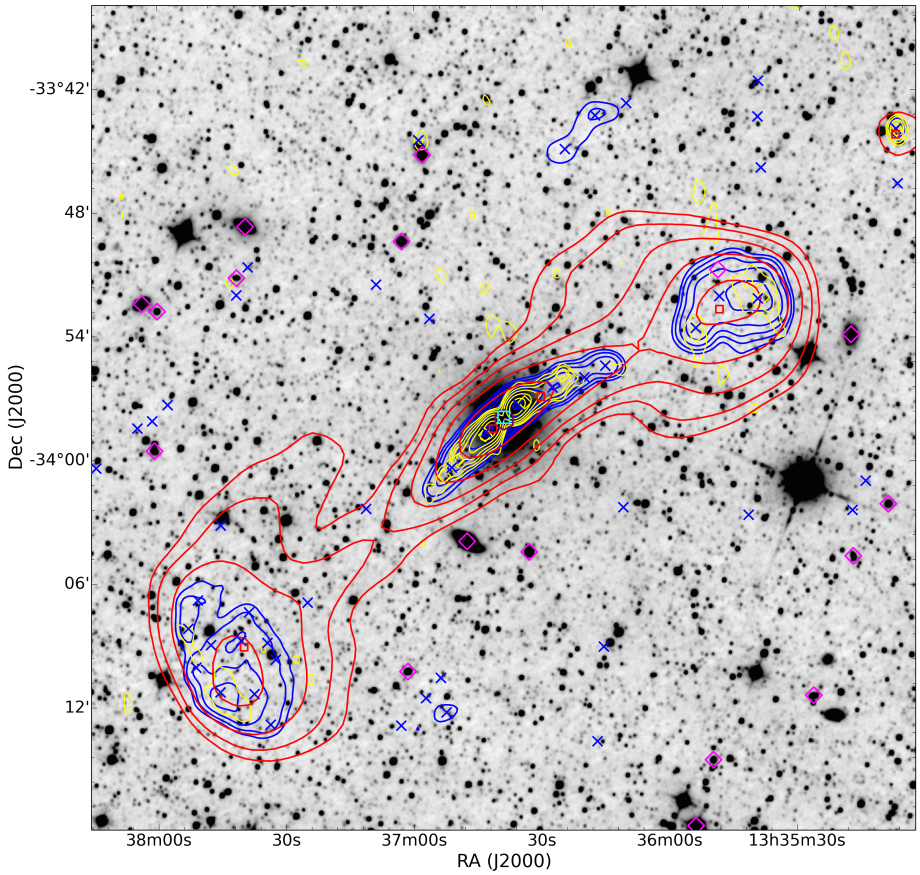

Figure 1. An overlay, centred at R.A. = 13:36:39, Dec. = −33:57:57 (J2000), for an extended radio-galaxy (also known as IC 4296) in the G4Jy Sample. Radio contours from TGSS (150 MHz; yellow), GLEAM (170–231 MHz; red) and NVSS (1.4 GHz; blue) are overlaid on a mid-infrared image from AllWISE (3.4 μm; inverted grey-scale). For each set of contours, the lowest contour is at the 3 σ level (where σ is the local rms), with the number of σ doubling with each subsequent contour (i.e. 3, 6, 12 σ, etc.). This source is an unusual example, in that its GLEAM-component positions (red squares) needed to be re-fitted using Aegean (Hancock et al. 2012, 2018). Also plotted are catalogue positions from TGSS (yellow diamonds) and NVSS (blue crosses). The brightness-weighted centroid position, calculated using the NVSS components, is indicated by a purple hexagon. The cyan square represents an AT20G (Australia Telescope 20-GHz Survey; Murphy et al. 2010) detection, marking the core of the radio galaxy. Magenta diamonds represent optical positions for sources in the 6-degree Field Galaxy Survey (Jones et al. 2004).

approved for follow-up by the Taipan Galaxy Survey (da Cunha et al. 2017), which is a new optical, spectroscopic survey over the southern hemisphere.

3. Constructing broadband radio spectra

A great strength of the GLEAM Survey is the ability to tightly constrain the radio spectrum at low radio-frequencies. We extend this frequency coverage for a subset of the G4Jy Sample, by also incorporating measurements (at 5, 9, and 20 GHz) from the Australia Telescope Compact Array. Doing so emphasises the degree of curvature in the radio spectrum, and that we cannot simply assume that radio emission follows a power-law description ($S_\nu \propto \nu^\alpha$, where S is the flux density at a particular frequency, ν, and α

is the spectral index). Instead, there are poorly-studied physical processes that need to be considered. For 'peaked-spectrum' sources (Callingham et al. 2017), which show 'convex' spectra, synchrotron self-absorption or free-free absorption by ionised gas may be the cause of the spectral turnover towards low frequencies. As for sources that show an upturn or flattening in flux density towards high frequencies (i.e. have 'concave' spectra), this may be due to renewed AGN activity or the orientation of the jet axis. At this point, we remind the reader that higher radio-frequencies probe more-recent/ongoing AGN activity, whilst observations at low frequencies reveal the cumulative effect of past epochs of activity. Therefore, spectral fitting allows constraints to be placed on the fraction of time that the central, supermassive black-hole is in active and quiescent phases (Turner 2018) – that is, the duty cycle of the AGN can be determined.

4. Summary and outlook

The G4Jy Sample comprises the brightest radio-sources below Dec. = 30 deg, following repeated visual inspection of overlays and labour-intensive checks against the literature. Most importantly, the associated catalogue provides mid-infrared positions of ∼1,800 host galaxies, allowing the brightest detections in the GLEAM catalogue to be more easily cross-matched with information at other wavelengths. This will form a highly-valuable, legacy dataset in preparation for science enabled by the Square Kilometre Array. Furthermore, such a large, complete, unbiased sample is required for investigating what conditions promote, or are associated with, the production of powerful radio-jets. By exploiting the excellent spectral-coverage provided by the MWA, we can also tightly constrain the spectral behaviour of the G4Jy sources, and determine the prevalence of 'restarted' AGN activity.

References

Best, P. N., & Heckman, T. M., 2012, *MNRAS*, 421, 1569
Callingham et al., 2017, *ApJ*, 836, 174
Condon, J. J., Cotton, W. D., Greisen, E. W., Yin, Q. F., Perley, R. A., Taylor, G. B., & Broderick, J. J., 1998, *AJ*, 115, 1693
da Cunha et al., 2017, *PASA*, 34, e047
Cutri et al., 2012, *Explanatory Supplement to the AllWISE Data Release Products*
Hancock, P. J., Murphy, T., Gaensler, B. M., Hopkins, A., & Curran, J. R., 2012, *MNRAS*, 422, 1812
Hancock, P. J., Trott, C. M., & Hurley-Walker, N., 2018, *PASA*, 35, e011
Hurley-Walker et al., 2017, *MNRAS*, 464, 1146
Intema, H. T., Jagannathan, P., Mooley, K. P., & Frail, D. A., 2017, *A&A*, 598, A78
Jackson et al., 2015, *Proceedings of Science*, The Many Facets of Extragalactic Radio Surveys: Towards New Scientific Challenges (Bologna)
Jones et al., 2004, *MNRAS*, 355, 747
Laing, R. A., Riley, J. M., & Longair, M. S., 1983, *MNRAS*, 204, 151
Mauch, T., Murphy, T., Buttery, H. J., Curran, J., Hunstead, R. W., Piestrzynski, B., Robertson, J. G., & Sadler, E. M., 2003, *MNRAS*, 342, 1117
Murphy, T., Mauch, T., Green, A., Hunstead, R. W., Piestrzynska, B., Kels, A. P., & Sztajer, P., 2007, *MNRAS*, 382, 382
Murphy et al., 2010, *MNRAS*, 402, 2403
Turner, R. J., & Shabala, S. S., 2015, *ApJ*, 806, 59
Turner, R. J., 2018, *MNRAS*, 476, 2522
Wang, Y., & Kaiser, C. R., 2008, *MNRAS*, 388, 677
Wayth et al., 2015, *PASA*, 32, e025

Astronomy in Focus, Volume 1
XXXth IAU General Assembly, August 2018
Volker Beckmann & Claudio Ricci, eds.

DOI: 00.0000/X000000000000000X

Understanding mechanical feedback from HERGs and LERGs

Imogen H. Whittam[1]

[1]Department of Physics and Astronomy, University of the Western Cape,
Robert Sobukwe Road, Bellville 7535, South Africa
email: iwhittam@uwc.ac.za

Abstract. The properties of $\sim$ 1000 high-excitation and low-excitation radio galaxies (HERGs and LERGs) selected from the Heywood et al. (2016) $1-2$ GHz VLA survey of Stripe 82 are investigated. The HERGs in this sample are generally found in host galaxies with younger stellar populations than LERGs, consistent with other work. The HERGs tend to accrete at a faster rate than the LERGs, but there is more overlap in the accretion rates of the two classes than has been found previously. We find evidence that mechanical feedback may be significantly underestimated in hydrodynamical simulations of galaxy evolution; 84 % of this sample release more than 10 % of their energy in mechanical form. Mechanical feedback is significant for many of the HERGs in this sample as well as the LERGs; nearly 50 % of the HERGs release more than 10 % of their energy in their radio jets.

Keywords. radio continuum: galaxies, galaxies: active, galaxies: evolution

1. Introduction

One of the key unknowns in galaxy evolution is how star-formation in galaxies becomes quenched; it is widely thought that feedback from active galactic nuclei (AGN) is responsible for this, but the mechanisms are not well understood. Observational evidence (e.g. Best & Heckman (2012)) suggests that AGN can be split into two distinct classes; high-excitation radio galaxies (HERGs; also known as cold mode, quasar mode or radiative mode sources) which radiate efficiently across the electromagnetic spectrum and posses the typical AGN accretion-related structures such as an accretion disk and a dusty torus, and low-excitation radio galaxies (LERGs; also known as hot mode, radio mode or jet mode sources) which radiate inefficiently and emit the bulk of their energy in mechanical form as powerful radio jets (see e.g. Heckman & Best (2014)).

It is thought that these two AGN accretion modes have different feedback effects on the host galaxy (see review by Fabian (2012)) and lead to the two different feedback paths in semi-analytic and hydrodynamic simulations, but despite being widely studied over the last decade (e.g. Hardcastle et al. (2007); Cattaneo et al. (2009); Heckman & Best (2014)) these processes are not well understood. In these proceedings I use a sample of $\sim$ 1000 HERGs and LERGs to investigate the host galaxy properties and accretion rates of the two classes, and explore the implications of these results for AGN feedback.

2. Data used and source classification

This work is based on a $1-2$ GHz Karl G. Jansky Very Large Array (VLA) survey covering 100 deg^2 in SDSS Stripe 82 which has a 1σ rms noise of 88 μJy beam^{-1} and a resolution of 16×10 arcsec; full details of the radio survey are given in Heywood et al. (2016). This radio catalogue was matched to the SDSS DR14 optical catalogue (Abolfathi et al. (2018)) by eye; details of the matching process are described in Prescott

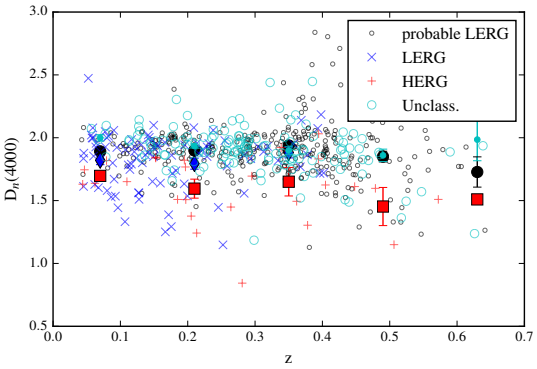

Figure 1. 4000 Å break strength as a function of redshift with the HERGs, LERGs, probable LERGs and unclassified sources shown separately. The filled shapes show the mean values in each luminosity bin for the different samples. From Whittam et al. (2018)

et al. (2018). We restrict our analysis to sources with a counterpart in the spectroscopic catalogue with $z < 0.7$, our sample therefore has 1501 sources which cover the range $0.01 < z < 0.7$ and $10^{21} < L_{1.4\ \mathrm{GHz}}/\mathrm{W\ Hz^{-1}} < 10^{27}$. We use the the value-added spectroscopic catalogues described in Thomas et al. (2013).

Sources are classified as either AGN or star-forming galaxies using information from their optical spectra, full details of this process are given in Prescott et al. (2018). The AGN in the sample are then classified as HERGs or LERGs using the criteria given in Best & Heckman (2012), which use a combination of emission line ratios and [OIII] equivalent width. This is explained in detail in Whittam et al. (2018). Additionally to the Best and Heckman classification scheme, we introduce a 'probable LERG' class for sources which cannot be classified according to the full criteria but which have an [OIII] equivalent width < 5 Å. The total number of sources in each category is as follows; HERGs = 60, LERGs = 149, probable LERGs = 600, QSOs = 81 and unclassified sources = 271, with 340 star-forming galaxies.

3. Host galaxy properties

Using the wealth of multi-wavelength data available in the field, we can compare the properties of the host galaxies of the HERGs and LERGs. 4000 Å break strength, which traces stellar age, is shown as a function of redshift in Fig 1. This shows that HERGs tend to be found in host galaxies with younger stellar populations than LERGs across the redshift range probed here. This is agrees with other results in the literature (e.g. Best & Heckman (2012)) and is consistent with the idea that HERGs have a supply of cold gas which provides the fuel for both star-formation and AGN activity. We refer the reader to Whittam et al. (2018) for further discussion of this and other host galaxy properties.

4. Accretion rates

There is a scenario building up in the literature that there are two distinct accretion modes which are responsible for HERGs and LERGs respectively; in this scenario there is a dichotomy in accretion rates between the two classes, relating to the two different modes. The radiative accretion rates of the AGN in this sample are estimated from their [OIII] 5007 line luminosity and the mechanical accretion rates are estimated from the 1.4-GHz radio luminosity using the Cavagnolo et al. (2010) relationship. Black hole masses

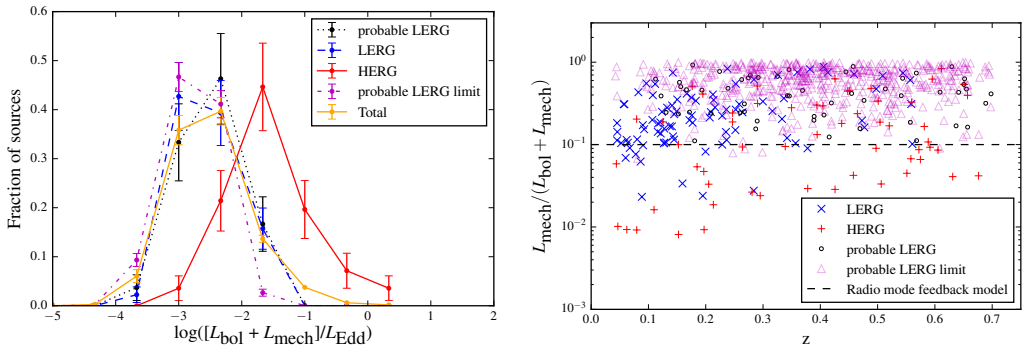

Figure 2. Left panel shows the distribution of Eddington-scaled accretion rates for the different source classifications. Right panel shows the fraction of the accreted energy released in the jets for the different source types as a function of redshift. Triangles represent sources with an upper limit on their radiative accretion rate, so the fraction of energy released in the jet is a lower limit. The dashed line is the radio mode feedback model used in Horizon-AGN from Dubois et al. (2014). The uncertainties in the scaling relations used to estimate $L_{\rm bol}$ and $L_{\rm mech}$ are 0.4 and 0.7 dex respectively. From Whittam et al. (2018).

are estimated from the local black hole mass - bulge mass relation, allowing Eddington-scaled accretion rates to be calculated as follows: $\lambda = (L_{\rm bol} + L_{\rm mech})/L_{\rm Edd}$. The left panel of Fig. 2 shows the distribution of Eddington-scaled accretion rates for the HERGs and LERGs in this sample. It is clear from this figure that the HERGs generally accrete at a faster Eddington-scaled rate than the LERGs, with a distribution that peaks just below 0.1 compared to 0.01. However, there is a significant overlap in accretion rates between the two classes, with HERGs found across nearly the full range of accretion rates.

The dichotomy in accretion rates between HERGs and LERGs is therefore less clear in this study than it is in other studies in the literature; for example Best & Heckman (2012) and Mingo et al. (2014) both find almost no overlap in accretion rates between the two classes. In contrast, our sample seems to suggest a more continuous range of accretion rates. Note the our sample probes fainter radio luminosities ($10^{21} < L_{1.4\ \rm GHz}/\rm W\ Hz^{-1} < 10^{27}$) than other results in the literature; this could be part of the reason for the difference in our results, although we see some overlap in the accretion rates of the HERGs and LERGs across the luminosity range sampled here. We also do not observe any dichotomy in the [OIII] equivalent width or Excitation Index distributions, the two main parameters used to classify the HERGs and LERGs, suggesting that any dividing value chosen in these parameters is perhaps arbitrary for our sample.

5. Implications for AGN feedback

AGN feedback is required in all leading hydrodynamical simulations of galaxy evolution to quench star-formation. Some simulations implement mechanical and radiative feedback (assumed to relate to LERGs and HERGs respectively) separately (e.g. Horizon-AGN; Dubois et al. (2014)) while others do not (e.g. MUFASA; Davé et al. (2016)).

The right panel of Fig. 2 shows $L_{\rm mech}/(L_{\rm bol} + L_{\rm mech})$, which provides an estimate of the fraction of the total accreted energy deposited back into the interstellar medium in mechanical form. The dashed line shows the mechanical feedback efficiency of 10 % assumed in Horizon-AGN; it is clear that this is a significant underestimate for the sources in this sample, with 84 % of the sample depositing more than 10 % of their energy in mechanical form. This plot also demonstrates that mechanical feedback can be

significant for HERGs as well as for LERGs; nearly 50 % (29/60) of the HERGs in this sample release more than 10 % of their accreted energy in mechanical form.

There is a scatter of $\sim$ 2 dex in $L_{\rm mech}/(L_{\rm bol} + L_{\rm mech})$, which shows that the assumption that there is a direct scaling between accretion rate and mechanical feedback which is used in most hydrodynamical simulations does not necessarily hold. This may be because environment plays a significant role.

6. Conclusions and future perspectives

We have used the Heywood et al. (2016) VLA 1-2 GHz radio survey covering 100 deg^2 in Stripe 82 along with optical spectroscopy to probe the properties of $\sim$ 1000 high- and low-excitation radio galaxies. They key results of this work are:

- HERGs tend to be found in host galaxies with younger stellar populations than LERGs, consistent with other results in the literature.
- While the HERGs in our sample tend to have higher accretion rates than the LERGs, we find considerable overlap in the accretion rates of the two samples.
- Mechanical feedback can be significant for HERGs as well as for LERGs, and may be underestimated for both populations in hydrodynamical simulations.

The advent of new radio telescopes, such as MeerKAT, LOFAR and ASKAP, means there is potential to make a large step forward in our understanding of radio galaxies and their mechanical feedback effects in the next few years. One example of a survey planned with a new instrument is the MeerKAT MIGHTEE survey (Jarvis et al. (2016)) which has just started to collect data and will survey 10 deg^2 to a depth of 1 μJy at 800 - 1600 MHz in four different fields. The unique combination of deep radio images over a significant cosmological volume along with excellent multi-wavelength coverage means we will be able to, amongst other things, extend the study described in this proceedings to significantly fainter luminosities and probe whether or not there is an accretion mode dichotomy, particularly at lower luminosities.

Acknowledgements The author thanks Matthew Prescott, Matt Jarvis, Kim McAlpine and Ian Heywood for their significant contributions to this work. This research was supported by the South African Radio Astronomy Observatory, which is a facility of the National Research Foundation, an agency of the Department of Science and Technology.

References

Abolfathi B., et al., 2018, *ApJS*, 235, 42
Best P. N., Heckman T. M., 2012, *MNRAS*, 421, 1569
Cattaneo A., et al., 2009, *Nature*, 460, 213
Cavagnolo K. W., et al., 2010, *ApJ*, 720, 1066
Davé R., Thompson R., Hopkins P. F., 2016, *MNRAS*, 462, 3265
Dubois Y., et al., 2014, *MNRAS*, 444, 1453
Fabian A. C., 2012, *ARA&A*, 50, 455
Hardcastle M. J., Evans D. A., Croston J. H., 2007, *MNRAS*, 376, 1849
Heckman T. M., Best P. N., 2014, *ARA&A*, 52, 589
Heywood I., et al., 2016, *MNRAS*, 460, 4433
Jarvis M., et al., 2016, *Proceedings of MeerKAT Science: On the Pathway to the SKA. 25-27 May, 2016 Stellenbosch, South Africa*, 6
Mingo B., et al., 2014, *MNRAS*, 440, 269
Prescott M., et al., 2018, *MNRAS*, 480, 707
Thomas D., et al., 2013, *MNRAS*, 431, 1383
Whittam I. H., Prescott M., McAlpine K., Jarvis M. J., Heywood I., 2018, *MNRAS*, 480, 358

Astronomy in Focus, Volume 1
XXXth IAU General Assembly, August 2018
Volker Beckmann & Claudio Ricci, eds.

DOI: 00.0000/X000000000000000X

The intermediate-power population of radio galaxies: morphologies and interactions

Diana M. Worrall[1], Ryan T. Duffy[2], and Mark Birkinshaw[3]

[1]HH Wills Physics Laboratory, University of Bristol,
Tyndall Avenue, Bristol BS8 1TL, U.K.
email: D.Worrall@bristol.ac.uk

[2]HH Wills Physics Laboratory, University of Bristol,
Tyndall Avenue, Bristol BS8 1TL, U.K.
email: R.Duffy@bristol.ac.uk

[3]HH Wills Physics Laboratory, University of Bristol,
Tyndall Avenue, Bristol BS8 1TL, U.K.
email: Mark.Birkinshaw@bristol.ac.uk

Abstract. Radio galaxies of intermediate power dominate the radio-power injection in the Universe as a whole, due to the break in the radio luminosity function, and so are of special interest. The population spans FR I, FR II, and hybrid morphologies, resides in a full range of environmental richness, and sources of all ages are amenable to study. We describe structures and interactions, with emphasis on sources with deep high-resolution *Chandra* X-ray data. As compared with low-power sources there is evidence that the physics changes, and the work done in driving shocks can exceed that in evacuating cavities. A range of morphologies and phenomena is identified.

Keywords. galaxies:active, galaxies:jets, radio continuum:galaxies, intergalactic medium, X-rays:galaxies

1. The intermediate-power population

Our motivation for studying intermediate-power radio galaxies is that the radio luminosity function breaks at intermediate powers (e.g., Best et al. 2005), where sources from the lower-power FR I and higher-power FR II populations (Fanaroff & Riley 1974) overlap (hereafter called the FR I/II boundary zone). This means that in weighting power by density it is the intermediate-power radio galaxies that dominate the overall radio power in the Universe. If radio power is a proxy for jet power, then these sources should dominate radio-galaxy heating in the Universe.

For radio galaxies in significant atmospheres in the local Universe, jet powers have been measured by combining the enthalpy of cavities evacuated of X-ray-emitting gas by the radio lobes with their ages (e.g., Bîrzan et al. 2004). Such work has led to correlations between jet and radio power (e.g., Bîrzan et al. 2008, Cavagnolo et al. 2010, O'Sullivan et al. 2011). Godfrey and Shabala (2016) have argued that common distance spreading, forcing correlations to slopes approaching unity, may be a strong factor driving the results, but more recently Ineson et al. (2017) have estimated jet powers for samples at higher radio power from measurements of lobe overpressuring with respect to the intergalactic medium (IGM). The conclusions are that correlations broadly hold, but that different radio-source morphology and composition contribute a large scatter (Croston, Ineson & Hardcastle 2018) . We find the sources in the FR I/II boundary zone to be intermediate both in radio power and estimated jet power, so supporting the hypothesis that their environmental heating is of particular importance.

FR I/II boundary sources span a wide range of atmosphere type. For example, the boundary-zone sources in the sample of radio galaxies with low excitation emission lines of Ineson et al. (2015) span three orders of magnitude in the X-ray luminosity of their environments.

In our work we concentrate on radio galaxies at redshift less than 0.1 for the best spatial resolution. This has given us two redshift-selected subsamples from two primary samples. One is 3CRR (Laing, Riley & Longair 1983) where there are 15 low-redshift boundary-zone sources, all of which are *Chandra* observed. Our matched southern-hemisphere sample is selected from MS4 (Burgess 1998, Burgess & Hunstead 2006a, Burgess & Hunstead 2006b), and is only partially observed with *Chandra*. Additionally we've observed other FR I/II boundary-zone sources falling outside those complete samples. As a rough approximation, about 30 per cent of the radio galaxies lie in significant group or cluster atmospheres.

2. A new rich-cluster atmosphere

One of our southern-sample sources, PKS B1416-493, led to a recent discovery with *Chandra* of a $z < 0.1$ 4.6-keV cluster (Worrall & Birkinshaw 2017). Finding new nearby rich clusters has become rare. The radio source lies central to the cluster emission which, unusually for such situations, is void of a strong cool core. Detection of lobe inverse Compton emission and an X-ray lobe cavity have enabled good estimates of source energetics, and this FR I/II boundary source is consistent with jet-radio-power correlations and so should be a fair representative of a source providing heating in a rich cluster environment.

3. Two sources in a poorer cluster

The poor cluster Abell 3744 at $z = 0.038$ contains two FR I/II boundary sources, NGC 7016 and 7018 (Worrall & Birkinshaw 2014, see also Birkinshaw et al., these proceedings). A pronounced cavity overlaps lobe emission from each source. The cluster temperature, at 3.5 keV, is much hotter than expected based on cluster temperature-luminosity correlations, but since it would take the energy from 85 cavities to provide such heating, a recent merger is the likely case of the excess heat. It is extraordinary that the large-scale plumes from the two radio galaxies seem to be hugging X-ray-emitting gas of different temperature. The radio plasma appears to be acting as a thermal barrier, perhaps due to magnetic-field compression and a smaller gyroradius inside the radio plasma than in the external gas.

4. Shocks

While earlier Chandra work argued for weak or absent shocks around radio galaxies (see McNamara & Nulsen 2007), the situation changes for FR I/II boundary-zone sources, perhaps due to their more representative range of atmospheres. Moderate Mach 2 shocks are seen in 3C 305 and 3C 310 from the 3CRR sample (Hardcastle et al. 2012, Kraft et al. 2012). In PKS B2152-699 from our southern sample, we measure shocks of roughly Mach 2.7 (Worrall et al. 2012). Here the detection of lobe inverse Compton emission coupled with *Chandra* measurements of the gas properties enables a secure estimate of the source energetics, leading to the important conclusion that the work in driving shocks dominates that in producing cavities, so jet power can be sorely underestimated from cavity estimates alone.

5. Protons not contributing to minimum energy

Our studies have led to an important conclusion concerning minimum energy. The argument is as follows. Measurements of X-ray inverse Compton emission from the lobes of FR II radio galaxies have found magnetic fields that are typically about a third of the minimum-energy value calculated using the radiating leptons as the only significant contributer to the particle energy density (e.g., Croston et al 2005). More recently we find the same situation for the lobes/plumes of FR I radio galaxies (Duffy, Worrall & Birkinshaw 2018). It's known from pressure-balance considerations that FR II lobes cannot contain significant proton pressure (Croston et al 2005, Ineson et al. 2017, Croston, Ineson & Hardcastle 2018) while FR Is do (e.g., Morganti et al 1988, Worrall & Birkinshaw 2000), for which the best candidate is re-energized entrained particles (Croston et al. 2008). So, similar departures from minimum energy are seen in FR Is and IIs, but only FR Is contain a significant proton pressure. The logical physics conclusion is that only electrons are relevant to the state of minimum energy, even in the presence of protons. This is perhaps because electrons are light, and so should react quicker to magnetic field irregularities. A further conclusion is that if relativistic protons enter lobes from FR II jets (including quasars) in similar numbers to electrons, they need a lower minimum Lorentz factor than the electrons so as not to increase lobe pressure significantly.

6. Local versus large-scale heating

A relatively small fraction of FR I/II boundary sources appears to be interacting with their environments on a scale that may provide large-scale heating. In some cases, significant environments appear already to have been lost, with heating complete. However, local heating is rather common.

In this regard, study of our 3CRR subsample of FR I/II boundary-zone sources finds almost half to show evidence of enhanced central belt-like gas structures, seen between and roughly orthogonal to the lobes (Duffy, Worrall & Birkinshaw 2018). Such gas can have originated from mergers, fossil groups or cool cores. Less clear is whether or not the radio plasma is driving the gas towards the AGN nucleus, as might assist fuelling, since measurements of temperature structure in the belt gas are generally insufficient for firm conclusions. The low-redshift radio galaxy best supporting inflow is 3C 386 (Duffy et al. 2016), but this source is underpowered for the FR I/II boundary zone by a factor of two to three.

On an even more localized scale, FR I/II boundary-zone sources show cases where the jets have bent appreciably in interactions with large gas clouds. A well-studied case is PKS 2152-699 at $z = 0.0282$, where the jet shows at least two distinct bends on its path to the northern hotspot (Worrall et al. 2012). The outer bend lies adjacent to a bright high ionization cloud (Tadhunter et al. 1987), and a recent kinematic study of the gas argues for a proton contribution to the jet to avoid ram-pressure deflection exceeding that observed (Smith et al. 2018). The gas cloud, of mass of order 10^8 $M_\odot$, has been heated to X-ray temperatures by the jet's passage (Worrall et al. 2012). The inner jet bend is embedded within galaxy emission and less amenable to study, but lies adjacent to a bright feature seen in HST data and which in a similar way is likely to be responsible for the jet deflection here. A further example is the FR I/II boundary-zone radio galaxy 3C 277.3 (Coma A) at $z = 0.0853$. Despite the source lying closer to the plane of the sky than PKS 2152-699, the projected deflection is greater, at 40°, and again the gas cloud adjacent to the bend is heated to X-ray temperatures (Worrall, Birkinshaw & Young 2016).

Both PKS 2152-699 and 3C 277.3 also show interfaces for heating on hundred-kpc scales. PKS 2152-699, which fills much of its 1-keV group atmosphere, is strongly shocking gas around its lobes, as mentioned above. At the outer extremities of the lobes of 3C 277.3 lie Hα-emitting filaments believed to be merger remnants (Tadhunter et al. 2000). An anti-correlation between the locations of arms of enhanced X-ray emission and the filaments suggests that shocks advancing around the lobe are inhibited by the dense colder material (Worrall, Birkinshaw & Young 2016).

References

Best, P.N., Kauffmann, G., Heckman, T.M., & Ivezić, Ž 2005, *MNRAS*, 362, 9

Bîrzan, L., Rafferty, D.A., McNamara, B.R., Wise, M.W., & Nulsen, P.E.J. 2004, *ApJ*, 607, 800

Bîrzan, L., McNamara, B.R., Nulsen, P.E.J., Carilli, C.L., & Wise, M.W. 2008, *ApJ*, 686, 859

Burgess, A.M. 1998, Ph.D. Thesis, University of Sydney

Burgess, A.M. & Hunstead R.W. 2006a, *AJ*, 131, 100

Burgess, A.M. & Hunstead R.W. 2006b, *AJ*, 131, 114

Cavagnolo, K.W., McNamara, B.R., Nulsen, P.E.J., Carilli, C.L., Jones, C., & Bîrzan, L. 2010, *ApJ*, 720, 1066

Croston, J.H., Hardcastle, M.J., Harris, D.E., Belsole, E., Birkinshaw, M., & Worrall, D.M. 2005, *ApJ*, 626, 733

Croston, J.H., Hardcastle, M.J., Birkinshaw, M., Worrall, D.M., & Laing, R.A. 2008, *MNRAS*, 386, 1709

Croston, J.H., Ineson, J., & Hardcastle, M.J. 2018, *MNRAS*, 476 1614

Duffy R.T., Worrall, D.M., Birkinshaw, M., & Kraft, R.P. 2016, *MNRAS*, 459, 4508

Duffy R.T., Worrall, D.M., & Birkinshaw, M. 2018, in preparation

Fanaroff, B.L., & Riley, J.M. 1974, *MNRAS*, 167, 31P

Godfrey, L.E.H., & Shabala, S.S. 2016, *MNRAS*, 456, 1172

Hardcastle, M.J., Massaro, F., Harris, D.E. et al. 2012, *MNRAS*, 424, 1774

Ineson, J., Croston, J.H., Hardcastle, M.J., Kraft, R.P., Evans, D.A, & Jarvis, M. 2015, *MNRAS*, 453 2682

Ineson, J., Croston, J.H., Hardcastle, M.J., & Mingo, B. 2017, *MNRAS*, 467 1586

Kraft, R.P., Birkinshaw, M., Nulsen, P.E.J. et al. 2012, *ApJ*, 748, 19

Laing, R.A., Riley, J.M., & Longair, M.S. 1983, *MNRAS*, 204, 151

McNamara B.R., & Nulsen P.E.J. 2007, *ARA&A*, 45, 117

Morganti, R., Fanti, R., Gioia, I.M., Harris, D.E., Parma, P., & de Ruiter, H. 1988, *A&A*, 189, 11

O'Sullivan, E., Giacintucci, S., David, L.P., Gitti, M., Vrtilek, J.M., Raychaudhury, S., & Ponman, T.J. 2011, *ApJ*, 735, 11

Smith, D.P., Young, A.J., Worrall, D.M., & Birkinshaw, M. 2018, *MNRAS*, submitted

Tadhunter, C.N., Fosbury, R.A.E., Binette, L., Danziger, I.J., & Robinson, A. 1987, *Nature*, 325, 504

Tadhunter, C.N., Villar-Martin, M., Morganti, R., Bland-Hawthorn, J., & Axon, D. 2000, *MNRAS*, 314, 849

Worrall, D.M., & Birkinshaw, M. 2000, *ApJ*, 530, 719

Worrall, D.M., & Birkinshaw, M. 2014, *ApJ*, 784, 36

Worrall D.M., & Birkinshaw, M. 2017, *MNRAS*, 467, 2903

Worrall D.M., Birkinshaw, M., Young, A.J., Momtahan, K., Fosbury, R.A.E., Morganti, R., Tadhunter, C.N., & Verdoes Kleijn, G. 2012, *MNRAS*, 424, 1346

Worrall, D.M., Birkinshaw, M., & Young, A.J. 2016, *MNRAS*, 458, 174

Astronomy in Focus, Volume 1
XXXth IAU General Assembly, August 2018
Volker Beckmann & Claudio Ricci, eds.

DOI: 00.0000/X000000000000000X

Optically-faint radio galaxies found by Subaru HSC-SSP and FIRST catalogs

T. Yamashita[1], T. Nagao[1], M. Akiyama[2], W. He[2], H. Ikeda[3], M. Tanaka[3], M. Niida[4], M. Kajisawa[1,4], Y. Matsuoka[1], C.-H. Lee[5], T. Morokuma[6], Y. Toba[7], T. Kawaguchi[8], A. Noboriguchi[4], and the WERGS collaborators

[1]Research Center for Space and Cosmic Evolution, Ehime University, 2-5 Bunkyo-cho, Matsuyama, Ehime 790-8577, Japan
email: takuji@cosmos.phys.sic.ehime-u.ac.jp

[2]Astronomical Institute, Tohoku University, 6-3 Aramaki, Aoba-ku, Sendai, Miyagi 980-8578, Japan

[3]National Astronomical Observatory of Japan, 2-21-1 Osawa, Mitaka, Tokyo 181-8588, Japan

[4]Graduate School of Science and Engineering, Ehime University, Bunkyo-cho, Matsuyama, Ehime 790-8577, Japan

[5]National Optical Astronomy Observatory, 950 N. Cherry Ave., Tucson, AZ 85719, USA

[6]Institute of Astronomy, Graduate School of Science, University of Tokyo, 2-21-1 Osawa, Mitaka, Tokyo 181-0015, Japan

[7]Department of Astronomy, Kyoto University, Kitashirakawa-Oiwake-cho, Sakyo-ku, Kyoto 606-8502, Japan

[8]Department of Economics, Management and Information Science, Onomichi City University, Onomichi, Hiroshima 722-8506, Japan

Abstract. We present results of optical identifications of FIRST VLA radio sources by Hyper Suprime-Cam Subaru Strategic Program survey (HSC-SSP). This study is part of an ongoing project, "a Wide and Deep Exploration of Radio Galaxies with Subaru HSC (WERGS)", which aims to explore high-z radio galaxies (RGs). The combination of Subaru HSC-SSP and FIRST successfully produced more than 3600 radio-AGNs in the 156 deg^2 of the HSC-SSP field. The photometric redshifts for most of the sources range up to $z_{\rm ph} = 1.5$. The optically-faint RGs ($i_{\rm AB} > 21$) are located at $z_{\rm ph} > 1$ and show higher radio-loudness than the optically-bright ones. The optical colors of the optically-faint RGs are not consistent with that of passive galaxies but can be explained by predominant young stellar populations. The optically-faint RG sample found by Subaru HSC-SSP and FIRST might include "evolving" RGs that are star-forming.

Keywords. galaxies: active, galaxies: statistics, radio continuum: galaxies

1. Introduction

RGs have powerful radio-jets, which could give a so-called feedback effect on host galaxies. Therefore, statistical studies on RGs along the cosmic timescale are important for understanding the evolution of galaxies, as well as the evolution of the nuclear supermassive black holes. While there exist wide and deep radio surveys, however, compatible wide optical surveys have been not enough deep. The redshifts of the statistical large-area RG sample produced with SDSS were limited to be $z < 0.5$ due to its sensitivity ($i < 21$, e.g., Best et al. 2005).

2. Method and Results

In order to explore high-z RGs, we carried out the search for optically-faint radio galaxies by combining both the Subaru HSC-SSP catalog and the FRIST catalog (Yamashita et al. 2018). The HSC-SSP compiles faint sources down to $i_{\rm AB} = 26$ mag in the

Wide layer. We successfully identified $\sim$ 3,600 radio-AGNs in the field of 156 deg^2. The number of the matches is equivalent to $\sim$ 50 % of FIRST sources in the search field. This matching fraction is significantly higher than that of SDSS-FIRST radio-AGN samples (e.g., Ivezić et al. 2002). The photometric redshift (photo-z, Tanaka et al. 2018) of most of the HSC-FIRST RGs ranges are $0 < z_{\rm ph} < 1.5$ (Figure 1A).

We found a large number of RGs with large radio-loudness ($\log R_{\rm rest} > 4$) at an optically-faint regime ($i_{\rm AB} > 21$ mag). These optically-faint RGs are mostly located at photometric redshifts $z_{\rm ph} > 1$ (Figure 1B). The optical color of optically-bright HSC-FIRST RGs at $z_{\rm ph} \lesssim 1$ is consistent with that of passive galaxies. Meanwhile, the optically-faint RGs at $z_{\rm ph} > 1$ show bluer color, which is not consistent with that of passive galaxies but can be explained by predominant young stellar populations (Figure 1C). These optically-faint RGs might be "evolving" RGs from star-forming galaxies to passive ones.

3. Conclusion

The combination of Subaru HSC-SSP and FIRST successfully identified more than 3600 radio-AGNs at $0 < z < 1.5$ in the 156 deg^2. The optically-faint RG sample found by Subaru HSC-SSP and FIRST might include "evolving" RGs that are star-forming.

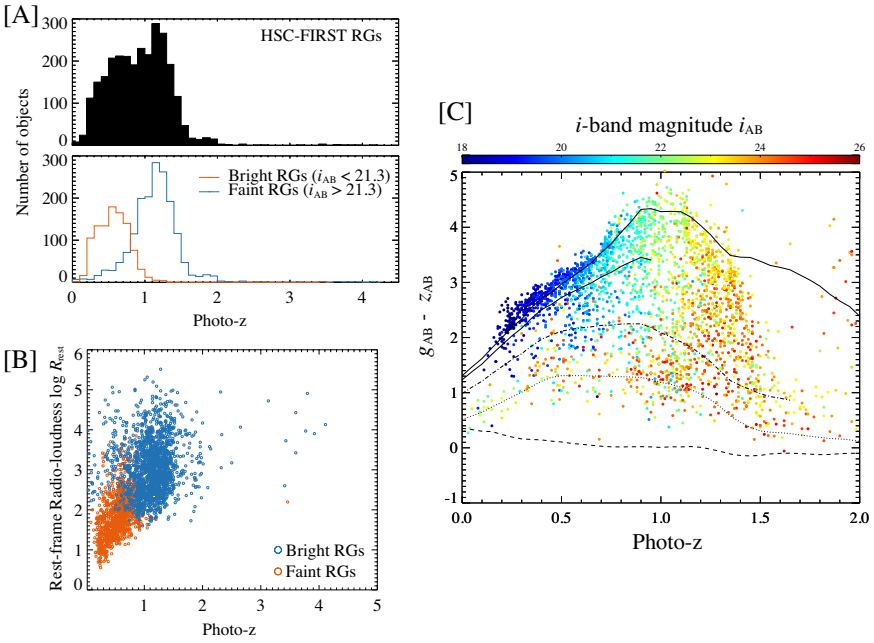

Figure 1. A: Photo-z for HSC-FIRST RGs (*upper panel*) and two sub-samples of the optically bright (orange) and faint (blue) RGs (*lower panel*). **B:** Radio-loudness at the rest-frame as a function of photo-z for the optically-bright (orange) and faint (blue) RGs. **C:** Optical color, $g_{\rm AB} - z_{\rm AB}$, as a function of photo-z for HSC-FIRST RGs. Colors of the data represent i-band magnitudes. Color tracks of model elliptical galaxies with a τ-model of $\tau = 1$ Gyr and ages of 2, 4, 6, and 8 Gy are shown as the solid, three-dots-dash, dot-dash, dotted curves, respectively. A color track for a star-forming model galaxy is also shown by the dash curve.

References

Best, P. N., Kauffmann, G., Heckman, T. M., & Ivezić, Ž. 2005, *MNRAS*, 362, 9

Ivezić, Ž., Menou, K., Knapp, G. R., et al. 2002, *AJ*, 124, 2364

Tanaka, M., Coupon, J., Hsieh, B.-C., et al. 2018, *PASJ*, 70, S9

Yamashita, T., Nagao, T., Akiyama, M., et al. 2018, accepted for publication in ApJ, arXiv:1804.03340

Astronomy in Focus, Volume 1
XXXth IAU General Assembly, August 2018
Volker Beckmann & Claudio Ricci, eds.

DOI: 00.0000/X000000000000000X

Modelling the jet kinematics of OJ287: Paradigm for other blazars?

M. Zajaček[1,2], S. Britzen[1], C. Fendt[3], G. Witzel[1], and V. Karas[4]

[1]MPIfR, Auf dem Hügel 69, D-53121 Bonn, Germany
email: zajacek, britzen@mpifr-bonn.mpg.de

[2]Universität zu Köln, Zülpicher Strasse 77, D-50937 Köln, Germany

[3]Max-Planck-Institut für Astronomie, Königstuhl, D-69117 Heidelberg, Germany

[4]Astronomical Institute, Academy of Sciences, Boční II 1401, CZ-14131 Prague, Czechia

Abstract. OJ287 belongs to one of the best candidates among active galactic nuclei to host a supermassive black hole binary (SMBHB) at very close separation. Based on a recent analysis of 120 VLBA (Very Long Baseline Array) observations at 15 GHz, we set up a simple kinematical model to explain the motion of jet components. The model involves the jet precession, on top of which we find an indication of additional nutation-like motion for the first time. The ratio of the precession and nutation periods is about 20. The precessing motion is quite natural in SMBHB systems, due to the torques exerted by the companion black hole on the accretion disc around the primary component. The other plausible explanation is provided by the disc misalignment with respect to the spin of a single black hole. The jet precession then occurs due to the Lense-Thirring effect. Both scenarios imply merger events during the evolution of OJ287, which may be a general characteristic of blazars. This model contribution is complementary to the observational contribution by Britzen et al. (this meeting).

Keywords. BL Lacertae objects: individual (OJ287), galaxies: jets, galaxies: nuclei

1. Summary

The BL Lac object OJ287 is characterized by one of the longest optical light curves (in the V-band) in the history, dating back to $\sim$ 1887, with the established quasi-periodicity of optical outbursts with the main period of $\sim 11.65\,\mathrm{yr}$ (Sillanpää et al., 1988). It was detected as a radio source for the first time in the Ohio sky survey in the 1960s. It belongs to low-synchrotron peaked BL Lac objects, having the redshift of $z = 0.306$. To explain the optical periodic outbursts, a scenario with a supermassive black hole binary was proposed (Lehto and Valtonen, 1996; Valtonen and Wiik, 2012), which has been successful in explaining the observed phenomena as well as in testing the general theory of relativity (Valtonen et al., 2010; Valtonen et al., 2016). The binary system is supposed to have an orbital period of $\sim 8.95\,\mathrm{yr}$ in the co-moving frame, with the large mass ratio of ~ 122 and the total binary mass that amounts to $\sim 10^{10}\,M_{\odot}$.

The analysis of VLBA data at 15 GHz showed that the Gaussian-fitted jet components change the position angle in the sky in a coherent way with the period of $\sim$ 20 years (Britzen et al., 2018). Based on the visual change of the jet position as well as the associated variability in the radio continuum, we set up a basic precession model, see also Fig. 1 (right panel), which was previously applied to OJ287 for a smaller number of components (Abraham, 2000). While Abraham (2000) fitted the precession model simultaneously to the apparent velocities and position angles of three components, Britzen et al. (2018) obtained 12 moving components, 3 stationary ones, and 9 from previous studies. The precession parameters obtained by Britzen et al. (2018) include the precession

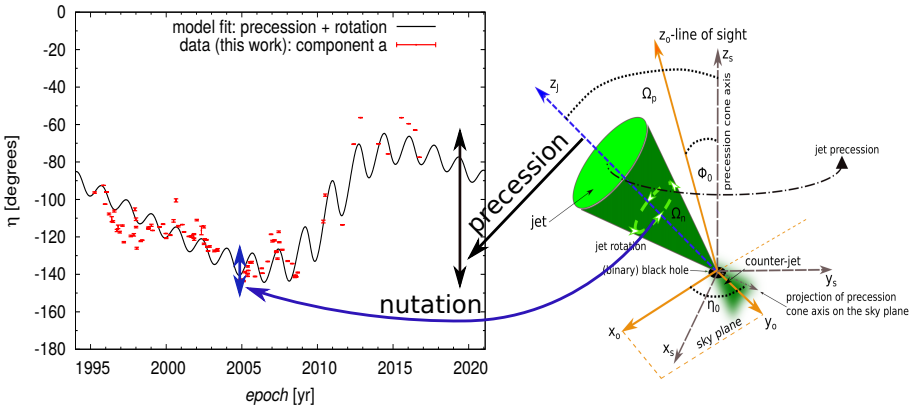

Figure 1. The model of the precessing and nutating jet (illustration on the right) applied to one of the stationary components of OJ287 jet - component **a** (left plot): the inferred position angles of the component (Britzen et al., 2018) are shown as red points whereas the model fit is depicted by a black solid line. For details, see Britzen et al. (2018).

period $P_{\rm p} = (24 \pm 2)\,{\rm yr}$, the Lorentz factor of the component motion $\gamma = 10 \pm 1$, the half-opening angle of the precession cone $\Omega = (10 \pm 3)^\circ$, the angle between the precession cone axis and the line of sight $\phi_0 = (12 \pm 3)^\circ$, and the projected angle of the cone axis in the sky plane $\eta_0 = (-149 \pm 40)^\circ$.

For three stationary components, an additional, weaker oscillation of the position angle was detected, which is consistent with the nutation-like motion of the jet. In Fig. 1 (left panel), we fitted the combined precession-nutation motion of the jet to the position angle of the component **a**. The obtained period of the nutation motion is $1.6 \pm 0.1\,{\rm yr}$, which is by a factor of ~ 20 smaller than the period of the precession motion. This is the first time that an indication of the nutation motion was detected for AGN jets. The similarity to X-ray binaries, specifically SS433, provides a hint for the potential binary nature of the source. The precession on the time-scale of ~ 24 years can be explained by either of the two following mechanisms:

(a) the supermassive black hole binary with a range of mass ratios and component separations,

(b) the Lense-Thirring precession of the inner compact ($\sim 100\,r_{\rm s}$) Advection-Dominated Accretion Flow (ADAF).

Both mechanisms require the perturbation of the inner, circularized accretion flow, which is expected to occur either during or after mergers of two massive black holes – scenarios (a) and (b) – or potentially the misalignment of the accretion flow may be caused by a non-spherical nuclear cluster that contains massive young stars whose strong stellar winds provide the material for accretion, which is relevant for the scenario (b).

References

Abraham, Z. 2000, *A&A*, 355, 915

Britzen, S., Fendt, C., Witzel, G., et al. 2018, *MNRAS*, 478, 3199

Lehto, H. J., & Valtonen, M. J. 1996, *Astrophysical Journal*, 460, 207

Sillanpää, A., Haarala, S., Valtonen, M. J., et al. 1988, *ApJ*, 325, 628

Valtonen, M. J., Mikkola, S., Lehto, H. J., et al. 2010, *Celestial Mechanics and Dynamical Astronomy*, 106, 235

Valtonen, M. J., & Wiik, K. 2012, *MNRAS*, 421, 1861

Valtonen, M. J., Zola, S., Ciprini, S. et al. 2016, *AJ* (Letters), 819, L37

Astronomy in Focus, Volume 1
XXXth IAU General Assembly, August 2018
Volker Beckmann & Claudio Ricci, eds.

DOI: 00.0000/X000000000000000X

Radio-spectral index distribution of SDSS-FIRST sources across optical diagnostic diagrams

M. Zajaček[1,2], G. Busch[2], M. Valencia-S.[2], A. Eckart[2,1], S. Britzen[1], N. Fazeli[2] and J. A. Zensus[1]

[1]MPIfR, Auf dem Hügel 69, D-53121 Bonn, Germany
email: zajacek, britzen@mpifr-bonn.mpg.de

[2]Universität zu Köln, Zülpicher Strasse 77, D-50937 Köln, Germany

Abstract. The unification model of active galactic nuclei (AGN) suggests that radio emission, and particularly radio spectral index, correlates with the accretion efficiency of the supemassive black hole. We performed 4.85 and 10.45 GHz observations of a few hundred SDSS-FIRST galaxies ($0.04 < z < 0.4$) with the Effelsberg 100-m telescope. We analysed the distribution of the radio-spectral index α (with $S_\nu \propto \nu^\alpha$) of the sources across the optical diagnostic diagrams. The objects can be grouped in three classes: (i) sources with steep radio index $\alpha < -0.7$, high ionization ratio and large radio loudness, (ii) sources with flat radio index $-0.7 \leqslant \alpha \leqslant -0.4$, lower ionization ratio and intermediate radio loudness, and (iii) sources with inverted radio spectra $\alpha > -0.4$, low ionization ratio and low radio loudness. The groups (i), (ii), and (iii) are concentrated on the transition from Seyferts to LINERs in the direction of the decreasing ionization-line ratio, where the trend of radio-spectral index flattening is found. These findings are interpreted in terms of the recurrent nuclear/jet activity, partially driven by galaxy interactions and mergers.

Keywords. galaxies: active, galaxies: jets, galaxies: nuclei

1. Summary

Several correlations between the mass of central supermassive black holes (SMBH) and the characteristics of their host bulges (stellar velocity dispersion, mass, luminosity) point towards their co-evolution (Kormendy & Ho 2013). In general, it is thought now that the enhanced accretion activity of SMBH in active galactic nuclei (AGN) can influence the star-formation activity in their hosts due to the input of energy and momentum, which heats the cold gas reservoir up and/or makes it more turbulent and/or expels it out of the host. These factors lead to the lack of cold gas and as a result, stars form less efficiently (Harrison 2017).

In particular, the role of radio AGN in the feedback process has remained unclear. In general, for sources at intermediate redshifts, the radio emission can be linked to the nuclear, jet, and jet-lobe emission with a variable spectral index, depending on the electron temperature (optical depth), see e.g. Eckart et al. (1986). The ratio of the radio and optical flux-densities, called the radio-loudness, was frequently reported to have a bimodal nature – radio-loud and radio-quiet sources are distinguished (Kellermann et al. 1989). However, because of the difficulty to unambiguously extend this definition to Type 2 AGN, it has been suggested that radio galaxies should be classified instead according to the presence (or absence) of relativistic jets (Padovani 2017). When plotted as a function of the Eddington ratio, the radio loudness derived from the total radio luminosity appears to evolve along two separate tracks, in which the radio-loudness generally tends to increase with the decreasing Eddington ratio (Sikora et al. 2007).

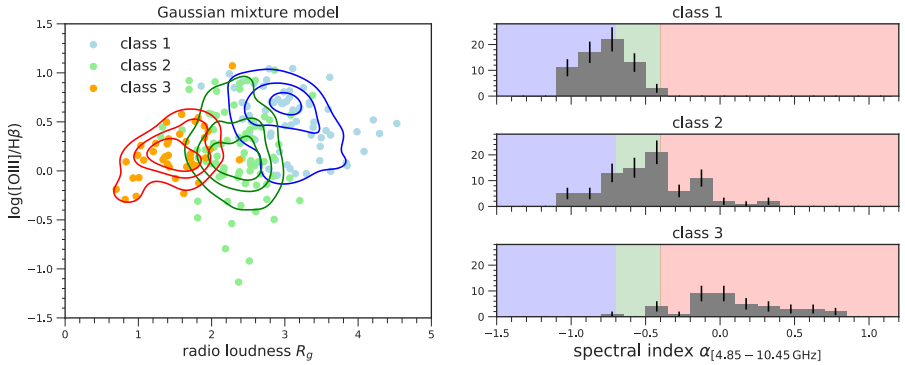

Figure 1. The three classes of radio sources in the space of radio-loudness, spectral index, and the ionization ratio $\log([\mathrm{O\,III}]/\mathrm{H}\beta])$ (left panel) and the corresponding distributions of spectral indices (right panel), where the spectral index α is defined using $S_\nu \propto \nu^\alpha$.

The broad-line radio galaxies, radio-loud quasars, and Fanaroff-Riley type I radio galaxies occupy more the upper track, while Seyfert, low-ionization nuclear emission-line region galaxies (LINERs), and Palomar-Green quasars lie along the radio-quiet track (Sikora et al. 2007). These distinctions in the radio-loudness–Eddington ratio plane disappear when the mass-corrected core radio luminosity is considered, which potentially decreases the importance of the black hole spin in determining the jet power (Broderick & Fender 2011).

Studying the relation between the radio-loudness and other quantities, such as the radio spectral index and the optical emission-line ratios, is vital to address fundamental questions of the role of black hole accretion and the jet formation and their connection to the feedback on galactic scales. To this goal, we performed radio-continuum observations at 4.85 and 10.45 GHz of several hundred intermediate-redshift galaxies to calculate their spectral indices. This information was complemented by the radio-loudness inferred from the core-dominated 1.4 GHz FIRST-survey luminosities and the emission-line ratio $\log([\mathrm{O\,III}]/\mathrm{H}\beta])$. We searched for the trends between these quantities both manually and using a machine-learning algorithm (Gaussian Mixture Model). We managed to recover three distinct groups in the 3D space of radio-loudness, spectral index, and the ratio $\log([\mathrm{O\,III}]/\mathrm{H}\beta])$, see also Fig. 1:

(1) sources with steep radio index, high ionization ratio and large radio loudness,

(2) sources with flat radio index, lower ionization ratio and intermediate radio loudness,

(3) sources with inverted radio spectra, low ionization ratio and low radio loudness.

References

Broderick, J. W., & Fender, R. P. 2011, *MNRAS*, 417, 184
Eckart, A., Witzel, A., Biermann, P. et al. 1986, *A&A* 168, 17
Harrison, C. M. 2017, *Nature Astronomy*, 1, id. 0165
Kellermann, K. I., Sramek, R., Schmidt, M. et al. 1989, *AJ*, 98, 1195
Kormendy, J., & Ho, L. C. 2013, *ARAA*, 51, 511
Padovani, P. 2017, *Nature Astronomy*, 1, id. 0194
Sikora, M., Stawarz, L., & Lasota, J.-P. 2007, *ApJ*, 658, 815

Astronomy in Focus, Volume 1
XXXth IAU General Assembly, August 2018
Volker Beckmann & Claudio Ricci, eds.

DOI: 00.0000/X000000000000000X

Proposed VLBI Observations in the FAST Commissioning Stage

Haiyan Zhang[1,2]†, Ru-Rong Chen[1,2], Chengjin Jin[1,2], Zhisheng Gao[1,2], Bo Zhang[3], Zhihan Qian[3], Xingwu Zheng[4] and Rendong Nan[1]

[1]National Astronomical Observatories of CAS, 100109, Beijing, People's Republic of China
[2]CAS Key Laboratory of FAST, NAOC, Chinese Academy of Sciences, 100109, Beijing, People's Republic of China
[3]Shanghai Astronomical Observatory of CAS, 200030, Shanghai, People's Republic of China
[4]Nanjing University, 210023, Nanjing, People's Republic of China

Abstract. The Five-hundred-meter Aperture Spherical radio Telescope (FAST) is the largest single dish radio telescope in the word, which could significantly improve the sensitivity of the current VLBI networks. In the FAST commissioning stage, the early VLBI sciences goals has been proposed, such as observing calibrators and strong OH maser sources. Till now, the VLBI backend and data storage system has been installed at the site, and the first VLBI fringe will be obtained in near future.

Keywords. VLBI, FAST

1. Introduction

The Five-hundred-meter Aperture Spherical radio Telescope (FAST) is a Chinese mega science project, and the main structure of the telescope had been completed in September 2016. Now the FAST is being busily commissioned (Li et al. 2018).

As the most sensitive single-dish radio telescope, Very Long Baseline Interferometry (VLBI) research with FAST is one of the key science goals (Nan et al. 2011). Due to its extremely collecting area and the location, FAST could greatly improve the sensitivity of the current VLBI networks and detect weaker radio sources than before. For instance, if FAST joins into the European VLBI Network (EVN), the image sensitivity will be comparable to the value of the Full High Sensitive Array (HSA) (Zhang 2017).

2. Proposed VLBI observations in the commissioning stage

Several science goals have been proposed for FAST VLBI observations, such as compact radio sources survey, Active Galactic Nuclei (AGNs) to study the physical mechanism, pulsar Astrometry to obtain the accurate distance and parallax, and radio stars etc. However, the complexity and the innovative nature of the FAST systems pose many challenges. The observations in draftscan mode have been proposed to avoid the complex scan patterns and fast driving/switching of the telescope. More than 40 new pulsars have been detected by FAST successfully recently.

For VLBI test observation with FAST, the objective is to establish VLBI observation system. In the commissioning stage, several adjustment and early sciences goals have been considered, such as observing the satellite or strong calibrators to detect the first fringe, detecting strong OH maser sources etc.

† Email: hyzhang@bao.ac.cn

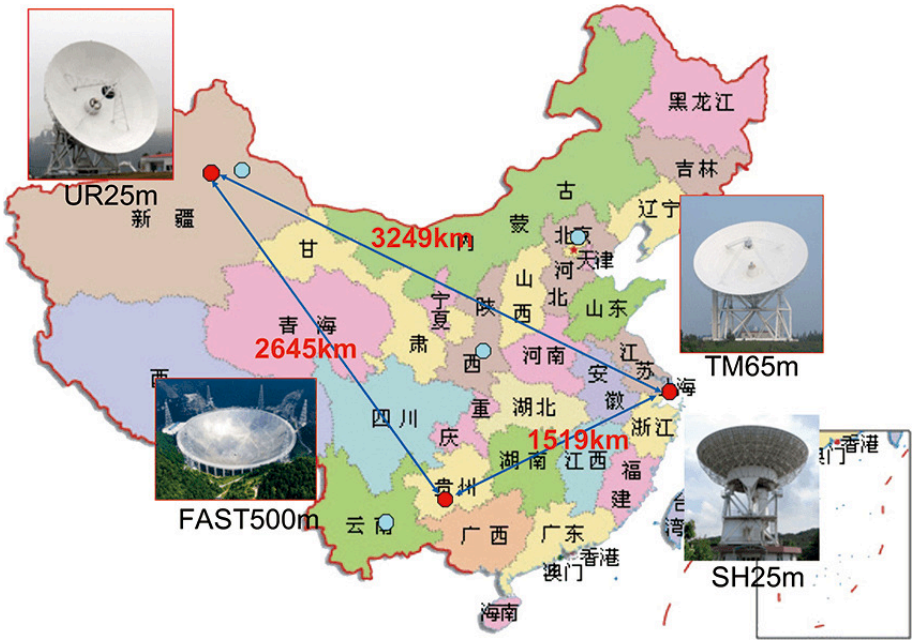

Figure 1. The radio telescopes with L band receivers in China.

3. Current status

Till now, the FAST VLBI backend using ROACH2 board has been developed and installed at the site. The disk-based Mark 6 has also been built to record the observing data with the total storage of 256 TB. Moreover, the Hydrogen maser clock has been used to provide the high-resolution time.

The 19-beam receiver at L band has been installed at the FAST. Now in China, the VLBI observations at L band have been carried out with Chinese VLBI networks including the 26-m telescope in Xingjiang, the Tianma 65-m telescope and Sheshan 25-m telescope (see Figure 1). FAST test observations with Chinese VLBI networks would be made in the near future, such as observing the satellite and the strong calibrators.

Acknowledgment

This work is partially supported by the National Scientific Foundation of China (No. U1831128 and 11503034), and by the CAS Key Laboratory of FAST.

References

Li, D., Wang, P., Qian, L., et al. 2018, *IMMag*, 19, 112
Nan, R., Li, D., Jin, C., et al. 2011, *IJMPD*, 20, 989
Zhang, B. 2017, *Sci Sin-Phys Mech Astron*, 47, 069501, 30, 490

Astronomy in Focus, Volume 1
XXXth IAU General Assembly, August 2018
Volker Beckmann & Claudio Ricci, eds.

DOI: 00.0000/X000000000000000X

Extremely Rapid X-Ray Flares of TeV Blazars in the RXTE Era

S. F. Zhu[1,2], Y. Q. Xue[2], W. N. Brandt[1], W. Cui[3], and Y. J. Wang[2]

[1]Dept. of Astronomy & Astrophysics, The Pennsylvania State University, University Park, PA 16802, USA; email: sxz89@psu.edu

[2]CAS Key Laboratory for Research in Galaxies and Cosmology, Dept. of Astronomy, University of Science and Technology of China, Hefei 230026, China; email: xuey@ustc.edu.cn

[3]Dept. of Physics and Astronomy, Purdue University, West Lafayette, IN 47907, USA

Abstract. Rapid flares from blazars in very high-energy (VHE) gamma-rays challenge the common understanding of jets of active galactic nuclei (AGNs). The same population of ultra-relativistic electrons is often thought to be responsible for both X-ray and VHE emission. We thus systematically searched for X-ray flares at sub-hour timescales of TeV blazars in the entire Rossi X-ray Timing Explorer archival database. We found rapid flares from PKS 2005−489 and S5 0716+714, and a candidate rapid flare from 1ES 1101−232. In particular, the characteristic rise timescale of PKS 2005−489 is less than half a minute, which, to our knowledge, is the shortest among known AGN flares at any wavelengths. The timescales of these rapid flares indicate that the size of the central supermassive black hole is not a hard lower limit on the physical size of the emission region of the flare. PKS 2005−489 shows possible hard lags in its flare, which could be attributed to particle acceleration (injection); its flaring component has the hardest spectrum when it first appears. For all flares, the flaring components show similar hard spectra with $\Gamma = 1.7$–1.9, and we estimate the magnetic field strength $B \approx 0.1$–1.0 G by assuming synchrotron cooling. These flares could be caused by inhomogeneity of the jets. Models that can only produce rapid gamma-ray flares but little synchrotron activity are less favorable. *[see Zhu et al. (2018) for details]*

Keywords. galaxies: active – BL Lacertae objects: general – galaxies: jets – X-rays: galaxies

---

1. Why care about rapid X-ray flares?

Rapid flares from blazars in very high-energy (VHE) gamma-rays challenge the common understanding of AGN jets. The same population of ultra-relativistic electrons is often thought to be responsible for both X-ray and VHE emission. A fundamental question is: *How rapid can an X-ray flare of TeV blazars ever be (is there a limit at all)?*

2. What have we done?

We have systematically searched for X-ray flares at *sub-hour timescales* of TeV blazars in the *entire* RXTE archival database.

3. What have we found?

We have discovered *3 new extremely rapid X-ray flares* from 3 TeV blazars, PKS 2005−489 (rising timescale $\tau_{\rm r} < 30$ s), S5 0716+714 ($\tau_{\rm r} < 180$ s), and 1ES 1101−232 ($\tau_{\rm r} < 60$ s), respectively (see Figure 1).

4. What is so special about this very flare with $\tau_{\rm r} < 30$ s from PKS 2005−489 that has a BH mass of $M_{\rm BH} > 10^{8.5} M_{\odot}$?

• Its characteristic rise timescale is less than 30 sec, which, to our knowledge, is the *fastest among known AGN flares* at any wavelengths (see Figure 2).

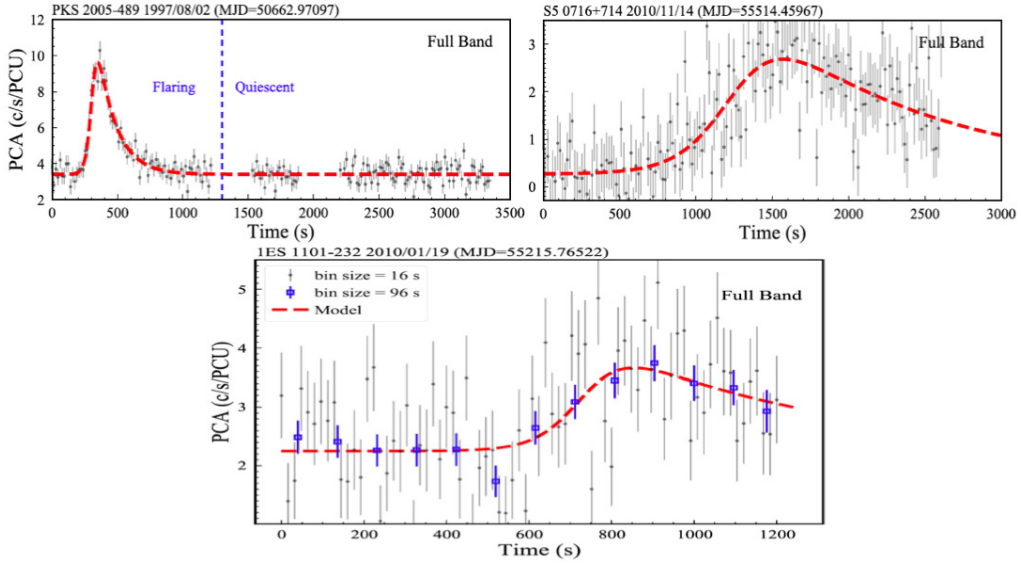

Figure 1. Three extremely rapid X-ray flares newly discovered for 3 TeV blazars.

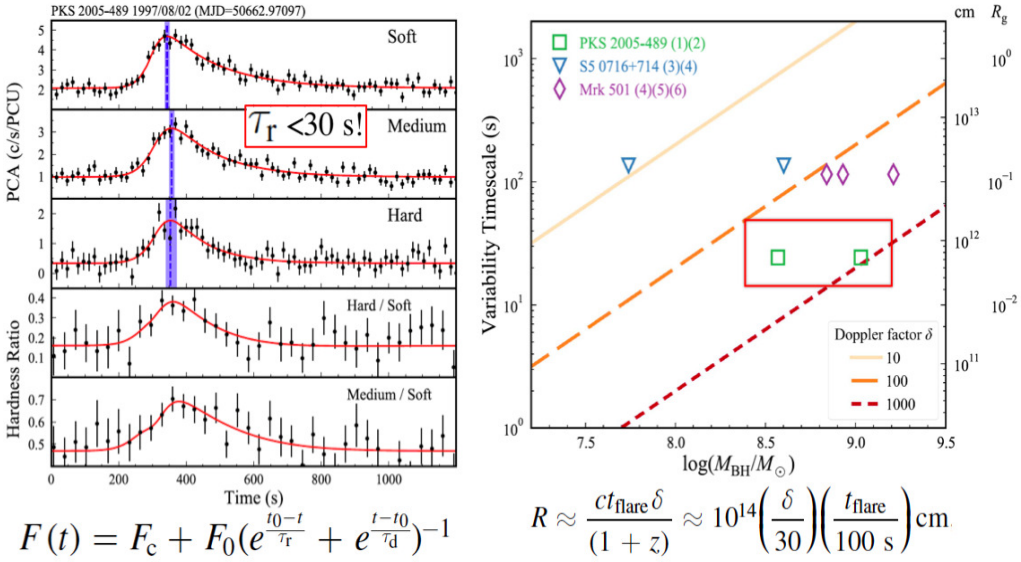

Figure 2. Fastest AGN flare ever that tightly constrains the size of its emission region.

• This indicates that the size of central supermassive black hole is *not a hard lower limit* on the physical size of emission region of the flare (see Figure 2).

5. Some take-home messages

- Hitherto the most rapid AGN flare ($\tau_r < 30$ s) has been discovered.
- BH size is not a hard lower limit on flaring emission region.
- Extremely rapid X-ray flares of TeV blazars could be caused by jet inhomogeneity.

References

Zhu, S. F., Xue, Y. Q., Brandt, W. N., Cui, W., & Wang, Y. J. 2018, *ApJ*, 853, 34

Astronomy in Focus, Volume 1
XXXth IAU General Assembly, August 2018
Volker Beckmann & Claudio Ricci, eds.

DOI: 00.0000/X000000000000000X

Optical monitoring of a sample of FR II-type QSOs

S. Zola[1,2], A. Kuzmicz[3], G. Bhatta[1], M. Jamrozy[1], W. Ogloza[2], M. Drozdz[2], M. Siwak[2], D. E Reichart[4], D. B Caton[5] and G. Stachowski[2]

[1]Astronomical Observatory, Jagiellonian University, ul. Orla 171, 30-244 Krakow, Poland
email: szola@oa.uj.edu.pl

[2]Mt. Suhora Observatory, Pedagogical University, ul. Podchorazych 2, 30-084 Krakow, Poland

[3]Center for Theoretical Physics, Polish Academy of Sciences Al. Lotnikow 32/46, 02-668 Warsaw, Poland

[4]University of North Carolina at Chapel Hill, Chapel Hill, North Carolina NC 27599, USA

[5]Dark Sky Observatory, Department of Physics and Astronomy, Appalachian State University, Boone, NC 28608, USA

Abstract. We present results derived from a monitoring program of a sample of FR-II type radio quasars. The variabilities detected in their densely covered light curves, which have being gathered over a period of more than 9 years, are analyzed with the structure function statistical method. Based on the shapes of the structure functions, for each target we can identify which proposed model (supernovae/starbursts, disk instability and gravitational microlensing) could be responsible for the optical variability, concluding that all three occur in this sample of QSOs.

Keywords. galaxies: photometry, galaxies: nuclei, quasars: individual (J0713+3656, J0952+2353, J1007+1248, HB1156+631, HB1525+267, J1504+6856, HB1721+343, J2042+7508)

1. Observations

An observing program aimed at long-term monitoring of a sample of 8 radio-quasars was started in 2009. The chosen sample consists of 8 objects located in the northern hemisphere, all belonging to the FR-II type and bright enough to allow photometric measurements with small telescopes with an accuracy better than a few hundredths of a magnitude. Observations are being taken primarily with two telescopes located in Poland: the 60 cm reflector at the Mt. Suhora Observatory of the Pedagogical University, and the 50 cm Cassegrain telescope of the Astronomical Observatory of the Jagiellonian University in Krakow. Both telescopes are equipped with CCD cameras with back illuminated chips and a set of wide band filters (made according to the Bessell prescription). In the case of prolonged periods of cloudy weather at the two sites, we gather data with two telescopes operated by the SKYNET Robotic Telescope Network: DSO-17 (40 cm) and/or RRRT (60 cm). Front illuminated CCDs are used at these telescopes. Due to the peak sensitivity of CCDs in the near infrared, we perform observations in the R filter in order to increase the S/N ratio, occasionally also measuring colors (BVRI) at the Mt. Suhora observatory. Reduction of observations, each consisting of 6 or more scientific images, is performed in the usual way: calibration for bias, dark and flatfield (usually taken on the sky) is done with the IRAF package, while extraction of magnitudes was done with the CMunipack program, an interface to the DAOPHOT code. For each target, we calculate a mean point from individual measurements, and a standard sigma is considered as its uncertainty. The light curves spanning more than 9 years are shown in Fig. 1.

2. Conclusions

We applied the structure function (SF) method (e.g. Vanden Berk *et al.* 2004) to quantify the optical variability seen in our targets' light curves.The observational SFs can be compared with predictions given by theoretical models: accretion disk instability (e.g. Kawaguchi *et al.* 1998), supernovae and starbursts (e.g. Aretxaga & Terlevich 1994); or gravitational microlensing causing variations with smaller amplitude (Hawkins 1996).

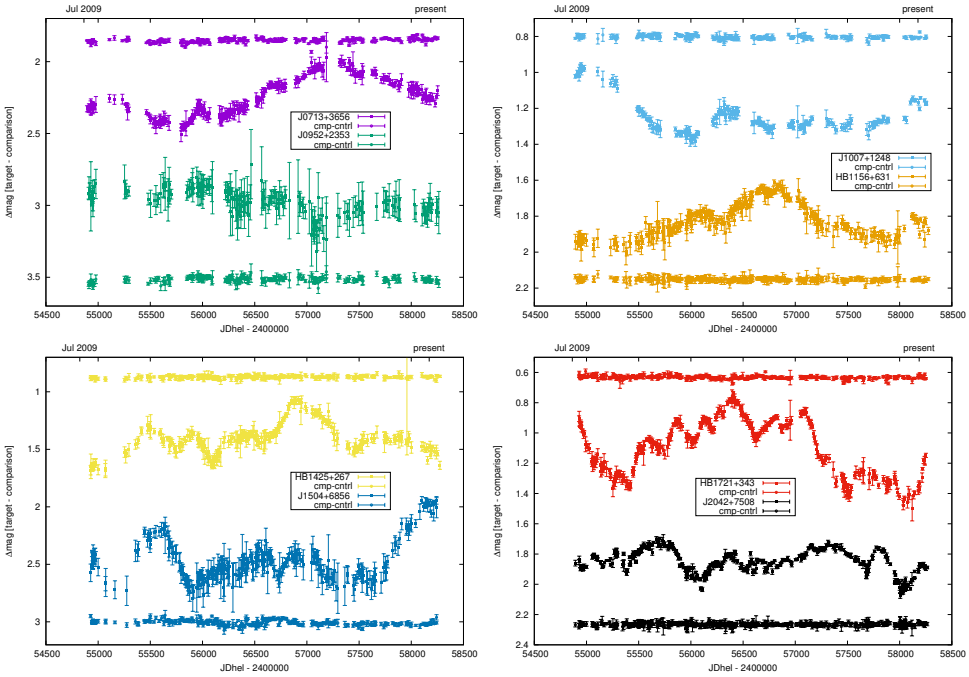

Figure 1. Light curves of eight monitored quasars (R filter).

Comparing the recent variability properties of the sample objects with those we estimated in 2015 based on a 4 year-long run (Zola *et al.* 2012) we notice an increase in the amplitude of variations for all our targets, suggesting a very long timescale of flux changes, however we do not notice any significant change in the SF slope steepness of any of the quasars except for J0713+3656, for which there is an increase from 0.48 to 0.67. The observed SF of J2042+7508 very closely resembles the theoretical one computed for the disk instability model. A multiwavelength analysis of this object by Bhatta *et al.* (2018) supports this finding by concluding that the flux in optical band is dominated by the accretion disk.

This work was partially supported by the NCN grants No. 2018/09/B/ST9/02004 and 2017/26/D/ST9/01178

References

Aretxaga, I., & Terlevich, R. 1994, *MNRAS*, 269, 462
Bhatta, G., Stawarz, L., Markowitz, A., et al. 2018, *ApJ*, 866, 132
Hawkins, M. R. S. 1996, *MNRAS*, 278, 787
Kawaguchi, T., Mineshige, S., Umemura, M., & Turner, E. L. 1998, *ApJ*, 504, 671
Vanden Berk, D. E., Wilhite, B. C., Kron, R. G., et al. 2004, *ApJ*, 601, 692
Zola, S., Kuzmicz, A., Jamrozy, M., et al. 2012, *ASI Conf. Ser.*, 7, 239